ANALYSIS OF THE CATALYTIC CYCLE
&
MANIPULATION OF SUBSTRATE SPECIFICITY
IN
FLAVOCYTOCHROME b_2

Simon N. Daff

THESIS PRESENTED FOR THE DEGREE OF
DOCTOR OF PHILOSOPHY
UNIVERSITY OF EDINBURGH
APRIL 1996

to my parents and my wife

Acknowledgements

Many thanks must go to my supervisors, Steve and Graeme, for their inspirational help and guidance. Thanks to Dr Forbes Manson for supplying mutants and to Dr John Ingledew for loaning freeze-quench equipment and for performing EPR experiments. Finally, thanks to the occupants, past and present, of Lab 275 (Chemistry) and the 8th floor (Darwin) for providing entertainment, refreshment, stimulation and unreserved help.

Abstract

The physiological role of flavocytochrome b_2 from *Saccharomyces cerevisiae* is to couple L-lactate dehydrogenation to respiration via the ubiquitous electron carrier cytochrome *c*. For each L-lactate molecule dehydrogenated two cytochrome *c* molecules are reduced, and as such the enzyme acts as a 'bio-electrical transformer'. The mechanism through which this process occurs can be simplified into five separate electron transfer events which form the catalytic cycle. L-lactate dehydrogenation results in the two electron reduction of flavin at the enzyme's active site. These electrons are passed individually to the b_2-haem (intramolecular electron transfer) and on to two cytochrome *c* molecules (intermolecular electron transfer). Using stopped-flow spectrophotometry, the intramolecular electron transfer steps have been investigated using several different experimental procedures. Electron transfer from fully reduced FMN to b_2-haem has been studied by monitoring both haem reduction and haem re-reduction (following oxidation by cytochrome *c*). In each situation this step proved too fast to be observed, and appeared only as a slight lag (relative to flavin reduction) in the b_2-haem reduction trace. Nevertheless a lower estimate for this rate constant was derived to be 1500±500 s^{-1}. The second intramolecular electron transfer step takes place from flavin semiquinone to b_2 haem and was observed as a component of the flavin oxidation process. This proved to be the slowest step in the catalytic cycle (at 120 s^{-1}) and is therefore responsible for determining the overall turnover rate. The product, pyruvate, was found to be an inhibitor of the flavin oxidation reaction (K_i = 40±15 mM), consistent with reports that it acts as a non-competitive inhibitor in the steady-state. Stopped-flow studies on the cytochrome *c* reductase activity of flavocytochrome b_2 yielded a second-order rate constant of 35 $\mu M^{-1}s^{-1}$, which represents the rate constant for cytochrome *c* association. The rate constant for electron transfer between b_2-haem and cytochrome *c* in the pre-formed complex proved to be too fast to be observed (i.e. >1000 s^{-1}). Inhibition of pre-steady-state cytochrome *c* reduction by ferrocytochrome *c* and also by zinc-substituted cytochrome *c* enabled a binding constant to be estimated for the catalytically competent complex (8 μM). However, the inhibition observed was only partial signifying that cytochrome *c* reduction is able to take place at sites other than the primary catalytic site, when this is occupied. This is advantageous for the enzyme in terms of efficiency, since the dissociation rate for the primary binding site is

estimated to be 280 s^{-1}, and so approaches the maximum turnover rate of 207 s^{-1}. Further evidence obtained showed that there is little or no dependence of the catalytic turnover rate on any step involving cytochrome *c* reduction or dissociation. A self consistent model for the catalytic cycle has been derived incorporating the electron transfer rate constants obtained. In order to test the model quenched-flow EPR experiments were conducted in an attempt to trap the dominant enzyme form in steady-state turnover. The results indicate that as expected, the majority of flavin present is in the semiquinone form.

In a separate study, the ability of flavocytochrome b_2 to distinguish its physiological substrate L-lactate from other 2-hydroxy-acids was examined by site-directed mutagenesis. Several 2-hydroxy-acids are able to act as reasonable substrates, but L-lactate is clearly preferred. Examination of the enzyme crystal structure reveals that the bound product molecule (pyruvate) interacts with various charged and polar side-chains, however selectivity for the substrate methyl group was considered to originate from hydrophobic interactions with the alkyl side-chains of residues Ala198, Leu230 and Ile326. The importance of these residues in controlling substrate specificity was probed by the generation of four mutant enzymes, each designed to accommodate larger substrates in favour of L-lactate. These were the point mutants; A198G (Ala→Gly); L230A (Leu→Ala) and I326A (Ile→Ala) and the double mutant A198G·L230A. Wild-type and mutant enzymes were characterised according to their ability to catalyse steady-state dehydrogenation of a range of substrates increasing in chain-length from 2 to 8 carbon atoms. Ala198 was found to be influential in substrate binding, the A198G mutation causing an increase in K_m for all substrates studied. The L230A mutation caused a dramatic decrease in specificity for L-lactate and created an enzyme which performed most efficiently with long-chain substrates (k_{cat}/K_m values were found to be comparable to the wild-type enzyme for these substrates). The double mutation A198G·L230A combined the effects caused by the two single mutations and generated an enzyme with poor substrate binding ability and specificity biased towards long-chain substrates. The I326A mutation generated a specific 2-hydroxyoctanoate dehydrogenase with better efficiency and specificity for its primary substrate than the wild-type enzyme exhibits for L-lactate.

INDEX

Chapter 1	INTRODUCTION	Page 1

1.1. Discovery 2

1.2. The Physiological Role of Flavocytochrome b_2 3

1.3. The Flavocytochrome b_2 Structure 5
The amino-acid sequence, The crystal structure.

1.4. The Flavin Domain 8
FMN binding, FMN and metabolism, *Redox potentials.*

1.5. The Active Site 12
Residues involved in substrate binding, Residues involved in catalysis.

1.6. The Mechanism of L-Lactate Dehydrogenation 15
Nucleophilic addition, Halide elimination, 5-Deaza-FMN, Structural analysis.

1.7. Substrate Specificity & Inhibition 24
Relative activities of some substrates, Flavocytochrome b_2 inhibitors.

1.8. The Haem Domain 26
The role of the haem domain, The catalytic cycle.

1.9. Protein Mediated Electron-Transfer 28
Non-adiabatic electron-transfer theory: Marcus theory.

1.10. Intramolecular Electron-Transfer 33
The photosynthetic reaction centre, Ruthenated proteins, FMN to b_2-haem electron transfer in flavocytochrome b_2.

1.11. Intermolecular Electron-Transfer 40
Cytochrome *c* : cytochrome *c* peroxidase, Cytochrome *c* : cytochrome b_5, Conclusions.

2.1. Site-Directed Mutagenesis 50

2.2. Transformation of *E. coli* 50

2.3. Growth of *E. coli* 50

Luria broth (growth medium), Luria agar plates.

2.4. Purification of Flavocytochrome b_2 51

Cell lysis, Ammonium sulphate fractionation, Dialysis, Column purification, Enzyme storage.

Phosphate buffer (for flavocytochrome b_2 purification)

2.5 SDS PAGE 54

Gel preparation, Electrophoresis.

Resolving gel, Stacking gel, Resolving buffer, Stacking buffer, Sample buffer, Running buffer, Gel stain, Destains.

2.6 Western Blotting 57

Western transfer, Developing the Western blot.

Western transfer buffer, Tris-buffered saline, Developing solution

2.7. Steady-State Kinetics 59

The Michaelis-Menten equation, Preparation of L-2-^{2}H-lactate.

Standard absorption changes for electron acceptors, Tris buffer (pH 7.5, I 0.10; for steady-state & stopped-flow kinetic experiments), Michaelis Menten Equation, L-2-^{2}H-lactate synthesis reaction mixture.

2.8 Determination of FMN content 61

CAPS buffer (pH 11, *I* 0.10)

2.9 Stopped-Flow Spectrophotometry 62

Introduction, Flavocytochrome b_2 reduction, b_2-haem re-reduction, Flavin oxidation, Cytochrome *c* reduction, Inhibition of cytochrome *c* reduction.

2.10 Preparation of Zinc-Substituted Cytochrome *c* 67

Phosphate buffer (molarity x, *pH y), Amberlite CG-50 equilibration.*

2.11 Rapid-Freezing Quenched-Flow EPR 69

MOPS buffer (pH 7.5, I 0.10).

Chapter 3 THE CATALYTIC CYCLE Page 72

3.1. Introduction 73
The model, The component steps

3.2 Results 76

(a) Flavocytochrome b_2 Reduction 76

(b) Re-reduction of b_2-haem 80

(c) Flavin Oxidation 82

(d) Pyruvate Inhibition 88
Inhibition of flavin oxidation, The effect of pyruvate on b_2-haem reduction

(e) Rapid-Mixing Quenched-Flow EPR Spectroscopy 93

3.3. Discussion 96

Chapter 4 THE INTERACTION WITH CYTOCHROME *C* Page 99

4.1. Introduction 100
Cytochrome *c* binding studies, Intermolecular electron-transfer

4.2 Results 103

(a) Pre-Steady-State Reduction of Cytochrome *c* 104

(b) Variation of the Second-Order Rate Constant for Cytochrome *c* Reduction with Ionic Strength 106
Low ionic strength
The Primary kinetic salt effect

(c) Inhibition of Cytochrome *c* 110
The model used to quantify inhibition of pre-steady-state cytochrome c reduction

(d) The Effect of Zinc-substituted Cytochrome *c* Binding on Flavocytochrome b_2 Reduction. 113

4.3 Discussion 114

Chapter 5	SUBSTRATE SPECIFICITY	Page 117
5.1.	**Introduction** Comparison with LDH from *B. stearothermophilus*	118
5.2	**Results & Discussion**	123
(a)	**Wild-Type**	123
(b)	**The L230A Mutation** Stopped-flow analysis of L230A, Kinetic isotope effects	125
(c)	**The A198G Mutation** The A198G:L230A mutant	132
(d)	**The I326A Mutation**	135
5.3.	**Conclusions**	137

APPENDICES

1	**References**	138
2	**Abbreviations**	150
3	**Courses & conferences attended**	153
4	**Publications**	155

List of Figures

1.1 The physiological location of flavocytochrome b_2 3

1.2 Respiratory pathways sustained by flavocytochrome b_2 4

1.3 Amino-acid sequence comparison 6

1.4 Structure of flavocytochrome b_2 tetramer & subunit 7

1.5 Riboflavin 9

1.6 Flavin mononucleotide: oxidation states & redox potentials 10

1.7 Active site structure 13

1.8 A mechanistic comparison: Hydride *v* Carbanion 15

1.9 Nitroethane, 2-hydroxy-3-butynoate & 5-Deaza-FMN 17

1.10 Proposed model for halide elimination 18

1.11 Active site viewed down the substrate's C1-C2 bond 21

1.12 Mechanisms involving pyridoxal phosphate 23

1.13 Haem *a* 26

1.14 The catalytic cycle 28

1.15 The energetics of non-adiabatic electron transfer 30

1.16 The energetics of 'activationless' electron transfer and electron transfer in the Marcus 'inverted' region 31

1.17 Plot of ln k_{et} *v* $-\Delta G$ 32

1.18 Experimentally derived activationless electron-transfer rate constants plotted against through-space distance and σ-tunneling distance 34

1.19 Electron-transfer pathways suggested for ruthenated His mutants of b_2-core 35

1.20 Variation of electron-transfer rate constant with hinge length 38

1.21 The dual role of Tyr143 39

1.22 The reacting face of yeast cytochrome *c* 42

1.23 Cytochrome *c* peroxidase:cytochrome *c* electron-transfer complex 43

1.24 Cytochrome b_5:cytochrome *c* electron-transfer complex 45

List of figures continued.....

2.1 SDS PAGE of mutant enzymes 55

2.2 An example of a stopped-flow trace 63

2.3 Visible absorption spectra of flavocytochrome b_2 64

2.4 Visible absorption spectra of flavocytochrome b_2 flavin domain 65

2.5 Visible absorption spectra of cytochrome *c* 66

2.6 Visible absorption spectra of zinc-substituted & porphyrin cytochromes *c* 68

2.7 EPR spectra used in ferricytochrome *c* quantitation 70

3.1 Kinetic model for the catalytic cycle of flavocytochrome b_2 73

3.2 Model for flavocytochrome b_2 reduction 76

3.3 b_2-haem reduction: stopped-flow trace 78

3.4 b_2-haem re-reduction: stopped-flow trace 80

3.5 Pre-steady-state flavin oxidation scheme 82

3.6 Flavin oxidation: stopped-flow traces 84

3.7 Flavin oxidation time-course 85

3.8 Inhibition plot of flavin oxidation rate constant *v* pyruvate concentration 89

3.9 b_2-haem reduction in the presence of pyruvate 90

3.10 EPR spectra used for semiquinone quantitation 94

3.11 Plot of free radical concentration *v* time 95

4.1 Postulated electron-transfer pathway from b_2-haem to cytochrome *c* 102

4.2 Cytochrome *c* reduction: stopped-flow trace 103

4.3 Possible kinetic models for pre-steady-state cytochrome *c* reduction 104

4.4 Derivation of the second-order rate constant for cytochrome c reduction 105

4.5 Debye-Hückel plot for pre-steady-state cytochrome *c* reduction 107

List of figures continued.....

4.6 Cytochrome *c* reduction: stopped-flow traces recorded at low ionic strength 109

4.7 Rate constants for cytochrome c reduction plotted against inhibitor concentration 111

4.8 Flavocytochrome b_2 reduction: stopped-flow traces recorded in the presence of zinc-substituted cytochrome *c* 113

5.1 Active site structure 118

5.2 Active site structure of LDH from *B. stearothermophilus* 121

5.3 A typical Michaelis-Menten plot, and steady-state data determined for the wild-type enzyme with different substrates 124

5.4 Substrate specifity profiles for L230A and wild-type, and steady-state data determined for L230A with different substrates 126

5.5 Reduction of L230A: stopped-flow traces, and model for electron redistribution 128

5.6 Rate constants for reduction of L230A plotted against substrate concentration 130

5.7 Typical Michaelis-Menten plots used in calculation of kinetic isotope effects, and data for wild-type, A198G and L230A 131

5.8 Substrate specifity profiles for A198G and wild-type, and steady-state data determined for A198G with different substrates 133

5.9 Substrate specifity profiles for L230A:A198G and L230A, and steady-state data determined for L230A:A198G with different substrates 134

5.10 Substrate specifity profiles for I326A and wild-type, and steady-state data determined for I326A with different substrates 136

CHAPTER 1

INTRODUCTION

1.1. Discovery

Flavocytochrome b_2 (L-lactate : cytochrome *c* oxidoreductase) was first identified by Bach *et al.* (1942 a & b) who surmised that the new soluble cytochrome they had discovered in an extract of bakers' yeast may have been responsible for the L-lactate dehydrogenase activity reported earlier by Bernheim (1928). Their suspicions were confirmed by Appleby & Morton (1954) who succeeded in crystallising the enzyme. They showed that one flavin mononucleotide (FMN) was bound for every b_2-haem and that it behaves as a prosthetic group rather than a weakly-bound cofactor. They correctly assigned L-lactate dehydrogenase activity to FMN, and electron transfer functionality to the b_2-haem, for which cytochrome *c* was the implied redox partner. It was later demonstrated, however, that the yeast preparations used in these early studies contained enzyme which had been modified by site-specific proteolytic cleavage. The resultant enzyme form (termed 'Morton' or 'nicked') consisted of two unequal polypeptide chains which, while folded, retained the general characteristics of the native enzyme. Lederer & Simon (1971) used SDS-PAGE to separate the denatured fragments, obtaining two bands (see *Figure 2.1*). The native enzyme was prepared from yeast by Jacq & Lederer (1972) in the presence of phenylmethylsulphonyl fluoride (PMSF, a potent inhibitor of serine proteases) and consisted of a single polypeptide chain with weight 57 kDa.

It should be noted that the earlier enzyme preparations are likely to have consisted of either pure Morton enzyme or a mixture of the Morton and native forms, therefore the kinetic results reported are not always comparable with more recent work. The Morton and native enzyme forms are differentiated by the ability of the former to be crystallised at low ionic strength. Whereas, in kinetic terms, the Morton enzyme has a significantly lower specific activity (~40%) and lower substrate affinity (Lederer, 1991).

Labeyrie *et al.* (1978) report that around 0.8 μmole of intact flavocytochrome b_2 can be prepared per kg of dried yeast. This situation has been improved dramatically by over-expression of the enzyme in a bacterial host (Black *et al.*, 1989).

A similar quantity of enzyme can now be purified from less than 10 g of *Escherichia coli* transformants.

1.2. The Physiological Role of Flavocytochrome b_2

Flavocytochrome b_2 is initially synthesised as a 68 kDa precursor in the cytoplasm of *Saccharomyces cerevisiae* before being proteolytically processed during its transport to the mitochondrial intermembrane space (Daum *et al.*, 1982; Gasser *et al.*, 1982). As a niche respiratory enzyme, flavocytochrome b_2 is induced by the presence of oxygen and more specifically by its substrate L-lactate. Its physiological role is illustrated in *Figures 1.1* and *1.2*, the latter of which places it in relation to the Krebs cycle. This is at the heart of normal aerobic respiration and involves the

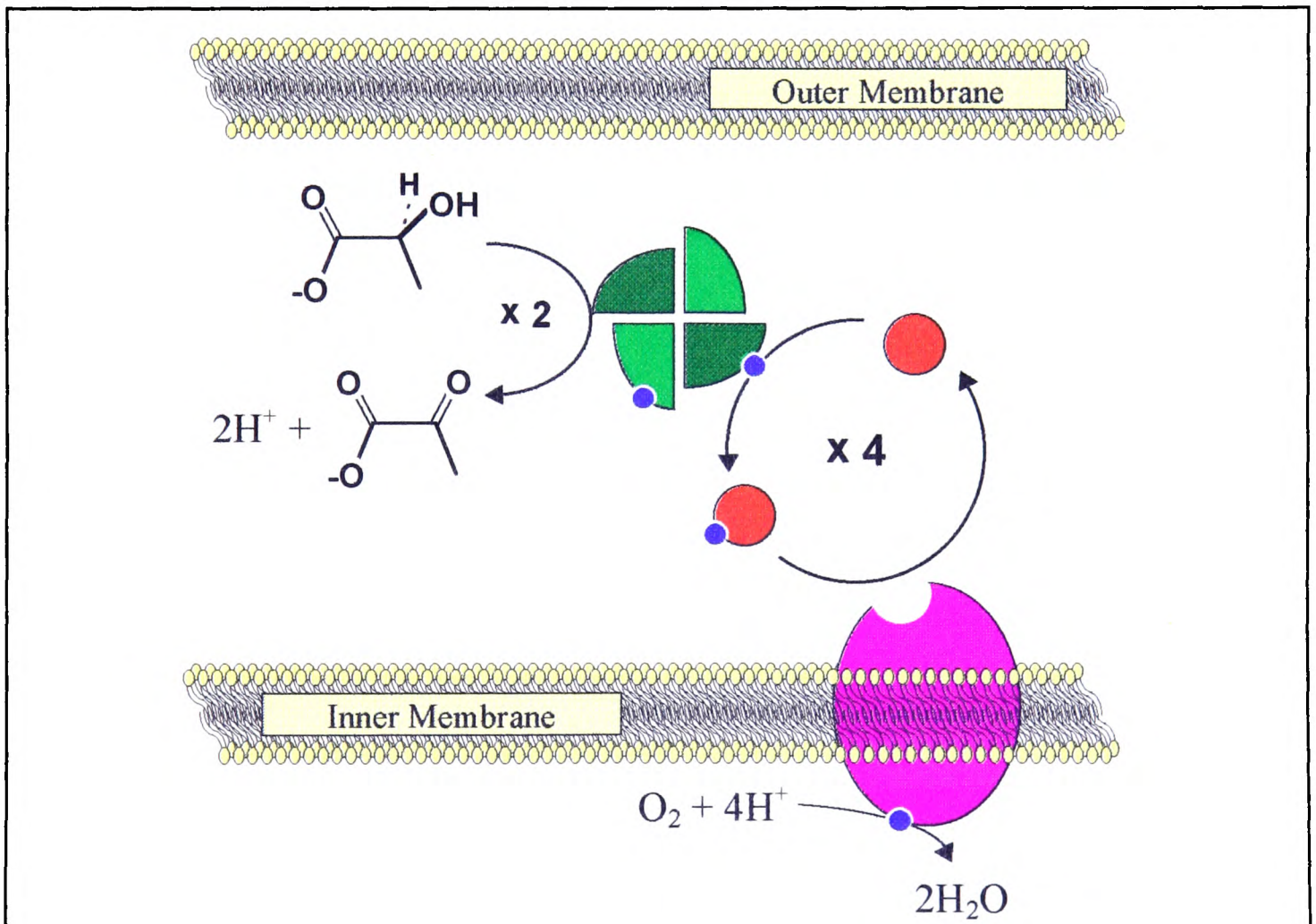

Figure 1.1 Schematic representation of the physiological role of flavocytochrome b_2 (green) within the mitochondrial intermembrane space of yeast. L-lactate dehydrogenation is coupled to cytochrome *c* (red) reduction by the enzyme. The transport of electrons (blue) to cytochrome *c* oxidase (magenta) and ultimately to dioxygen completes the short respiratory pathway.

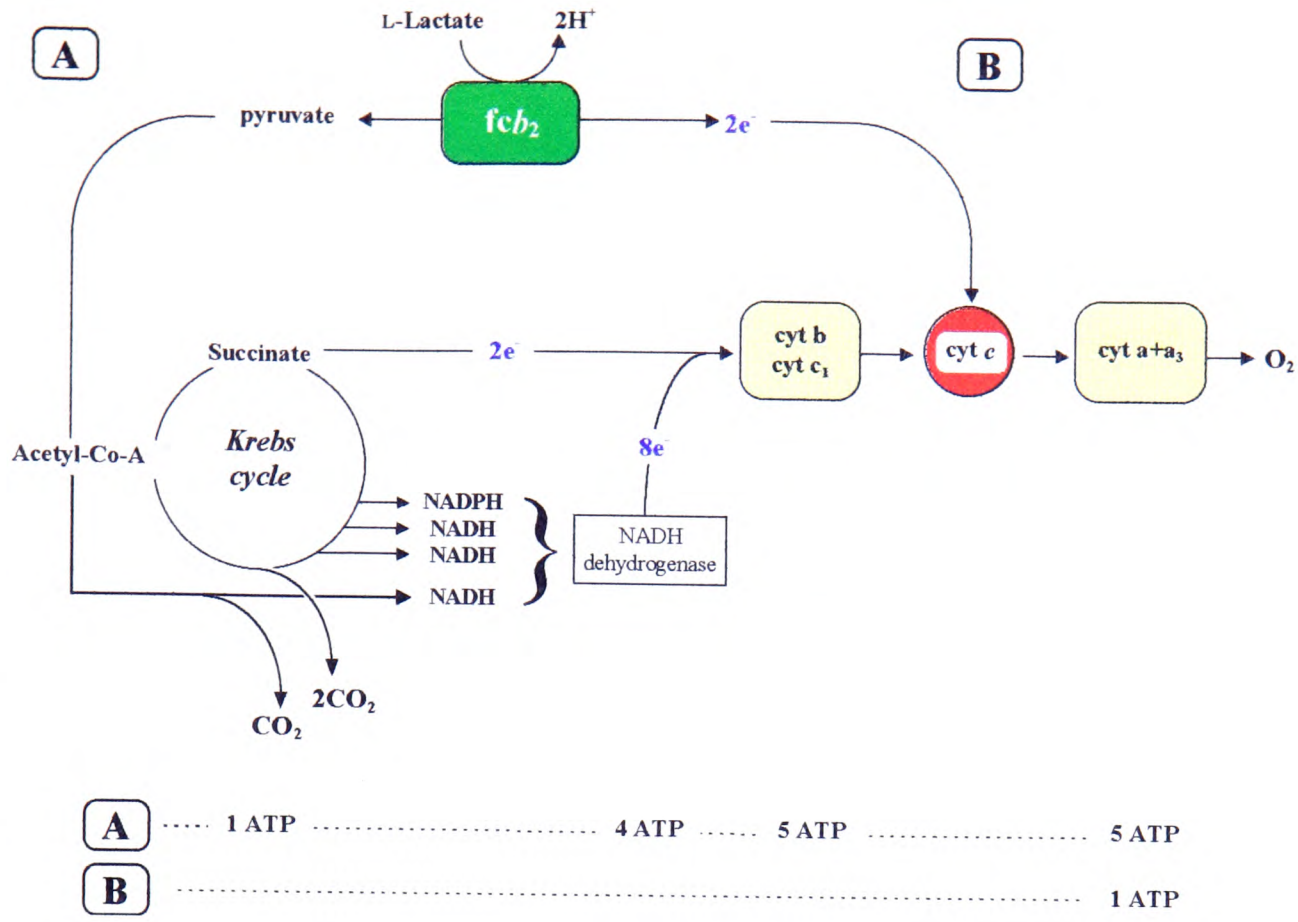

Figure 1.2 Aerobic respiration of L-lactate by yeast can yield 16 equivalents of ATP. 15 of these are derived from the normal respiratory pathway (A) as pyruvate passes through the Krebs cycle. However, during L-lactate dehydrogenation by flavocytochrome b_2 a shorter path (B) is utilised, involving direct electron transfer to cytochrome *c*.

Adapted from Pajot & Claisse (1974).

systematic degradation of pyruvate to carbon dioxide and water (Baldwin & Krebs, 1981). As well as providing pyruvate for the Krebs cycle, the role of flavocytochrome b_2 is to direct the energy generated by L-lactate dehydrogenation (in the form of electrons) ultimately to oxygen. In this shorter respiratory chain flavocytochrome b_2 acts as a cytochrome *c* reductase and by-passes the Krebs cycle. Via this pathway alone L-lactate dehydrogenation yields one equivalent of ATP (adenosine triphosphate) per L-lactate. In a key series of experiments Pajot & Claisse (1974) showed that when the Krebs cycle is blocked by the addition of antimycin the yeast are able to survive entirely by utilising this single process. Under these extreme circumstances keto-acids are exported from the cell. However, as *Figure 1.2* illustrates, the normal degradation of pyruvate in the Krebs cycle is able to yield 15 equivalents of ATP, making L-lactate a very attractive source of energy.

1.3. The Flavocytochrome b_2 Structure

The amino-acid sequence

The primary structure of flavocytochrome b_2 was determined by both amino-acid (Lederer *et al.*, 1985) and DNA sequencing (Guiard, 1985). While the former method identified all 511 amino-acids, the gene sequence also identified the 80 amino-acid N-terminal extension important for labelling the gene product for transportation to the mitochondrial intermembrane space. *Figure 1.3* aligns the amino-acid sequence with that of the equivalent enzyme from *Hansenula anomala* (Black *et al.*, 1989), along with several related flavin-containing dehydrogenases and oxidases not containing b_2-haem. The most obvious deduction to be made from this is that b_2-haem binds within a separate domain comprising the first 100 amino-acids. Further, it appears likely that, as Morton *et al.* (1961) suggested, the enzyme evolved from an act of gene-fusion. *Figure 1.3* also aligns the b_2-haem domain with the sequence of bovine cytochrome b_5 (Cristiano & Steggles, 1989), a membrane-bound electron-transfer protein which clearly possesses a similar evolutionary background. Such evidence has stimulated attempts to build genetic 'family-trees' (e.g. Lederer, 1991; 1994).

The crystal structure

The X-ray crystal structure of flavocytochrome b_2 was solved by Xia & Mathews (1990) to a resolution of 2.4 Å (*Figure 1.4*). It is clear from the crystal structure that the enzyme exists as a homotetramer with a four-fold axis of symmetry, however two distinguishable subunits were observed in the asymmetric unit. One of these contains a molecule of pyruvate (product) bound in close proximity to the FMN. In this subunit the entire b_2-haem-binding domain is unresolved. This anomaly together with the unusually sharp NMR lines observed for b_2-haem resonances (Labeyrie *et al.*, 1988) was used as evidence that the b_2-haem-binding domain possesses intrinsic mobility with respect to the FMN-binding domain. The two

```
                                                    43                                  66
                                                    ↓                                   ↓
Scb2        EPKLDMNKQK ISPAEVAKHN KPDDCWVVIN GYVYDLTRFL PNHPGGQDVI KFNAGKDVTA IFEPL.HAPN VIDKYIAPEK    79
Hab2         DVPHWKDIE LTPEIVSQHN KKDDLWVVLN GQVYDLTDFL PNHPGGQKII IRYAGKDATK IFVPI.HPPD TIEKFIPPEK    78
b5              SKAVKY YTLEEIQKHN NSKSTWLILH YKVYDLTKFL EEHPGGEEVL REQAGGDATE NFEDVGHSTD ARELSKTF..    72

                    ——— hinge ———                                                   143
                                                                                    ↓
Scb2        KLGPLQGSMP PELVCPPYAP GETKEDIARK EQLKSLLPPL DNIINLYDFE YLASQTLTKQ AWAYYSSGAN DEVTHRENHN   159
Hab2        HLGPLVGEFE QE......EE ELSDEEIDRL ERIER.KPPL SQMINLHDFE TIARQILPPP ALAYYCSAAD DEVTLRENHN   151
b5          IIGELHPDDR SKI(87)
MsLox                             SNWGDYENEI YGQGLVGVAP TLPMSYADWE AHAQQALPPG VLSYVAGGSG DEHTQRANVE    60
EcLdh                                        MII SAA...SDYR AAAQRILPPF LFHYMDGGAY SEYTLRRNVE    40
PpMdh                                         MS QNLFNVEDYR KLRQKRLPKM VYDYLEGGAE DEYGVKHNRD    42
SpGox                                            MEITNVNEYE AIAKQKLPKM VYDYYASGAE DQWTLAENRN    40
Haox                                               PLVCLADFK AHAQKQLSKT SWDFIEGEAD DGITYSENIA    39

                                                  198                                   230
                                                  ↓                                     ↓
Scb2        AYHRIFFKPK ILVDVRKVDI STDMLGSEVD VPFYVSATAL CKLGNPLEGE KDVARGCGQG VTKVPQMIST LASCSPEEII   239
Hab2        AYHRIFFNPK ILIDVKDVDI STEFFGEKTS APFYISATAL AKLGHP.EGE VAIAKGAGRE ..DVVQMIST LASCSFDEIA   228
MsLox       AFKHWGLMPR MLMAATERDL SVELWGKTWA APMFFAPIGV IALC.AQDGH GDAASAQASA RTGVPYITST LAVSSLEDIR   139
EcLdh       DLSEVALRQR ILKNMSDLSL ETTLFNEKLS MPVALAPVGL CGMYAR.RGE VQAAKAADAH ..GIPFTLST VSVCPIEEVA   117
PpMdh       VFQQWRFKPK RLVDVSRRSL QAEVLGKRQS MPLLIGPTGL NGALWP.KGD LALARAATKA ..GIPFVLST ASNMSIEDLA   119
SpGox       AFSRILFRPR ILIDVTNIDM TTTILGFKIS MPIMIAPTAM QKMAHP.EGE YATARAASAA ..GTIMTLSS WATSSVEEVA   117
Haox        AFKRIRLRPR YLRDMSKVDT RTTIQGQEIS APICISPTAF HSIAWP.DGE KSTARAAQEA ..NICYVISS YASYSLEDIV   116

                    254                                                                 loop ——
                    ↓                                                                   ——————
Scb2        EAAPSDKQIQ WYQLYVNSDR KITDDLVKNV EKLGVKALFV TVDAPSLGQR EKDMK...LK FSNTKAGP.. ..........   304
Hab2        DARIPGQQ.Q WYQLYVNADR SITEKAVRHA EERGMKGLFI TVDAPSLGRR EKDMK...MK FEADSDVQ.. ..........   292
MsLox       KHA..GDTPA YFQLYYPEDR DLAESFIRRA EEAGYDGLVI TLDTWIFGWR PRDLTISNFP FLRGLCLTNY VTDPVFQK..   215
EcLdh       PAIKR.P..M WFQLYVLRDR GFMRNALERA KAAGCSTLVF TVDMPTPGAR YRDAH.SGMS GPNA.AMRRY LQAVTHPQWA   192
PpMdh       RQC.DGD..L WFQLYVIH.R EIAQGMVLKA LHTGYTTLVL TTDVAVNGYR ERDLH.NRFK IPMSYSAKVV LDGCLHPRWS   194
SpGox       STGP.G..IR FFQLYVYKDR NVVAQLVRRA ERAGFKAIAL TVDTPRLGRR EADIK.NRFV LPPFLTLK.. ..........   181
Haox        AAAPEG..FR WFQLYMKSDW DFNKQMVQRA EALGFKALVI TIDTPVLGNR RRDKR.NQLN LEANILLK.. ..........   181

                                                  326
                                                  ↓
            ——————————————————
Scb2        .......... KAMKKTNVEE SQGASRALSK F....IDPSL TWKDIEELKK KTKLPIVIKG VQRTEDVIKA AEIGVSGVVL   370
Hab2        .......... G..DDEDIDR SQGASRALSS F....IDPSL SWKDIAFIKS ITKMPIVIKG VQRKEDVLLA AEHGLQGVVL   356
MsLox       ........KF KAHSGVEAEG LRDNPRLAAD FWHGLFGHSV TWEDIDWVRS ITKMPVILKG IQHPDDARRA VDSGVDGIYC   287
EcLdh       WDVGLNGRPH DLGNISAYLG KPTGLEDYIG WLGNNFDPSI SWKDLEWIRD FWDGPMVIKG ILDPEDARDA VRFGADGIVV   272
PpMdh       LDFVRHGMP. QLANFV..SS QTSSLEMQAA LMSRQMDASF NWEALRWLRD LWPHKLLVKG LLSAEDADRC IAEGADGVIL   271
SpGox       .......... NFEGIDLGKM DKANDSGLSS YVAGQIDRSL SWKDVAWLQT ITSLPILVKG VITAEDARLA VQHGAAGIIV   251
Haox        .......... DLRAL...KE EKPTQSVPVS FPKA....SF CWNDLSLLQS ITRLPIILKG ILTKEDAELA MKHNVQGIVV   244

                373 376
                ↓   ↓
Scb2        SNHGGRQLDF SRAPIEVLAE TMPILEQRNL KDKLEVFVDG GVRRGTDVLK ALCLGAKGVG LGRPFLYANS CYGRNGVEKA   450
Hab2        SNHGGRQLDY TRAPVEVLAE VMPILKERGL DQKIDIFVDG GVRRGTDVLK ALCLGAKGVG LGRPFLYAMS SYGDKGVTKA   436
MsLox       SNHGGRQANG GLPALDCLPE VVK......A SGDTPVLFDS GIRTGADVVK ALAMGASAVG IGRPYAWGAA LGGSKGIEHV   361
EcLdh       SNHGGRQLDG VLSSARALPA I.....ADAV KGDIAILADS GIRNGLDVVR MIALGADTVL LGRAFLYALA TAGQAGVANL   347
PpMdh       SNHGGRQLDC AISPMEVLA. .......QSVA KTGKPVLIDS GFRRGSDIVK ALALGAEAVL LGRATLYGLA ARGETGVDEV   344
SpGox       SNHGARQLDY VPATIMALEE VVK.....AA QGRIPVFLDG GVRRGTDVFK ALALGAAGVF IGRPVVFSLA AEGEAGVKKV   326
Haox        SNHGGRQLDE VSASIDALRE VVA.....AV KGKIEVYMDG GVRTGTDVLK ALALGARCIF LGRPILWGLA CKGEDGVKEV   319

                                                  ——————— Tail ———————
Scb2        IEILRDEIEM SMRLLGVTSI AELKPDLLDL STLKARTVGV PNDVLYNEVY EGPTLTEFED A          511
Hab2        IQLLKDEIEM NMRLLGVNKI EELTPELLDT RSIHNRAVPV AKDYLYEQNY QRMSGAEFRP GIED      500
MsLox       ARSLLAEADL IMAVDGYRNL KELTIDALRP TR                                         393
EcLdh       LNLIEKEMKV AMTLTGAKSI SEITQDSL.. VQGLGKELPA ALAPMAKGNA A                    396
PpMdh       LTLLKADIDR TLAQIGCPDI TSLSPDY... LQNEGVTNTA PVDHLIGKGT HA                   393
SpGox       LQMMRDEFEL TMALSGCRSL KEISRSHIAA DWDGPSSRAV ARL                             369
```

Figure 1.3 An amino-acid sequence comparison between *S. cerevisiae* flavocytochrome b_2 (Scb_2; Guiard, 1985), *H. anomala* flavocytochrome b_2 (Hab_2; Black *et al.*, 1989), bovine cytochrome b_5 (b_5; Cristiano & Steggles, 1989), lactate mono-oxygenase from *Mycobacterium smegmatis* (MsLox; Giegel *et al.*, 1990), *E. coli* lactate dehydrogenase (EcLdh; Dong *et al.*, 1993), mandelate dehydrogenase from *Pseudomonas putida* (PpMdh; Tsou *et al.*, 1990), spinach glycolate oxidase (SpGox; Volokita & Somerville, 1988) & rat kidney hydroxy-acid oxidase (Haox; Lê & Lederer, 1991).

Amino-acids which are catalytically important are marked with arrows. His 43 & His 67 are the haem axial ligands, whereas residues 143, 254, 373 & 376 are implicated in substrate binding and activation. The regions marked with a line are the inter-domain hinge, the proteolytically sensitive loop and the C-terminal tail. None of these are well conserved.

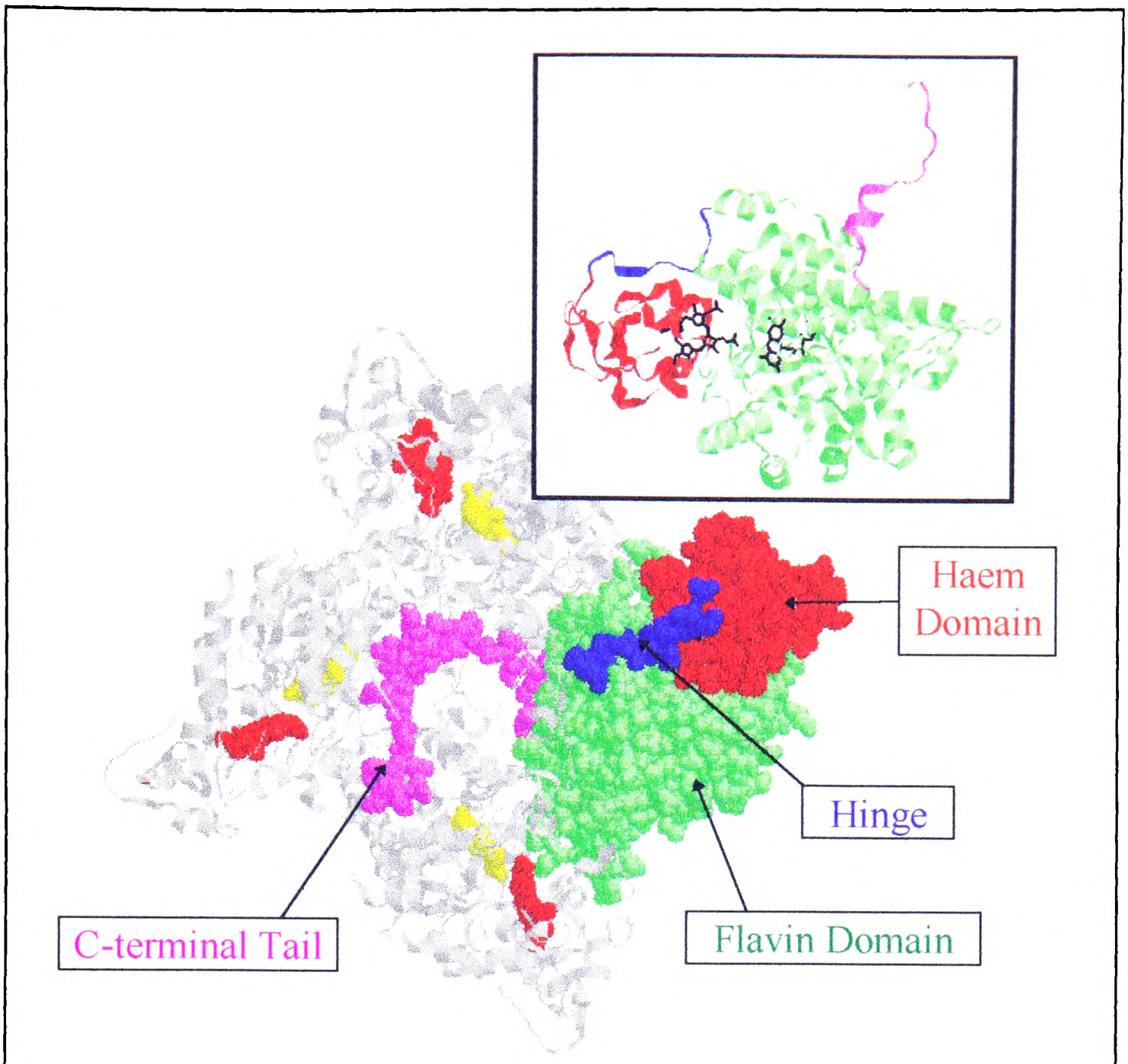

Figure 1.4 The structure of the flavocytochrome b_2 tetramer based on the X-ray crystal structure (Xia & Mathews, 1990). A single subunit is shown in spacefill representation with b_2-haem- and flavin-binding domains in red and green respectively. The prosthetic groups themselves are shown in red and yellow respectively. **Inset:** a single subunit of flavocytochrome b_2 with the protein backbone shown in ribbon format and the two prosthetic groups in black.

domains are linked by a single strand of polypeptide eleven residues in length, as such this region is referred to as the *inter-domain hinge*. In addition to the disorder observed in alternate b_2-haem-binding domains, a length of polypeptide within the FMN-binding domain was unresolved in the crystal structure. Its position (293 to 314) is consistent with the location of the site for proteolytic cleavage inherent in early flavocytochrome b_2 purifications (Lederer & Simon, 1970). Therefore this

length of protein is often referred to as the *disordered* or *proteolytically-sensitive loop*. The tetrameric nature of the enzyme is attributed to the large number of inter-subunit contacts made by the FMN-binding domains. Of particular note is the position of the C-terminal tail which winds around the four-fold axis of symmetry making contact with all three other subunits in the process.

The expression of flavocytochrome b_2 (Black *et al.*, 1989) in the bacterial host *Escherichia coli* represented a significant advancement in the study of the structure/function relationship. In addition to increasing the yield of enzyme per weight of cells, it has allowed site-directed mutagenesis to be employed in the analysis of the roles of individual amino-acids. Several gross structural changes have also been made. These include the expression of the separate FMN-binding (Pallister *et al.*, 1990) and b_2-haem-binding (Brunt *et al.*, 1992) domains, the deletion of the C-terminal tail (White *et al.*, 1989) and insertions/deletions within the hinge region (White *et al.*, 1993; Sharp *et al.*, 1994).

Despite the fact that the first five amino-acids from the N-terminus are missing, the recombinant enzyme was found to possess no significant functional (Black *et al.*, 1989) or structural difference (Tegoni & Cambillau, 1994) to the native form.

1.4. The Flavin Domain

The FMN-binding domain consists of residues 101 to 511 (*Figure 1.3;* p6) which fold into a classic $\alpha_8\beta_8$ TIM-barrel structure (Banner *et al.*, 1975), i.e. 8 β sheets surrounded by 8 α helices (*Figure 1.4 Inset;* p7). Several other flavoenzymes share this structural motif and consequently possess a degree of sequence homology, this is particularly apparent for enzymes which are functionally similar. *Figure 1.3* aligns the flavocytochrome b_2 sequence with those from *M. smegmatis* lactate monooxygenase, *E. coli* lactate dehydrogenase, *P. putida* mandelate dehydrogenase, spinach glycolate oxidase and rat kidney hydroxy-acid oxidase. All these enzymes

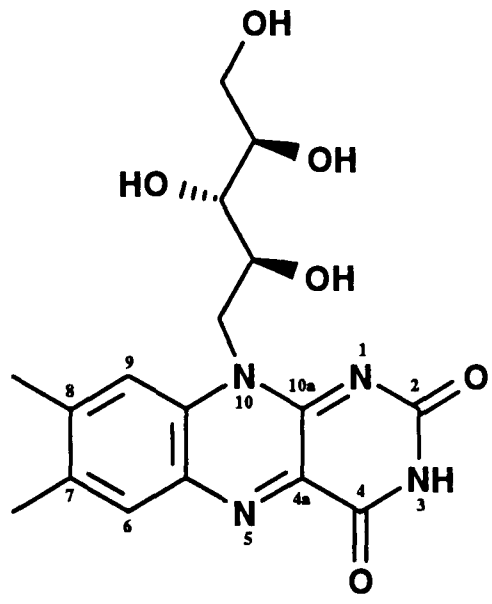

Riboflavin

Figure 1.5 The structure of riboflavin (vitamin B_2) including the numbering system used to define the atoms in the isoaloxazine ring system.

catalyse S-2-hydroxy-acid dehydrogenation, although some preferentially utilise substrates other than L-lactate. As *Figure 1.3* shows, the active site residues are well conserved within this enzyme family and the active site architecture is always constructed around flavin mononucleotide.

FMN binding

FMN is a common enzyme cofactor based on riboflavin (vitamin B_2). It consists of an isoaloxazine ring system attached at N3 to phosphorylated D-ribose (*Figure 1.5*). The reason for the presence of FMN in flavocytochrome b_2 and related enzymes is linked to the redox potentials tabulated in *Figure 1.6*. The midpoint potentials of the lactate/pyruvate and free flavin ($FMN/FMNH_2$) couples are close together, whereas that for enzyme bound flavin is more than 100 mV more positive. The enzyme is therefore able to catalyse lactate dehydrogenation by facilitating flavin reduction. The nature of the interactions between protein and bound FMN were derived from close examination of the X-ray crystal structure (Xia & Mathews, 1990) and mainly consist of a network of hydrogen bonds. Of these, a few have been attributed particular significance (Lederer, 1991). Lys349 positions a positive charge in the immediate vicinity of the flavin N1 (see *Figure 1.5*) and is believed to aid flavin reduction by stabilising a negative charge at this position. Significantly,

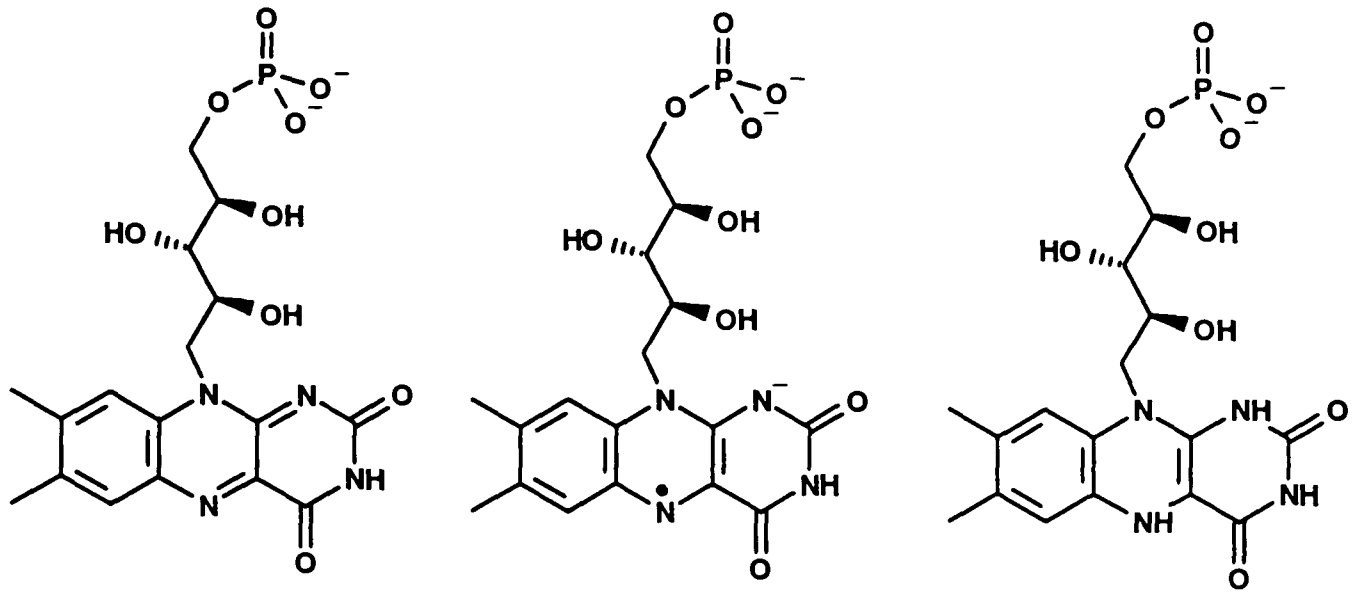

oxidised (ox) **semiquinone (sq)** **hydroquinone (red)**

Figure 1.6 The three different oxidation states of flavin mononucleotide, which refer to the redox potentials below (mV; pH 7, 25°C; *vs* Pt/H_2):

	$E_{ox/red}$	$E_{ox/sq}$	$E_{sq/red}$
$FMN/FMNH_2$ (free)[a]	-205	-238	-172
S.c. flavocytochrome b_2 (FMN; 24°C)[b]	-64	-94	-34
H.anomala flavocytochrome b_2 (FMN; 30°C)[c]	-34 ± 10	-23 ± 10	-45 ± 12
H.a. flavocytochrome b_2 (FMN; 18°C; + 10mM pyruvate)[d]	-31 ± 5	+74 ± 4	-133 ± 7
b_2-haem (pH 7.5)[e]	-20		
lactate/pyruvate[f]	-185		
cytochrome c[f]	+254		
$NAD^+/NADH$[f]	-320		
O_2/H_2O[f]	+816		

[a] Stankovich (1991); [b] Walker & Tollin (1991); [c] Cappelleire-Blandin *et al.,* (1986); [d] Tegoni *et al.,* (1986); [e] White *et al.,* (1993); [f] Loach (1971).

flavocytochrome b_2 and its related flavoenzymes all favour the generation of a red, anionic semiquinone (Capeillère-Blandin *et al.,* 1975) to the blue, neutral semiquinone found in high-potential flavodoxins (Mayhew & Ludwig, 1975). Furthermore, they all form strong, reversible covalent complexes with sulphite at position N5 leading to bleaching of the cofactor (Massey *et al.,* 1969; Tegoni & Mathews, 1988). Lys349 is conserved in all the flavooxidases (see *Figure 1.3;* p6) and the corresponding residue has been mutated to Met in L-lactate monooxygenase (Müh *et al.,* 1994a). The midpoint potential for FMN in this mutant was found to be more than 100 mV more

negative than for the wild-type enzyme and the affinity of the flavin for sulphite was found to be substantially lower.

FMN and metabolism

Unlike many organic reagents, flavins are able to take part in single electron transfer reactions by virtue of their stable semiquinone oxidation state. This is particularly useful in processes which ultimately require electrons to be passed to molecular oxygen, e.g. respiration. The reason behind this does not involve thermodynamics, since the midpoint potential for the O_2/H_2O couple indicates that oxygen should spontaneously react with lactate. Rather, the barrier is a kinetic one which arises from the molecular electronic orbital structure of O_2. Its degenerate π^* orbitals are both singlely occupied and so it is unable to accommodate an electron pair without first undergoing a spin-forbidden triplet to singlet electronic transition. This does not apply to single electron transfers so the flavoenzymes are able to couple 2-hydroxy-acid dehydrogenation to O_2 reduction.

Many of the flavoenzymes react directly with dioxygen (oxidases) whereas flavocytochrome b_2 does so via the cytochrome *c*/cytochrome *c* oxidase system (*Figures 1.1 & 1.2;* p3 & 4). In order to couple lactate dehydrogenation to the generation of ATP its ability to perform as an oxidase appears to have been evolutionarily suppressed, while the gene-fusion with a *b*-type cytochrome has provided the flavin with a conveniently located redox partner. The role of the b_2-haem domain as an intrinsic electron-transfer mediator is discussed is *Section 1.8*.

L-lactate dehydrogenation is also accomplished by an abundant family of enzymes which utilise NADH as a cofactor in place of FMN. It is clear from the redox potential of the NAD^+/NADH couple that this strong reductant will drive the L-lactate/pyruvate equilibrium in the opposite direction to FMN. These enzymes perform a different role to the flavoenzymes and are not directly involved in the reduction of oxygen; NAD is unable to stabilise an unpaired electron and so maintains the kinetic barrier. However, vertebrate L-lactate dehydrogenases are nevertheless involved in metabolism by aiding the relocation of pyruvate (a key component of the Kreb's Cycle, see *Figure 1.2*) in the body via the bloodstream by converting it to L-lactate. Following transport, the lactate is converted back to pyruvate before being

metabolised. This inter-conversion of L-lactate and pyruvate, coupled with relocation, forms the basis of the Cori Cycle. Interestingly, NADH is metabolised via NADH dehydrogenase which also uses FMN as a cofactor and ultimately allows the high potential electron-pair to be separated (see *Figure 1.2*).

1.5. The Active Site Structure

Although there remains some dispute as to the exact mechanism of L-lactate dehydrogenation in flavocytochrome b_2, the high resolution crystal structure of the enzyme has helped to clarify many points. *Figure 1.7* focuses in on the active site and allows the catalytically important residues to be identified. Included in *Figure 1.7* is an inset picture derived from the crystal structure of spinach glycolate oxidase (Lindquist *et al.,* 1991). The striking similarity of the two active sites reinforces the theory derived from sequence comparisons (see *Figure 1.3;* p6) that these enzymes share their ancestral roots. Further, it implies that the enzymes retain mechanistic similarities despite diverging in terms of substrate specificity. It is therefore considered pertinent to discuss evidence derived from the whole family of enzymes when referring to the mechanism of dehydrogenation.

Residues involved in substrate binding

Figure 1.7 shows a molecule of pyruvate bound in the flavocytochrome b_2 active site in close proximity to the FMN. The carboxylate end of pyruvate forms a salt-bridge with Arg376 which contributes strongly to the binding interaction. Evidence to this effect comes from the study of the point mutant *R376K* (Arg→Lys) which was found to have a K_m 100-fold higher than the wild-type enzyme (Miles, 1992). This is despite the fact that the charge balance has been maintained. As illustrated in *Figure 1.3,* Arg376 is conserved throughout this family of FMN-binding dehydrogenases, however, the corresponding mutation in L-lactate monooxygenase led to a severe drop in k_{cat} but a relatively small change in K_m (Müh *et al.,* 1994b). Although the nature of the change is inconsistent, the importance of this particular residue to catalytic function is assured.

Tyr143 is also shown in *Figure 1.7* to be hydrogen bonding to the carboxylate end of the substrate. Its role has also been examined by site-directed mutagenesis, which allowed the creation of the *Y143F* mutant (Tyr→Phe). This mutant had a larger K_m value than the wild-type enzyme indicating a decrease in substrate binding affinity and a larger rate for pre-steady-state FMN reduction (Miles *et al.*, 1992). Both of these observations were attributed to destabilisation of the Michaelis complex. This mutation also had a dramatic effect on the rate of electron transfer from FMN to b_2-haem, providing evidence of an additional role for Tyr143 in hydrogen-bonding to one of the b_2-haem propionates (see *Section 1.10*). Tyr143 is conserved in all but one of the related enzymes sequence-aligned in *Figure 1.3* (p6) and has also been mutated in L-lactate monooxygenase (Müh *et al.*, 1994b). Again this mutation causes a large

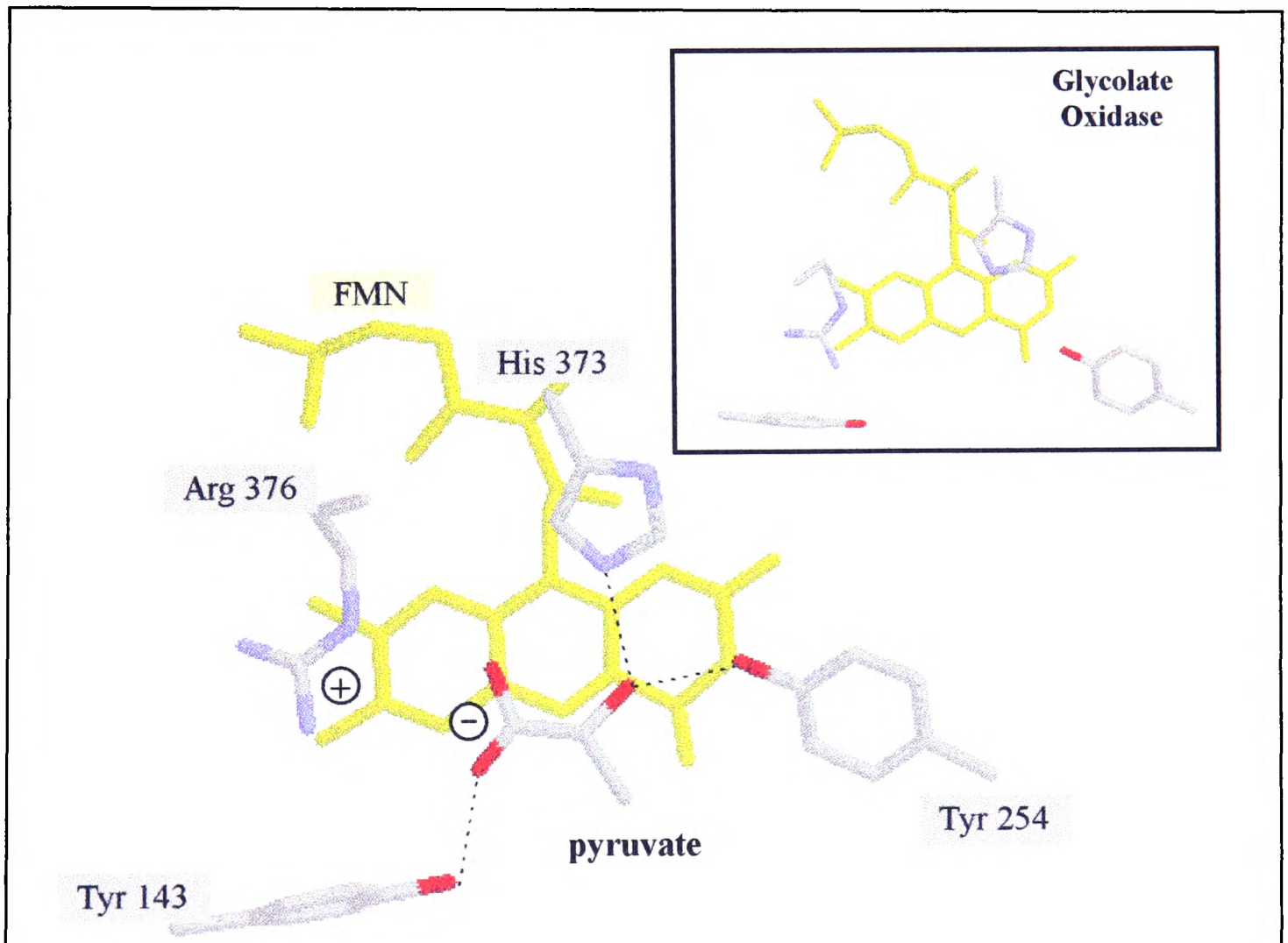

Figure 1.7 The structure of the flavocytochrome b_2 active site (Xia & Mathews, 1990). FMN is shown in yellow and four active site residues surround a molecule of pyruvate (the product of L-lactate dehydrogenation). **Inset:** a similar view of the spinach glycolate oxidase active site (Lindquist *et al.*, 1991).

decrease in the rate of enzyme turnover but not substrate binding affinity. The effects of both the tyrosine and arginine mutations on L-lactate monooxygenase are explained in terms of an adjustment in binding orientation.

Residues involved in catalysis

Tyr254 is shown in *Figure 1.7* to be hydrogen-bonding to the carbonyl group of the pyruvate molecule, but its role in catalysis is less clear than for the two amino-acids discussed in the previous paragraphs. Its mutation to phenylalinine resulted in a decrease in k_{cat} but left the K_m unaltered (Miles, 1992). Similar effects have been reported for the corresponding mutations to L-lactate monooxygenase (Müh *et al.*, 1994b) and spinach glycolate oxidase (Macheroux *et al.*, 1993). The obvious conclusion from this is that Tyr254 does not contribute to the stabilisation of the Michaelis complex, but this is not universally accepted.

His373 is generally accepted to be the key catalytic residue of flavocytochrome b_2 with regard to lactate dehydrogenation. Its mutation to glutamine (*H373Q*) resulted in an enzyme with very little reported activity (Miles, 1992). However, this has recently been reconsidered in light of the potential of the Gln codon substituted in this case for being misinterpreted during DNA translation for that of the wild-type amino-acid. The activity reported for the H373Q mutant (0.1%) is consistent with the error expected during translation, therefore the actual activity of this mutant is now considered to be minimal. This is supported by results taken from the corresponding mutant in L-lactate monooxygenase (Müh *et al.*, 1994c). The role of this residue is central to the catalytic mechanism and crucially, whether it is reponsible for abstraction a proton from thehydroxylor the α-carbon of L-lactate. The former leads to the 'hydride' mechanism and the latter leads to the 'carbanion' mechanism.

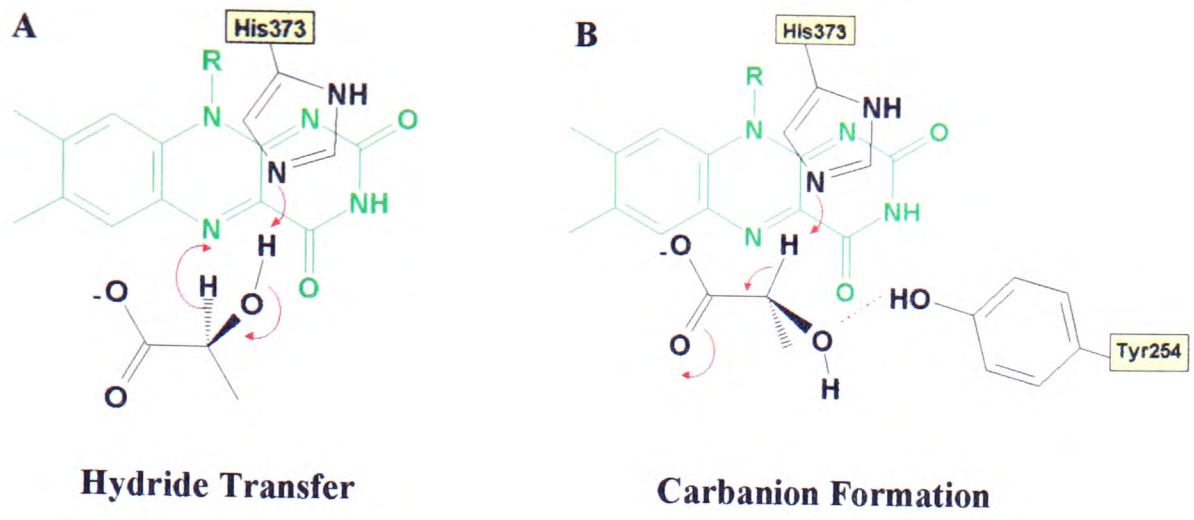

Figure 1.8 The mechanism of L-lactate dehydrogenation by flavocytochrome b_2 is one of two possibilities. A) Hydride transfer to flavin N5. B) Generation of a carbanion intermediate which is followed by addition of this to flavin N5. In both cases the postulated transition state is shown.

1.6 The Mechanism of L-Lactate Dehydrogenation

The rate-limiting step in the L-lactate dehydrogenation/FMN reduction process has been shown to be abstraction of the hydrogen from the α-carbon of L-lactate. This conclusion was derived from the primary kinetic isotope effect observed (8.1 ± 1.4) for pre-steady-state reduction of FMN, when α-deuterated L-lactate was used as reductant (Miles *et al.,* 1992). Both mechanisms illustrated in *Figure 1.8* are compatible with this. The first of these involves the transfer of the α-H as a hydride ion from lactate to FMN in a concerted process instigated by deprotonation of the hydroxy group by His 373. The second involves the formation of a stabilised carbanion intermediate as an active-site base (His 373) removes the α-H as a proton. The carbanion is then postulated to form a covalent bond with the N5 of FMN before direct breakdown to pyruvate and reduced FMN.

A large amount of effort has been expended in the hope of providing a solution to this debate which is heavily cited to be in favour of the carbanion mechanism (Lederer, 1991; Ghisla & Massey, 1991; Ghisla, 1982). The simplicity of

the hydride mechanism makes its unambiguous proof difficult and so much of the evidence revolves around the existence of a stabilised carbanion intermediate.

Nucleophilic addition

Both mechanisms illustrated in *Figure 1.8* involve nucleophilic addition to N5 of FMN. However, such reactions are not expected from studies on free FMN (Hemmerich *et al.,* 1977). It has been postulated therefore that carbanion formation may be followed by single electron transfers from substrate to FMN. Because such a process involves formation of a substrate free-radical, this theory seems unlikely and covalent bond formation is generally favoured. Unlike free FMN, the enzyme bound form does react with certain nucleophiles and is particularly sensitive to sulphite. The reversible co-ordination of sulphite has been shown by X-ray crystallography to occur at position N5 of the FMN isoalloxazine ring system (Tegoni & Mathews, 1988; Tegoni & Cambillau, 1994).

Covalent bond formation has also been achieved by reaction with nitroethane (in the case of D-amino-acid oxidase only; Porter *et al.,* 1973) and 2-hydroxy-3-butynoate. The latter is particularly interesting because it also acts as a competent substrate of flavocytochrome b_2 (Pompon & Lederer, 1979), while concurrently inactivating the enzyme via an alternative process. The degradation products purified from inactivated enzyme indicate that the substrate forms covalent bonds with both N5 and C4a of the FMN. The degree of partition between inactivation and normal turnover was found to be strongly in favour of turnover for flavocytochrome b_2, but could be enhanced by the presence of the product 2-keto-3-butynoate which stimulates reverse-turnover or transhydrogenation. L-lactate monooxygenase on the other hand was rapidly inactivated by this substrate in either direction (Ghisla *et al.,* 1976). The mechanism proposed for the inactivation reaction involves the nucleophilic attack of an allenic anion at C4a of FMN. However the evidence far from proves the existence of a carbanion during normal L-lactate turnover for several reasons. Firstly, the substrate is more susceptible to carbanion formation owing to the greater acidity of its α-H. Secondly, it possesses an alternative acidic proton which may be removed preferentially and thirdly, there is no proof that inactivation doesn't occur after substrate has reacted with FMN i.e. by product reacting with reduced FMN. The

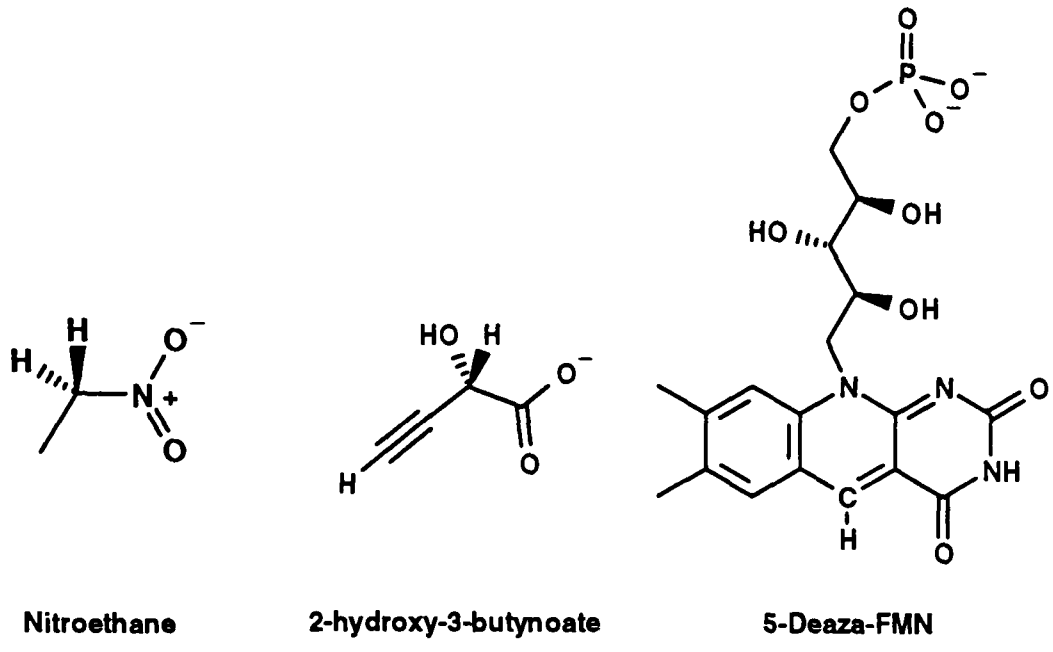

Figure 1.9

latter proposal may indicate why L-lactate monooxygenase is more susceptible to inactivation than flavocytochrome b_2, since this enzyme has a greater affinity for its product, the dissociation of which is slow (Ghisla & Massey, 1991).

L-Lactate monooxygenase also, uniquely, forms stable adducts on reaction with glycolate (Ghisla & Massey, 1980). the major product is shown to be catalytically competent, while the minor, which results from the removal of stereoscopically the 'wrong' α-H, is not. The authors consider that a strong active site base is capable of removing either α-H to generate stereoactive carbanions and that these form direct covalent bonds to FMN. Great emphasis is placed on the catalytically inactive species, which cannot be directly formed from the addition of glyoxalate (the product) to reduced enzyme. This species was also generated by photodecomposition of tartronate in the active site of the enzyme which proceeds via an identical carbanion to that created by proton abstraction from glycolate and is accompanied by evolution of carbon dioxide. While this evidence indicates that carbanions can be formed on complexation with L-lactate monooxygenase, it does not prove that a carbanion lies on the normal catalytic pathway. The action of glycolate on both flavocytochrome b_2 and glycolate oxidase is that of a normal substrate and therefore this behaviour could be construed as being non-representative. L-lactate monooxygenase certainly exhibits

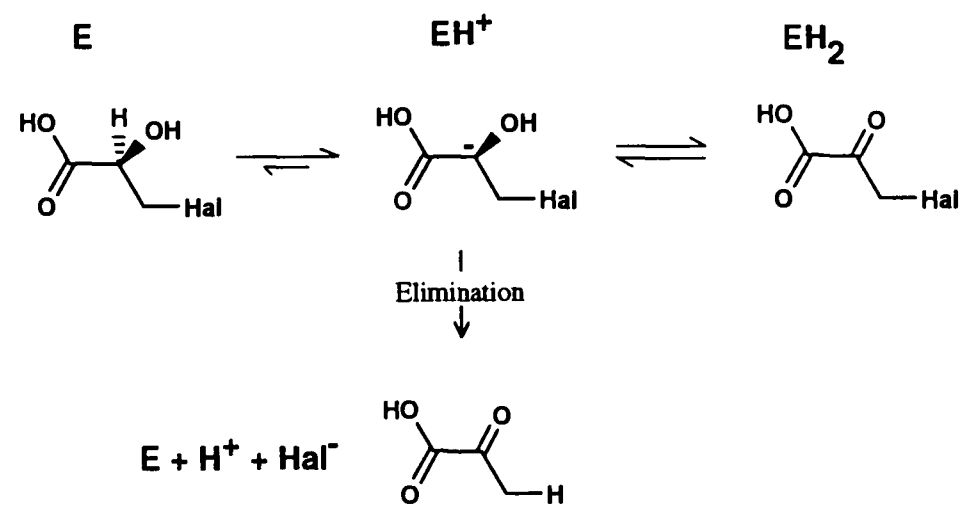

Figure 1.10 The model used to explain the reverse isotope effect found on halide elimination following reduction of the enzyme (E) with deuterated substrate (Urban & Lederer, 1985).

functional anomalies e.g. it is capable of catalysing decarboxylation of substrates following dehydrogenation.

Halide elimination

L-Lactate monooxygenase and D-amino-acid oxidase were first shown to catalyse halide elimination from β-chloro- and β-bromo- substrates (Bright & Porter, 1975; Massey *et al.*, 1976). This property was shown to be emulated by flavocytochrome b_2 under transhydrogenation conditions (Urban & Lederer, 1984), (i.e. reduced enzyme incubated with the β-halo-keto-acid). In this respect the situation is similar to the inactivation reaction with 2-hydroxy-3-butynoate (see above). Both are explained by "faster processing of the carbanion intermediate" in flavocytochrome b_2 (Lederer, 1991), although it is unclear why this might be the case. Alternatively both the halide elimination and butynoate inactivation reactions could originate from complexes between reduced FMN and the appropriate keto-acid. This possibility was dismissed by Lederer (1991) following a series of more elaborate transhydrogenation/halide elimination experiments. Transhydrogenation between α-^{3}H-L-lactate and β-bromo-pyruvate led to the formation of α-^{3}H-bromo-lactate, while concurrent bromide elimination led to partial formation of ^{3}H-pyruvate (Urban & Lederer, 1985). This indicated that during elimination, some ^{3}H migrates from the α position of lactate to the β position of pyruvate. This was interpreted as being due to

the enol-keto tautomerisation of pyruvate following halide elimination in the active site. Direct substitution of bromide by $^3H^-$ was ruled out by the incomplete nature of migration following quantitation of radioactivity in the different products.

Evidence for a common intermediate in the transhydrogenation and halide elimination reactions was construed from a study of the 2-^{2}H-kinetic isotope effects (Urban & Lederer, 1985). Hydrogenation of β-bromo-pyruvate by flavocytochrome b_2 was found to proceed 4.4 times more slowly when 2-^{2}H-lactate was used as reductant than when 2-^{1}H-lactate was used, giving a primary kinetic isotope effect of 4.4 ± 0.4 (lower estimate; no correction was made for the rate of proton exchange with buffer or for the contribution of elimination). However, the rate of bromide elimination was found to increase by a factor of 2, which constitutes an inverse effect. This phenomenon was proposed to occur indirectly as a result of the large isotope effect on transhydrogenation, which would affect the rate at which the carbanion intermediate is protonated (see *Figure 1.10*). No other intermediate has been suggested to be a realistic alternative to the carbanion in this case. The viability of the model proposed in *Figure 1.10* is dependent on a shift in the rate-determining step from carbanion formation (in the reverse direction) to carbanion protonation by $^2H^+$, only under these circumstances would the concentration of carbanion be expected to change. This aspect of the model has thus far not been discussed and it is alarming to consider that in the forward direction the isotope effect is 4.7 (Urban *et al.,* 1983), although this value refers only to steady-state turnover. However, the implication that protonation of the carbanion is rate-determining seems to be the most remarkable aspect of the model.

5-Deaza-FMN

Substitution of FMN by 5-Deaza-FMN (see *Figure 1.9*) has been carried out with both L-lactate monooxygenase (Averill *et al.*, 1975) and flavocytochrome b_2 (Pompon & Lederer, 1979) as well as with a wide variety of other flavoenzymes (Hemmerich *et al.,* 1977). 5-deaza-FMN simply has the flavin N5 replaced by CH and so has broadly similar properties to FMN, indeed it is bound strongly by both enzymes in the same way as FMN. The redox potential for free 5-deaza-FMN is approximately -300 mV for the 2-electron couple which is 100 mV more negative than free FMN

(Stankovich, 1990). However, the semiquinone oxidation state of 5-deaza-FMN is far less stable than for FMN resulting in this cofactor being a poor one electron transferase (Blankenhorn, 1977). 5-deaza-FMN is often compared to NAD in its hydride-transfer ability (Hemmerich *et al.*, 1977). The studies on both flavocytochrome b_2 and L-lactate monooxygenase showed that reduction of enzyme bound 5-deaza-FMN by substrate occurs very slowly and cannot be coupled to ferricyanide reduction. However reoxidation of the cofactor by excess product (pyruvate) was found to occur rapidly. Pompon & Lederer (1979) report an electrode potential for flavocytochrome b_2-bound 5-deaza-FMN of -230 mV, which is almost 200 mV more negative than that of enzyme-bound FMN (see *Figure 1.6;* p10), this is consistent with the relative reactivities reported for reduction and oxidation by substrate and product. Transhydrogenation between L-lactate and pyruvate was shown by 2-^{3}H- labelling to occur without significant exchange with the solvent, suggesting that the location of this label when enzyme bound possesses different chemical properties to that for the FMN-based enzyme. Further, no inactivation was observed when the enzyme was incubated with 2-hydroxy-3-butynoate. This is a surprising result for a cofactor which is known to be more susceptible to nucleophilic attack by carbanions than FMN in free solution (Hemmerich *et al.*, 1977).

Thus far, the results collected for the 5-deaza-FMN-substituted enzymes all indicate that L-lactate dehydrogenation proceeds by hydride transfer from lactate to C5 of the cofactor. This is referred to by Ghisla (1982) as "The Deazaflavin Dilemma", but is qualified by suggestions that FMN is different enough to render a direct comparison dubious. Hemmerich *et al.*, (1977) tabulate the properties of FMN, 5-deaza-FMN and NAD, to demonstrate that 5-deaza-FMN resembles NAD more closely than FMN. In summary, FMN is resistant to attack by nucleophiles, including sulphite and hydride, but is able to undergo one electron reduction, in contrast to the two other cofactors. However, enzyme-bound FMN has clearly evolved its ability to react with nucleophiles, as illustrated by the tight complex formed with sulphite. Further, NADH and NADPH reductases have evolved to catalyse direct hydride transfer to flavin. The remaining difference is the one electron-transferase ability

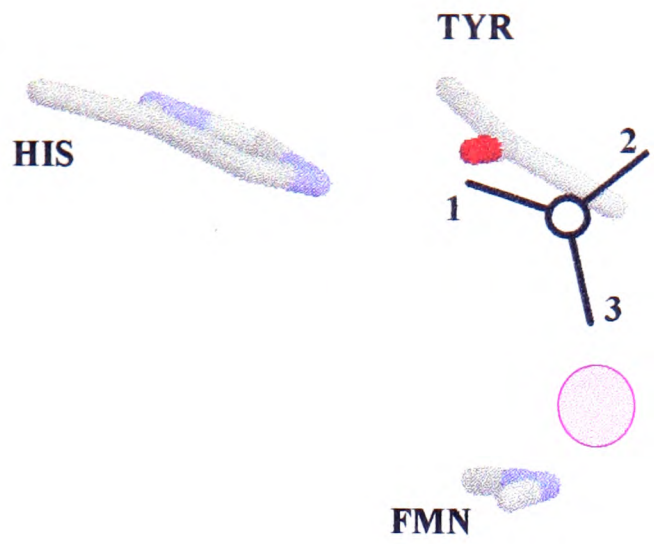

Figure 1.11 The active site of flavocytochrome b_2 viewed down the C1-C2 bond of L-lactate. FMN N5, His373 and Tyr254, the mechanistically implicated groups, are shown in the same positions as in *Figure 1.8*. The position of L-lactate is implied from the position of pyruvate in the crystal structure, but should be considered to be flexible. For the 'hydride mechanism': 1 ≡ -OH; 2 ≡ $-CH_3$; 3 ≡ -H. For the carbanion mechanism 1 ≡ -H; 2 ≡ -OH; 3 ≡ $-CH_3$. The pink shaded region represents the approximate position of the accepting FMN π^* orbital, which would be involved in either mechanism.

retained by FMN, which is clearly the underlying reason for the evolution of FMN-based L-lactate dehydrogenases/oxidases in addition to NADH-dependent ones.

Structural analysis

The majority of the evidence discussed so far was collected prior to the availability of a high resolution X-ray crystal structure (Xia & Mathews, 1990). Therefore, in recent reviews the viability of the 'hydride' and 'carbanion' mechanisms have been discussed in more specific terms (Lederer, 1991; Ghisla & Massey, 1991). *Figure 1.7* (p13) illustrates the orientation of pyruvate in the active site of flavocytochrome b_2 with respect to the catalytically active amino acids. The structure is essentially unchanged when pyruvate is not present or when sulphite is bound (Tegoni & Cambillau, 1994), even the active site of glycolate oxidase bears an uncanny similarity (*Figure 1.7:* inset). It therefore seems unlikely that gross structural changes could occur during the dehydrogenation process, so the lock and key analogy appears to be justified in this case. *Figure 1.11* illustrates the active site down the C1-

C2 axis of the substrate. Relative to *Figure 1.7*, the view is directly away from Arg 376 which would form a salt bridge with the carboxylate of pyruvate orienting the plane of this horizontally in the centre of the picture. The exact position of L-lactate should remain at the readers discretion, but is assumed to be held by the Arg-carboxylate salt-bridge with free rotation around C2 (as illustrated). The rotational position of the 3 substituents of C2 (-H, -OH, $-CH_3$) would be decided by the interactions with surrounding amino-acids and would define the Michaelis complex.

The carbanion mechanism relies on the direct interaction of His373 with the -H substituent, however this results in the other two substituents being placed in less favourable environments. The methyl group would be close to the flavin N5 and the side-chain of Ala198. The hydroxyl group would be in a hydrophobic environment, making contact with the side chains of Leu230 and Leu286. It has been argued that a hydrogen-bond could be made with the hydroxyl of Tyr254 following a minor structural change (Lederer, 1991), but results from mutational studies indicate that this is doubtful (Miles, 1992; Macheroux *et al.*, 1993). The alternative orientation, for the hydride mechanism, allows the hydroxyl group to hydrogen-bond to His373, the methyl group to interact with the side-chain of Leu230 and Leu286 (see *Section 1.6* and *Chapter 5*) and the α-hydrogen to be positioned optimally for direct entry into the FMN-N5 π* orbital. The putative role of Tyr254 would be to hydrogen-bond to His373 prior to substrate binding and to hydrogen-bond to the hydroxyl/carbonyl in the transition state.

The analogous dehydrogenation by NADH dependent L-lactate dehydrogenase follows a similar pathway to that described for the flavocytochrome b_2 hydride mechanism. The substrate is bound via a carboxyl salt-bridge to an arginine residue and a hydroxyl hydrogen-bond to a histidine residue, which facilitates hydride transfer to NAD. As in flavocytochrome b_2, the active site histidine also hydrogen bonds to an aspartate residue (Clarke *et al.*, 1989 a & b).

There is no doubt as to the viability of the hydride mechanism for flavocytochrome b_2, whereas several questions remain with regard to the carbanion mechanism. Is His373 really capable of removing the α-hydrogen as a proton? The pK_a of the lactate α-H is estimated to be 25-30 (Williams & Bruice, 1976). It has been

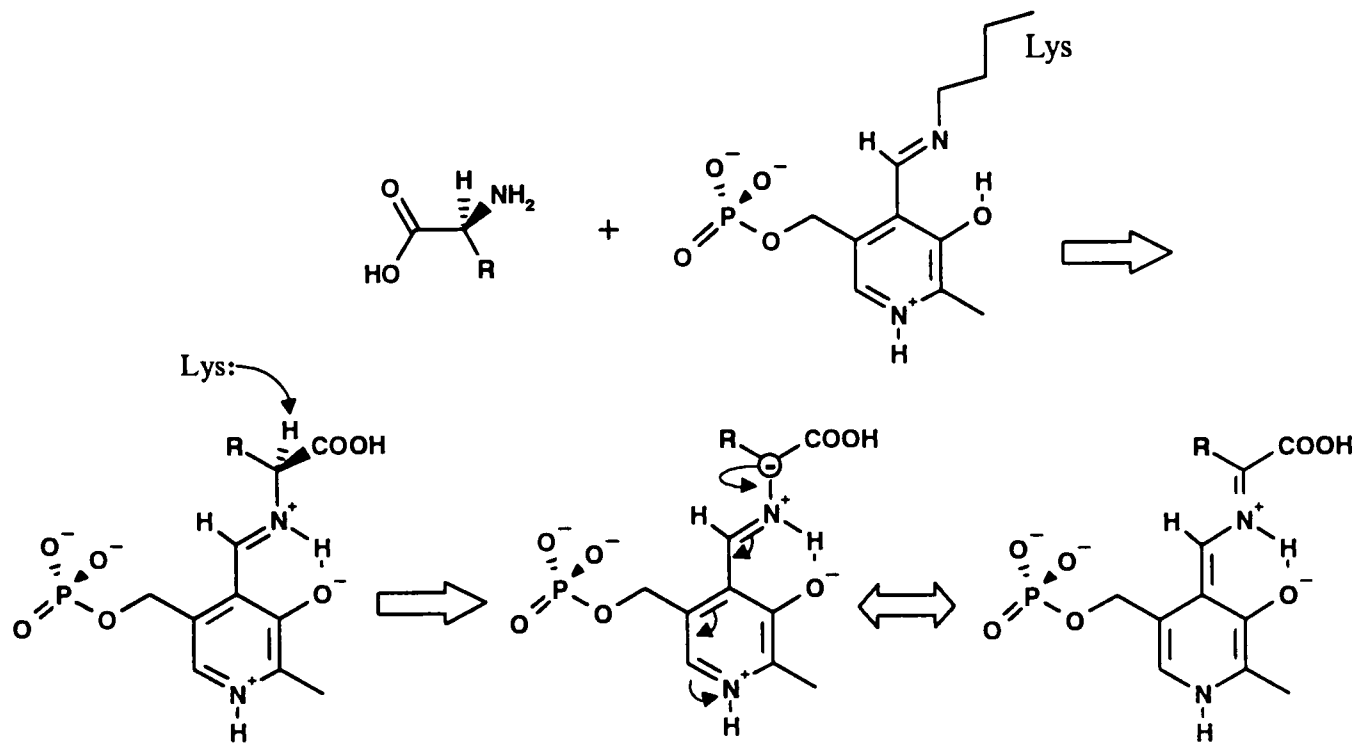

Figure 1.12 Pyridoxal phosphate (attached to the protein via a lysine reside) condenses with amino acids (top) and facilitates carbanion formation at the α-carbon.

(Adapted from Fersht, 1985 & Hayashi, 1995)

suggested that the acidity could be dramatically shifted on binding (Ghisla, 1982), but no detailed explanation has been proposed. It should be noted that for an isotope effect of 8.1 on hydrogen abstraction (Miles *et al.*, 1992), the transition state would be expected to be evenly balanced between protonation and deprotonation, i.e. the competing groups should have very similar pK_a's. The suggestion that carbanion formation could be facilitated by electron delocalization to the carboxylate-arginine salt-bridge conflicts with the necessary transition-state orientation, which would position the orbital lobe approximately 90° out of alignment (see *Figures 1.7,1.8 & 1.11*; the C1 pπ orbital is aligned vertically). It should be noted that substantial reorientation of the carbanion would be required for a covalent bond to be formed with FMN N5, including a 120° torsion by the hydroxyl group around the C1-C2 axis (see *Figure 1.11*). This process must be rapid in both forward and reverse directions for transhydrogenation to occur, since carbanion processing in either direction is required to be faster than protonation/deprotonation.

Stabilised carbanions are known to exist as intermediates in the catalytic mechanisms of pyridoxal-phosphate-dependent enzymes (Hayash, 1995) and have

been used to support the theory that a carbanion is a viable species on the pathway of FMN-catalysed L-lactate dehydrogenation (Ghisla, 1982). *Figure 1.12* illustrates how stabilisation is achieved by such enzymes. Carbanion formation occurs only after direct complexation with pyridoxal phosphate, which allows the negative charge to be stabilised over a large conjugated system. It would seem illogical to attempt carbanion formation prior to stabilisation, as proposed for the L-lactate dehydrogenation mechanism.

In summary, the structural evidence strongly supports the 'hydride' mechanism, as does the study of 5-deaza-FMN-substituted enzymes. Whereas the detailed, quantitative solution studies involving transhydrogenation and dehydrohalogenation, along with the study of the L-lactate monooxygenase-glycolate complex, appear to support the 'carbanion' mechanism.

1.7. Substrate Specificity and Inhibition

Flavocytochrome b_2 acts exclusively as an L-2-hydroxy-acid dehydrogenase and exhibits a strong preference for its physiological substrate L-lactate. Substrate recognition is achieved by the careful positioning of active site amino-acid residues as illustrated in *Figure 1.7.* Arg376 and Tyr143 appear to interact with the substrate carboxylate and His373 with the hydroxyl (see *Section 1.5;* p12). However, recognition of the L-lactate methyl-group appears to arise from interactions with the hydrophobic side-chains of Ala198, Leu230 and Leu286 (see *Figure 5.1;* p118). *Table 1.1* compares the activities found with alternative substrates relative to L-lactate.

In *Chapter 5* substrate specificity is discussed in greater detail, site-directed mutagenesis has been employed in an attempt to exert a degree of control over the kinetic parameters. This is partly spurred on by the successful attempts of others to create biosensors based on flavocytochrome b_2 by immobilising the enzyme in electrically conducting polymer matrices (Bartlett & Caruana, 1994). Flavocytochrome b_2 is ideal for such a role because substrate dehydrogenation is

coupled directly to electron transfer by the enzyme, this allows a signal to be detected electronically. Clearly, if protein engineering can be used to manipulate substrate specificity, then the substrate range of the biosensor can be increased.

In addition to sulphite (see p10) several carboxylic-acid derivatives inhibit the turnover of flavocytochrome b_2. Those of particular note are collated in *Table 1.2* with reported inhibition constants. Most are classified as competitive inhibitors which, on binding, mimic the substrate-enzyme Michaelis complex. Pyruvate exhibits more complex behaviour, which is thought to originate from the stability it imparts on the semiquinone oxidation state of bound flavin. This was demonstrated by Tegoni *et al.*, (1990) for the *H. anomala* enzyme and by Walker & Tollin (1991) for the *S.cerevisiae* enzyme and is examined further in *Chapter 3*.

Table 1.1 ***Relative activities of some substrates*** (Chapman *et al.*, 1991)

Substrate	Relative Rate
L-lactate	1.00
DL-Chlorolactate	0.35
DL-Fluorolactate	0.10
DL-Bromolactate	0.91
L-Glycerate	0.50
DL-Phosphoglycerate	0.25
Glycolate	0.04
DL-α-Hydroxybutyrate	0.30
DL-α-Hydroxycaproate	0.18
DL-α-Hydroxyisocaproate	0.17
DL-Isocitrate	0.01
L-Malate	0.01
L-Tartrate	0.05

Table 1.2 ***Flavocytochrome b_2 Inhibitors*** (Lederer, 1991)

Inhibitor	Inhibition type	K_d
L-lactate	Excess substrate	150 mM
L-lactate	Competitive	1.4 mM
Propionate	Competitive	28 mM
L-Mandelate	Competitive	0.26 mM
Oxalate	Competitive	1.1 mM
Sulphite	Competitive	0.0014 mM
Pyruvate	Competitive	3 mM
	Non-competitive	30 mM

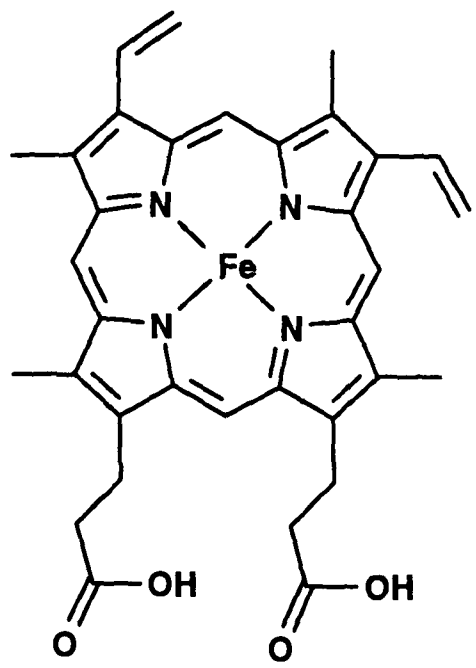

Figure 1.13 Haem *a* is composed of iron ligated to protoporphyrin IX. It is bound by the haem domain of flavocytochrome b_2 via axial co-ordination to the imidazoles of His43 and His66.

1.8. The Haem Domain

The flavocytochrome b_2 haem-binding domain consists of a 90 amino-acid polypeptide folded into a β-sheet/α-helix sandwich in which two hydrophobic pockets are formed (Xia & Mathews, 1990). One of these pockets is the haem-binding crevice and contains a pair of histidine residues (43 and 66) which axially co-ordinate to the haem iron. As predicted from sequence alignments (see *Figure 1.3;* p6), the b_2-haem domain has a similar structure to that of cytochrome b_5 and possesses sequence similarities with individual domains of *Nicotiana tabacum* nitrate reductase and chicken sulphite oxidase (Lederer, 1994). It has been separated from the flavin domain by both genetic engineering (Brunt *et al.,* 1992) and tryptic hydrolysis (Labeyrie *et al.,* 1966). The resultant b_2-core protein is around 11 kDa in weight and is of course monomeric. On mixing b_2-core with the separately expressed flavin domain of flavocytochrome b_2, no haem reduction was observed. This result underlines the importance of the inter-domain hinge for the effective functioning of the enzyme and has been addressed further by mutagenesis. Mutant enzymes have

been generated in which the hinge has been truncated (Sharp *et al.,* 1994) and replaced by the hinge region of *H anomala* flavocytochrome b_2 (White et al., 1993). Both mutations cause disruption to inter-domain electron-transfer.

The role of the haem domain

As mentioned in *Section 1.2* (p3) the physiological redox partner of flavocytochrome b_2 is cytochrome *c*. It was demonstrated by Brunt *et al.* (1992) that the separately expressed flavin domain of flavocytochrome b_2 could not efficiently transfer electrons to cytochrome *c*, despite the large driving force for the reaction, yet could function unhindered as a L-lactate dehydrogenase if given a suitable redox partner (e.g. ferricyanide). Therefore the b_2-haem domain appears to be an integral electron-transfer mediator with a single role: facilitating transfer from reduced FMN to cytochrome *c*. Given that FMN is a two-electron acceptor/one-electron donor, while b_2 haem can only accommodate one electron ($Fe^{III} \leftrightarrow Fe^{II}$), we are able to specify a catalytic cycle based on electron flow.

The catalytic cycle

Figure 1.14 illustrates how five individual electron-transfer events constitute the flavocytochrome b_2 catalytic cycle, which directly couples L-lactate dehydrogenation to cytochrome *c* reduction. Each subunit is treated as functionally independent since inter-subunit electron-transfer is a relatively slow process (Capeillère-Blandin, 1975). This also justifies the exclusion of a three-electron reduced species in the cycle. The first step in the cycle is the two-electron reduction of FMN on conversion of L-lactate to pyruvate. These two electrons are passed individually to b_2-haem and then to cytochrome *c*, making up steps 2 & 3 and 4 & 5 respectively. Steady-state reduction of cytochrome *c* by flavocytochrome b_2 occurs at 207 ±10 s^{-1} (Miles *et al.*, 1992), but since two equivalents of cytochrome *c* are reduced per circuit, the cycle itself turns at approximately 100 s^{-1} (at 25°C, pH 7.5, *I* 0.10).

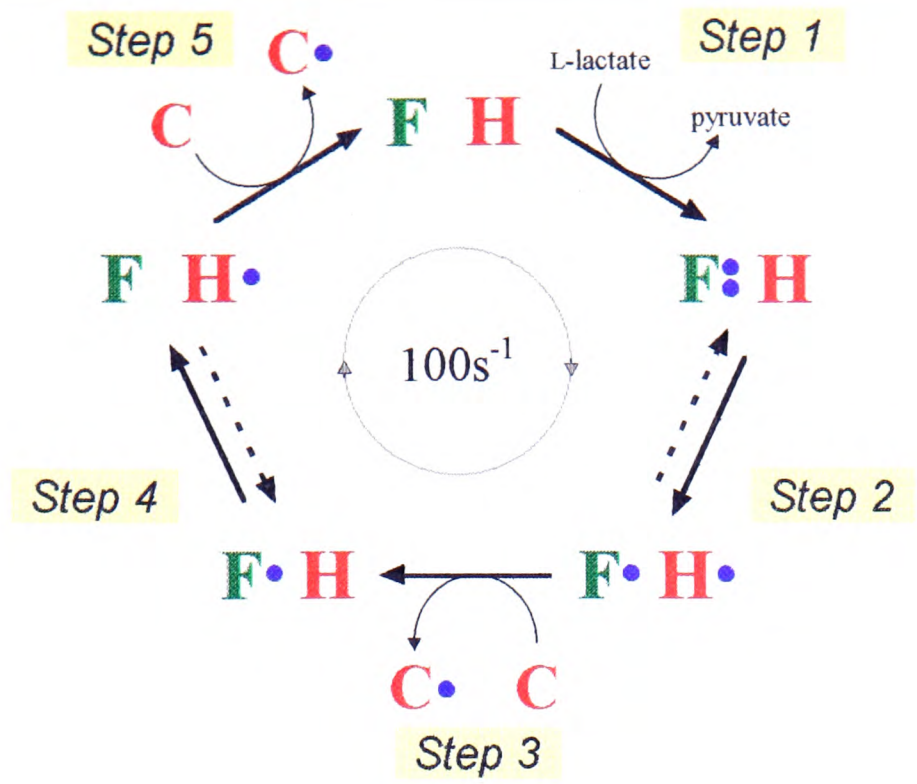

Figure 1.14 The catalytic cycle of flavocytochrome b_2 based on single electron-transfer events. The five sequential steps result in an overall turnover rate of approximately 100 s^{-1}.

F H single subunit of flavocytochrome b_2 (F ≡ FMN, H ≡ b_2-haem)

C cytochrome *c*

• a reducing equivalent of electrons.

The cycle is discussed in greater detail in *Chapter 3* where an attempt has been made to develop a self-consistent kinetic model based on the individual electron-transfer events. More specifically, the interaction between flavocytochrome b_2 and cytochrome *c* is discussed in *Chapter 4*.

1.9 Protein Mediated Electron-Transfer

Electron transfer is Nature's solution to the fundamental problem of coupling organic chemistry to one-electron redox chemistry and is conducted largely by proteins. Respiration uses the large amount of energy gained from the four-electron reduction of oxygen for the production of ATP, which in turn drives many other biological processes. The mini respiratory pathway directed by flavocytochrome b_2 in yeast demonstrates this in microcosm (see *Section 1.2;* p3). The same problem arises

in photosynthesis, which involves the reduction of carbon dioxide and water to oxygen. Photosynthesis is an endothermic process which provides carbon for carbohydrate synthesis in plants and as such requires an input of energy in terms of solar light. The complex mechanism of photon harvesting involves single-electron-transfer chemistry which ultimately leads to the generation of NADH and ATP, the universal energy carriers. Common to both respiration and photosynthesis is the generation of and controlled release of energy through an electrical potential gradient. During respiration, electrons are passed from NADH (-320 mV) to O_2 (820 mV) through a potential of more than 1 V, whereas during photosynthesis electrons are excited through a similar potential on absorption of visible light.

There is a general need for organisms to be able to direct energy to where it is required and this is achieved by the effective isolation of electron transfer processes. Where physical separation is inconvenient, redox events are isolated by the use of molecular recognition. Examples of electron transfer will therefore be considered in two halves: *1.10 Intramolecular Electron-transfer* and *1.11 Intermolecular Electron-transfer.* Flavocytochrome b_2 acts as a simple and convenient model for both.

Non-adiabatic electron-transfer: Marcus theory

Marcus theory (Marcus & Sutin, 1985) simplifies the problem of calculating the activation energy for long-range electron transfer reactions by considering reactants and products to be systems undergoing simple harmonic oscillation, such that both lie in separate parabolic potential energy wells (see *Figure 1.15*). Electron transfer is assumed to take place instantaneously without change in nuclear configuration according to the Franck-Condon principle ('nuclear configuration' refers to the spatial arrangement of all nuclei influenced by the reaction and is dependent on bond-lengths etc.). However, the location of the mobile electron influences the nuclear configuration such that the two parabolas do not overlay. The activation energy (ΔG^*) is therefore determined from the point of intersection between the two parabolas.

The reorganisation energy (λ) is the amount of energy required for the reactant nuclei to assume the configuration of the product nuclei without undergoing

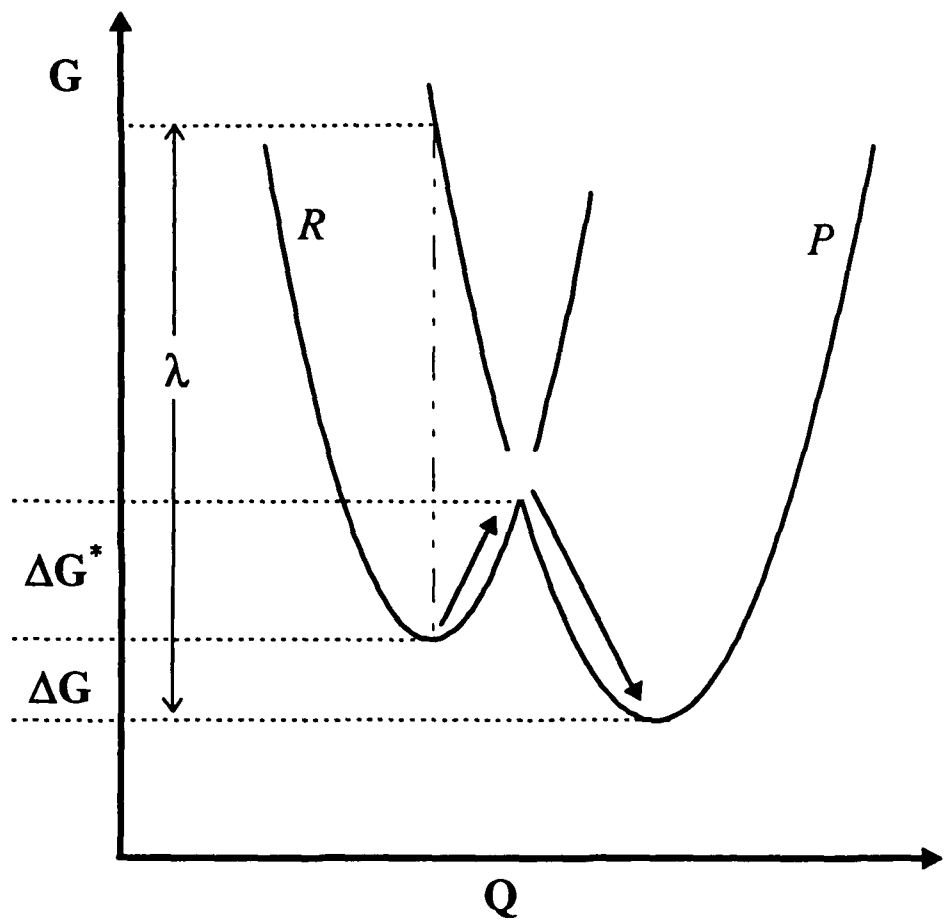

Figure 1.15 Plot of nuclear displacement (Q) against free energy (G) for reactants (*R*) and products (*P*) during an electron transfer reaction. The parabolas describe the respective nuclear configurations during harmonic oscillation. ΔG is the free energy change of the reaction, ΔG^* the activation energy, and λ the reorganisational energy.

electron transfer. It is related to the activation energy according to the following equation:

$$\Delta G^* = (\Delta G + \lambda)^2/4\lambda \qquad (1)$$

and to the rate of electron transfer according to the Gaussian function:

$$k_{et} = k_{MAX} e^{-(\Delta G + \lambda)^2/4\lambda kT} \qquad (2)$$

According to Marcus theory, for a given system, variation of ΔG (with constant λ) causes the two parabolas to move relative to one another along the y axis. The extreme possibilities created by this procedure are depicted in *Figure 1.16(b & c)* and are compared to the usual situation *(a)*. 'Activationless' electron transfer occurs when $\lambda = -\Delta G$ *(b)* and there is no energy barrier to be overcome, at this point $k_{et} = k_{MAX}$. When $\lambda > -\Delta G$ *(c)* electron transfer slows down as a potential energy barrier

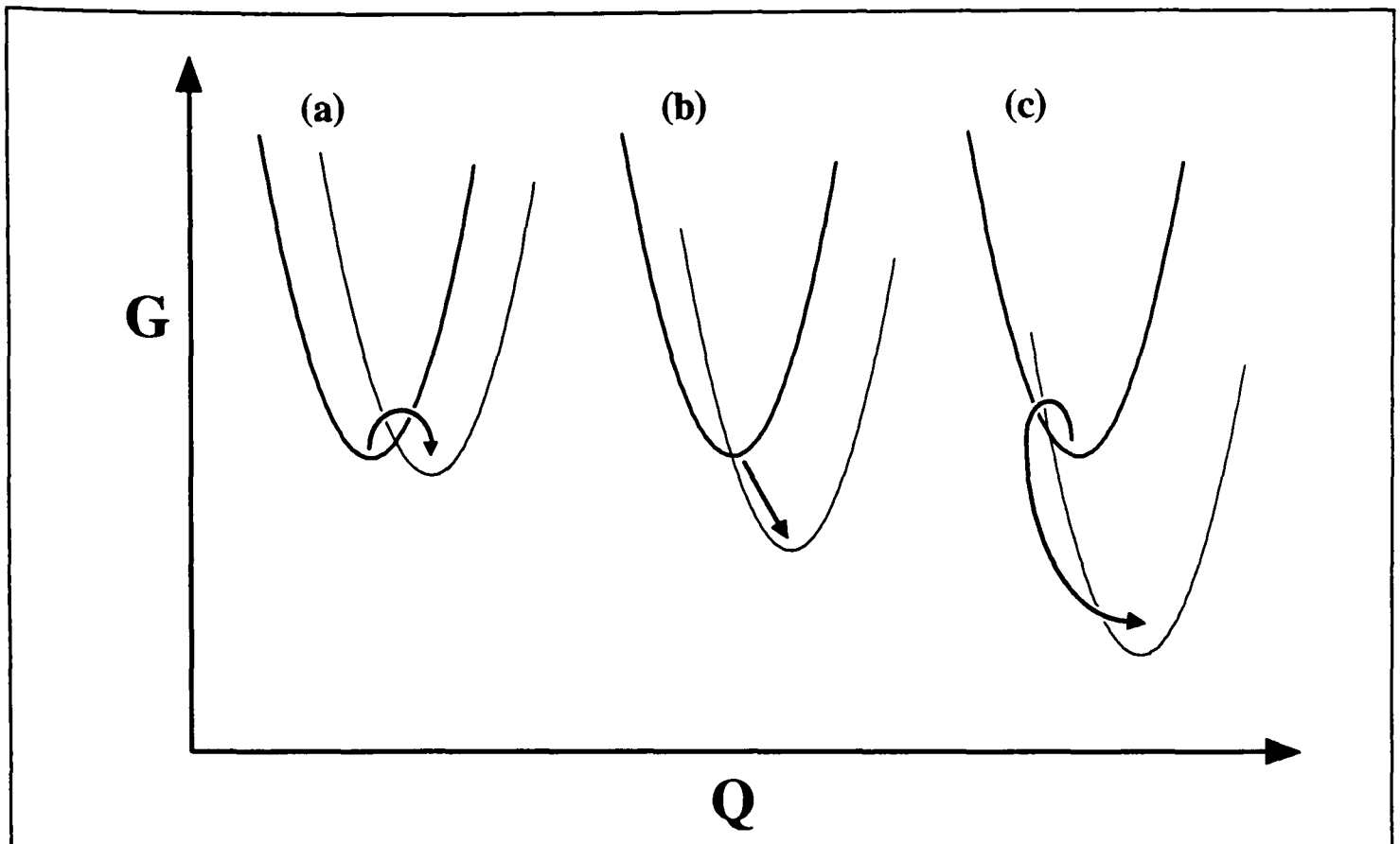

Figure 1.16 Potential energy wells illustrating the conditions required for (a) 'normal' electron transfer, (b) 'activationless' electron transfer, (c) electron transfer in the Marcus 'inverted' region. The axes are labelled as in *Figure 1.15*.

reforms, despite the application of a larger driving force. This is known as the Marcus 'inverted' region. The relationship between k_{et} and ΔG is plotted in *Figure 1.17*.

For the simplest model the value of k_0 is limited by two factors: the distance from donor to acceptor and the nature of the intervening medium. Both directly influence the amount of tunnelling overlap between the donor and the acceptor electronic orbitals. The degree of overlap and therefore the rate of electron transfer are predicted to decay exponentially with distance (overlap is small for long-range electron transfer). The rate of decay is given the value β such that:

$$k_{MAX} \propto e^{-\frac{1}{2}\beta(d-d_0)} \qquad (3)$$

For a vacuum $\beta = 2.8$ Å^{-1} and for a direct protein link $\beta = 0.7$ Å^{-1} (Moser *et al.*, 1995). However, in real biological systems the value of β is often similar to that in a frozen organic solvent (1.4 Å^{-1}). According to classical Marcus theory, the proportionality constant for equation 3 is $(4\pi^3/h^2\lambda kT)^{1/2}H_0^2$, where H_0 is the coupling matrix element for the donor and acceptor orbitals at distance d_0. This raises the

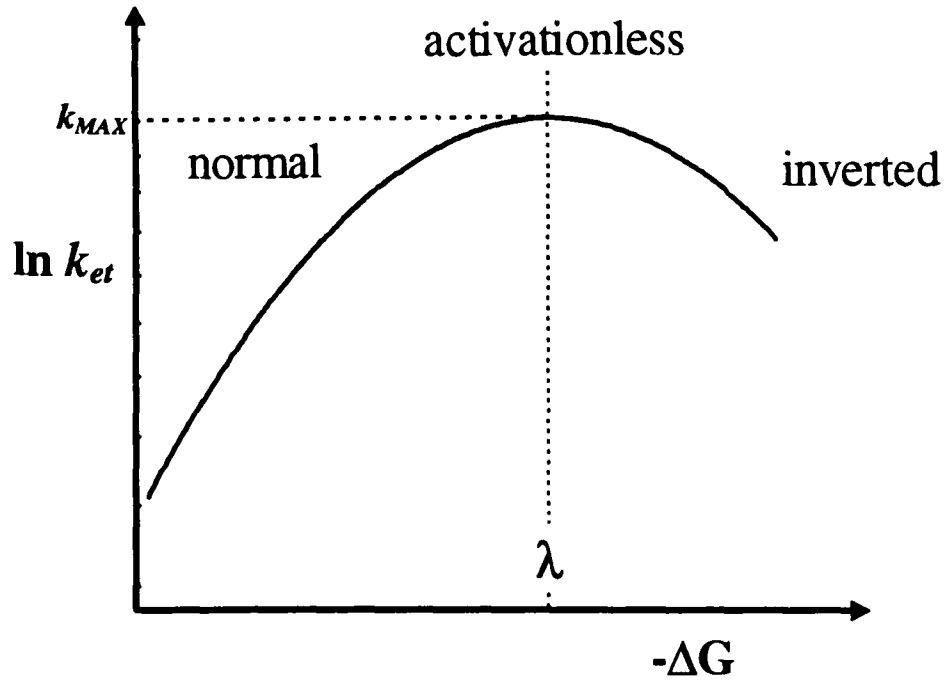

Figure 1.17 For a fixed system, a plot of $\log_e$ of electron-transfer rate against activation energy reaches a maximum when $-\Delta G = \lambda$. Following this, increases in driving force cause the electron transfer rate to decrease, this is the Marcus 'inverted' region.

question of where the electron is actually localised before and after transfer. Distance cannot be measured from the centre of a redox cofactor, whether this is a co-ordinated metal atom or a π-conjugated system, because the β value within any given redox centre is effectively zero. However, the exact extent of the electronic orbitals involved can be difficult to predict (Newton, 1988) and they are unlikely to be well localised or spherical. The values of d_0 and H_0 are therefore mutually dependent. The situation is complicated further by adjustments made to Marcus theory in light of quantum mechanics (Moser *et al.*, 1992, 1995)

Despite the complications noted above, the dominant factors in long-range biological electron-transfer are the driving-force dependence of *Equation 2* and the distance dependence of *Equation 3*. The methodology employed for elucidating the variables in these two equations is best illustrated using examples taken from the intramolecular electron-transfer reactions of well characterised systems (see *Section 1.10*).

1.10 Intramolecular Electron-Transfer

The application of Marcus theory to a real biological system depends on the availability of well defined structural, thermodynamic and kinetic models. These are essential for the derivation of d, ΔG and k_{et} respectively. In order to solve *Equation 2* (p30) rate constants (generally obtained by photo-excitation methods) are tabulated against ΔG, which can be varied by site-directed mutagenesis or cofactor substitution (Moser *et al.*, 1995). Attempts must be made to ensure that structural integrity is maintained and that replacement cofactors are as similar as possible to the original ones. From a plot of log k_{et} *v* ΔG, approximations for both λ and k_{MAX} can then be derived (see *Figure 1.17*). Values for k_{MAX} obtained from a variety of systems can then be used in *Equation 3*, along with distance parameters obtained from high resolution crystal structures, to estimate β and define the role played by the protein matrix in mediating electron transfer.

The photosynthetic reaction centre

The bacterial photosynthetic reaction centre consists of a number of membrane-spanning polypeptides which bind several redox centres in close proximity (Allen *et al.*, 1987; Chang *et al.*, 1986; Michel *et al.*, 1986). It is therefore an ideal system in which to study protein mediated electron-transfer and has been exploited most successfully (Moser *et al,* 1995; 1992). Rate constants for the electron transfer reactions between quinone A, quinone B, bacteriopheophytin, bacteriochlorophyl dimer and bacteriopheophytin monomer have been deduced for the reaction centre systems from *Rb. sphaeroides* and *Rp. viridis*. Mutagenesis and cofactor replacement have been employed to vary the driving force for individual steps so that an extensive list of individual k_{MAX} values has accumulated (Moser *et al,* 1992). *Figure 1.18(a)* depicts a plot of $\log_{10}(k_{et})$ against 'd', the direct edge-to-edge distance between cofactors. The x-axis begins at 3.6Å which represents the Van der Waal's contact range of the two cofactors and therefore the point at which Marcus theory becomes redundant. Moser *et al.* (1992) fit the data to a straight line according to *Equation 3*, which gives a y-axis intercept (at 3.6Å) of 10^{13} s^{-1} and a β value of 1.4 $Å^{-1}$. The implication of this result is that physiological electron-transfer decreases with

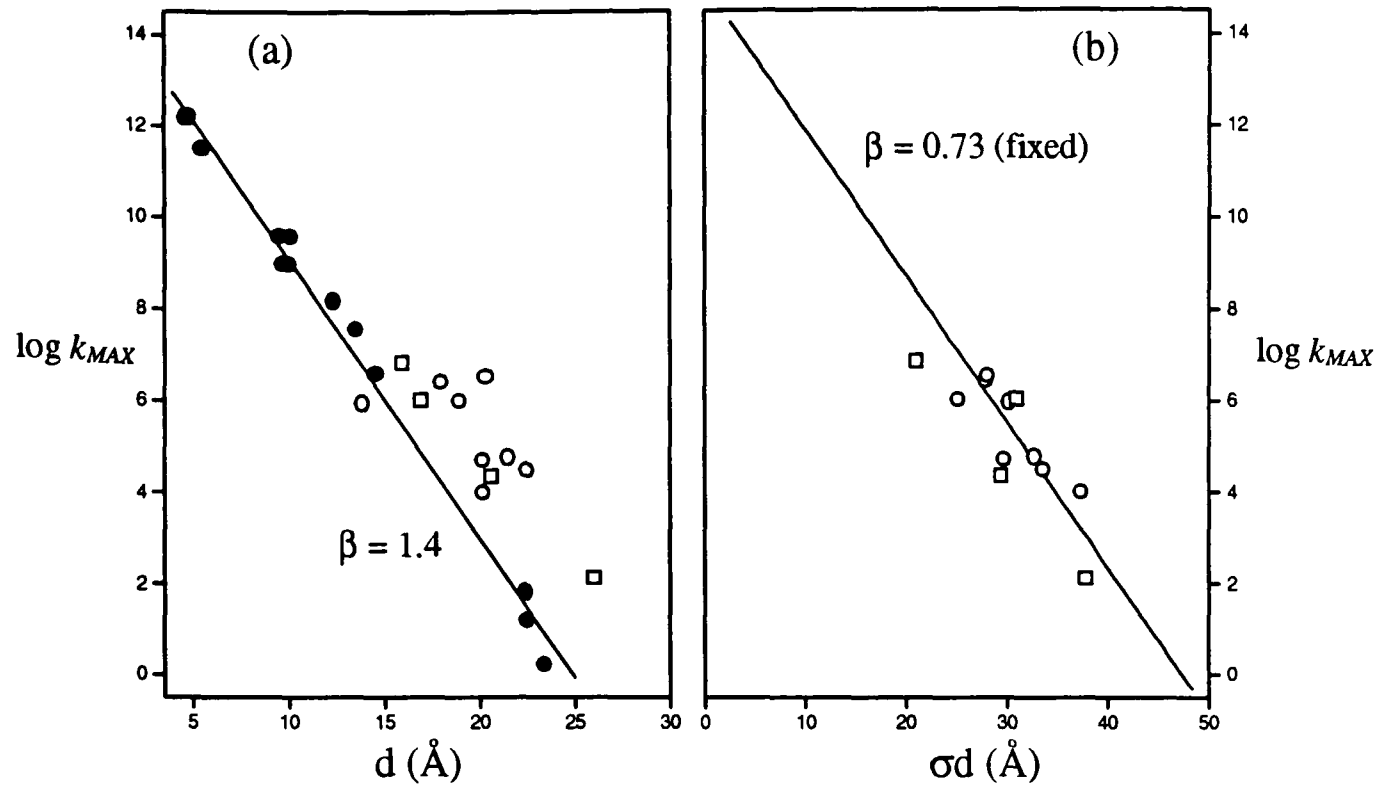

Figure 1.18 The log of activationless electron-transfer rate plotted against (a) through space distance 'd' and (b) σ tunnelling distance 'σd' for several physiological and synthetic systems.

- taken from Moser *et al.* (1992), based on electron transfers in the photosynthetic reaction centre. These points are fitted to a function with $\beta = 1.4$ Å^{-1}, 'd' is taken to be the edge to edge distance between quinone, chlorophyl & pheophytin cofactors.

o taken from Bjerrum *et al.* (1995), based on electron transfers in $Ru(bpy)_2$-modified cytochromes *c* ($Fe^{II} \rightarrow Ru^{III}$). In plot (b) these points are fitted to a function with β fixed at 0.73 Å^{-1}. 'd' is the distance between redox centres.

taken from Bjerrum *et al.* (1995), based on electron transfers in $Ru(bpy)_2$-modified azurins ($Cu^{I} \rightarrow Ru^{III}$). 'd' is the distance between redox centres.

increasing distance in a mono-exponential manner with a decay factor of 1.4 Å^{-1}. This is apparently independent of variations in the intervening protein structure. However, in a comparison of synthetic systems, Moser *et al.* (1992) acknowledge that variations in β can occur when direct links are formed between redox centres.

The general prognosis presented by Moser *et al.* (1992; 1995) is that electron transfers in physiological systems will fall roughly in line with the reaction centre and that β values will approximate to 1.4 Å^{-1}. This would certainly be expected if protein matrices are randomly organised and behave like frozen organic solvents. This doctrine is not universally accepted and much effort is being expended in the analysis

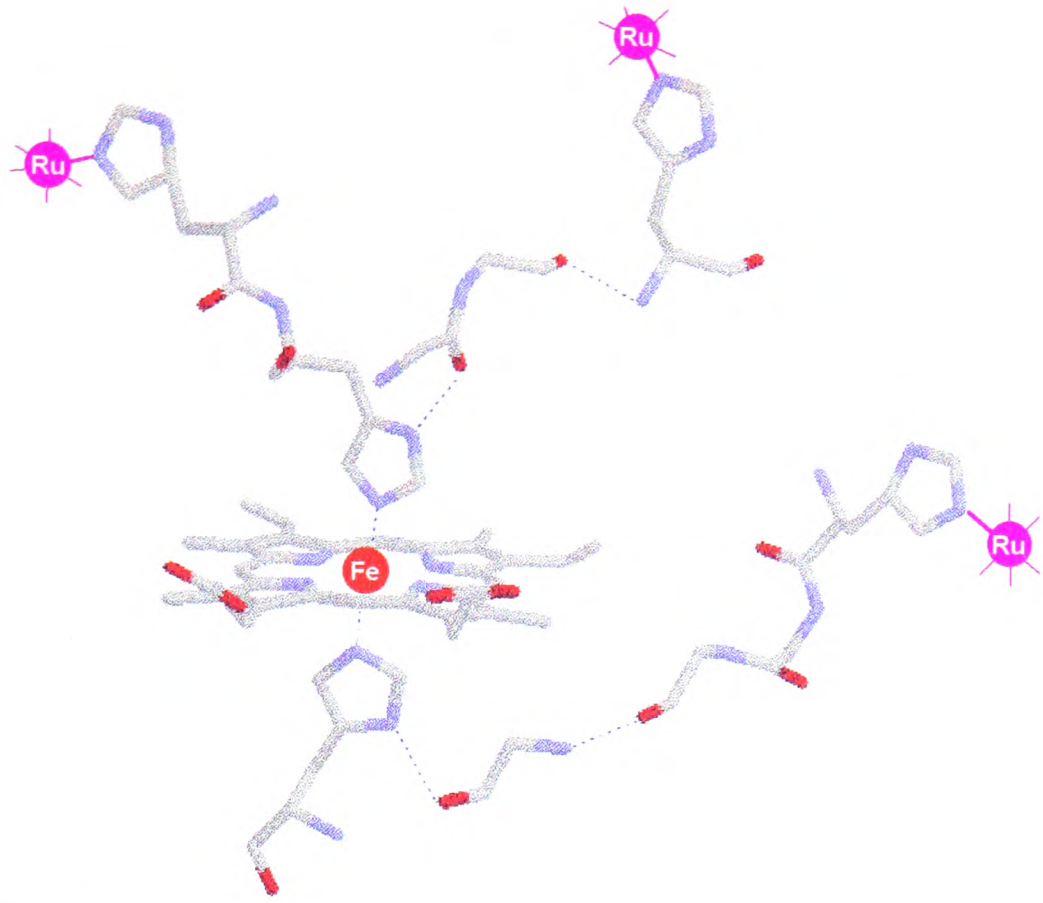

Figure 1.19 Electron-transfer pathways suggested for three ruthenium-modified His-mutants of cytochrome b_2 core (Lloyd *et al.*, 1994). Electron transfer coupling-coefficients are derived from the path-length (σd) which is a function of both distance and path type, to account for variations in coupling across covalent bonds, hydrogen-bonds and through-space jumps.

of alternative systems, with the aim of deriving a methodology to account for all intervening structural motifs. The most popular systems in use recently consist of transition metal complexes chemically attached to simple redox proteins. The most popular transition metal in use is ruthenium.

Ruthenated proteins

Electron transfer between protein redox centres and Ru^{III} complexes have been conducted on a variety of systems including cytochrome b_2 core (Lloyd *et al.*, 1994). In this case select surface residues were mutated to histidines and directly treated with $Ru^{II}(NH_3)_5H_2O^{2+}$ anaerobically. On oxidation, non-labile $Ru^{III}(NH_3)_5$-His-Protein complexes were formed. Rate constants were then measured for the electron transfer from b_2-haem-Fe^{II} to Ru^{III} by first reducing the b_2-haem with radiolytically excited methyl viologen radical. The authors suggest electron-transfer pathways (*Figure 1.19*)

based on the flavocytochrome b_2 X-ray crystal structure (Xia & Mathews, 1990), but find a poor correlation for rate verses distance according to *Equation 3* (p31), whether the pathway or direct through-space distance is taken. Their conclusion, that, when k_{et} is used in place of k_{MAX} small variations in reorganisation energy (λ) are amplified by *Equation 2* (p30), illustrates the requirement for ΔG variation in the application of Marcus theory (as in the photosynthetic reaction centre model).

A more thorough treatment has been applied to the cytochrome *c* and azurin systems reviewed by Winkler & Gray (1992) and Bjerrum *et al.* (1995). The general procedure adopted involves mutation of surface histidines and complexation of these with $Ru^{II}(bpy)_2CO_3$. The resultant $Ru^{II}(bpy)_2$im-His-Protein complexes are subjected to various flash-quench procedures to obtain electron-transfer rate constants, photoelectronic excitation of Ru^{II} in the presence of quenching agents has allowed $Ru^{II}\rightarrow M$, $Ru^{I}\rightarrow M$ and reverse processes to be monitored individually. The use of bpy derivatives and alternative ligands to vary ΔG has enabled λ and k_{MAX} values to be obtained. Some of these k_{MAX} values are plotted in *Figure 1.18*. It should be noted, however, that in these plots 'd' is measured directly between metal centres and so up to 8 Å should be deleted from each distance. As mentioned earlier, estimates of the exact extent of the donor/acceptor orbitals of metal complexes remains somewhat speculative, perhaps more so than the π-systems surveyed by Moser *et al.* (1992; 1995). The apparent failure of these points to lie on the $\beta = 1.4$ $Å^{-1}$ line has encouraged the development of more sophisticated approaches to the analysis of the effect of intervening medium on long-range biological electron-transfer (Curry *et al.*, 1995). *Figure 1.18(b)* is a plot of k_{MAX} verses the σ-tunnelling distance 'σd' between donor and acceptor. This is calculated by assigning different β values to individual steps in the pathway, covalent bond < hydrogen bond < through-space jump, as in *Figure 1.19*. Bjerrum *et al.* (1995) fit the cytochrome *c* data to a slope with a fixed β of 0.73 $Å^{-1}$ consistent with the model used and obtain an intercept of 10^{15} s^{-1}.

Unfortunately the intercept value cannot be regarded as a known quantity in this plot, since it depends on the proportionality constant of equation 3, therefore fixing the value of β assumes the validity of the model, making it difficult to draw positive conclusions from the data. Clearly, the degree of scatter in *Figure 1.18(b)* is not significantly different from the scatter caused by the same data in *Figure 1.18(a)*, therefore the model used cannot be considered a significant improvement. More elaborate models are being devised which remove some of the approximations made in the simple pathway model (Curry *et al.*, 1995; Siddarth & Marcus, 1993; Gruschus & Kuki, 1993) and protein matrices are being treated as multi-pathway systems in which quantum-interference effects must be incorporated.

The inherent uncertainty in much of the experimental data, often magnified in the calculation of k_{MAX} will always hinder the theoreticians. The success achieved by Moser *et al.* (1992) using the reaction centre as a model was aided by the large variation in distance ($\rightarrow$20 Å) and rate ($1\rightarrow10^{12}$ s^{-1}) achieved (Chapman & Mount, 1995). More localised comparisons will obviously suffer more from experimental uncertainty.

FMN to b_2-haem electron transfer in flavocytochrome b_2

Unlike in the rigid systems discussed above, intramolecular electron-transfer in flavocytochrome b_2 is complicated by the relative mobility of the redox groups implied from crystallographic and NMR evidence (see *Section 1.4*). This mobility has therefore been the subject of particular attention. Essentially, two aspects of the inter-domain region have been studied using a combination of site-directed mutagenesis and stopped-flow spectrophotometry, namely the 'hinge' linker and key hydrogen-bonding interactions.

The idea that that the length of the hinge polypeptide is evolutionarily optimised for FMN to b_2-haem electron transfer has been tested by the generation of deletion and insertion mutants (Sharp *et al.*, 1994; 1996a & b). Both hinge shortening by the removal of 3, 6 and 9 amino-acids and hinge extension by the insertion of 3, 6 and 9 amino-acids caused a step-wise erosion of the electron-transfer rate constant. This is represented by the bar plot in *Figure 1.20*, the value of k_{et} used for wild-type (position zero) is a minimum estimate derived from Chapman *et al.* (1994) and

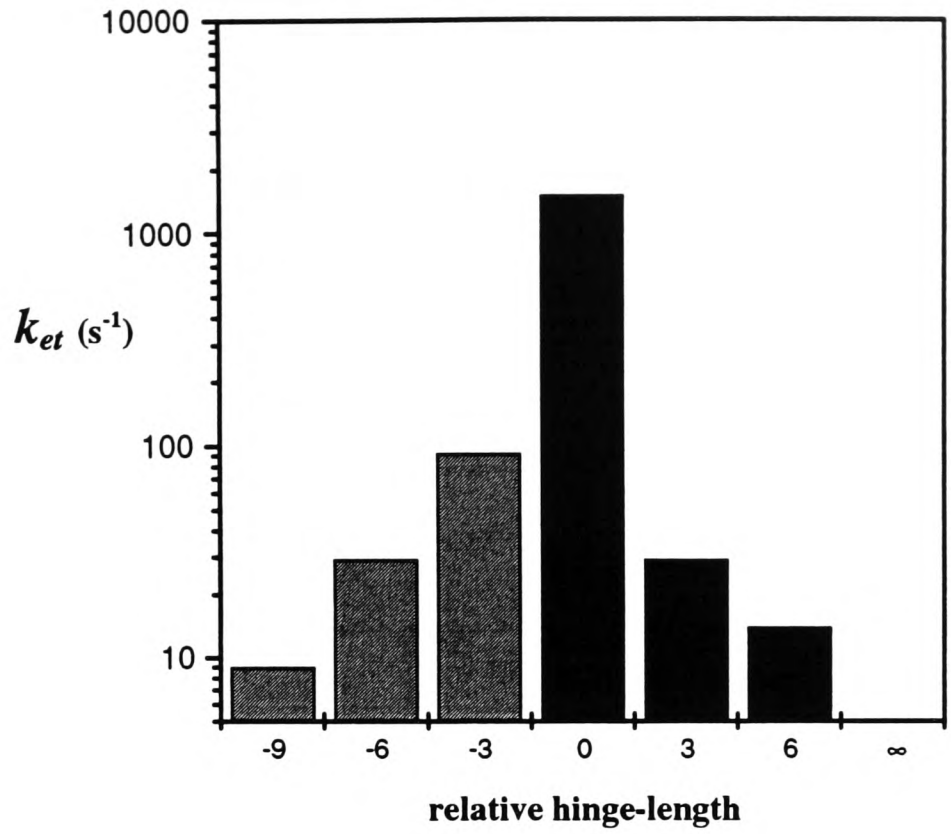

Figure 1.20 Plot of the FMN (fully reduced) to b_2-haem electron-transfer rate constant against hinge-length for flavocytochrome b_2 hinge deletion/insertion mutants (Sharp *et al.*, 1994; 1995a & b). When the hinge is cleaved (∞) there is negligible electron transfer (Brunt *et al.*, 1992).

Chapter 3 of this thesis. The fact that the plot of hinge length verses electron transfer rate peaks sharply at that of the native enzyme suggests that the hinge is of the optimum length. However this is unlikely to be strictly a distance-related phenomenon, although crystal structures have not been determined. Sharp *et al.* (1994, 1996a & b) consider that the rate of electron transfer is limited by the number of productive encounters between the two domains and therefore depends on the mobility of the b_2-haem-domain.

White *et al.* (1993) replaced the hinge polypeptide with that of *H. anomala* flavocytochrome b_2 by site-directed mutagenesis. Although this enzyme is strongly related to *S. cerevisiae* flavocytochrome b_2 by amino-acid sequence (see *Figure 1.3;* p6) the hinge region is shorter and of widely different composition. This mutation also decreased the rate constant for FMN to b_2-haem electron transfer implying that hinge-length optimisation is particular to the two individual enzymes.

The presence of strong inter-domain binding forces seems to be ruled out by the mobility reported for the b_2-haem domain in the wild-type enzyme and the lack of interaction found when the two separate domains are mixed (Brunt *et al.*, 1992). Nevertheless the mutation of Tyr143 to Phe caused a large change in the rate of intramolecular electron-transfer (Miles *et al.*, 1992).

Figure 1.21 compares the active sites found in the two asymmetric units of the flavocytochrome b_2 X-ray crystal structure. In subunit 1 the hydroxyl group of

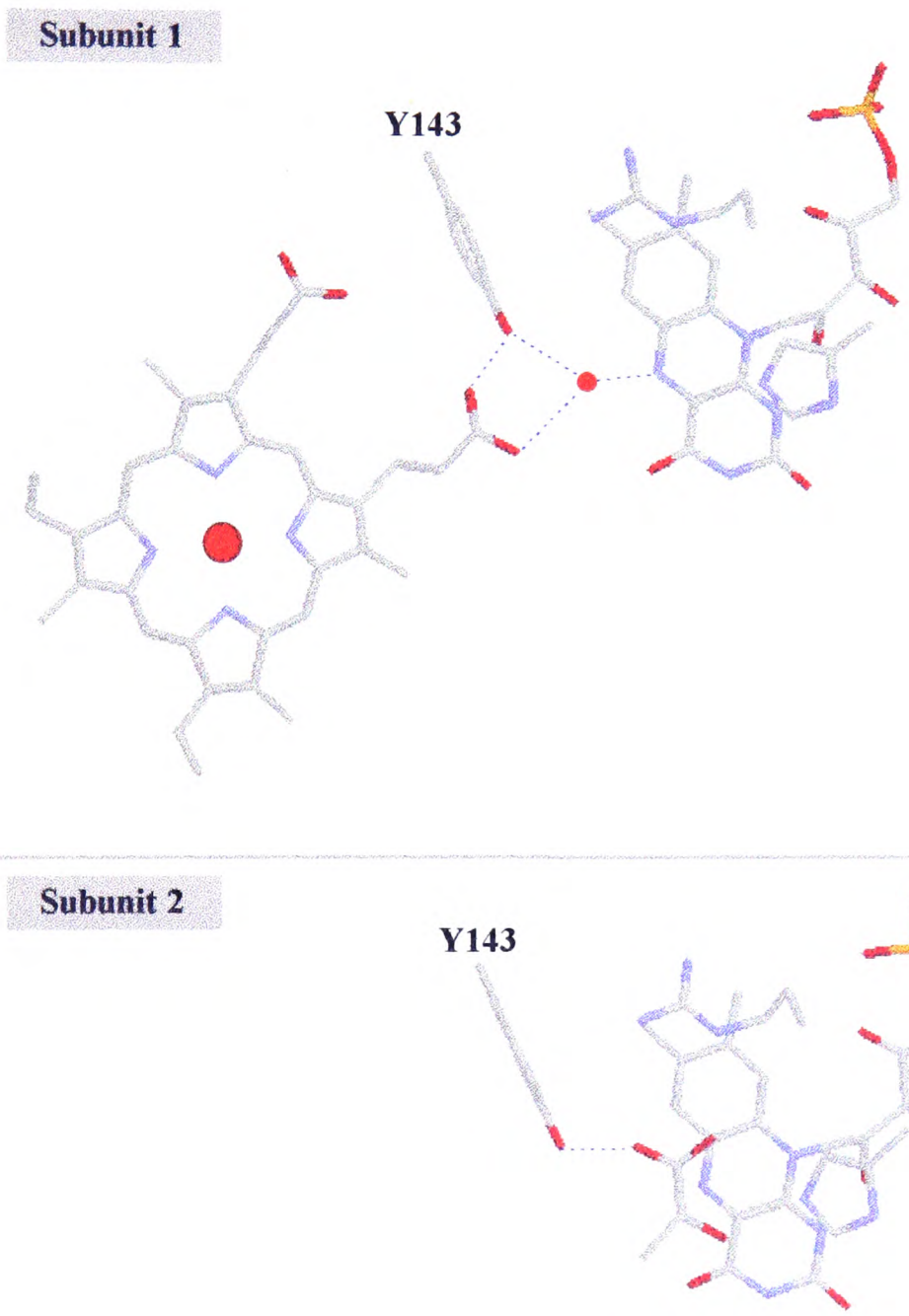

Figure 1.21 The X-ray crystal structure of flavocytochrome b_2 (Xia & Mathews, 1990) contains two non-equivalent subunits. In one of these the b_2-haem domain can be resolved and a haem propionate group hydrogen-bonds to Tyr143. In subunit 2 the b_2-haem domain is disordered and Tyr143 appears to hydrogen-bond to a product molecule (pyruvate).

Tyr143 hydrogen-bonds to one of the b_2-haem propionates, whereas in subunit 2 the entire b_2-haem domain is disordered and the hydroxyl group hydrogen-bonds to a molecule of pyruvate. As well as causing a decrease in the electron-transfer rate constant the Tyr143→Phe mutation also caused an increase in K_m for L-lactate oxidation and a slight increase in the rate of FMN reduction by L-lactate. Both changes were interpreted as evidence for destabilisation of the Michaelis complex. Miles *et al.* (1992) proposed that the decrease in the rate of intramolecular electron-transfer was due to a decrease in the number of productive encounters between the two domains. This implies that the hydrogen-bond aids the inter-domain complexation process and decreases mobility. In subunit 1 the closest FMN to b_2-haem distance is 9.8 Å which is relatively short for protein mediated electron-transfer and, in the authors opinion, too short to limit the rate-constant to 700 s^{-1}, although the rate is certainly faster than this (Chapman *et al.*, 1995; Hazzard *et al.*, 1994). Considering the electron transfer process in terms of the pathway model, it is easy to imagine the b_2-haem propionate group increasing the coupling between donor and acceptor orbitals (see *Figure 1.21*). If such a pathway were valid, the hydrogen-bond could play a significant part in facilitating electron transfer more directly. Taking this a stage further, the hydrogen bond could also facilitate concurrent proton transfer, thereby maintaining the balance of charge in the active site.

1.11 Intermolecular Electron-Transfer

The study of electron transfer between proteins is complicated by similar factors as those described above for electron transfer between the mobile domains of flavocytochrome b_2. Added complications arise from concentration dependent kinetics, which can often be characterised in terms of the dissociation constant for the protein:protein complex. Further, in order to understand a system at a molecular level, it is imperative that an accurate structural model be devised for the active complex. Two different approaches are often employed in the generation of a model, the first, exemplified by the cytochrome *c*:cytochrome *c* peroxidase complex (below) involves the generation of cocrystals and structural analysis by X-ray crystallography.

However, the complex formed within a crystal lattice may be very different to the transient species active in solution, so refinement of the model is often necessary. Alternatively, a model can be designed entirely by the computer-aided energy minimisation of component structures at a putative binding site, as exemplified by the cytochrome *c*:cytochrome b_5 complex (below).

Cytochrome *c*:cytochrome *c* peroxidase

Cytochrome *c* peroxidase couples the oxidation of cytochrome *c* to the reduction of peroxide to water, like flavocytochrome b_2, in the mitochondrial intermembrane space of yeast. A minimum catalytic cycle for the enzyme involves three basic steps (Yonetani *et al.*, 1966; Kim *et al.*, 1990):

$$\text{ccp} + H_2O_2 \rightarrow \text{ccpI(IV R}\bullet) + H_2O \qquad (1)$$

$$\text{ccpI(IV R}\bullet) + \text{cyt}c\bullet \rightarrow \text{ccpII(IV R)} + \text{cyt}c \qquad (2)$$

$$\text{ccpII(IV R)} + \text{cyt}c\bullet \rightarrow \text{ccp} + \text{cyt}c + H_2O \qquad (3)$$

Millett *et al.*, (1995) present the mechanism above as being the most likely sequence of events. Initially cytochrome *c* peroxidase (ccp) reacts with peroxide to form an oxyferryl species with oxidation state IV and generates a free-radical cation on Trp191 (cmpIV R•). This species then oxidises two equivalents of ferrocytochrome *c* (cyt*c*•), with the radical probably being reduced before the Fe^{IV}=O species, although conflicting results suggest the converse may be true or that an equilibrium between ccpI(IV R•) and ccpI(III R) is formed (Coulson *et al.*, 1971; McLendon & Hake, 1992). Purcell & Erman (1976) estimate the redox potential of the oxyferryl species to be 1.0 V and Miller *et al.* (1994) estimate that of the Trp191 indolyl radical cation to be 0.65 V. Both steps 1 and 2 involve intermolecular electron transfer, as ferrocytochrome *c* donates an electron to the ccpI and ccpII intermediates of cytochrome *c* peroxidase. These two steps have been examined extensively by stopped-flow spectrophotometry and photoexcitation of ruthenated mutants under several different ionic strength and pH conditions (Millett *et al.*, 1995).

An initial model for the intermolecular complex was proposed by Poulos & Kraut (1980) involving a significant electrostatic component. This is a prominent feature of the physiological interactions between cytochrome *c* and its redox partners.

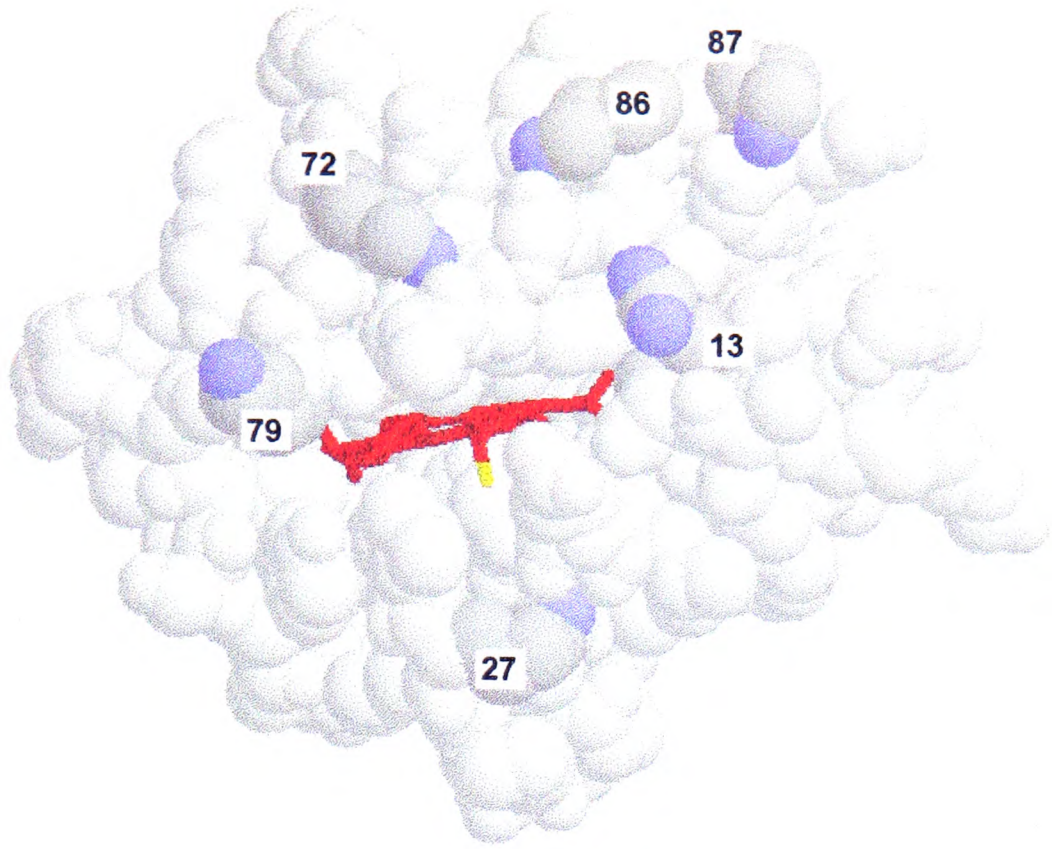

Figure 1.22 The reacting face of yeast cytochrome c, showing the exposed haem edge (red) and positively charged amino-acids Arg13, Lys27, Lys72, Lys79, Lys86 and Lys87 implicated in electrostatic binding interactions with various redox partners (Louie & Brayer, 1990).

As *Figure 1.22* shows, the active face of cytochrome *c* is scattered with positively charged amino-acid residues, which surround the exposed haem edge. Poulos & Kraut (1980) effectively matched these with patches of negative charge on the surface of cytochrome *c* peroxidase thought to influence binding affinity. The complex was also subjected to Brownian dynamics simulations by Northrup *et al.* (1988) who concluded that 'favourable electrostatic interactions facilitate long-lived non-specific encounters that allow the severe orientational criteria for reaction to be overcome by rotational diffusion during encounters'.

After several unsuccessful attempts, Pelletier & Kraut (1992) succeeded in obtaining cocrystals of cytochrome *c* and cytochrome *c* peroxidase. They present two structures, one obtained with cytochrome *c* from horse heart, but the other with the native yeast cytochrome *c* (and therefore physiologically more relevant). As well as

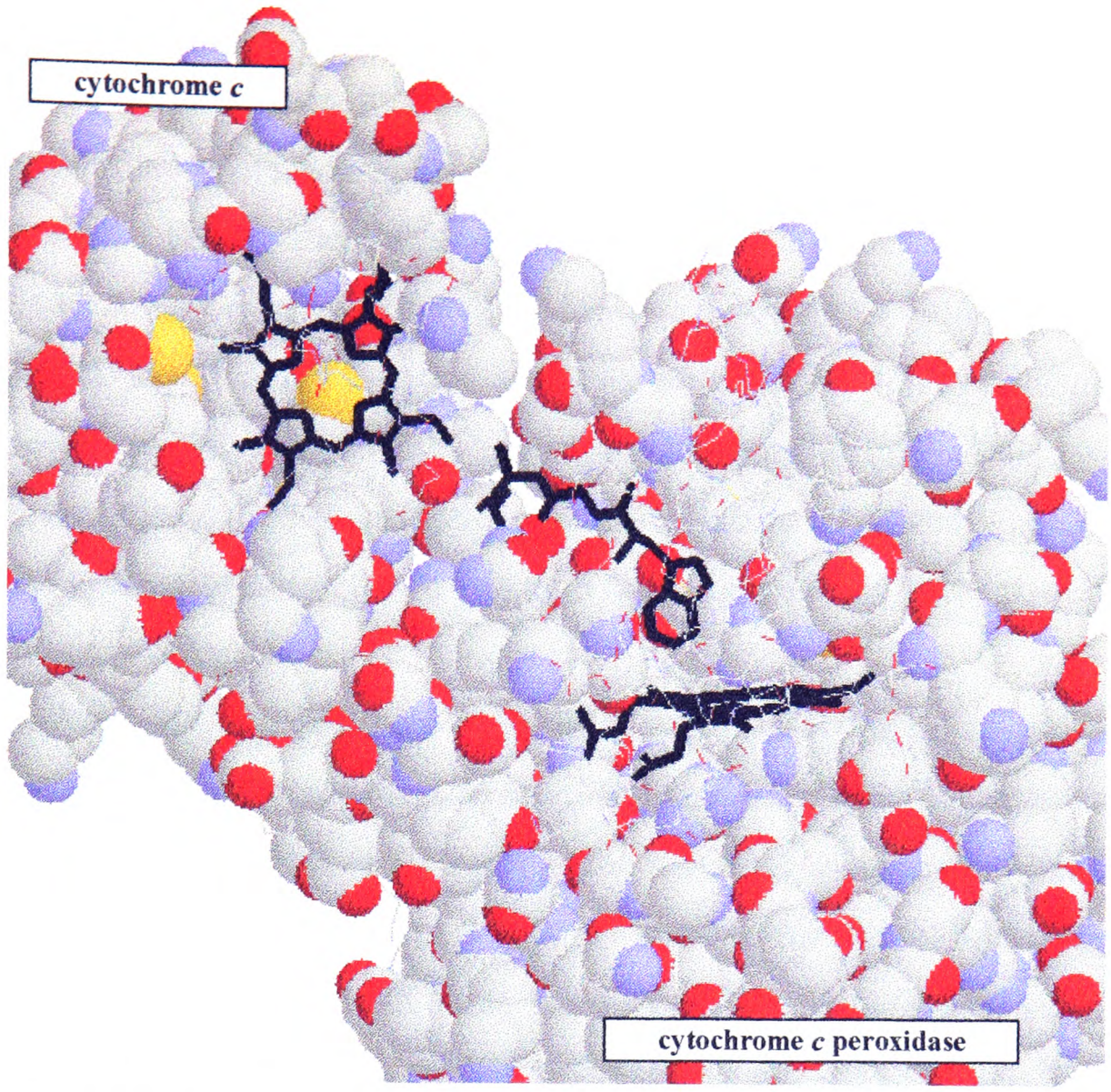

Figure 1.23 The complex formed between cytochrome *c* peroxidase and its physiological redox partner, yeast cytochrome *c*, when the two proteins are cocrystallised (Pelletier & Kraut, 1992). The two haem cofactors are shown in black along with a putative electron-transfer pathway. The pathway consists entirely of cytochrome *c* peroxidase residues (191 to 194 inclusive) which interact at one end with the cytochrome *c* haem (top left) and at the other end with the cytochrome *c* peroxidase haem (bottom right). Trp191 (the latter end) acts as a redox centre itself by converting to/from a stabilised free radical form.

containing several electrostatic contacts, the binding region for the latter also involves significant hydrophobic interactions. One of these is considered by the authors to be a potential route for electron transfer. The pathway extends from the CBC haem methyl of cytochrome *c* across a van der Waal's contact to Ala193/194 and directly along the protein chain to Trp191, which is an integral part of the cytochrome *c* peroxidase redox centre (see *Figure 1.23*).

Various aspects of the cytochrome *c* peroxidase mechanism have been tested by site-directed mutagenesis (e.g. Fitzgerald *et al.*, 1994; Liu *et al.*, 1994) and location of the binding site has been scrutinised by mutagenesis of both cytochrome *c* and cytochrome *c* peroxidase (e.g. Witt *et al.*, 1995; Miller *et al.*, 1994; Mauk, 1991). Miller *et al.* (1994) paid particular attention to the Pelletier & Kraut model, generating several mutants designed to disrupt cytochrome *c* binding. The proposed electron transfer pathway was also tested by the mutation Ala193→Phe, which was designed to increase the distance between redox centres. In general, stopped-flow kinetic analysis of the point mutants provided evidence consistent with the model in terms of general decreases (up to around 5 fold) in the second-order rate constant for cytochrome *c* reduction.

Summarising a wealth of data Millett *et al.* (1995) propose a general kinetic scheme based on the three processes described earlier and including rate constants for binding and dissociation steps. However, the actual rate constants for intra-complex electron-transfer are estimated at 2×10^6 s^{-1} and 5×10^3 s^{-1} for the first and second steps respectively. The first of these is considered to be consistent with estimates derived from applying a σ-tunnelling approach to the Pelletier & Kraut electron-transfer pathway. The second electron transfer is thought to be influenced by the location of the first electron which, because of the nature of the pathway, may require prior transfer from Trp191 to the oxyferryl haem.

Cytochrome *c*:cytochrome b_5

Cytochrome b_5 is a small membrane-bound redox protein consisting of a 92 amino-acid soluble cytochrome domain and a 36 amino-acid hydrophobic membrane anchor. It is found in various physiological locations and is known to interact with several different redox partners (Mauk *et al.*, 1995; Pettigrew & Moore, 1987). Much of the experimental data reported for cytochrome b_5 refers to the solubilised form of the microsomal enzyme, which is unlikely to interact directly with cytochrome *c* due to biological compartmentalisation. This is justified by the occurrence of several b_5-like domains which function physiologically as cytochrome *c* reductases (e.g. flavocytochrome b_2 and sulphite reductase) and the occurrence of a mitochondrial cytochrome b_5 (Lederer *et al.*, 1983). Cytochrome b_5 has an overall surface charge of

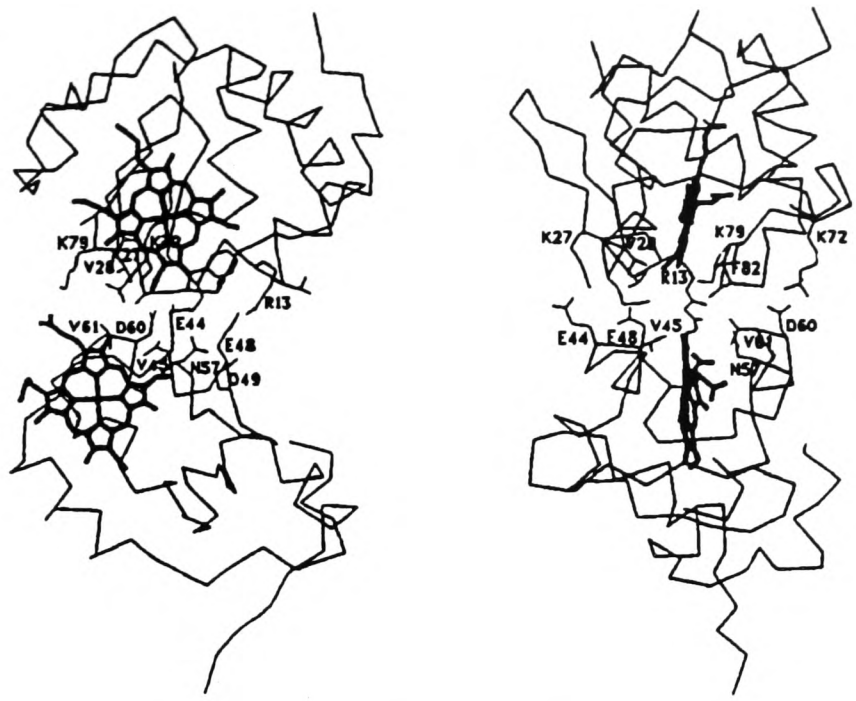

Figure 1.24 The model complex proposed for the interaction between cytochrome b_5 and cytochrome *c* (Salemme, 1976), refined by Guillemette *et al.*, (1994).

-9 and a redox potential of +10 mV, whereas cytochrome *c* has a surface charge of +7 and a redox potential of +260 mV (Moore & Pettigrew, 1987; Eltis *et al.*, 1991). Superficially therefore, ferricytochrome *c* would be expected to oxidise cytochrome b_5 within a tight electrostatic complex. Using the known X-ray crystal structures of the two proteins Salemme (1976) constructed a model for an electrostatically stabilised complex in which the two haem groups were placed parallel and close together (8 Å apart). Thus far, attempts to generate cocrystals of the complex have been unsuccessful and despite refinement using energy minimisation (Guillemette *et al.*, 1994) and Brownian dynamics simulations (Northrup *et al.*, 1993) the model remains largely unaltered (see *Figure 1.24*).

The electrostatic basis of the Salemme model was validated by steady-state ionic-strength studies and the specific roles of certain lysine residues of cytochrome *c* were demonstrated by chemical modification (Ng *et al.*, 1977; Smith *et al.*, 1980). Numerous techniques have been employed in the analysis of the complex including optical difference spectroscopy (Mauk *et al.*, 1982; 1986) and NMR spectroscopy (Eley & Moore, 1983; Whitford *et al.*, 1990). Most of this work supports the formation of a 1:1 complex in solution, although Whitford *et al.* (1990) find evidence

in favour of a ternary complex (this is disputed by Mauk *et al.,* 1995). Mauk *et al.* (1991) used potentiometric titrations to determine the pH dependency of the complex and concluded that 10 to 12 titratable groups are influenced by complex formation (although variations in the conformation of the complex are expected). Rodgers *et al.* (1988) and Rodgers & Sligar (1991) used a combination of mutagenesis and hyperbaric visible difference spectroscopy to evaluate the influence of specific salt bridges between the proteins, they concluded that 3 to 4 such interactions occur. NMR has also been used to acquire more specific information, particularly with regard to the binding region on cytochrome *c*. Lysine dimethylation and acetimidylation using ^{13}C-labelled reactants followed by NMR of free and complexed cytochrome *c* has implicated at least six of these residues, while the use of redox inactive shift reagents (e.g. $Cr(ox)_3^{3-}$, $Cr(CN)_6^{3-}$) to perturb ^1H resonances has confirmed the involvement of Lys72, Ile81, Ala83, Phe82 and Ile85 as predicted by the Salemme model (Eley & Moore, 1983; Mauk *et al.*, 1995). The large number of interactions found in the NMR studies was considered as evidence for the dynamic nature of the complex.

Computer-aided docking and simulation studies have shown that the model can sample several conformations of comparable stability and in fact the interaction can be improved by allowing a degree of molecular flexibility (Wendoloski *et al.,* 1987; Northrup *et al.,* 1993). This need for flexibility is extrapolated to the initial association process in which electrostatics are also believed to influence orientation both prior to and during complexation. All these factors were introduced into Brownian simulations by Northrup *et al.* (1993) in an attempt to calculate second-order rate constants for the reduction of yeast ferricytochrome *c* (and mutants of) by trypsin-solubilised ferrocytochrome b_5 using semi-empirical means. Marcus theory was incorporated into the calculations with $\beta = 1.0$ Å^{-1}, $l = 0.7$ eV and $k_0 = 1.3 \times 10^{11}$ (for wild-type) but the significance of this aspect of the simulations is perhaps less relevant than the influence of Brownian motion itself. The reasonable correlation between theory and experiment achieved illustrates the necessity for motion to be accounted for in any theoretical assault on intermolecular electron-transfer. The most probable docking geometry predicted by Northrup *et al.* (1993) involved the b_2:*c*

interactions Glu44:Lys27, Glu48:Arg13, Asp60:Tmlys72 and b_2-haem-propionate:Lys27. However, they also predicted a low-energy structure similar to the Salemme model involving the interactions Glu44:Lys27, Glu48:Arg13, Asp60:Tmlys72 and b_2-haem:Lys79 in which the haem groups were only 8.4 Å apart (compared to 12 Å).

Rate constants for electron transfer within the pre-formed complex have been measured most successfully by Willie *et al.* (1992; 1993) at low ionic strength (1 mM phosphate) by photoexciting ruthenated solubilised-cytochrome b_5 (Durham *et al.*, 1995). Ru-65-cytochrome b_5 was created from the Thr65→Cys mutant by chemical reaction with 4-bromomethyl-4'-methylbipyridine$Ru(bpy)_2^{2+}$, which had little effect on the cytochrome *c* reductase ability of the enzyme, but placed the Ru^{II} complex close enough to achieve b_5-haem reduction at a rate of $12 \times 10^6 s^{-1}$. Willie *et al.* (1992) found that electron transfer to horse-heart cytochrome *c* occurred in two separate phases with rate constants of $4 \times 10^5 s^{-1}$ and $3.4 \times 10^4\ s^{-1}$. The rate constant for the slow phase was found to increase with increasing ionic strength and was considered to be limited by conformational changes. At higher ionic strengths the authors were able to recreate the data presented by Eltis *et al.* (1991) for the bimolecular reaction between native cytochrome b_5 and cytochrome *c* obtained using stopped-flow spectrophotometry. Willie *et al.* (1993) also measured the fast and slow electron transfer rate constants using yeast cytochrome *c* and obtained values of $1 \times 10^5\ s^{-1}$ and $1.8 \times 10^4\ s^{-1}$ which are slightly slower than those obtained using the horse-heart derivative. However, neither of substrates have particular physiological relevance to the form of cytochrome b_5 used.

Conclusions

It is clear from the two systems described above that the study of inter-protein electron transfer is dominated by the dynamics of complexion. Generation of a model complex is therefore fundamental to the understanding of such systems, although interpretations become strained when a model is adhered to implicitly. The transient/random nature of molecular collisions in solution would make formation of rigid/specific complexes inefficient and as such, electron transfer is likely to occur

from a variety of different conformations (Williams, 1989; McLendon & Hake, 1992). Furthermore, tight complexation would be unfavourable since rapid dissociation is physiologically as essential as rapid association. These conflicting factors must be balanced against the necessity for protein recognition.

This discussion is resumed in *Chapter 4* where the interaction between flavocytochrome b_2 and cytochrome *c* is considered.

CHAPTER 2

MATERIALS & METHODS

2.1. Site-Directed Mutagenesis (Dr F.D.C. Manson)

Site-directed mutagenesis was performed by the Kunkel method of non-phenotypical selection (Kunkel, 1985) to generate the A198G, L230A, A198G:L230A, L286A, I326A and L230A:I326A mutations (Daff *et al.*, 1994). The mutant sequences were transferred into the expression vector pDSb2 (Black *et al.*, 1989) by replacing the wild-type flavocytochrome b_2 coding sequence. Standard methods for growth of *E. coli*, plasmid purification, DNA manipulation and transformation were employed (Sambrook *et al.*, 1989).

2.2. Transformation of *E. coli*

5 to 10 ng of supercoiled plasmid DNA were added to 100 µl of competent *E. coli* cells (pre-treated with $CaCl_2$) in a 1.5ml microcentrifuge tube and left on ice for 30 minutes. The cells were then heat-shocked at 45°C for 90 seconds and returned to ice for 5 minutes. Luria broth (1 ml), was added to the cells, which were incubated at 37°C for 1 hour. The cells were then pelleted in a microfuge and resuspended in 100 µl of Luria broth. Aliquots (25 µl and 75 µl) were spread onto Luria agar plates containing 100 mgl^{-1} ampicillin (Sigma). The plates were incubated overnight at 37°C.

2.3. Growth of *E. coli*

Starter cultures of *E. coli* were grown in Luria broth (150 ml, see below) containing 50 mgl^{-1} carbenicillin at 37°C inoculated from single colonies on Luria agar plates (see below) using a sterile wire loop. A 1.5 ml aliquot from each culture was centrifuged generating a small pellet, the colour of which (red) was used as an indication of flavocytochrome b_2 over-expression in the bacteria. Larger pellets (from 50 ml of culture) were frozen in $N_{2(l)}$, lysed and used to test for L-lactate dehydrogenation activity i.e. active flavocytochrome b_2. This was characterised by the

ability of the lysis supernatent to catalyse the reduction of 1 mM ferricyanide by 10 mM L-lactate in Tris buffer solution, as indicated by the colour change (see *Section 2.7;* p59).

Litre flasks containing 500 ml of Luria broth and 50 mgl^{-1} carbenecillin were inoculated by sterile transfer of 250 µl aliquots of a 150 ml culture and grown overnight at 37°C in a shaker-incubator. Cells were harvested by centrifugation (5 min. at 28 000 g) in a Sorvall RC-5B centrifuge using a GSA head and stored at -20°C as frozen wet pellets prior to protein purification. A typical batch, harvested from 5 litres of culture, yielded approximately 20 g of cells (wet weight).

Luria broth (growth medium)

Tryptone (Difco Bacto)	10 gl^{-1}
Yeast extract (Difco Bacto)	5 gl^{-1}
NaCl	5 gl^{-1}

Luria broth was autoclaved in growth flasks and cooled to 50°C before addition of antibiotic via a sterile millipore filter:

Carbenecillin (Sigma)	50 mgl^{-1}

Luria agar plates

Luria broth	(above)
Agar (Difco)	15 gl^{-1}

The Luria agar solution was autoclaved and supplemented with carbenecillin (as above) and poured into sterile petri dishes before setting. Plate cultures were streaked out from starter cultures using a sterile wire loop and grown overnight at 37°C.

2.4. Purification of Flavocytochrome b_2

Cell lysis

Each batch of frozen cells was defrosted and snap-frozen in $N_{2(l)}$ before being suspended in approximately 200 ml of 0.1 M phosphate buffer pH 7 containing 5 mM L-lactate and 1 mM EDTA (see below). The presence of L-lactate ensures that the enzyme is maintained in its more stable reduced form on release from the cell and EDTA aids lysis by chelating Ca^{2+} ions as they are released from the cell membranes. Approximately 0.2 mgl^{-1} lysozyme (grade III, chicken egg white, Sigma) was added

and the suspension was stirred at 4°C for 1 hour. After lysis the cell debris was removed by centrifugation at 39 000 g for 10 min. (using SS-34 centrifuge head). If necessary the process was repeated to release more enzyme, and the resultant supernatents pooled.

Phosphate buffer (for flavocytochrome b_2 purification)

H_2O	750 ml	
L-lactate (Li salt, Sigma)	0.96 g	(5 mM)
EDTA (Na salt, Fisons)	0.74 g	(1 mM)
NaH_2PO_4 (0.2 M)	375 ml	
$NaHPO_4$ (0.2 M)	~625 ml	(→ pH 7)
H_2O	(→ 2 litres)	

Ammonium sulphate fractionation

The lysis supernatent was fractionated by addition of ammonium sulphate, utilizing the phenomenon of 'salting out'. By adding enough $(NH_4)_2SO_4$ to 35% saturate the solution a proportion of proteins was precipitated. This fraction was removed by centrifugation at 39 000 g and discarded. Further addition of $(NH_4)_2SO_4$, to take the total concentration to 70% saturated, caused precipitation of flavocytochrome b_2 within a second fraction of proteins. This precipitate was collected by centrifugation, and the supernatent fraction discarded.

At this point the enzyme activity was measured using a standard steady-state assay (*Section 2.7;* p59), to be used for assessing activity loss during purification.

Dialysis

Prior to column purification the enzyme pellets were collectively dissolved in a minimum volume of phosphate buffer and dialysed for 4 hours (or overnight) at 4°C against a 40-fold excess of half strength buffer under an N_2 atmosphere. Dialysis tubing (Sigma) with a molecular weight exclusion limit of 12 kDa was used to ensure that $(NH_4)_2SO_4$ and other small contaminants diffused out. Following dialysis the enzyme solution was centrifuged at 39 000 g for 10 min. to remove any aggregated protein.

Column purification

The flavocytochrome b_2 was further purified by column chromatography, which was conducted entirely at 4°C. The first column (DE-52) removes many contaminants, but does not bind flavocytochrome b_2 and is therefore a useful and rapid pre-treatment for purification on hydroxylapatite.

DE-52 ion exchange column. Whatman DE-52 ion exchange resin consists of diethyl-aminoethyl groups which are covalently cross-linked to a cellulose matrix. When equilibrated at pH 7 (as in this case) it forms a positively charged binding surface for negatively charged proteins. Equilibration was conducted by adjusting the pH of a suspension of the column material in phosphate buffer by addition of $HCl_{(dil)}$. After pouring, the column (20 x 2.5 cm) was further equilibrated by elution with two column volumes of buffer. The protein solution was loaded onto the column and elution with phosphate buffer continued. Unlike many of the contaminating proteins, flavocytochrome b_2 passes directly through this column, and was therefore collected as elution progressed and loaded directly onto the hydroxylapatite column. After use the DE-52 column material was regenerated by washing with 3x five column volumes of 1 M NaCl and re-used once.

At this stage, the purity of flavocytochrome b_2 was typically 10-25% based on the UV/Vis peak height ratio Abs(423 nm)/Abs(269 nm) for which 2 = 100%. This method uses the soret peak height to quantitate the amount of flavocytochrome b_2 and the UV peak height as a crude measure of total protein concentration (Pajot & Groudinsky, 1970).

Hydroxylapatite column. Hydroxylapatite (Bio-rad) consists of crystalline $Ca_{10}(PO_4)_6OH_2$ and is often used as the basis for association columns, in that it is able to bind proteins tightly. Since the column material is believed to interact with proteins via negatively charged phosphate groups it behaves in the opposite manner to the DE-52 column, binding neutral and positively charged species which can be eluted with an ionic strength gradient.

Hydroxylapatite was equilibrated by washing with 5 volumes of phosphate buffer, and poured to form a column 10 x 2.5 cm. The flavocytochrome b_2 was

directly loaded onto the column to which it bound, forming a tight band. After washing with 5 column volumes of buffer, the enzyme was eluted using a 0-10% gradient of ammonium sulphate and fractions were collected. All fractions containing pure flavocytochrome b_2 were pooled, and the enzyme was precipitated by addition of $(NH_4)_2SO_4$ up to 70% saturation. The precipitate was collected by centrifugation at 39 000 g for 10 min. and pellets stored under N_2 at 4°C. Under these conditions the enzyme retained activity for several days.

Enzyme storage

For short term storage (days) the above conditions proved to be adequate, however for long term storage the $(NH_4)_2SO_4$ pellets were dissolved in a minimum volume of Tris buffer pH 7.5 and passed down a Sephadex G25 column (15 x 1.5 cm, Sigma) equilibrated in the same buffer (see *Section 2.7*). Drops of the L-lactate free, oxidised enzyme (at a typical concentration of 200 μM) were then immediately snap frozen in $N_{2(l)}$ and stored at -194°C. In this state activity was retained indefinitely.

Sephadex G25 consists of cross-linked dextran and epichlorohydrin, the degree of crosslinking determining the size exclusion limit. G25 can be used for separation within the range 1000-5000 Mr, but is also used to separate very small molecules from large proteins. The protein band is fast-moving because such large molecules are excluded from the polymeric grains, whereas $(NH_4)_2SO_4$, free FMN, lactate, pyruvate etc are all contained within a slow moving band. The desalted protein fraction therefore consists only of pure protein in the required buffer.

2.5 SDS PAGE

SDS (sodium dodecyl sulphate) polyacrylamide gel electrophoresis was used to verify that the flavocytochrome b_2 protein chain remained intact throughout purification. Protein separation by molecular weight (Laemmli, 1970) should lead to a single band at 57.5 kDa for the intact enzyme. However, since flavocytochrome b_2 is prone to proteolytic cleavage within the loop region (Lederer & Simon, 1971), two

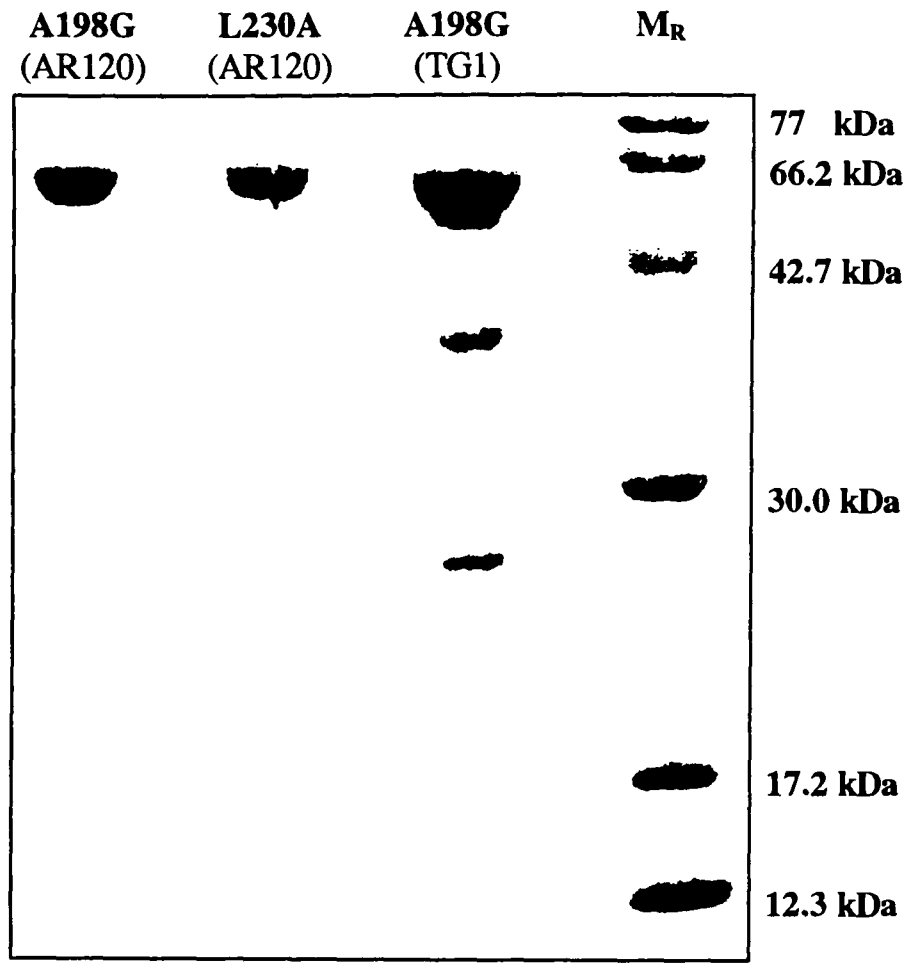

Figure 2.1 SDS PAGE of flavocytochrome b_2 mutant enzymes. The mutants A198G and L230A, prepared from two different bacterial strains (TG1 and AR120), are compared to standard molecular weight markers (M_R). The intact enzyme gives a single band at 57.5 kDa, whereas site-specific proteolysis within the loop region causes extra bands at 36 and 21 kDa, as observed in the TG1 preparation.

further bands at 36 and 21 kDa are sometimes observed. *Figure 2.1* illustrates this by comparing protein samples purified from different strains of *E. coli*. The A198G mutant prepared from the TG1 strain produces two bands clearly absent in preparations of L230A and A198G from the AR120 strain. This latter bacterial strain was used to express all the mutant enzymes discussed here since its proteolytic deficiencies are an obvious advantage.

Gel preparation

After mixing the resolving gel (see below), filtering and degassing, 50 µl N,N,N',N'-tetramethylethylene diamine (TEMED) was added and the gel poured between two plates. Water-saturated butanol was added to form a clean layer at the

top. The gel was left for 1 hour to set and the butanol layer poured off. The stacking gel was mixed in the same way and poured on top of the resolving gel, a comb was inserted to create sample wells. This was left to set for 30 minutes. The stacking gel helps to concentrate the protein samples before they are drawn into the resolving gel.

Resolving gel (10%; 30 ml)		
Protogel (30% acrylamide; 0.8% bis acrylamide)	10 ml	
4X resolving buffer	7.5 ml	
H_2O	12.3 ml	
10% Ammonium persulphate (Sigma)	190 µl	
The gel was filtered and degassed before addition of:		
TEMED (Sigma)	50µl	

Stacking gel (5%; 10ml)		
Protogel (30% acrylamide; 0.8% bis acrylamide)	1.6 ml	
4X stacking buffer	2.5 ml	
H_2O	5.9 ml	
10% Ammonium persulphate	30 µl	
The gel was filtered and degassed before addition of:		
TEMED	50µl	

Resolving buffer (4X)		
H_2O	750 ml	
Trisma base (Sigma)	181.6 g	
SDS (Sigma)	4 g	
HCl (conc.)	10 ml	(→ pH 8.8)
H_2O	~250 ml	(→ 1 litre)

Stacking buffer (4X)		
H_2O	400 ml	
Trisma base	30.3 g	
SDS	2 g	
HCl (conc.)	15 ml	(→ pH 6.8)
H_2O	~100 ml	(→ 0.5 litres)

Electrophoresis

The gel was clamped into a vertical electrophoresis tank which was filled with running buffer (see below). The comb was removed and samples injected into the

wells created. The gel was then run at 10 Vcm^{-1} (approximately 0.02 Amps) for 4 to 5 hours, until the dye front reached the end of the gel. After removal from the electrophoresis tank, the gel was stained overnight and then destained in three successive steps. To make a permanent copy the gel was dried to blotting paper under vacuum.

Sample buffer (2X)	
H_2O	80 ml
Tris/HCl pH 6.8 (1 M)	3.3 ml
SDS	2 g
Glycerol	9 ml
2-mercaptoethanol (Sigma)	5 ml
Bromophenol blue (1%, Sigma)	1 ml
Running buffer (5X)	
H_2O	500 ml
Trisma base	15.1 g
Glycine	94 g
SDS	2 g
HCl (1 M)	(→ pH 8.8)
Gel stain	
H_2O	375 ml
Isopropanol	125 ml
Acetic acid	50 ml
Coomassie brilliant blue (Sigma)	0.5 g

Destains		
1	25% Isopropanol	10% Acetic acid
2	10% Isopropanol	10% Acetic acid
3	-	10% Acetic acid

2.6 Western Blotting

Positive identification of a specific protein is possible by Western blotting which uses antibody raised against this particular protein. This primary antibody is then recognised by a secondary antibody which is conjugated to horse radish

peroxidase. Addition of peroxide and dianisidine results in the catalytic production of an orange dye identifying the correct protein band.

Western transfer

The protein bands from a fresh SDS PAGE were transferred onto a nylon membrane (Hybond-N) in a Western transfer tank. Firstly however the gel was soaked in transfer buffer for 2 minutes along with a sandwich containing 2 x 2 layers of 3 MM filter paper, the nylon membrane and foam sponge. The sandwich was then reconstructed with the gel on the negative side of the membrane and placed in the tank filled with transfer buffer (proteins migrate to the positive electrode). A corner was cut off the gel/nylon sandwich for later identification. A current of 1 Amp was passed through the sandwich for 2 hours.

The membrane was soaked overnight in 5% skimmed milk powder/Tris-buffered saline and then placed in 20 ml of 2% skimmed milk/TBS. The anti-flavocytochrome b_2 polyclonal antibody from rabbit (30 µl) was added and the membrane incubated for 2 hours. After washing four times in 100 ml Tris-buffered saline the membrane was placed in fresh 2% skimmed milk/TBS and the secondary antibody added (10 to 20 µl).

Western transfer buffer	
Tris/HCl pH 8.3 (1 M)	250 ml
Glycine	112.6 g
H_2O	(→ 1 litre)
Tris-buffered saline (TBS)	
Tris/HCl pH 7.5 (1 M)	10 ml
NaCl	8.78 g
H_2O	(→ 1 litre)

Developing the Western blot

After incubation with the secondary antibody (goat, anti-rabbit, IgG; Scottish Antibody Production Unit) the membrane was washed thoroughly and developed in 10 ml of developing solution (see below). Once the orange band appeared the

membrane was rinsed in distilled water and left to dry. The membrane was photographed to preserve the image.

Developing solution	
Dianisidine (5 $mgml^{-1}$, Sigma)	0.5 ml
Imidazole (0.1 M, pH 7.4, Sigma)	1 ml
H_2O_2 (30%)	0.1 ml
H_2O	8.5 ml

2.7. Steady-State Kinetics

Initial velocity steady-state assays were conducted on a Beckman DU 65 or Shimadzu 2101PC spectrophotometer by monitoring the consumption of electron acceptor with time. It should be noted therefore that since two electrons are produced per substrate molecule consumed, the rate constants quoted throughout this thesis should be halved if required in terms of substrate.

Standard absorption changes for electron acceptors

	λ	Δε	
Ferricyanide (K salt, BDH)	420 nm	1 010	
Cytochrome *c* (horse heart, Sigma)	550 nm	22 640	(Hazzard *et al.*, 1986)

All steady state experiments were performed at 25.0°C in Tris/HCl buffer pH 7.5, *I* 0.10. Catalytic amounts of flavocytochrome b_2 were used to initiate each assay by addition via a syringe of a typical volume of 10 to 25 µl to 3 ml of reaction solution (in a 1 cm cuvette). The concentration of enzyme added was determined by the absorbance of the soret peak at 423 nm (for reduced flavocytochrome b_2, ε = 183 000; Pajot & Groudinsky, 1970). All substrate solutions were prepared by dissolving an appropriate amount of the acid in Tris buffer and titrating to pH 7.5 by addition of $NaOH_{(dil)}$. Chirally pure (S)-2-hydroxy- long-chain acids were obtained from Oxford Asymmetry Ltd (Oxford), DL-substrates were obtained from either Sigma or Aldrich chemical companies (see *Table 5.1*).

Tris buffer (pH 7.5, *I* 0.10; for steady-state and stopped-flow kinetic experiments)

H_2O	750 ml
NaCl	5.26 g
HCl (1 M)	10 ml
Trisma base	(→ pH 7.5)
H_2O	(→ 1 litre)

The Michaelis-Menten equation

All steady-state initial-rate data was analysed by non-linear least-squares regression using the Michaelis Menten equation. Curve fitting was conducted using the PC based software, Origin (Microcal). The Michaelis Menten equation applies for an enzyme catalysed reaction in which substrate binding is rapid and reversible and where product formation is rate determining.

Michaelis Menten Equation

$$v = \frac{k_{cat}[S][E_0]}{[S] + K_m}$$

v	reaction velocity
$[S]$	substrate concentration
$[E_0]$	total enzyme concentration
k_{cat}	rate constant at substrate saturation
K_m	substrate dissociation constant

Preparation of L-2-^{2}H-lactate

^{2}H-kinetic isotope effects were determined in the steady-state by conducting parallel experiments with ^{1}H- and ^{2}H-L-lactate. The latter was prepared enzymatically by the method of Shapiro & Dennis (1965). In this reaction the production of L-lactate by beef-heart lactate dehydrogenase (LDH) is coupled to the dehydrogenation of hexadeuterated ethanol by yeast alcohol dehydrogenase via the hydride reduction/oxidation of NAD/NADH. The reaction mixture (see below) was incubated at 37°C for 24 hours with shaking before being heated briefly at 75°C to stop the reaction.

L-2-^{2}H-lactate synthesis reaction mixture

Pyruvate (Na salt, Sigma)	0.385 g	(70 mM)
NAD (Sigma)	30 mg	
Phosphate buffer (10 mM)	50 ml	(→ pH 7)
Hexadeuterated ethanol (Sigma)	1 ml	
ADH (yeast, Sigma)	2 mg	
LDH (beef heart, Sigma)	12 mg	

The L-2-^{2}H-lactate solution was loaded onto a Dowex 1 x 8-200 column (15 x 2.5 cm) equilibrated with water and fractions were collected as it was washed with a column volume of water. Since the resin is strongly basic in nature it binds the negative lactate and pyruvate molecules. These were eluted in a gradient of formic acid (0-0.36 M). Lactate fractions were collected first (pKa = 3.73) followed by pyruvate (pKa =3.39). All fractions were tested for lactate by observing decolouration of a ferricyanide/flavocytochrome b_2 solution, and also for pyruvate by using a pyruvate diagnostic kit (Sigma). The lactate containing, pyruvate free samples were pooled and concentrated on a high vacuum rotary evaporator to approximately 5 ml which were diluted into Tris buffer solution. The stock concentration was then determined by introducing a known volume to an assay containing 1 mM ferricyanide and a catalytic amount of flavocytochrome b_2 while monitoring the absorbance change at 420 nm.

2.8 Determination of FMN content

Dissociation of flavin mononucleotide from flavocytochrome b_2 is a common cause of activity loss. Therefore each mutant characterised was examined for this phenomenon by separating and quantifying the FMN and haemoprotein fragments. Approximately 10 mg of enzyme was dissolved in a minimum amount of 10 mM CAPS buffer, pH 11, *I* 0.1 (see below) and eluted through a sephadex G-25 column (1 x 15 cm) equilibrated in the same buffer. The red (haemoprotein) and yellow (FMN) fractions were collected as separate bands and diluted to exactly 10 ml and 5 ml respectively. The concentrations of these two solutions were then calculated from known standard absorption coefficients: Abs.(450 nm) = 12 500 for FMN (Dawson et al., 1987) and Abs. (413 nm) = 121 500 for the deflavo-enzyme (Pajot & Groudinsky,

---

CAPS buffer (pH 11, *I* 0.10)

H_2O	750 ml
NaCl	5.26 g
NaOH (1 M)	10 ml
CAPS (Sigma)	(→ pH 11)
H_2O	(→ 1 litre)

1970). During this entire procedure the FMN fraction was shielded from all light by foil-wrapping both column and containers. This precaution was taken to prevent the rapid photo-decomposition of FMN known to occur at high pH.

2.9 Stopped-Flow Spectrophotometry

All stopped-flow experiments were conducted on an Applied Photophysics SF.17 Micro Volume stopped-flow spectrofluorimeter path-length 1 cm at single wavelengths specified for each experiment. Enzyme samples were always oxidised and desalted on a Sephadex G25 column equilibrated in 10 mM Tris/HCl buffer pH 7.5, *I* 0.10 (Section 2.4). Generally, all reacting solutions were also made up in this buffer and maintained at 25.0 ±0.1°C during each experiment. All data were analysed using both the instrument's software and Origin (Microcal).

Introduction

Stopped-flow spectrophotometry involves the rapid mixing of two equal volume solutions within a spectrophotometric cell of fixed path length. On mixing, the instrument is immediately triggered to record the absorbance of the reacting solution and to generate a 'trace' with a specified time-base. The resolution of the instrument is limited by its dead-time, a value which is derived by calculating the time difference between the point at which the reaction can be traced back to (time = 0) and the point at which absorbance is actually recorded (t = dt). The dead-time can be measured by recording any single exponential reaction over which the total absorbance change is known. The dead-time for the Applied Photophysics instrument is estimated to be 0.9 to 1.1 ms. However resolution is also impaired by the mixing time, a value which is more difficult to quantify. Once the two solutions are in the reaction chamber observation will begin, but until mixing is complete the reaction will not be up to full speed and a lag will be observed. This phenomenon, as well as the dead-time itself, will depend on the physical attributes of the reacting solutions, including temperature and viscosity. Generally, reactions occurring faster than 1000 s^{-1} are impossible to resolve and, depending on the dead-time, a significant percentage of the absorbance change is lost.

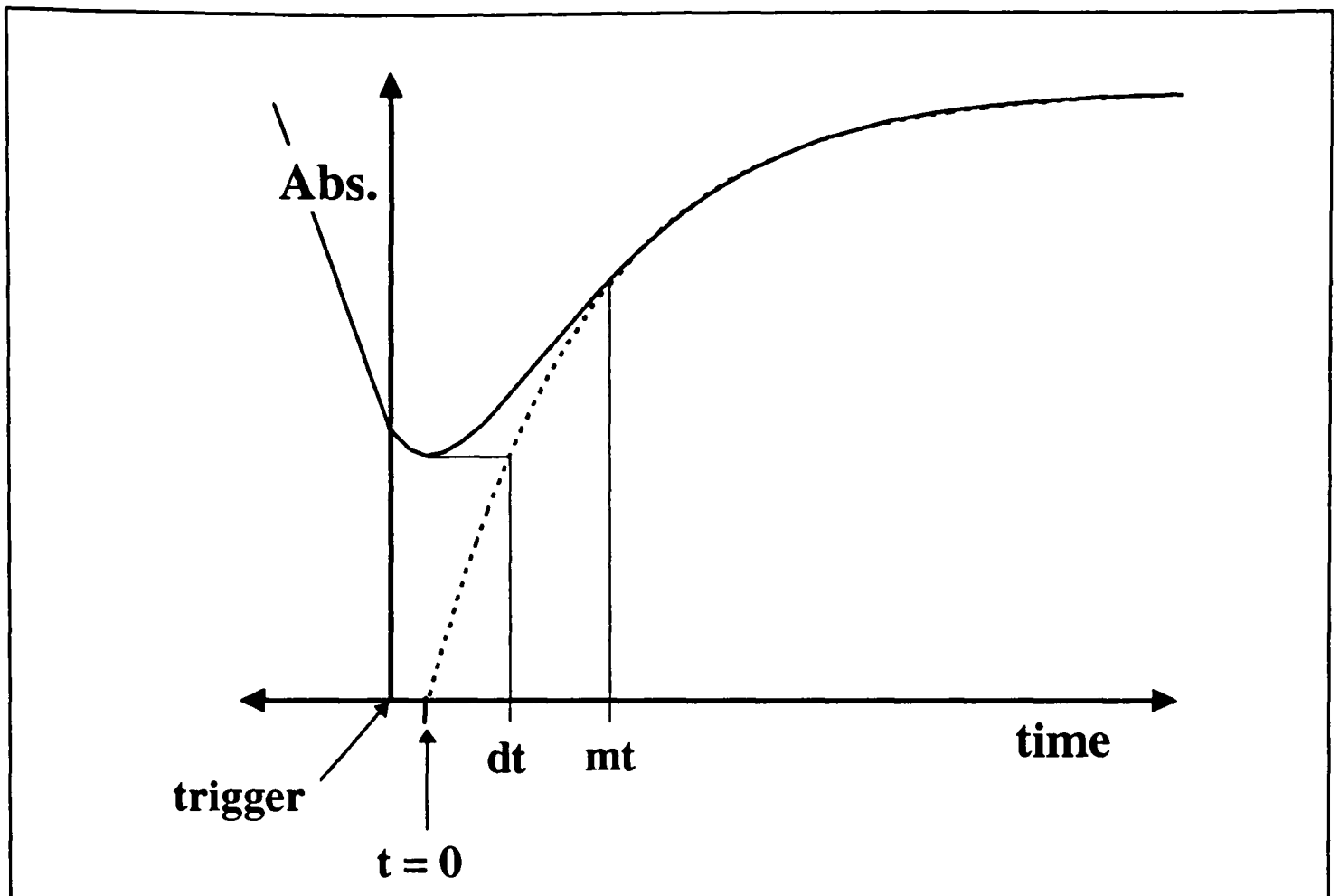

Figure 2.2 An example of a stopped-flow trace (absorbance vs time), fitted to a single exponential function ------- to illustrate the quantities dead-time (dt), mixing time (mt), the zero time point (t = 0) and the trigger point where observation begins.

Flavocytochrome b_2 reduction

Enzyme reduction by substrate was monitored in two separate experiments by observing FMN and b_2-haem reduction at the appropriate wavelengths. FMN reduction was observed at the b_2-haem isosbestic point of 438.3 nm and b_2-haem reduction at 557 nm where FMN absorbance is essentially zero. When conducted in the presence of Zn-cytochrome c, this was introduced by pre-mixing with the oxidised enzyme.

b_2-haem re-reduction

In addition to monitoring b_2-haem reduction as a component of total enzyme reduction, it was also followed during rapid oxidation by cytochrome *c* at the cytochrome *c* isosbestic of 408.4 nm. For this experiment the enzyme was pre-reduced with 20 mM L-lactate before stopped-flow mixing with a substoichiometric amount of cytochrome *c*. Typical concentrations after mixing were 20 μM

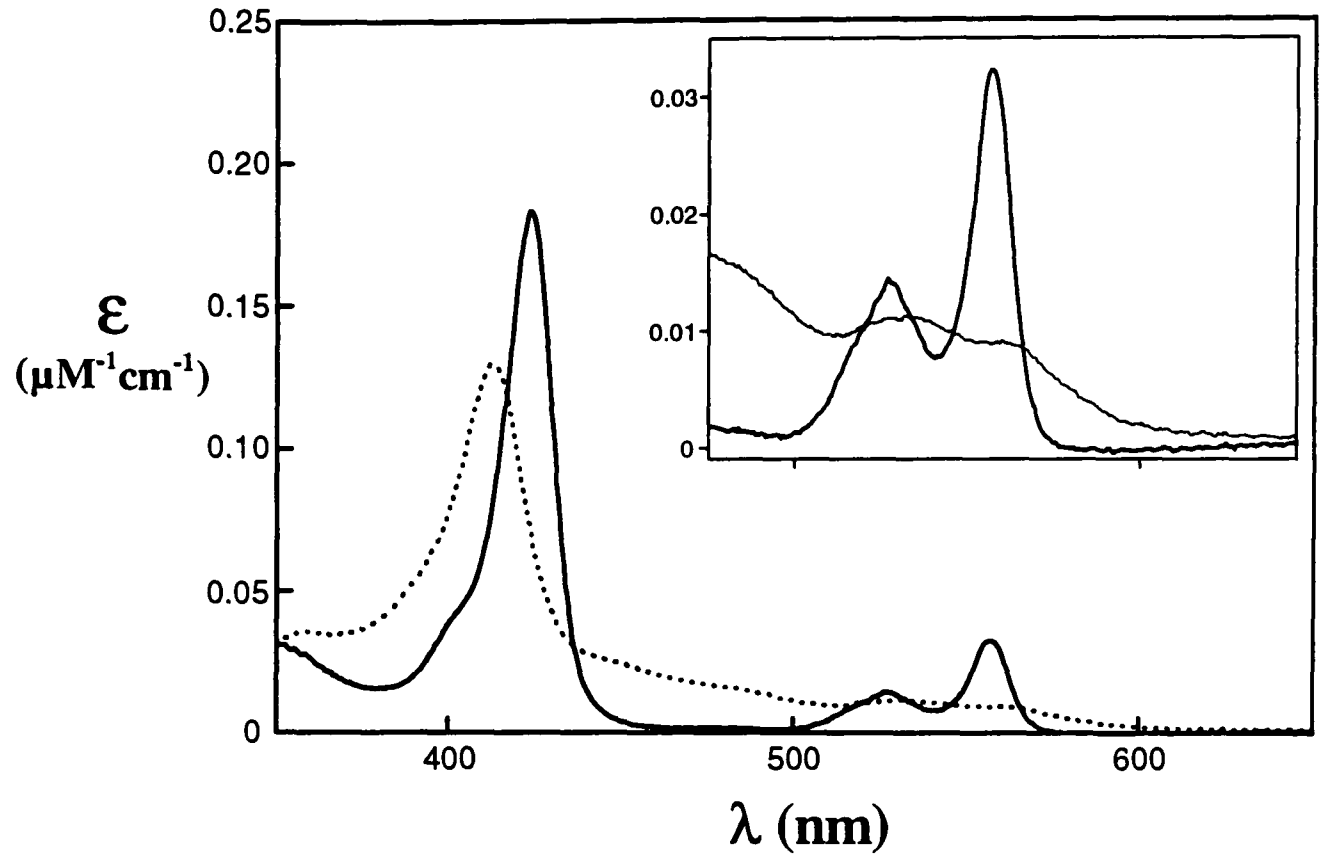

Figure 2.3 Visible absorption spectra of flavocytochrome b_2: reduced —— ; oxidised ····· and inset: the α and β bands shown on an expanded scale.

	λ (nm)	ε ($M^{-1}cm^{-1}$)	
oxidised	413	129500	(Pajot & Groudinsky, 1970)
reduced	423, 557	183 000, 30 900	"
isosbestic	544.8		(Janot *et al.*,1990)
isosbestic (b_2-haem)	438.3		

flavocytochrome b_2 and 4μM cytochrome *c*. Since at this concentration of flavocytochrome b_2 cytochrome *c* reduction happens too fast to be observed by stopped-flow spectrophotometry, b_2 haem reduction by the flavin hydroquinone can be observed more directly.

Flavin oxidation

FMN oxidation by an excess of cytochrome *c* was monitored at the b_2-heme isosbestic wavelength of 438.3 nm, where standard absorption coefficients for the various redox states have been previously determined to be approximately 1200, 3000 and 10 000 ($M^{-1}cm^{-1}$) for reduced, semiquinone and oxidized respectively (Capeillère-Blandin, 1991). Flavocytochrome b_2 was initially reduced by 1 mM glycolate, a poor substrate with maximum turnover rate of 3.5 moles substrate.s^{-1}, in order to prevent rapid re-reduction of the enzyme. Since 438.3 nm is not an isosbestic for cytochrome

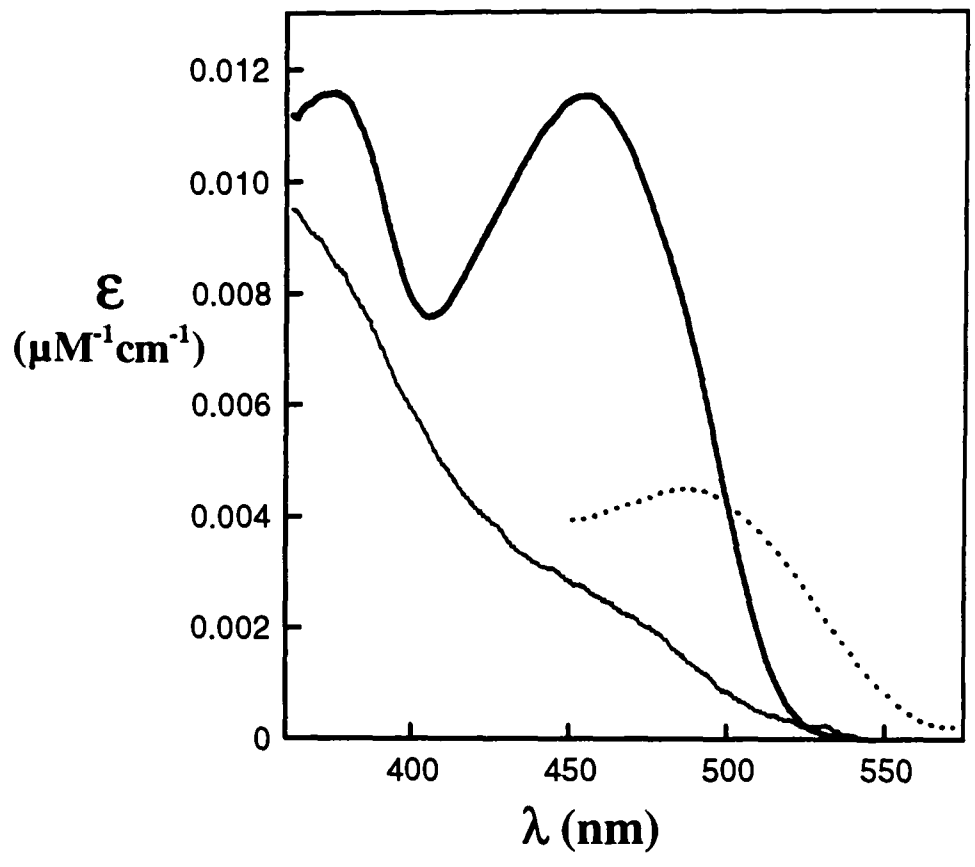

Figure 2.4 Visible absorption spectra of flavocytochrome b_2 flavin domain: —— oxidised; —— reduced with L-lactate; ····· an estimation of the semiquinone spectrum as adapted from the L-lactate monooxygenase from *Mycobacterium smegmatis* (Ghisla & Massey, 1990). ε (453 nm) = 11 100 $M^{-1}cm^{-1}$ (Iwatsubo *et al.*, 1977).

c, its absorbance contribution at this wavelength was subtracted. This was achieved by generating a cytochrome *c* reduction trace at the b_2-heme/FMN isosbestic of 544.8 nm (Janot *et al.*,1990). A pure FMN trace could be produced according to Absorbance(438.3 nm) + 107%[Absorbance(544.8 nm)]. Typical concentrations used were 10 μM flavocytochrome b_2 and 80 μM cytochrome *c* (after mixing). The traces were collected using a split time-base and the period of slow turnover, dependent on glycolate oxidation was used to determine the addition percentage used above. During a true steady-state period the absorbance of the FMN will be constant, and therefore the modified trace should be flat. In addition, once all the cytochrome *c* has reacted, the enzyme is reduced by the excess of glycolate and should therefore return to its original absorbance. Bearing these facts in mind the value was derived by inspection. Once modified, the fast phase of each trace, representing the time course for flavin oxidation and occurring largely within the first 100 ms, was fitted to a single exponential function.

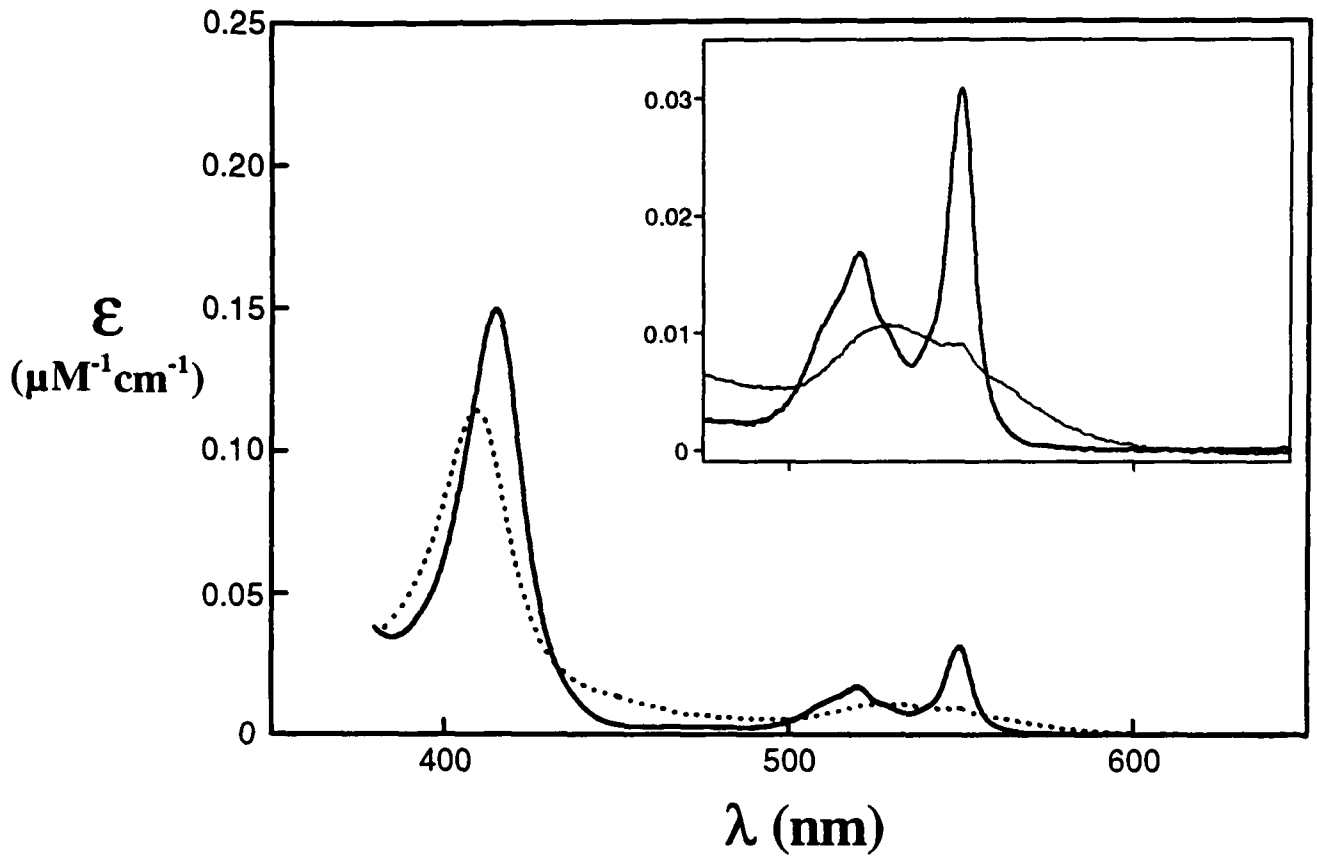

Figure 2.5 Visible absorption spectra of horse-heart cytochrome *c*: reduced —— ; oxidised ····· and inset: the α and β bands shown on an expanded scale.

	λ (nm)	ε ($M^{-1}cm^{-1}$)	
oxidised	550	8 160	(Hazzard *et al.*, 1986)
reduced	550	30 800	
isosbestic	408.4		

Inhibition of FMN oxidation by pyruvate was studied by introducing a range of different concentrations (0 to 50 mM) via the cytochrome *c* syringe. The kinetic analysis was then carried out as described above.

Cytochrome *c* reduction

Cytochrome *c* reduction by pre-reduced flavocytochrome b_2 was monitored at 416.5 nm, a flavocytochrome b_2-heme isosbestic point. To ensure that the reduction occurred under pseudo-first-order conditions, flavocytochrome b_2 was always present in excess. Reduction was carried out over a range of flavocytochrome b_2 concentrations, typically 2-15 μM. The cytochrome *c* concentration was 1 μM after mixing. The traces were fitted to monophasic exponentials by non-linear regression analysis. At least five runs were performed at each flavocytochrome b_2 concentration.

Throughout each set of experiments involving ionic strength variation, L-lactate was added to the flavocytochrome b_2 solution to a concentration of 2 mM (before mixing), to fully reduce the enzyme. Over the time scale of the experiment (5 mins) no autooxiadation of the enzyme occurred and it remained fully reduced. For all other experiments the L-lactate concentration was 10 mM after mixing.

Inhibition of cytochrome *c* reduction

Pre-steady-state cytochrome *c* reduction was inhibited by the introduction of ferro- or zinc-substituted cytochrome *c* into the flavocytochrome b_2 solution. A typical concentration range would be 0 to 100 μM (after mixing). In order to compensate for the larger absorbance of the solution this experiment was conducted at 544.8 nm (a flavocytochrome b_2 isosbestic point), and the concentration of oxidised cytochrome c was increased to 2 μM (after mixing). Inhibition was followed at a single flavocytochrome b_2 concentration, approximately 8 μM, where rates were well within the range for accurate stopped-flow determination and concentration was significantly in excess of stoichiometric.

2.10 Preparation of Zinc-Substituted Cytochrome *c*

Porphyrin cytochrome *c* was prepared essentially as described by Vanderkooi & Erecinska (1975). Approximately 100 mg freeze dried horse-heart cytochrome *c* (Sigma) was placed in an open PTFE test tube and cooled in liquid nitrogen. HF gas was then condensed onto the cytochrome *c* while stirring with a PTFE rod. The HF was generated by bubbling nitrogen gas through a HF-saturated pyridine solution (Sigma) contained in a sealed PTFE vessel, the only exit from which lead directly to the cytochrome *c* via a length of PTFE tubing. This apparatus was contained within a well ventilated fume hood. Once the cytochrome *c* was covered entirely by solid HF, the flow was stopped and reaction tube removed from liquid nitrogen. While stirring, the HF was evaporated in a steady stream of nitrogen gas. The flakey purple residue was dissolved in approximately 5 ml 0.1 M phosphate buffer pH 8 to neutralise any remaining HF, and acidified to pH 4 with 30% acetic acid. The purple solution was

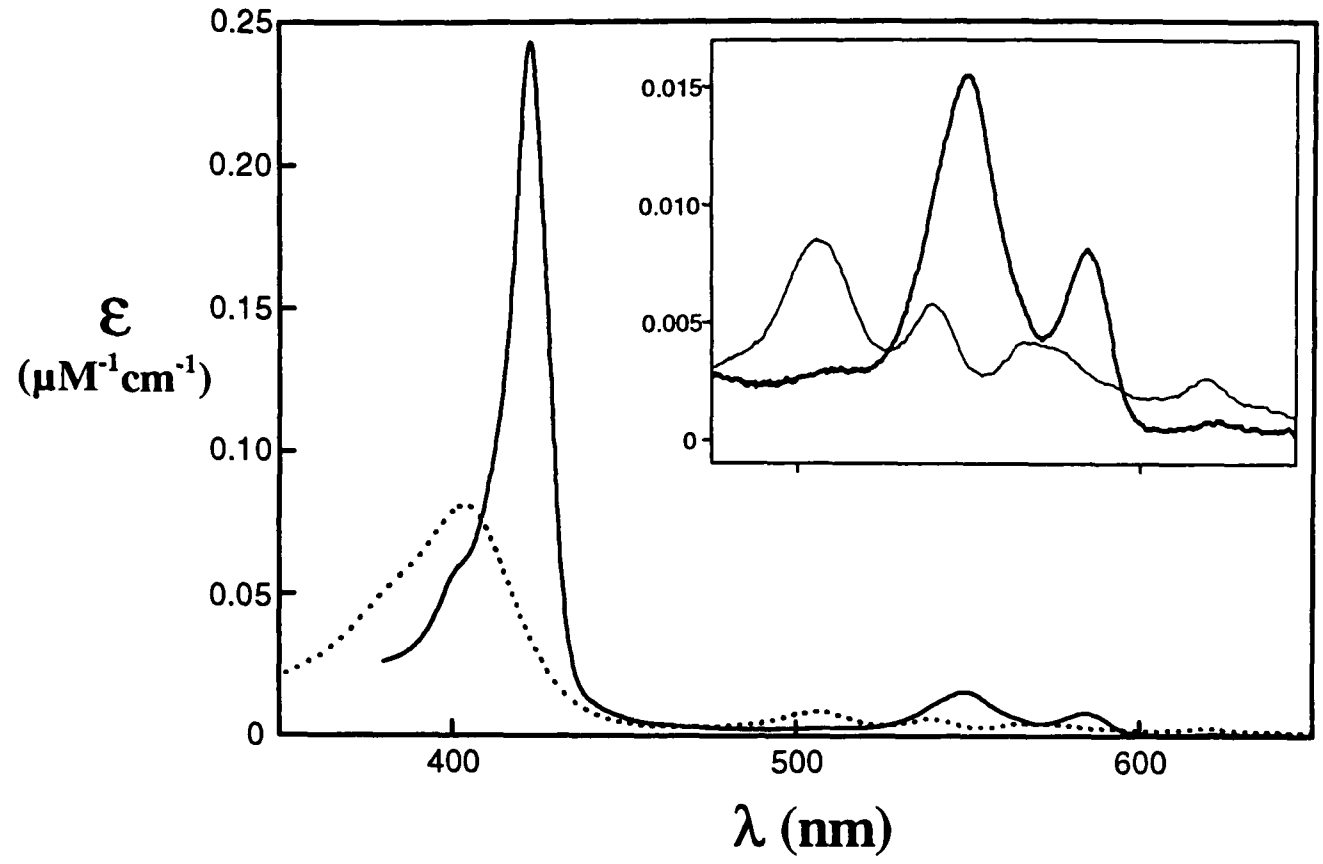

Figure 2.6 Visible absorption spectra of zinc-substituted cytochrome *c* (——) and porphyrin cytochrome *c* (·····). Inset: the α and β bands shown on an expanded scale.

	λ (nm)	ε ($M^{-1}cm^{-1}$)	
Zn-cytochrome c	423	243 000	(Vanderkooi *et al.*, 1976)
porphyrin-cyt c	404	81 000	

then purified by eluting down a G25 column 30 x 2 cm equilibrated in 20 mM phosphate acidifed to pH 4 with acetic acid. This step was conducted at 4°C in a foil wrapped column. Porphyrin cytochrome c was collected as the major purple band.

Freshly made porphyrin cytochrome *c* was converted entirely to zinc-substituted cytochrome *c* as described by Vanderkooi *et al.*, (1976). The fraction taken from the column was acidified to pH 2.5 with 30% acetic acid and a 10-fold excess of $ZnCl_2$ was added before incubating at 50°C in the dark for 1 hour. Aliquots were removed during this time period and the conversion of porphyrin cytochrome c to zinc-substituted cytochrome c was monitored spectrophotometrically (*Figure* 2.6). The Zn-cytochrome *c* was dialysed for 3 hours at 4°C in the dark against 2 litres each of: pH 3 acetic acid, water and 10 mM phosphate pH 7.4. It was then applied to an amberlite CG-50 column (1 x 5 cm; Sigma) equilibrated in the same buffer and eluted with 0.5 M phoshate buffer pH 7.4. This was then dialysed for 3 hours at 4°C in the

dark against 2 litres each of 20 mM phosphate pH 7.4, water and 10mM Tris/HCl buffer pH 7.5 *I* 0.10. The Zn-cytochrome c was then concentrated using Centricon tubes (Amicon) to approximately 250μM and aliquots were snap frozen in $N_{2(l)}$ and stored at -20°C. Concentrations were calculated from previously reported extinction coefficients (Vanderkooi *et al.*, 1976).

***Phosphate buffer, molarity* x, *pH* y.**		
	KH_2PO_4 (x M)	
	K_2HPO_4 (x M)	(→ pH y)
Amberlite CG-50 equilibration		(Margoliash & Walasek, 1967)
step 1		
	NaOH (2 M)	2 x 8 volumes
	H_20	5 x 8 volumes
	HCl (2 M)	2 x 8 volumes
	H_20	5 x 8 volumes
	repeat	
step 2		
	acetone	5 x 8 volumes
	H_20	10 x 8 volumes
	repeat step 1 twice, ending in Na^+ form.	
step 3		
	H_20	10 x 8 volumes
	equilibrate at pH 8 using H_3PO_4 (1.5 M) with 5-6 hours stirring.	
step 4		
	H_20	2 volumes
	suspend in 2 volumes 20 mM phosphate pH 8 and check pH	
	if necessary repeat step 3.	

2.11 Rapid-Freezing Quenched-Flow EPR

Rapid-freezing quenched-flow EPR was performed in 10 mM MOPS (morpholinopropanesulphonic acid, Sigma)/KOH buffer pH 7.5 adjusted to *I* 0.10 by addition of NaCl (see below). For each experimental data point, 1 ml reaction mixture containing 470 μM oxidized cytochrome *c*, 20 μM flavocytochrome b_2 and 10 mM L-lactate was generated by a rapid mixer, forced through a variable length of HPLC steel tubing before being sprayed into a bath of isopentane (Probalo), maintained at -140°C by a liquid nitrogen cooled cryostat (Moodie *et al.*,1990). In order to vary the

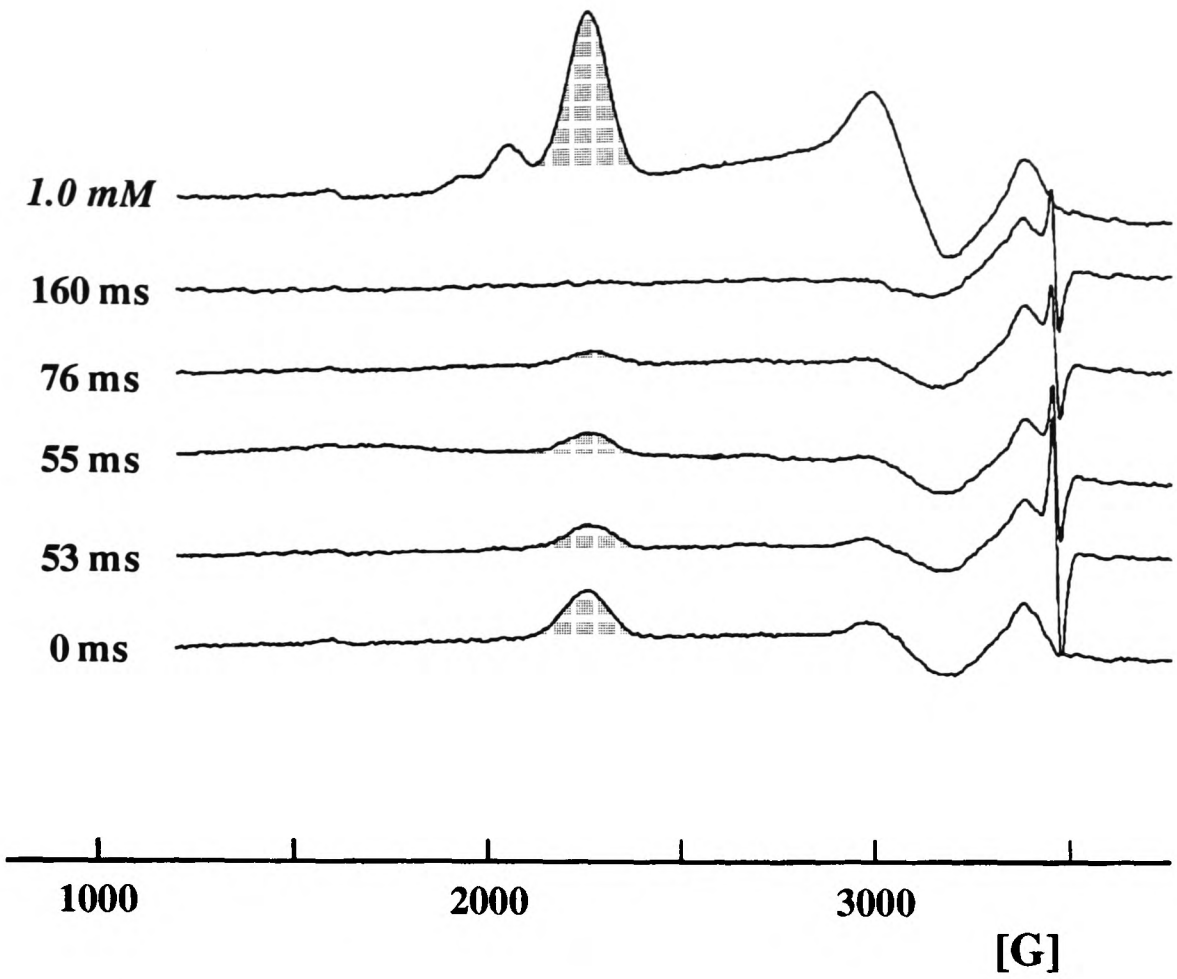

Figure 2.7 EPR spectra recorded at -270°C of freeze-quenched samples showing the steady-state reduction of 470 μM cytochrome *c* catalysed by 20 μM flavocytochrome b_2 in a solution containing 10 mM L-lactate. Ferricytochrome *c* concentrations were calculated at different time-points relative to the 1 mM standard (top) by integrating the shaded peak. The derivative at ~3500 G results from the presence of FMN semiquinone (see *Figure 3.10;* p94).

time-base for the experiment, different lengths of steel tube were used, to allow different degrees of aging. The frozen reaction mixture was then packed into an EPR tube and stored in liquid nitrogen.

All EPR measurements were performed on a Bruker instrument by Dr W.J. Ingledew, University of St. Andrews. Integrals were calculated for the FMN semiquinone signal at -194°C, and for the ferricytochrome *c* signal at -270°C (*Figure* 2.7). These were corrected for packing with respect to a standard ferricytochrome *c* sample produced in an identical way but in the absence of flavocytochrome b_2. The ferricytochrome *c* integrals were used to calibrate the time-base for the data by fixing them to a spectrophotometrically collected cytochrome *c* trace which had been

adjusted to account for the higher concentration of flavocytochrome b_2 and faster reaction rate observed in the quenched-flow experiment (see *Figure 3.11*).

MOPS buffer (pH 7.5, *I* 0.10; for quenched-flow EPR)

H_2O	750 ml
NaCl	5.26 g
KOH (1 M)	10 ml
MOPS (Morpholinopropanesulphonic acid, Sigma)	(→ pH 7.5)
H_2O	(→ 1 litre)

CHAPTER 3

THE CATALYTIC CYCLE

3.1 Introduction

The model

The catalytic cycle for flavocytochrome b_2 is illustrated in *Figure 1.14* (p28) in terms of its component electron-transfer processes. This provides a convenient frame of reference for experiment since each electron transfer corresponds to a change in the visible absorption spectrum. It is important to note however that the rate-determining factor in each electron transfer step may be dependent on a chemical or conformational change directly preceding the electron transfer, as such, the observed colour changes serve only as convenient observation points. A multi-faceted kinetic approach has been used to observe each individual step under various different circumstances. This has lead to the derivation of a self-consistent model for the

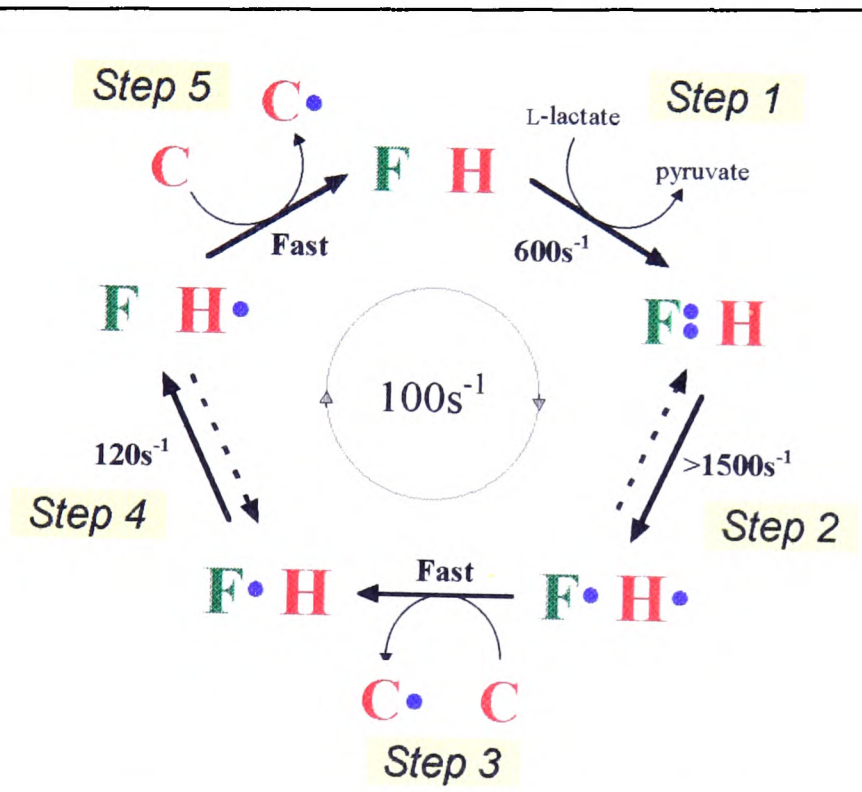

Figure 3.1 The kinetic model derived for the catalytic cycle of flavocytochrome b_2 based on individual electron-transfer steps (compare to *Figure 1.14* p28). The action of a single subunit of the enzyme is described as it turns over at its maximum rate of ~100 s^{-1} in the presence of saturating amounts of L-lactate and ferricytochrome *c* at 25°C in Tris/HCl buffer pH 7.5, *I* 0.10. Two equivalents of cytochrome *c* are reduced in each turnover so in these terms the k_{cat} is 207 (±10) s^{-1} (Miles *et al.*, 1992). *Step 1*: Reduction of FMN to its hydroquinone form, and oxidation of L-lactate to pyruvate. *Step 2*: Inter-domain electron-transfer from fully reduced FMN to b_2-haem, generating reduced haem and FMN semiquinone. *Step 3 & 5*: Binding and reduction of ferricytochrome *c* by b_2-haem (see *Chapter 4*). *Step 4*: Inter-domain electron-transfer from FMN semiquinone to b_2-haem.

catalytic cycle (*Figure 3.1*).

Flavocytochrome b_2 catalyses L-lactate dehydrogenation and cytochrome *c* reduction at a rate of 207 (±10) s^{-1} per electron transferred (Miles *et al.*, 1992). Since two equivalents of cytochrome *c* are reduced for every revolution of the cycle, the turnover rate is approximately 100 s^{-1}. However, this only applies when the concentrations of both ferricytochrome *c* and L-lactate are at saturation. The K_m for the former was determined to be 10 (±1) μM and for the latter to be 0.49 (±0.05) mM (Miles *et al.*, 1992).

The component steps

Step 1 represents the reduction of FMN by L-lactate, which probably proceeds via hydride transfer (see *Section 1.6;* p15). It has been studied previously using stopped-flow spectrophotometry (Miles *et al.*, 1992) and the rate constant reported to be 604 (±60) s^{-1}. This rate constant is 6-fold greater than that for overall turnover and for this reason FMN reduction should contribute little towards limiting the rate of turnover, provided the concentration of L-lactate remains saturating. By using 2-^{2}H-L-lactate, Miles *et al.* (1992) also discovered a ^{2}H-kinetic isotope effect of 8.1 (±1.4) on α-H abstraction. The magnitude of this value suggests that during the process of FMN reduction, α-H abstraction is entirely rate-limiting. This work confirmed the previous study of Pompon *et al.* (1980) and Capeillère-Blandin *et al.* (1975), who conducted similar experiments on the 'cleaved' form of the enzyme (see *Section 1.1*).

Steps 2 and *4* are inter-domain electron-transfer processes which are distinctly different. The first involves electron transfer from FMN hydroquinone and the second from FMN semiquinone. Both are expected to be equilibrium processes, although during normal turnover, the rapid reaction between b_2-haem and cytochrome *c* (which is essentially irreversible) prevents the reverse reactions.

Capeillère-Blandin *et al.* (1975), using the 'cleaved' form of the enzyme and later the *H. anomala* enzyme (Capeillère-Blandin, 1991), observed a lag-phase, corresponding to *Step 2* of the catalytic cycle, when monitoring the pre-steady-state reduction of flavocytochrome b_2 by L-lactate. In general, the lag-phase is manifested as a small difference in timebase between the traces for reduction of flavin and b_2-haem (this effect was also noted for the intact *S. cerevisiae* enzyme; Miles *et al.*,

1992; and is examined further in *Section 3.2a*). Full, three-electron reduction of flavocytochrome b_2 is complicated by the necessity for inter-subunit electron transfer and the disproportionation of flavin semiquinones. Capeillère-Blandin (1975) and Pompon (1980) present elaborate models which simulate the observed kinetics.

Intramolecular electron transfer from flavin semiquinone to b_2-haem (*Step 4;* see *Section 3.2c;* p82) has proved more difficult to observe. Previous attempts to rationalise the flavocytochrome b_2 catalytic cycle have therefore relied upon simulation and assumption (Capeillère-Blandin, 1991; Pompon *et al.*, 1980). Tegoni *et al.* (1984a) used a T-jump method to create transient displacements in the redox equilibrium (using the *H. anomala* enzyme) and obtained a rate constant of 160 (±40) s^{-1} at 16°C. However, the authors considered a value of 225 s^{-1} to be more in line with the observed steady-state rate constant. Both *Step 2* and *Step 4* for the *S. cerevisiae* enzyme have recently been examined in laser flash photolysis experiments. For *Step 2* a rate constant of 1900 s^{-1} was observed at 24°C (Walker & Tollin, 1991), but no process corresponding to *Step 4* could be observed in the absence of pyruvate. In contrast, Tegoni *et al.,* (1984a & b) showed that pyruvate stabilises the flavin semiquinone of the *H. anomala* enzyme and inhibits the electron transfer to b_2-haem. This effect is considered in *Section 3.2(d),* p88.

It should be noted at this stage that kinetic parameters determined for *H. anomala* flavocytochrome b_2 deviate considerably from those determined for *S. cerevisiae* flavocytochrome b_2. Further, the 'cleaved' form of the *S. cerevisiae* enzyme, used in earlier studies, has a lower specific activity than the intact form and therefore cannot be compared quantitatively (Lederer, 1991). Qualitative comparisons are nevertheless valid, since all three enzymes follow similar catalytic mechanisms.

Steps 3 and 5 both represent electron transfers from the b_2-haem to cytochrome *c,* while also involving binding and dissociation processes. A full characterisation of the interaction between flavocytochrome b_2 and cytochrome *c* is included in *Chapter 4,* but it is apparent that the contribution of *steps 3* and *5* to rate limitation of normal catalytic turnover is negligible, provided that the concentration of cytochrome *c* is saturating.

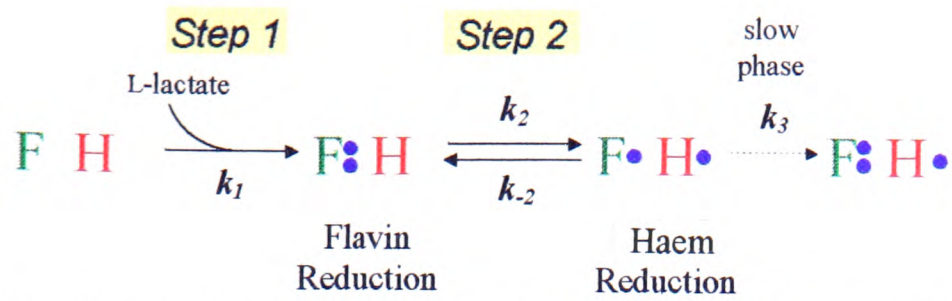

Figure 3.2 The individual electron-transfer steps leading to the reduction of flavocytochrome b_2 by L-lactate. Steps 1 & 2 form part of the catalytic cycle, whereas the third step is a composite process involving inter-subunit electron transfer.

(see *Figure 1.14;* p28, for legend)

3.2 Results

3.2(a) Flavocytochrome b_2 Reduction

Stopped-flow reduction of flavocytochrome b_2 by L-lactate is an ideal way to monitor *Step 1* of the catalytic cycle. Miles *et al.* (1992) determined rate constants for this process by monitoring FMN reduction at an isosbestic in the absorption spectrum of b_2-haem (438.3 nm). The rate constant for FMN reduction was observed to be dependent on the concentration of L-lactate with a K_m value of 0.84 (±0.1) mM, saturating at 604 (±60) s^{-1}. Stopped-flow traces monitoring b_2-haem reduction were studied in tandem with FMN reduction and appeared to lag behind by only a small amount, suggesting that the rate constant for electron transfer from FMN to b_2-haem is faster than that for FMN reduction. These experiments were conducted as described in *Section 2.9* (p62).

Figure 3.2 illustrates the steps observed during flavocytochrome b_2 reduction. *Steps 1* and *2* relate directly to the catalytic cycle, but a slow phase is always observed during both FMN and b_2-haem reduction which complicates data interpretation. This process ultimately results in the three-electron reduction of the enzyme. It probably consists of a series of steps including inter and intra-tetramer electron transfers between both flavin and haem groups. Cappeillère-Blandin (1975) used a simplified model to account for the slow phase, which considered only two subunits and included only one inter-subunit electron transfer (between FMN semiquinones). Pompon (1980) elaborated on this, but failed to generate any real clarity.

The slow phase is often treated as a single step and is represented by a mono-exponential function in stopped-flow data fitting exercises. For traces in which FMN reduction is monitored, it constitutes around 20% of the total amplitude, which is derived mainly from the conversion of FMN semiquinone to hydroquinone. Therefore, when complete traces are fitted to double exponential functions, the fast phase corresponds to *Step 1* (Miles *et al.,* 1992). For traces in which b_2-haem reduction is monitored, the contribution of the second phase is of similar magnitude, but originates entirely from perturbation of the *Step 2* equilibrium. The position of equilibrium is derived from the redox potentials of the FMN semiquinone/hydroquinone and the b_2-haem(III)/b_2-haem(II) couples and is expected to lie approximately 80% in favour of haem reduction (Walker & Tollin, 1991). Miles *et al.* (1992) also fitted b_2-haem traces to double exponential functions, obtaining a rate constant of 445(±50) s^{-1} for the fast phase. However, this procedure is only valid if *Step 2* is much faster than *Step 1,* in which case the fast phase for b_2-haem reduction would be expected to be the same as that for FMN reduction, unless it is much slower, which is most unlikely. The presence of a lag phase between FMN and b_2-haem reduction indicates that *Step 2* should not be ignored and that the first two steps cannot be adequately represented by a single exponential.

Figure 3.3 displays a stopped-flow trace for b_2-haem reduction, produced as described in *Section 2.9* (p62) using a concentration of 10 mM L-lactate (saturating). The starting absorbance was measured by mixing enzyme with L-lactate-free buffer and the end-point was measured a few seconds after reaction. These values were used to determine the scale of the y-axis. Much of the absorbance change was lost in the dead-time of the instrument (see *Section 2.9*), since the rate of reaction is relatively fast. This makes the task of analysing the data particularly difficult. The trace shown is fitted to a function describing an A→B→C reaction, where k_a and k_b are the rate constants for the forward and reverse steps and A is the amplitude of the trace:

$$A\left(1 + \frac{k_b e^{-k_a t} - k_a e^{-k_b t}}{k_a - k_b}\right) \qquad \textbf{\textit{Equation 3.1}}$$

over the fast-phase region of the curve. This method ignores the second phase which should significantly lag behind the first. The starting absorbance was fixed (zero

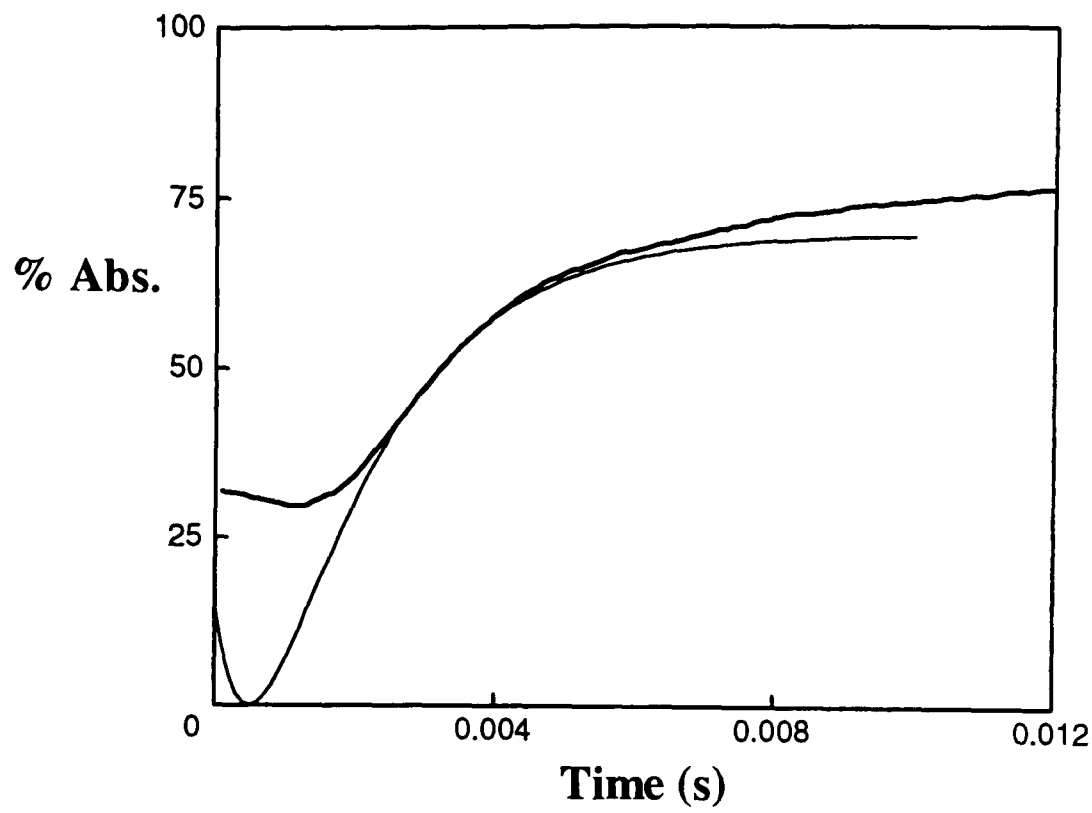

Figure 3.3 An example of a stopped-flow trace for b_2-haem reduction, generated on mixing 10 mM L-lactate with 10 μM flavocytochrome b_2. The % absorbance (y-axis) has been calculated from the start & end points. The trace is fitted to *Equation 3.1* describing an A→B→C reaction with t_0 = 0.5 ms (fixed), k_a = 600s^{-1} (fixed), k_b = 1800 (±200) s^{-1}.

in *Figure 3.3*) and the value of k_a fixed at 600 (±60) s^{-1}, in accordance with the rate constant derived for *Step 1 (k_1: Figure 3.2)*. The value of t_0 (the zero time point: see *Section 2.9*) was adjusted between 0.5 and 1.2 ms, dead-time values were calculated for each fit and the value of k_b was noted. The dead-time of the stopped-flow instrument used is expected to be around 1.2 (±0.1) ms under ideal conditions, but will depend somewhat on the experiment being conducted. Through the range of t_0 values considered the dead-time varied from 1.5 ms to 0.75 ms and the value of k_b from 1600 (±300) s^{-1} to infinity. The latter value would result in a single exponential function from Equation 3.1, but the corresponding dead-time (0.75 ms) is unrealistic.

It is clear from Figure 3.3 that the fit quality is impaired by the small fit range, which is due in part to both the unfortunate presence of *phase 2* and the limitations imposed by the instrument dead-time. Consequently, the rate constants calculated for the intervening dead-times suffer from large errors. However, it is considered unlikely that the dead-time would be greater than 1.5 ms and therefore the rate constant calculated at t_0 = 0.5 ms (fixed) can be considered to be a reasonable lower estimate.

Observed rate constants for reversible steps are equivalent to the sum of the rate constants for the forward and reverse processes, unless a consecutive step is faster than the reverse process. Therefore if $k_3 >> k_{-2}$ then $k_b = k_2$, but if $k_3 << k_{-2}$ then $k_b = k_2 + k_{-2}$. Because the steps involved in the slow phase (k_3) cannot be reconciled in these simple terms both mathematical extremes must be included in the estimate. The ratio of k_2 to k_{-2} is known from the appropriate redox potentials to be approximately 5½ : 1 (Walker & Tollin, 1991) allowing lower estimates of both values to be derived. The forward step (electron transfer from $FMNH_2$ to b_2-haem) proceeds with minimum rate constant k_2 = 1500 (±500) s^{-1}. The reverse step proceeds with minimum rate constant k_{-2} = 270 (±90) s^{-1}. It should be noted that these are lower estimates and that the actual values could be an order of magnitude greater.

Accuracy is clearly compromised by the stopped-flow procedure, which cannot generate reliable data for reactions which occur at this velocity and faster. However, laser flash photolysis has also been used to study this electron-transfer process and a value of 1900 s^{-1} derived for the forward rate constant (Hazzard *et al.*, 1994; at 24°C in pH 7, 100 mM phosphate buffer). This is consistent with the stopped-flow result although the circumstances of the electron-transfer event may be different owing to the different methodology. It appears, therefore, that this step is too fast to have any significant influence on the overall rate of catalytic turnover, but if pre-steady-state rate constants are to be applied directly to a steady-state situation it is important to match the conditions as closely as possible. In the b_2-haem reduction experiment described above, intramolecular electron transfer is only observed after FMN reduction and, in this respect, mimics *Step 1* and *Step 2* of the catalytic cycle. However one factor missing from this experiment is the presence of cytochrome *c*, which may bind strongly to the enzyme and affect either step. For this reason b_2-haem reduction was carried out in the presence of zinc-substituted cytochrome *c*, a redox inactive form of the electron acceptor known to bind to flavocytochrome b_2. The results, presented in *Section 4.2(d)* (p113), show that the stopped-flow traces overlay almost exactly, thereby demonstrating that the binding of cytochrome *c* to flavocytochrome b_2 is unlikely to affect either *Step 1* or *Step 2*. Further evidence is presented in the following section.

3.2(b) Re-reduction of b_2-Haem

In order to study $FMNH_2$ to b_2-haem electron transfer in the presence of redox-active cytochrome *c*, the rapid b_2-haem to cytochrome *c* electron-transfer process was exploited. This intermolecular step is dependent on the concentration of enzyme, and at high concentration (>20 μM) is known to occur within the dead-time of a stopped-flow experiment (see *Section 4.2a;* p104). By inducing the FMN to b_2-haem electron transfer in fully reduced enzyme using a substoichiometric amount of cytochrome *c* to first partially oxidise the b_2-haem, a 'b_2-haem re-reduction' trace is generated (*Figure 3.4*). The y-axis gives the % of oxidised b_2-haem expected, based on the amount of ferricytochrome *c* used. The obvious point to note is that, in the

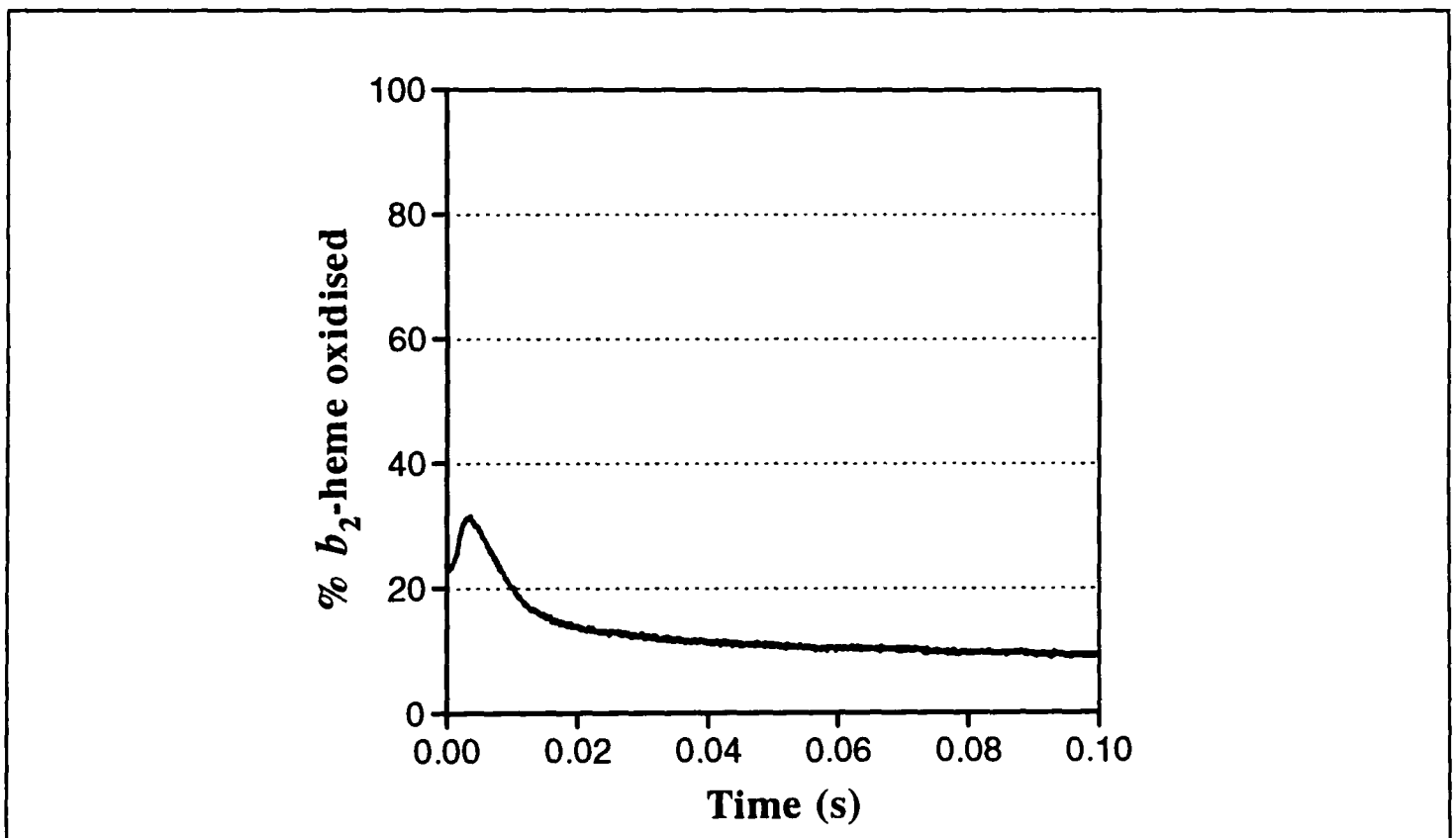

Figure 3.4 An example of a trace showing re-reduction of b_2-haem, generated by stopped-flow spectrophotometry at 408.4 nm (a cytochrome *c* isosbestic) using 20 μM flavocytochrome b_2 (after mixing) at 25°C in Tris/HCl buffer pH 7.5, *I* 0.10. Partial b_2-haem oxidation is initiated by rapid reduction of a sub-stoichiometric amount of ferricytochrome *c* (4 μM after mixing). Re-reduction then takes place by inter-domain electron transfer from the FMN hydroquinone. The change in absorbance (y-axis) has been converted to `% b_2-haem oxidised' based on $\Delta\varepsilon$ = 44 000 (see *Section 2.9;* p62), referring to the absorbance change expected from the amount of ferricytochrome *c* used.

example shown, the proportion of oxidised b_2-haem never exceeds 30%, indicating that electron transfer from the fully reduced FMN to b_2-haem is happening too fast to be observed by this method, i.e. the rate constant must be in excess of 1000 s^{-1}. Some oxidised haem is observed because electron transfer from the fully reduced FMN to oxidised b_2-haem will initially result in an equilibrium being established between the two prosthetic groups, based on their electrode potentials (Capeillère-Blandin, 1975; Chapman *et al.,* 1994). This equilibrium is eventually disrupted by disproportionation of flavin semiquinones followed by reduction by L-lactate. This is an overall slower process than the initial electron transfer but leads to fully reduced enzyme which accommodates three electrons (i.e. back to the starting absorbance). An additional factor which will also contribute to the amount of oxidised haem observed, is the small amount of flavocytochrome b_2 which may have lost FMN during preparation. Although this amount should be less than 10% of the total, it may be significant in terms of the small effect observed. This experiment was repeated using different substrates (S-2-hydroxyvalerate, S-2-hydroxyoctanoate) at different concentrations to reduce the enzyme, but in each case the maximum absorbance observed was never significantly different from that described above. In these experiments it is very unlikely that substrate (e.g. L-lactate) is bound in the active site when the enzyme is fully reduced (Urban *et al.,* 1983), especially at low substrate concentrations. Further, since the product (e.g. pyruvate) is present only in a slight excess over the enzyme, this is also unlikely to be bound. Therefore rapid FMN to b_2-haem electron transfer must be possible when the active site of the enzyme is unoccupied.

This observation is complementary to the b_2-haem reduction experiment, which demonstrates that rapid electron-transfer occurs directly after FMN reduction by L-lactate. Following reduction, pyruvate is bound in the active site, but it is not certain whether or not it dissociates prior to the electron-transfer event. However, we can conclude that either the presence of pyruvate has little effect on this electron-transfer step (in terms of the catalytic cycle), or that pyruvate dissociation is too fast to cause a detectable change in the rate. The influence of pyruvate on the catalytic cycle is considered further in *Section 3.2(d).*

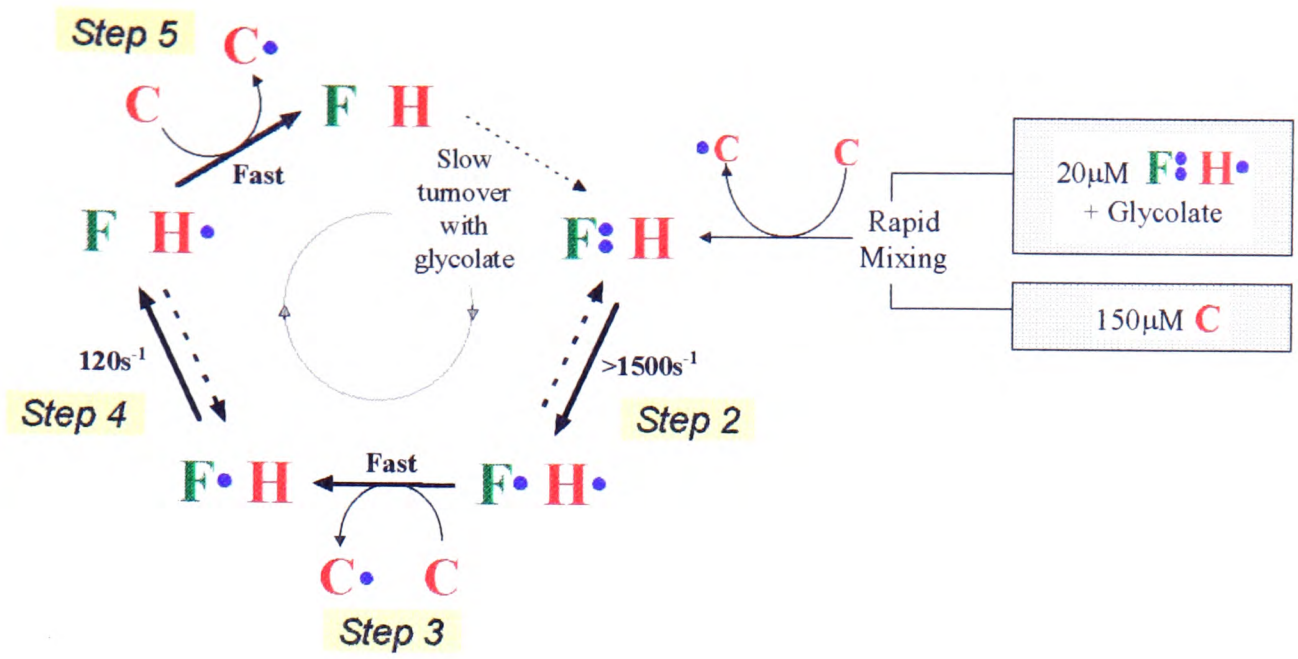

Figure 3.5 The electron-transfer processes occurring during the flavin oxidation stopped-flow experiment (see *Section 2.9;* p62). An excess of ferricytochrome *c* is used to oxidise flavocytochrome b_2 by entering the catalytic cycle (see *Figure 3.1;* p73) immediately before *Step 2*. The use of glycolate as substrate enables the enzyme to be fully reduced initially, but dramatically slows down the overall turnover rate at *Step 1* (see *Figure 3.1*). This allows *Step 4*, FMN oxidation, to be monitored as a pre-steady-state process. Examples of the stopped-flow traces derived from this experiment are illustrated in *Figures 3.6* and *3.7*. The introduction of pyruvate into the ferricytochrome *c* solution before mixing allows inhibition to be studied in the pre-steady-state.

3.2(c) Flavin Oxidation

Flavin oxidation traces were collected as described in *Section 2.9* (p62; see *Figures 3.5-3.7*). By using a poor substrate (e.g. glycolate) to pre-reduce a solution of enzyme (20 μM before mixing) and mixing with an excess of ferricytochrome *c* (150 μM before mixing), *Step 4* of the cycle could be studied with the assurance that *Step 1*, flavin reduction, would be slowed down enough to effectively rate-limit enzyme turnover. As already discussed, *Steps 2* and *3* occur too fast to be detected by stopped-flow spectrophotometry (*Section 3.2a;* p76 and *Section 4.2a;* p104 respectively) and therefore the change observed with regard to FMN, during the pre-steady-state period, is limited to the conversion of the semiquinone to oxidised FMN.

The cytochrome *c* trace monitored at 544.8 nm gives an overall indication of the processes occurring (see *Figure 3.6*). The fast phase (first 100 ms; *Phase [1]*) consists of a large absorbance change corresponding to approximately three electron equivalents. These three electrons are removed on the first rapid circuit of the catalytic cycle, before flavin re-reduction by glycolate slows turnover dramatically (see *Figure 3.5*). Once this point has been reached, a steady-state period occurs lasting approximately one second (*Phase [2]*), during which the concentration of reduced cytochrome *c* increases linearly with time, at a rate consistent with glycolate turnover. Finally, after 7.5 electron equivalents have been transferred, all of the cytochrome *c* has been reduced and turnover stops. The ferricytochrome *c* concentration was chosen to be as high as possible to ensure that the first two electron equivalents could be reduced while the flavocytochrome b_2 was still saturated. The K_m for cytochrome *c* reduction has been reported to be 10 (±1) μM (Miles *et al.,* 1992) and so even after the first two electron equivalents have been reduced (≡20 μM) 55 μM ferricytochrome *c* remains i.e. five fold excess over the K_m.

Since there is no convenient isosbestic point at which to monitor FMN absorbance, the corresponding flavin timecourse was generated by subtracting the cytochrome *c* contribution away from a trace recorded at 438.3 nm (a b_2-haem isosbestic point; see *Figure 3.6* and *Section 2.9;* p62). In the flavin trace (*Figure 3.7*) a rapid absorbance increase, caused by FMN oxidation, occurs initially (*Phase [1]*). This is followed by a flat steady-state period (*Phase [2]*) in which the oxidation state of the enzyme is maintained. Finally a slow reduction phase is observed once all the cytochrome *c* has been reduced (*Phase [3]*). The amplitude of the FMN contribution to the absorbance change at 438.3 nm was typically around 0.07. This is compatible with the expected change for the semiquinone to oxidised FMN redox change based on previously determined absorption coefficients (Capeillère-Blandin, 1991). Further, the rate of reduction occurring in *Phase [3]* was found to be compatible with the rate of reaction with glycolate.

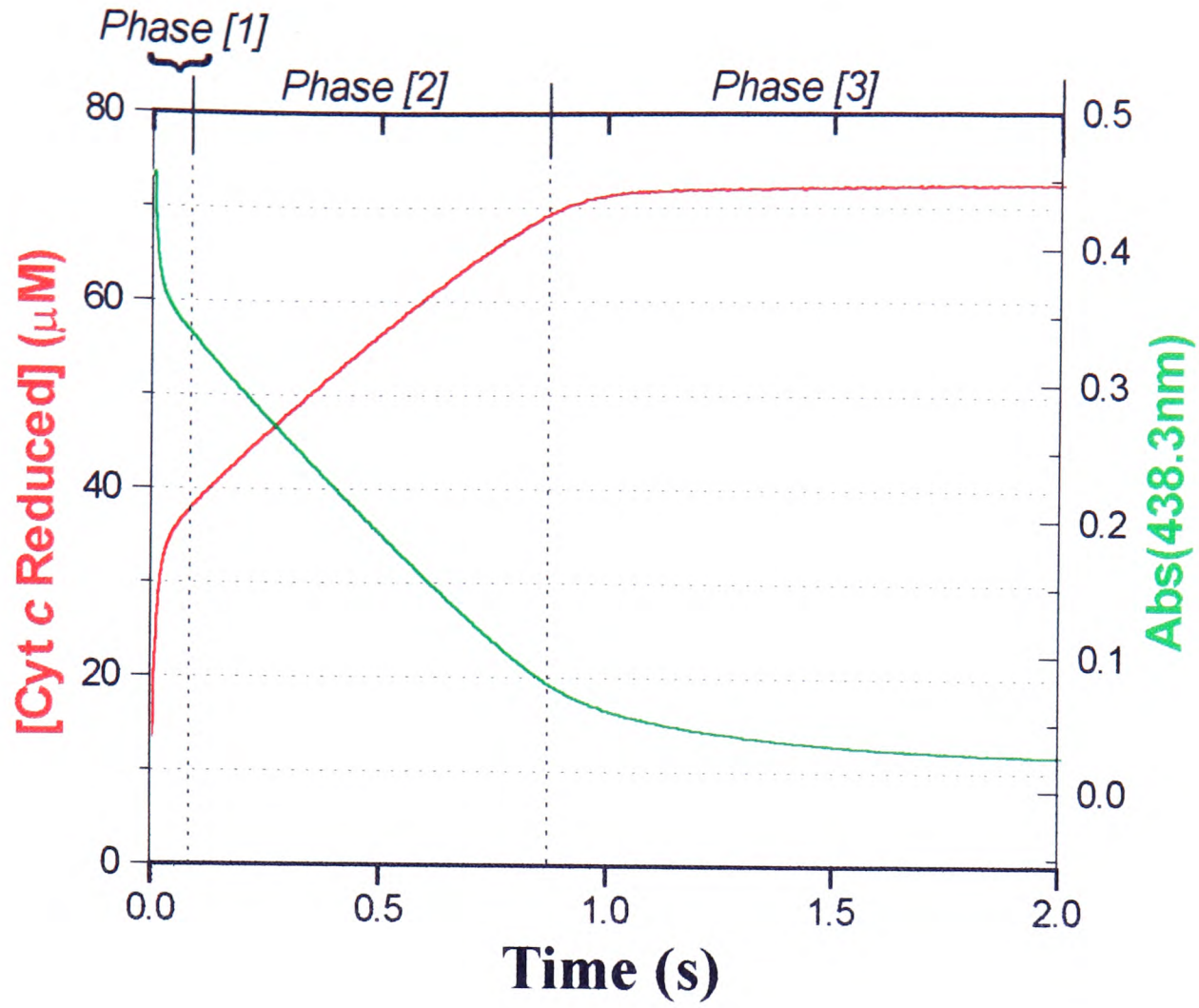

Figure 3.6 Examples of stopped-flow traces generated from a flavin oxidation experiment (see *Figure 3.5*) containing 10 μM flavocytochrome b_2, 75 μM cytochrome *c* and 15 mM pyruvate at 25°C in Tris/HCl buffer (*Section 2.7;* p59). The cytochrome *c* trace (left axis) was recorded at the b_2-haem isosbestic of 544.8 nm where an absorbance increase is observed as ferricytochrome *c* is reduced. The y-axis for this trace has been converted to concentration of ferrocytochrome *c* by using $\Delta\varepsilon$ = 7 000 (see *Section 2.9;* p62). This allows the steps described in *Figure 3.5* to be followed in terms of molar equivalents, i.e. since flavocytochrome b_2 is present at a concentration of 10 μM (after mixing), each 10 μM ferrocytochrome *c* produced represents one molar equivalent. The cytochrome *c* trace is split into 3 distinct phases; **1**, a rapid pre-steady-state phase in which 3 molar equivalents of ferrocytochrome *c* are generated; **2**, a slow steady-state phase in which turnover is limited by glycolate oxidation; **3**, turnover ends when all the cytochrome *c* has been reduced.

The trace recorded at the b_2-haem isosbestic 438.3 nm (right axis) is almost a mirror image of the cytochrome *c* trace, due to a large negative contribution from cytochrome *c* to the absorbance change at this wavelength. However there is a significant contribution from the flavin manifested in phase **1**, due to flavin oxidation, and phase **3**, as flavin reduction occurs. Weighted addition of the two traces to eliminate the common cytochrome *c* contribution leads to the flavin time-course illustrated in *Figure 3.7*.

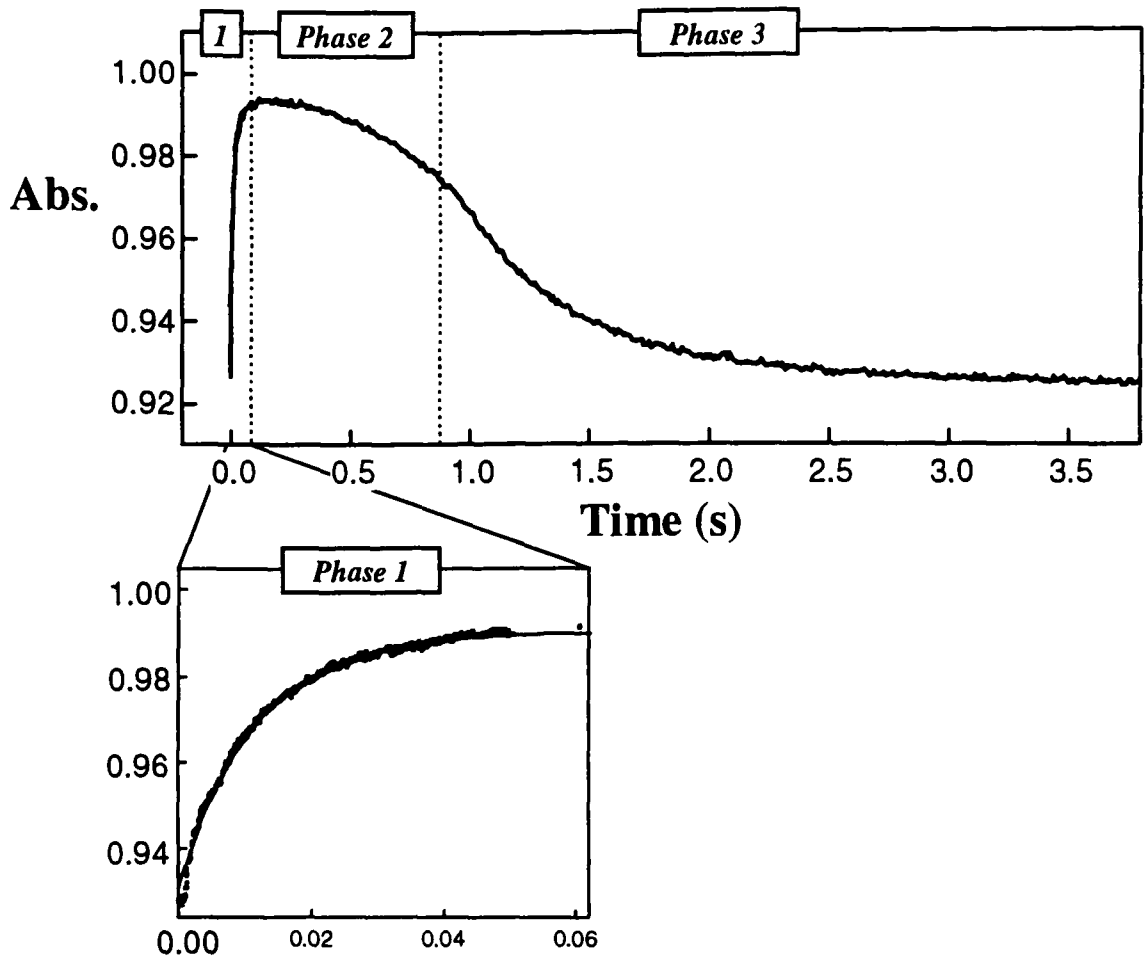

Figure 3.7 An example of a flavin absorbance time-course generated by the addition of the stopped-flow traces shown in *Figure 3.6* according to Abs(438.3 nm) + 1.07Abs(544.8 nm) as described in *Section 2.9* (p62). The three phases described for *Figure 3.6* are apparent here as; 1, flavin oxidation causes an absorbance increase at 438.3 nm; 2, steady-state period during which time the flavin absorbance is approximately constant; 3, flavin reduction, which occurs in the presence of excess glycolate once exhaustion of ferricytochrome *c* has ended the steady-state reaction and returns the absorbance back to its starting point. Phase 1 is shown expanded to illustrate the flavin oxidation process. Although the entire trace contains 1000 data points the use of split time-bases has enabled this small region of the time-course to contain 500 data points, allowing it to be accurately fitted to a single exponential function (as shown).

The rate constant for the flavin oxidation process was determined to be 120 s^{-1} by fitting the fast phase to a single exponential function (see *Figure 3.7, inset,* and *Table 3.1*). Therefore although several other steps occur before flavin oxidation they were deemed to be too fast to affect the shape of the trace and it was treated as a single-step reaction. The quality of fit typically achieved by this method suggests that this is a valid assumption. However, one should not ignore the implications of such assumptions when considering the error involved in the rate constant. Taking this into

account, along with errors generating from the subtraction of cytochrome *c* absorbance (see *Section 2.9;* p62) the rate constant calculated for FMN semiquinone to b_2-haem electron transfer is estimated to have 10-20% uncertainty in addition to the observed experimental error.

Table 3.1 lists rate constants for flavin oxidation derived for a variety of different conditions. The use of (S)-2-hydroxyvalerate as the initial reductant produced similar results as with glycolate. However, this substrate has a marginally higher turnover rate than glycolate and so is less ideal for this type of experiment (see *Section 5.2a;* p124). The concentration of glycolate was also varied, causing a moderate increase in rate. This effect is at least partly attributable to simultaneous changes in ionic strength, which were studied independently by the addition of NaCl.

Table 3.1 Observed rate constants for flavin oxidation in the presence of several different substrates and inhibitors (see also *Figure 3.8*). Averaged traces were fitted to single exponential functions with rate constants k_{obs} and amplitudes as indicated. Fit limits were varied, generating a spread of values as indicated by the confidence limits.

Substrate	Inhibitor	k_{obs} (s^{-1})	Amplitude
1 mM glycolate	-	120 ± 2	0.074
1 mM glycolate	5 mM pyruvate	116 ± 2	0.074
1 mM glycolate	7.5 mM pyruvate	102 ± 3	0.066
1 mM glycolate	10 mM pyruvate	94 ± 5	0.065
1 mM glycolate	15 mM pyruvate	87 ± 2	0.058
1 mM glycolate	25 mM pyruvate	69 ± 4	0.051
1 mM glycolate	40 mM pyruvate	64 ± 6	0.051
1 mM glycolate	50 mM pyruvate	50 ± 8	0.044
1 mM glycolate	50 mM NaCl	162 ± 5	0.066
1 mM glycolate	75 mM NaCl	210 ± 30	0.095
5 mM glycolate	25 mM oxalate	135 ± 20	0.085
5 mM glycolate	-	108 ± 10	0.081
20 mM glycolate	-	130 ± 10	0.080
45 mM glycolate	-	135 ± 20	0.080
100 mM glycolate	-	150 ± 15	0.084
4 mM s-2-hydroxy-valerate	-	100 ± 10	0.055

Unfortunately, at high ionic strength the simplicity of the experimental model breaks down as alternative steps begin to affect the rate of reaction. The result is traces which can no longer be represented accurately by single exponential functions. The steps involving cytochrome *c* reduction are an obvious source of disruption since, as demonstrated in *Chapter 4*, they are very sensitive to ionic strength (see *Figure 4.5;* p107). However, the most striking effect observed was the inhibition caused by introducing pyruvate into the reaction mixture. This is examined in *Section 3.2(d).*

Electron transfer from flavin semiquinone to b_2-haem has previously been studied by Walker & Tollin (1991), who used a laser flash photolysis method to generate highly reactive deazaflavin semiquinones (see *Section 1.6*, p19) in the reaction cell. In the presence of excess oxidised flavocytochrome b_2, the free radical species were observed to deposit single electrons on both FMN and b_2-haem species. This initial phase of the reaction occurred within 0.5 ms (depending on the concentrations of enzyme and deazaflavin) allowing reactions occurring at up to 10^4 s^{-1} to be resolved. However, intramolecular electron-transfer between flavin and b_2-haem was only observed in the presence of pyruvate, which appeared to prevent initial FMN reduction by the exogenous semiquinones. Pyruvate is known to stabilise the semiquinone oxidation state of FMN in flavocytochrome b_2 (Walker & Tollin, 1991; Tegoni *et al.,* 1986) and so electron transfer from b_2-haem to FMN is favoured in this case. Walker & Tollin (1991) report that the rate constant for this process varies between 400 s^{-1} and 1200 s^{-1} at ionic strengths between 0.50 and 0.010.

It is difficult to compare rate constants for the reverse reaction, measured in the presence of pyruvate, with the results of flavin oxidation stopped-flow experiments which are driven in the forward direction. The effect of pyruvate on the redox potential of FMN semiquinone is one complication and its possible conformational influence, resulting from disruption of the b_2-haem propionate to Tyr143 hydrogen-bond, is another (see *Sections 1.11;* p37 *& 3.3;* p96).

3.2(d) Pyruvate Inhibition

The steady-state turnover of flavocytochrome b_2 is known to be inhibited by the presence of pyruvate (product) in the reaction mixture (Lederer, 1978). However, the mechanism by which inhibition occurs is complex, Lederer (1978) reported inhibition constants of 3 mM and 30 mM for Michaelis-Menten straight line fits to competitive and non-competitive reciprocal plots. These observations, when coupled with reports that pyruvate stabilises the semiquinone oxidation state of FMN in both *H. anomala* (Tegoni *et al.,* 1986) and *S. cerevisiae* (Walker & Tollin, 1991) flavocytochromes b_2, suggest that pyruvate targets *Step 4* of the catalytic cycle. This premise was examined by conducting flavin oxidation experiments in the presence of pyruvate.

Inhibition of flavin oxidation

The experiments were performed as described in *Sections 2.9* (p62) & *3.2(c)* by introducing pyruvate into the ferricytochrome *c* solution before mixing (see *Figure 3.5*). The reason for this was to avoid FMN oxidation by excess pyruvate, although this process is sufficiently slow so as not to compete with the usual catalytic cycle (Urban *et al.,* 1983). *Figure 3.8* plots the rates calculated for pre-steady-state flavin oxidation against pyruvate concentration (see *Table 3.1*). At high pyruvate concentrations the traces obtained fitted less well to single exponentials and the data is less accurate as a result, therefore *Figure 3.8* is restricted to a concentrations below 50 mM. Complicating factors include the effect of increasing ionic strength with increasing pyruvate concentration. As discussed in *Section 3.2(c)* this has a tendency to speed the reaction up (see *Table 3.1*). Deviation from ideality with respect to pyruvate binding may also occur (i.e. the association or dissociation rates may be too slow to create a genuine equilibrium for binding during the pre-steady-state reaction). Oxalate is also known to inhibit the action of flavocytochrome b_2 (Lederer, 1991) but was not found to inhibit flavin oxidation.. In this respect pyruvate is unique.

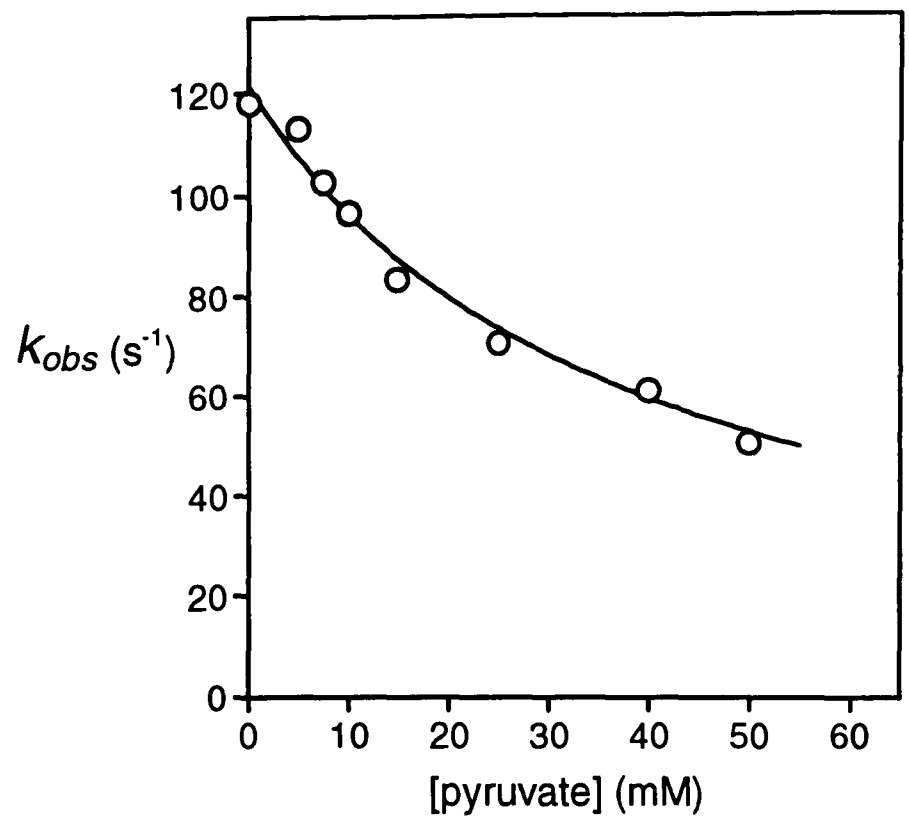

Figure 3.8 Inhibition plot of flavin oxidation rate v pyruvate concentration. All experiments were conducted as described in the *Section 2.9* (p62), flavocytochrome b_2 concentration 10 μM, cytochrome *c* concentration 75 μM (after mixing), in Tris/HCl buffer (*Section 2.7;* p59) at 25°C. Data (see *Table 3.1*) was fitted to *Equation 3.2* using non-linear least-squares regression analysis. k_0 is the rate constant in the absence of inhibitor, and k_∞ the minimum rate constant at saturation, this was constrained to > 0 during fitting. K_i = 40 (±17) mM, k_0 = 123 (±2) s^{-1}, k_∞ = 0 (±26) s^{-1}.

The data in *Figure 3.8* was fitted to a standard Michaelis-Menten inhibition curve, in which the lower-limit rate constant was allowed to vary (parameters as defined in *Figure 3.8*):

$$k = k_0 - \frac{(k_0 - k_\infty)[I]}{([I] + K_i)} \qquad \textbf{\textit{Equation 3.2}}$$

because of the tendency for fitting to force k_∞ below zero, this parameter was constrained to greater than zero. The ultimate result was $k_\infty = 0$, but at least we have a reasonable estimate of the error caused by uncertainty in k_∞. The inhibition constant obtained from least squares fitting (40 ±17 mM) is really only qualitative, due to the limited range of data points available. It is nevertheless reassuring that the inhibition constant derived for non-competitive steady-state inhibition is of similar magnitude (30 mM; Lederer, 1978). The origin of the competitive inhibition reported by Lederer (1978) at low concentrations of pyruvate remains a mystery. It is inconceivable that

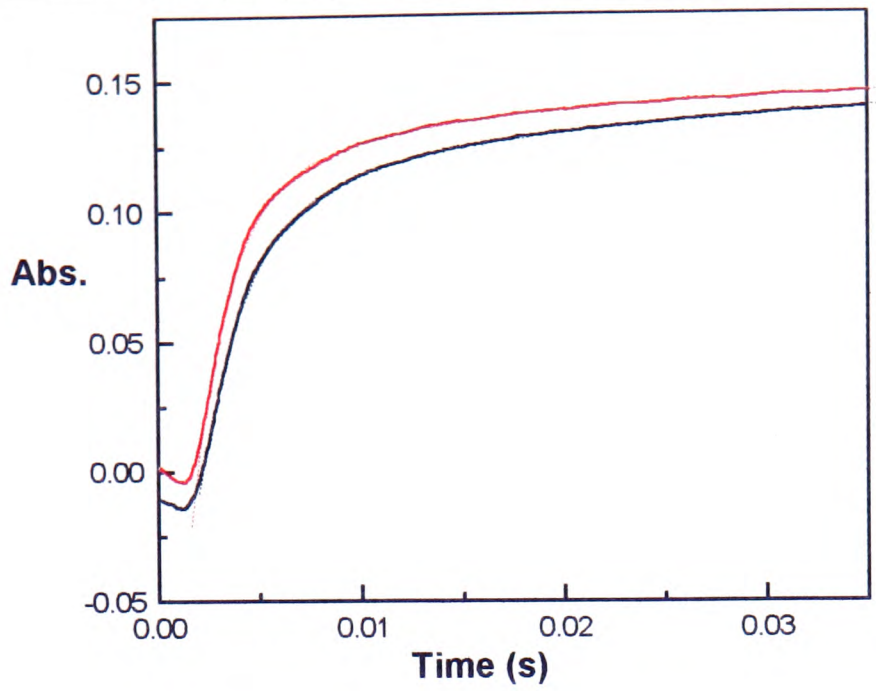

Figure 3.9 Stopped-flow traces showing b_2-haem reduction by 3.5 mM L-lactate (red) and a mixture of 3.5 mM L-lactate and 50 mM pyruvate (black; concentrations after mixing). The concentration of flavocytochrome b_2 was 7.5μM after mixing. Both traces are fitted to double exponential functions (dotted lines) the parameters of which are:

	k_1	k_2	$\mathbf{Amp_1}$	$\mathbf{Amp_2}$
no pyruvate	554 (±3)	74 (±1)	0.31	0.045
50 mM pyruvate	422 (±2)	46 (±1)	0.26	0.050

true competitive inhibition at the site for L-lactate dehydrogenation could be partial in nature. However, partial non-competitive inhibition of *Step 4* of the catalytic cycle would certainly produce unusual effects when studied using reciprocal plots. It appears likely, therefore, that k_∞ is greater than zero and that electron transfer can occur, albeit more slowly, even when pyruvate is bound. This is backed up by the laser flash photolysis experiments of Walker & Tollin (1991) who observed b_2-haem to FMN electron transfer in the presence of pyruvate.

The effect of pyruvate on b_2-haem reduction

Several experiments were also conducted in order to assess the effects of pyruvate on the other steps in the catalytic cycle, in particular *Steps 1* and *2*. It is a flaw in the flavin oxidation procedure that several other steps are necessary before *Step 4* can be monitored, some of which could be influenced by pyruvate. *Figure 3.9* compares stopped-flow traces for b_2-haem reduction (see *Section 2.9;* p62) by 3.5

mM L-lactate with and without the presence of 50 mM pyruvate. As discussed in *Section 3.2(a)*, haem reduction occurs via the sequential *Steps 1* and *2* and therefore gives a good indication of the influence exerted on both processes. The presence of 50 mM pyruvate certainly effects the rate of haem reduction, although the lag between the two traces is slight. In *Figure 3.9* the traces are fitted to double exponential functions, as such, the fast phase accounts largely for *Steps 1* and *2*, while the slow phase accounts for the entry of a third electron per subunit and the disruption of the equilibrium formed by *Step 2* (see *Figure 3.2;* p76). Unfortunately single exponential functions do not adequately represent either phase and the rate constants calculated can therefore be used only for qualitative assessment. In terms of the catalytic cycle, the effect on the overall rate of turnover would be minimal if the combination of *Step 1* and *2* result in a rate constant of around 420 s^{-1}. This leads us to the surprising conclusion that pyruvate does not have any significant affinity for the oxidised form of the enzyme and is therefore unable to cause competitive inhibition (i.e. inhibit *Step 1*). This was also apparent during the flavin oxidation experiments, in which the presence of up to 50 mM pyruvate had no effect on the rate of turnover with 1 mM glycolate, i.e. the length of the steady-state period (*Phase 2, Figure 3.7;* p85).

The repercussions for *Step 2* are less clear, as the rate constant for this step is much faster than for *Step 1* (see *Section 3.2a;* p76). Weak inhibition of both b_2-haem reduction and steady-state turnover has also been observed in the presence of excess substrate (K_i = 175 mM; Miles, 1992) and it is possible that this effect is analogous. Interestingly, the Y143F mutant (see *Section 1.10;* p37 & *Figure 1.21;* p39) appeared to be less susceptible to this form of inhibition despite the fact that intramolecular electron-transfer is rate determining in its catalytic cycle. In contrast, the hinge deletion/insertion mutants (see *Section 1.10* & *Figure 1.20;* p38) characterised by Sharp *et al.,* (1994; 1996a & b), which also exhibit rate-limiting intramolecular electron-transfer, are particularly susceptible to inhibition by excess substrate. The dual role of the Tyr143 side-chain may be central to this mechanism of inhibition, which may be induced by substrate or product binding at the active site during *Step 2*. For wild-type flavocytochrome b_2, Urban *et al.* (1983) determined a Michaelis constant (7.4 mM) for the transhydrogenation reaction between L-lactate and

pyruvate. In these terms, the concentration of pyruvate used in our experiment is approaching saturation, indicating that the inhibition is a partial effect. Overall, we can be reasonably confident that the weak inhibition of *Step 2* does not cause the decrease observed in the rate of flavin oxidation on addition of pyruvate.

Contrary to these findings, Hazzard *et al.* (1994) reported that pyruvate inhibits *Step 2* with a K_i of 3.8 mM. However the inhibition was manifested as a decrease in the amplitude of signal return during laser flash photolysis experiments, while the observed rate constant did not change (traces were generated by rapidly oxidising the b_2-haem using photoexcited 5-deazariboflavin in a premixed system). Such an effect would be produced if the concentration of 'active' enzyme decreased as the pyruvate concentration increased. A mechanism for this effect is well documented. Tegoni *et al.* (1986) showed that bound pyruvate stabilises the flavin semiquinone oxidation state of the *H. anomala* enzyme dramatically and shifts the midpoint potentials of the redox couples formed with both oxidised and reduced states by around 100 mV. This property was also confirmed for the *S. cerevisiae* enzyme (Walker & Tollin, 1991). Therefore, if the concentration of pyruvate is increased in a solution of flavocytochrome b_2 and L-lactate (stoichiometric in this case), the dominant FMN species will become the pyruvate/semiquinone complex. On haem oxidation, the increased stability of the flavin semiquinone would reverse the driving force for the electron transfer reaction and make it thermodynamically unfeasible. This would essentially decrease the amount of 'active' enzyme in the solution prior to the laser flash. In our flavin oxidation experiments, pyruvate was deliberately introduced via the alternative stopped-flow syringe to counteract this problem.

Although the accuracy is poor, it is clear that inhibition does occur during the rate-determining electron-transfer step. There are several possibilities for the mechanism of inhibition based on pyruvate binding to the semiquinone form of the enzyme: 1) pyruvate acts as a physical barrier to electron transfer from FMN to b_2-haem by changing the properties of the intervening medium (and therefore the value of β; see *Section 1.9;* p28). 2) pyruvate stabilises the semiquinone state thereby altering its redox potential and making electron transfer thermodynamically less

favourable (this possibility is discussed in detail by Tegoni *et al.* (1990) for the related enzyme from *Hansenula anomala).* 3) pyruvate competes with one of the haem propionates for the key hydrogen bond to Tyr143 (see *Section 1.10 & Figure 1.21;* p39) causing the haem group to be `disconnected' from the active site. This could result in an increase in the flavin-haem separation which would disfavour electron transfer.

Regardless of the mechanism, the fact that pyruvate is able to cause this inhibition suggests that, immediately prior to electron transfer, dissociation of pyruvate has already occurred, and that the active site is vacant. Furthermore the observation that *Step 4* (in the absence of pyruvate) occurs at the same rate as in the catalytic cycle suggests that pyruvate dissociation contributes little to the overall rate of turnover.

3.2(e) Quenched-Flow EPR

In order to test the model derived for the catalytic cycle, quenched-flow EPR was used to quantitate the amount of flavin semiquinone present when the enzyme is turning over at its maximum rate in the presence of saturating amounts of L-lactate (10 mM) and cytochrome *c*. The experiments were conducted as described in *Section 2.11* (p69). In order to maximise the EPR signal to noise ratio, a large concentration of enzyme was required (20 μM after mixing) and therefore a large concentration of ferricytochrome *c* (470 μM) in order to fuel the reaction for a reasonable time period. The EPR traces recorded at -194°C show large signals for the flavin semiquinone free radical (see *Figure 3.10*) and conveniently, at this temperature, no signal due to ferricytochrome *c* (Fe^{III}), which is quenched by rapid relaxation phenomena. The semiquinone concentrations were calculated by comparing the signal integrals with those of a Cu^{II} standard and were adjusted for sample packing dilution by comparison with an identically packed standard. This correction is probably the largest source of error in the entire procedure. Ferricytochrome *c* concentrations were similarly calculated from EPR spectra recorded at -270°C as described in *Section 2.11* and illustrated in *Figure 2.7* (p70).

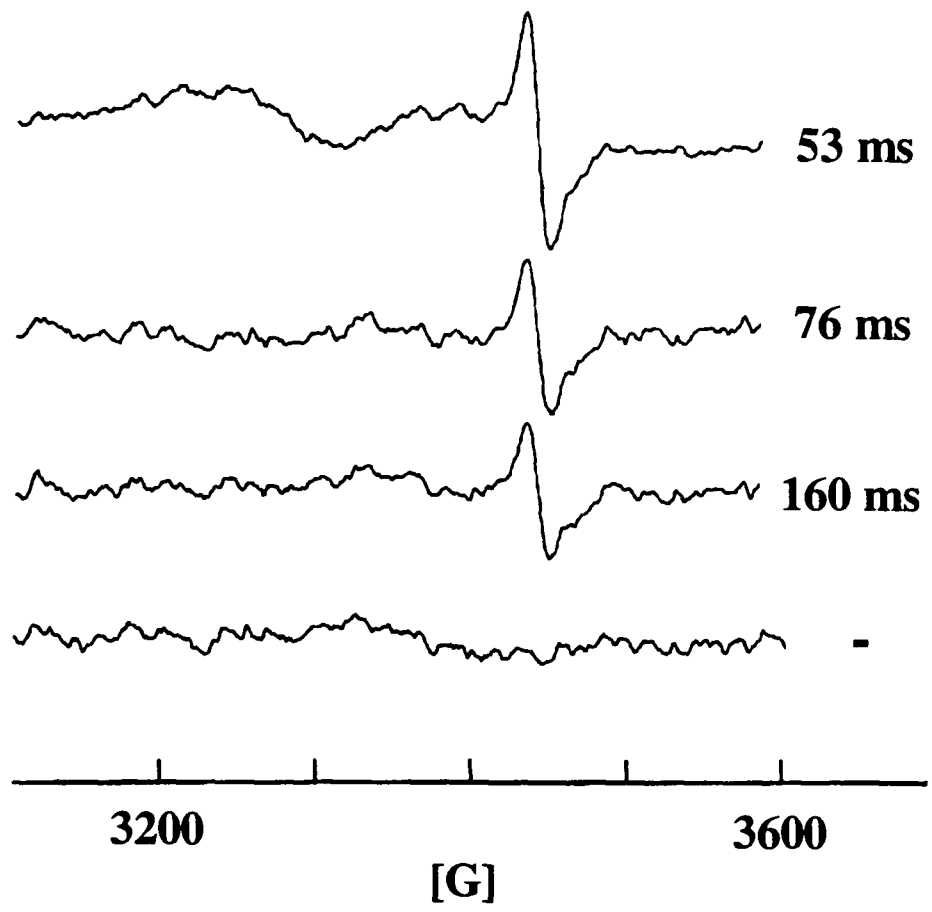

Figure 3.10 EPR spectra recorded at -194°C showing the FMN semiquinone signals of flavocytochrome b_2 samples freeze-quenched in liquid isopentane at -140°C during steady-state turnover in the presence of 10 mM L-lactate and 470μM ferricytochrome *c*. Integrations of these signals were used to calculate the semiquinone concentrations displayed in *Figure 3.11*.

Figure 3.11 plots the concentrations of flavin semiquinone and ferricytochrome *c* in each frozen sample relative to the reaction timebase. The ferricytochrome *c* quantitations provide an internal indication of the extent of the reaction, and therefore allow the semiquinone concentration values to be fixed to their correct positions along the time axis. This calibration was performed using a spectrophotometrically collected trace identical to the above reaction, but using only a catalytic amount of flavocytochrome b_2, which was then scaled up to provide an approximate simulation of the quenched-flow experiment. Although the free-radical concentrations are imprecise, due mainly to the problem of achieving uniform sample packing within the EPR tube, the data show that after 50 ms, during the rapid turnover period, around 75% of the total enzyme present is in the semiquinone form. This result is entirely compatible with the kinetic model proposed (*Figure 3.1;* p73).

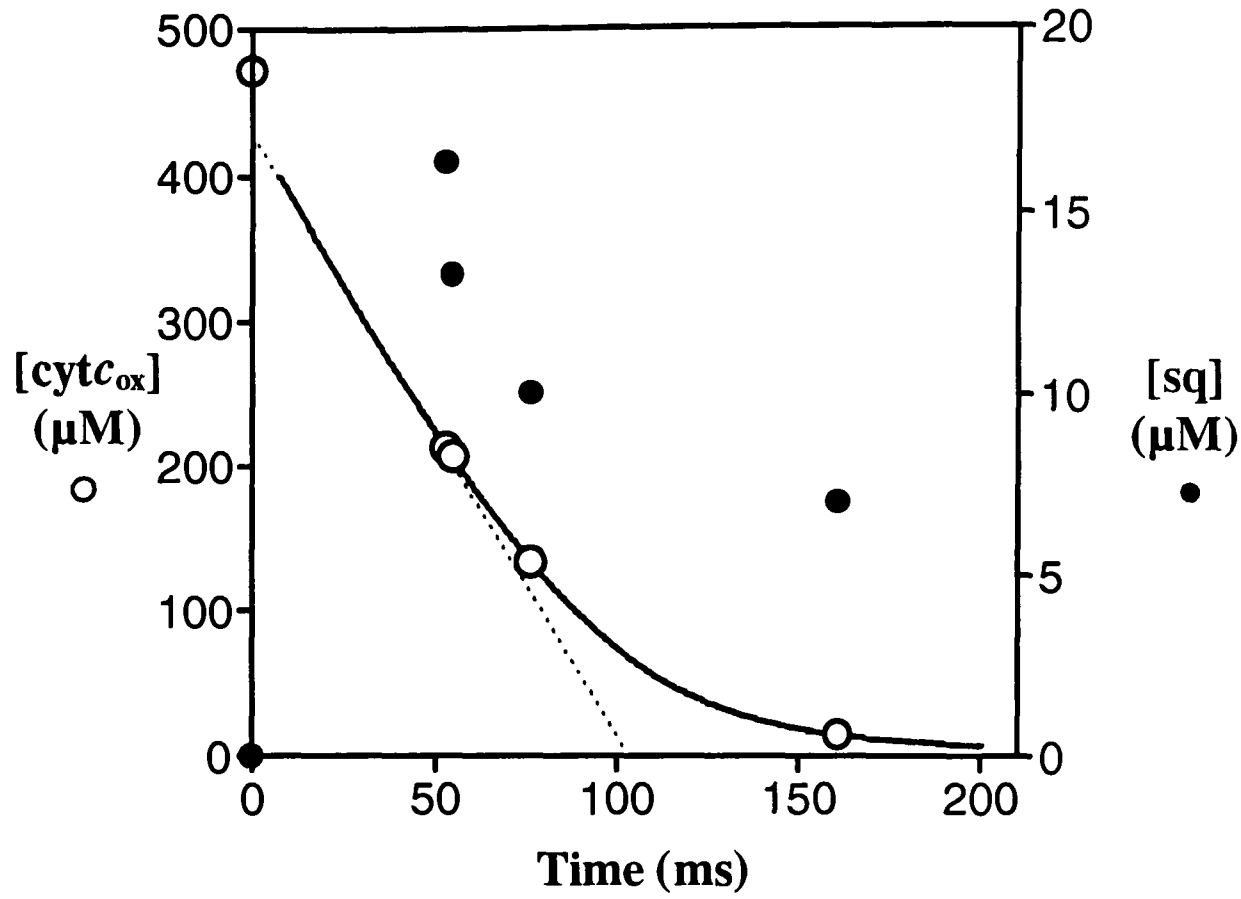

Figure 3.11 Plot of free radical concentrations for both ferricytochrome *c* and flavin semiquinone derived from EPR spectroscopic quantitations of frozen samples of a reaction mixture containing 470 μM cytochrome *c*, 10 mM L-lactate, 20 μM flavocytochrome b_2 mixed at 25°C in MOPS buffer pH 7.5 (see *Section 2.11;* p69) and freeze-quenched in isopentane liquid at -140°C. The ferricytochrome *c* quantities have been used to calibrate the time-base for this plot by fixing them to a simulation of the reaction ———— , derived by scaling up an assay collected by a visible spectrophotometer with a catalytic amount of flavocytochrome b_2. Each of the EPR quantitations have been corrected for the dilution caused by loose packing of the frozen, powdered sample in the EPR tube relative to a standard ferricytochrome *c* sample. Inconsistencies in packing are likely to constitute most of the significant error in the data.

Sample	**[FMN$^{\bullet}$] (μM)**	**[cytc$_{ox}$] (μM)**	**time (ms)**
1*	-	470	0
2	16.4	212	53
3	13.3	206	55
4	10	133	76
5	7	15	161

* sample used as a standard for calibrating the ferricytochrome *c* concentrations relative to the EPR signal. [FMN$^{\bullet}$] ≡ concentration of flavin semiquinone; [cytc$_{ox}$] ≡ concentration of ferricytochrome *c*.

A significant proportion of semiquinone remains after the steady-state period has ceased, which will eventually be reduced by excess L-lactate according to *Figure 3.2* (p76). However, the slow phase illustrated requires inter-subunit and inter-tetramer electron transfer to have taken place before the process is complete (see *Section 3.2a;* p76).

3.3 Discussion

Many of the steps within the catalytic cycle of flavocytochrome b_2 have been studied before, but the intramolecular electron transfer between FMN semiquinone and b_2-haem has proved difficult to observe. Monitoring the pre-steady-state flavin oxidation process using stopped-flow spectrophotometry is a method for achieving this which is of particular relevance to the catalytic cycle. The rate constant obtained for the electron transfer is 120 s^{-1}, which appears to rate-limit the overall catalytic cycle to 100 s^{-1} (see *Figure 3.1;* p73). Confirmation of this comes from quenched-flow EPR experiments which show that during steady-state turnover, around 75% of the enzyme is in the FMN semiquinone form.

The reason why FMN semiquinone to b_2-haem electron transfer is so slow in comparison to that from FMN hydroquinone to b_2-haem (>1500 s^{-1}) is unclear. Based on electrode potentials for the redox couples involved in the two one electron transfers, one would expect semiquinone to haem electron transfer to be faster than that for hydroquinone to haem (Walker & Tollin, 1991), although these electrode potentials are by no means certain and other workers find the reverse to be true (Cappeillère-Blandin *et al.*, 1986- 'nicked' enzyme; Tegoni *et al.*, 1986- *H. anomala* enzyme). The scope for conformational influences on electron-transfer rate constants is extensive in this case owing to the significant mobility of the two prosthetic groups with respect to each other. Such factors mean that the electron-transfer rate constants are likely to be altogether less predictable than for systems in which electron-transfer distance and prosthetic group orientation are fixed. Evidence for the mobility of the b_2-haem domain is derived from crystallographic (Xia & Mathews, 1990) and NMR

data (Labeyrie *et al.,* 1988), while the significance of the inter-domain hinge region has been studied by mutagenesis (Sharp *et al.,* 1994; White *et al.,* 1993).

The effect of pyruvate observed on FMN oxidation offers a credible explanation for the steady-state inhibition reported in early studies. The inhibition constant obtained (K_i = 40 ±17 mM) is consistent with the steady-state value reported for non-competitive inhibition. The mechanism by which this occurs is likely to involve thermodynamic stabilisation of the semiquinone coupled with competition for a hydrogen bond to a key active site residue (Tyr143). The enhanced stability of the flavin semiquinone on pyruvate binding would surely increase the enzyme's affinity for pyruvate. However, the inhibition constant observed for flavin oxidation is not indicative of tight binding. Therefore, it may be the role of the haem propionate to dislocate pyruvate from the active site prior to electron transfer by competing for the hydrogen-bond to Tyr143 (see *Figure 1.21;* p39). The reason for the enhanced stability of the FMN semiquinone in the presence of pyruvate may simply be due to the forced retention of the His373 proton, which would position a positive charge immediately adjacent to the FMN ring (see *Figures 1.7;* p13 & *1.8;* p15). However, the distinct stacking position of pyruvate when bound may also allow a degree of electronic stabilisation through pπ orbital overlap.

The physiological reason for this phenomenon is a matter for speculation, but it may simply be an evolutionary redundancy. The related enzyme, L-lactate monooxygenase, has a particularly slow substrate dissociation rate (~2 min^{-1}) which can rate-limit catalytic turnover. This enzyme uses dioxygen as a substrate, which has a low redox potential for the first electron reduction ($E_o(O_2/O_2^{\cdot-})$ = -160 mV; Ingram & Meyer, 1985) and a high potential for the second ($O_2^{\cdot-}/O_2^{2-}$ = +750 mV). Therefore a stabilised semiquinone would allow the two steps to balance offering an evolutionary edge in increased efficiency. The L-lactate monooxygenase semiquinone species binds pyruvate with a K_d of 13.6 μM (Choong & Massey, 1980), which shifts the FMN redox potentials by 150 mV to $FMN^{\bullet-}/FMNH^{-}$ = +80mV and $FMN/FMN^{\bullet-}$ = -370 mV (Ghisla & Massey, 1989; Stankovich & Fox, 1983). Flavocytochrome b_2 is believed to have evolved from a similar FMN-binding oxidase by gene fusion with a small cytochrome (see *Section 1.3;* p5). The switch in redox partner from oxygen to

cytochrome *c* may have induced the mechanism for rapid pyruvate release to speed up the catalytic cycle. This may explain why the b_2-haem propionate protrudes into the enzyme's active site (see *Figure 1.7*).

Tegoni *et al.* (1990) report that pyruvate binds to *H. anomala* flavocytochrome b_2 with a K_d of 0.2 mM under equilibrium conditions. This value is clearly much lower than the inhibition constant derived for the *S. cerevisiae* enzyme from flavin oxidation studies. The inconsistency may be attributable to differences in enzyme structure or, alternatively, to differences between the semiquinone species formed at equilibrium and that formed as a transient during turnover. One potential explanation lies in the redox state of the haem, which is reduced in the equilibrium study, but oxidised in the kinetic study. The haem redox state may affect the ability of the haem propionate to hydrogen-bond to Tyr143 and dislocate pyruvate. This coupling between electron transfer and H-bonding is definitely a strong feature of the flavocytochrome b_2 catalytic cycle, as shown by the mutagenesis study of Miles *et al.* (1992; see *Section 1.10;* p37). The postulation that simultaneous proton transfer also occurs (*Section 1.10*) offers further explanation for the perceived difference. Ultimately, proton transfer steps must be included in the catalytic cycle. It is possible that one of these may be affecting the rate of semiquinone oxidation both in the presence and absence of pyruvate.

CHAPTER 4

THE INTERACTION WITH CYTOCHROME *C*

4.1. Introduction

By catalysing L-lactate dehydrogenation, the FMN-binding domain of flavocytochrome b_2 is able to generate two electrons for a short respiratory chain which culminates in the reduction of molecular oxygen (*Section 1.2;* p4). The latter process is conducted by the multi-subunit complex cytochrome *c* oxidase which uses the energy generated to fuel trans-membrane proton pumping. The electron transport chain linking $FMNH_2$ oxidation to O_2 reduction utilises two distinct electron transferases, the b_2-haem domain and cytochrome *c*. The role of the b_2-haem domain (see *Section 1.8;* p26) is to facilitate the transfer of electrons between $FMNH_2$ and cytochrome *c*. For the separately expressed flavin domain, cytochrome *c* reduction has been shown to occur at only 0.01% of the usual rate (Balme *et al.*, 1995). The electron transfer reaction between the b_2-haem domain and cytochrome *c* has therefore been the subject of considerable interest. In addition, the structural similarity between the b_2-haem domain and cytochrome b_5 makes this an interesting model system to compare to the cytochrome b_5:cytochrome *c* system, for which a great deal of data has already been accumulated (see *Section 1.11;* p40).

Cytochrome *c* binding studies

Several studies report binding between flavocytochrome b_2 and cytochrome *c*, but the lack of correlation between these results makes interpretation difficult. Stoichiometries reported vary between one cytochrome *c* per flavocytochrome b_2 tetramer to one per subunit (Tegoni *et al.*, 1993). Previous studies on the flavocytochrome b_2 L-lactate dehydrogenase from *H. anomala*, which is related to the *S. cerevisiae* enzyme by a 60% sequence identity (Black *et al.*, 1989; *Figure 1.3;* p6), have lead to the conclusion that the cytochrome *c* binding site involves both flavin and b_2-haem domains. Thomas *et al.*, (1983a & b) used the fluorescence quenching of zinc-substituted *H. a.* cytochrome *c* to show that binding occurs to both the flavin and haem domains. Capeillère-Blandin & Albani (1987) observed that the second order rate constants for pre-steady-state cytochrome *c* reduction were faster for the

holoenzyme than the isolated b_2-core, indicating that the catalytically competent complex involved interactions with both domains. Further, ionic strength studies showed that the complex involved a degree of electrostatic attraction, which was less pronounced for the b_2-core. This is examined for the *S. cerevisiae* enzyme in *Section 4.2(b),* p106. Vanderkooi *et al.* (1980) used the fluorescence energy transfer from metal substituted cytochromes *c* to *S. cerevisiae* flavocytochrome b_2 to estimate the distance between redox centres (18 Å). They also found that redox inactive cytochrome *c* derivatives inhibit the steady state reduction of ferricytochrome *c* with a K_i of 13μM (assuming 1:1 stoichiometry). Inhibition of pre-steady-state cytochrome *c* reduction by zinc-substituted cytochrome *c* is considered in *Section 4.2(c),* p110.

Attempts to obtain a crystal structure of the flavocytochrome b_2:cytochrome *c* complex by growing cocrystals (as with cytochrome *c* peroxidase:cytochrome *c*; *Section 1.10;* p33) have failed, but Tegoni *et al.* (1983) reported that diffusion of cytochrome *c* into crystals of flavocytochrome b_2 lead to the formation of a catalytically competent complex with a stoichiometry of 1:1. Based on this premise, and considering the kinetic observations reported for the *H. anomala* enzyme, Tegoni *et al.* (1993) constructed an energy-minimised hypothetical complex for *S. cerevisiae* flavocytochrome b_2 and cytochrome *c*. The model contains a large amount of electrostatic stabilisation through the formation of inter-protein ion-pairs. These involve the positively charged residues on the surface of cytochrome *c* (see *Figure 1.22;* p42) and Glu91, Glu105, Glu110 and Asp510 of flavocytochrome b_2. These acidic residues are positioned around the hinge region of one subunit and on the C-terminal tail of another, interactions with a third subunit were also implicated. *Figure 4.1(a)* illustrates the electron transfer pathway between the two haem redox centres proposed by Tegoni *et al.* (1993) as being the most probable. The alternative orientation shown in *Figure 4.1(b)* raises doubts concerning the credibility of this pathway by illustrating that the closest distance between flavocytochrome b_2 Phe52 and the porphyrin ring of haem *c* is actually 10 Å, whilst Tegoni *et al.* (1993) claim that these are touching. Recently, experimental evidence has been collected which is entirely inconsistent with the model (Daff *et al.,* 1995a).

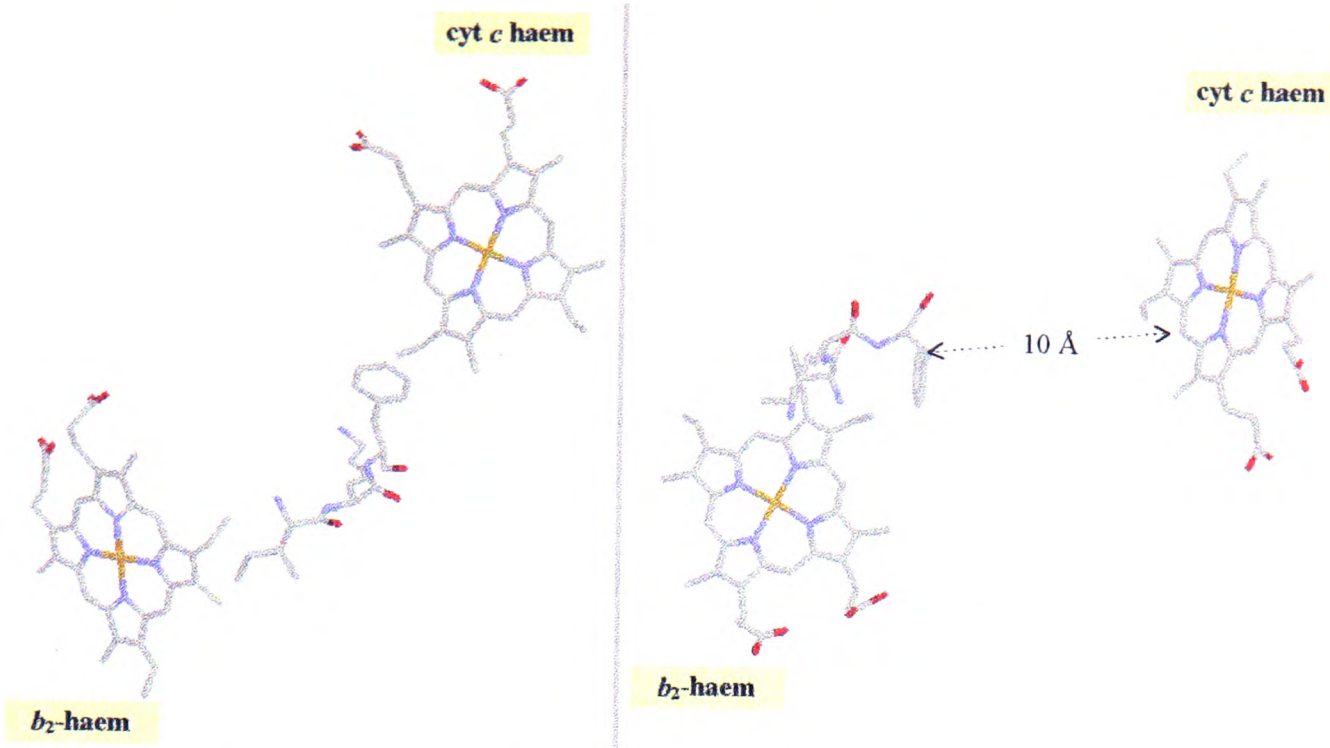

Figure 4.1 The electron transfer pathway from flavocytochrome b_2 to cytochrome *c* proposed by Tegoni & Cambillau (1991), based on their model for the inter-protein complex. The pathway includes the residues Ile50, Lys51 and Phe52, but as the reoriented figure shows, the shortest distance from Phe52 to the cytochrome *c* haem edge is 10 Å. The shortest inter-haem distance is 14 Å.

Intermolecular electron-transfer

The rate constant for electron transfer from b_2-haem to cytochrome *c* within the pre-formed complex has also been studied using a variety of techniques. Capeillère-Blandin (1982) reported that at 5°C the maximum rate of pre-steady-state cytochrome *c* reduction by flavocytochrome b_2 from *H. anomala* was 380 s^{-1}. McLendon *et al.* (1987) used metal-substituted cytochrome *c* derivatives to vary ΔG in electron-transfer reactions within the *S. cerevisiae* flavocytochrome b_2 :cytochrome *c* complex formed at low ionic strength. Analysis of the data in light of Marcus theory (*Section 1.9;* p28) lead them to conclude that the rate constants observed were essentially independent of driving force and that the electron transfer reaction is limited by conformational gating. The rate constant for electron transfer between flavocytochrome b_2 and ferricytochrome *c* was reported to be 200 ±80 s^{-1} at 24°C. This is considered further in *Section 4.2(a).*

4.2 Results

4.2(a) Pre-Steady-State Reduction of Cytochrome *c*

Reduction of a sub-stoichiometric amount of cytochrome *c* (1 μM after mixing) by reduced flavocytochrome b_2 (2-15 μM after mixing) was monitored by stopped-flow spectrophotometry at 416.5 nm as described in *Section 2.9* (p62). *Figure 4.2* shows an example of a stopped-flow trace fitted to a single exponential function to give a pseudo-first-order rate constant for the process. Since the concentration of cytochrome *c* is sub-stoichiometric and the b_2-haem is being continually reduced by L-lactate (10 mM), the reaction can be considered essentially first order. *Figure 4.4* shows a plot of observed rate constant against wild-type flavocytochrome b_2 concentration, which shows an approximately linear dependency up to 10 μM, with the rate constant approaching 350 s^{-1}. Each of the generated traces fitted well to a single exponential function (see *Figure 4.2*), indicating that the reduction process is controlled by a single rate-determining step. The two possibilities

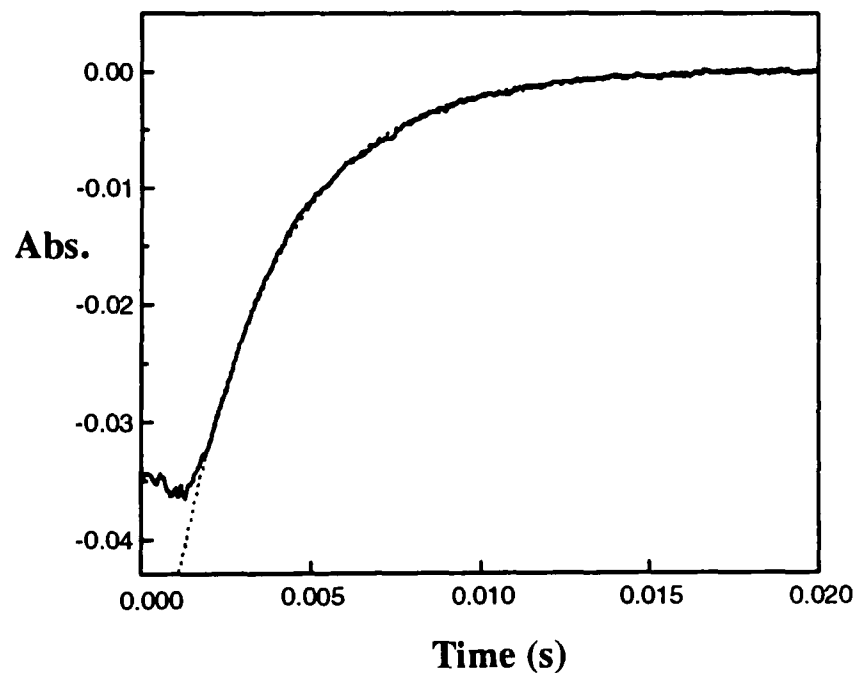

Figure 4.2 An example of a stopped-flow cytochrome *c* reduction trace: generated by mixing 1 μM ferricytochrome *c* with 10 μM flavocytochrome b_2 in Tris/HCl buffer pH 7.5, *I* 0.10 (see *Section 2.7*; p59). The trace is fitted to a single exponential function with rate constant 340 s^{-1} (·····).

for this mechanism are shown in *Figure 4.3*. Either (i) complex formation is rapid and reversible, while electron transfer within the pre-formed complex is slow, or (ii) cytochrome *c* binding is slow while electron transfer is faster than both binding and dissociation. Model (i) would generally produce a hyperbolic curve saturating at the electron-transfer rate with $K_m = K_d$ for the bound complex. The linear region observed in *Figure 4.4* would therefore have to occur at concentrations much less than the K_d for the bound complex. Model (ii) would generate a linear plot until the rate of binding approached the rate of electron transfer at which point single exponential functions would no longer fit to the experimental traces. The curvature shown in *Figure 4.4* cannot, however, be used as conclusive evidence in favour of model (i) since the pseudo-first-order rate constants are approaching levels at which a significant proportion of the absorbance change is lost to the instrument dead-time. The error bars shown indicate also how accuracy decreases with increasing rate constant. Under such circumstances it would be impossible to predict the reason for the curvature, the traces could for example be subject to deviation from first-order kinetics as described by model (ii). The further information required to solve this problem is presented in *Section 4.2(c)* in terms of a dissociation constant for cytochrome *c*. The value arrived at by studying inhibition of the cytochrome *c* reduction process is a K_d of approximately 8 μM for ferro- and zinc-substituted cytochrome *c*. In contrast with this, *Figure 4.4* shows a fit to a Michaelis-Menten

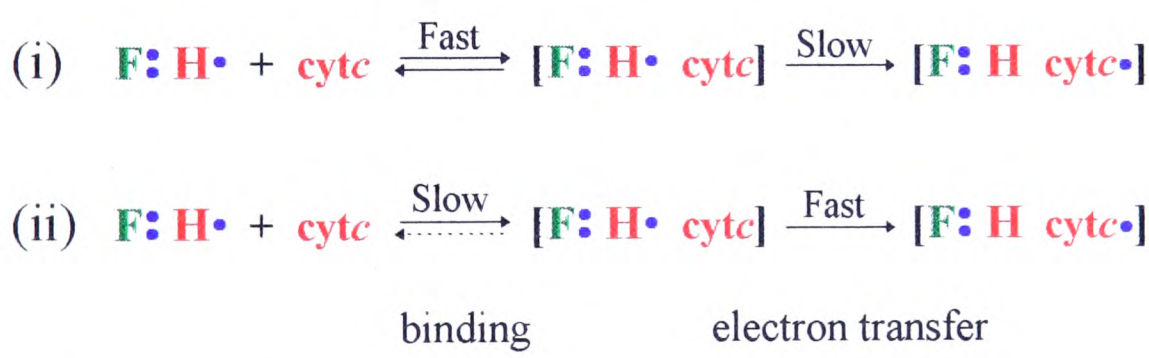

Figure 4.3 Pre-steady-state reduction of cytochrome *c* by excess flavocytochrome b_2 (two possible models). Under standard conditions cytochrome *c* reduction follows a single exponential function. This is only possible if one of the two schemes illustrated above is satisfied by the reaction mechanism. Therefore either (i) cytochrome *c* binding is fast and reversible and electron transfer slow by comparison, or (ii) cytochrome *c* association/ dissociation is slow and electron transfer is fast. For legend, see *Figure 1.14* (p28).

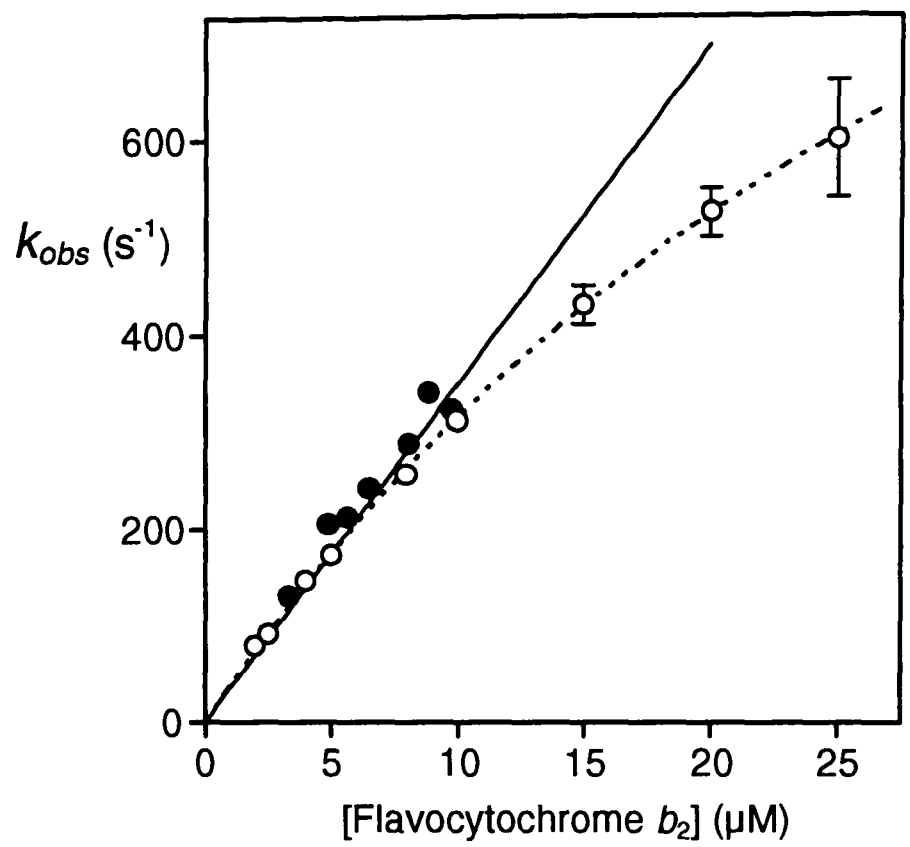

Figure 4.4 Derivation of the second-order rate constant for cytochrome c reduction. Pseudo-first order rate constants for cytochrome *c* reduction (k_{obs}) are plotted against flavocytochrome b_2 concentration. Data points < 10 μM are fitted to a straight line, gradient 35 ± 1 μMs^{-1} (———). • data points collected by D. Short in an independent experiment. ------ fit to Michaelis Menten equation, K_m = 41 ± 2 μM, k_{cat} = 1585 ± 45 s^{-1}. Error bars represent the range of values generated from different single exponential fits.

function with K_m = 41 μM. Unless the dissociation constant for ferricytochrome *c* really is 5-fold higher than for ferrocytochrome *c* this allows model (i) to be eliminated. The second-order rate-constant therefore represents the actual rate constant for cytochrome *c* binding and the rate constant for electron transfer can be expected to be much faster than that for cytochrome *c* dissociation.

For flavocytochrome b_2, the rate constant for electron transfer from b_2-haem to cytochrome *c* within the pre-formed complex has been estimated by photochemical excitation to be 200 (± 80) s^{-1} at 25°C (McLendon *et al.*, 1987). For the *H. anomala* enzyme, the rate constant has been determined from stopped-flow/ionic strength experiments to be 380 s^{-1} at 5°C (Capeillère-Blandin, 1982). In our experiments on the *S. cerevisiae* enzyme (at 25°C), cytochrome *c* reduction occurs at rates beyond the reliable range of the stopped-flow technique, and must be in excess of 1000 s^{-1}.

While the second value is not inconsistent with this, in view of the lower temperature used and different enzyme form, it seems unlikely that the electron-transfer rate constant could be as low as 200 s^{-1} as determined by photochemical excitation. As *Figure 4.4* shows, rate constants for cytochrome *c* reduction are observed to be well in excess of $500s^{-1}$. Beyond this, accompanying faster reaction rates, a decrease in signal amplitude due to the stopped-flow dead-time is observed (see *Section 2.9;* p62). A similar effect occurs as the ionic strength is decreased (*Figure 4.6;* p109).

4.2(b) Variation of the Second-Order Rate Constant for Cytochrome *c* Reduction with Ionic Strength

Second-order rate constants were determined for cytochrome *c* reduction at a series of different ionic strengths using the same methodology as described in *Section 4.2(a)*. All experiments were conducted in 10 mM Tris/HCl buffer pH 7.5 (see *Section 2.7;* p59) containing 1 mM L-lactate (after mixing), the ionic strength was adjusted by mixing with the appropriate amount of buffer containing 1 M NaCl . At each ionic strength pseudo-first-order rate constants were determined at least four

---

The Primary kinetic salt effect

$$\log(k_2) = \log(k_2^\circ) + 2AZ_+Z_-\sqrt{I}$$

Is derived by incorporating the Debye-Hückel limiting law into Bronsted's kinetic relation. Debye-Hückel theory uses the notion of an ionic atmosphere to calculate the free energy of an ion in solution. For two reacting charged species, the affect of the ionic atmosphere is found to be different on the reactive complex than on the individual ions. The limiting law applied above assumes the ions are point charges and ignores some solvent effects, such shortcomings are therefore important to note when studying macromolecules at high ionic strength.

Z_+, Z_-	unit ionic charges.
I	ionic strength of the solution determined according to $\Sigma_i \frac{1}{2}c_iZ_i^2$ where c_i is the concentration of ion i.
A	a temperature and solvent dependent constant; for water at 25°C A = 0.5115 $mole^{-1/2}l^{1/2}$
k_2	second-order rate constant.
k_2°	second-order rate constant at I 0

Perlmutter-Hayman (1973), Robinson & Stokes (1959)

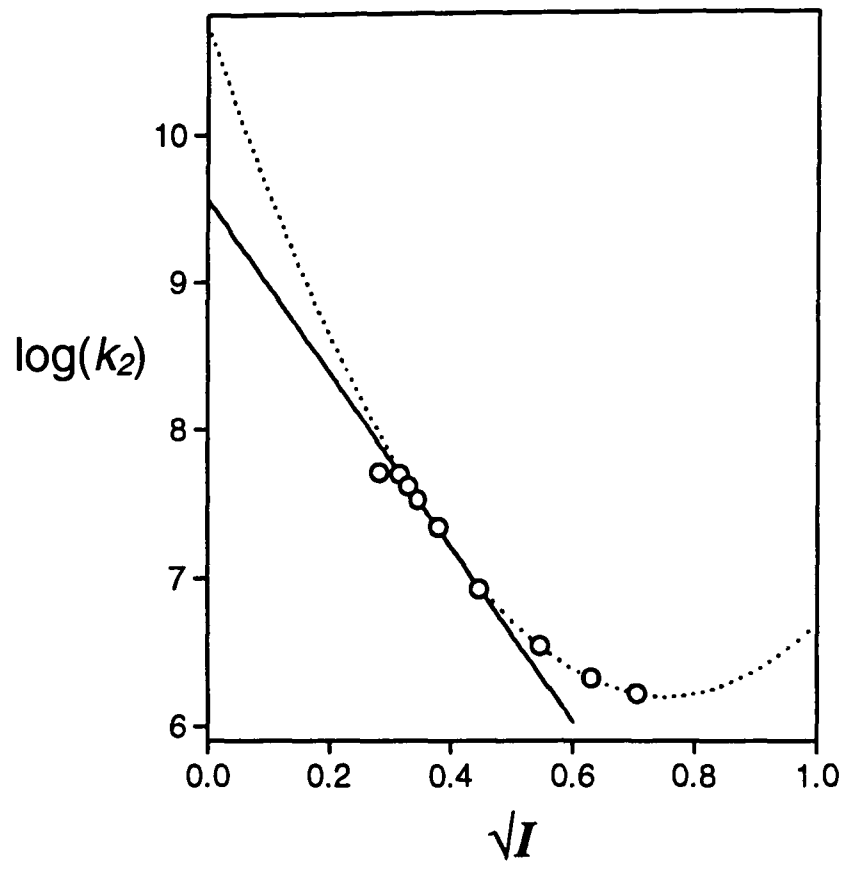

Figure 4.5 Debye-Hückel plot of the second-order rate constants for cytochrome *c* reduction. The rate constants (as log(k_2)) are plotted against the square-root of ionic strength. ——— fit to the Debye-Hückel limiting law ($\log(k_2) = \log(k_2^\circ) + 2AZ_+Z_-\sqrt{I}$) gradient ($2AZ_+Z_-$) = -5.9 ± 0.1 (NB/ Fit restricted to 5 data points *I* 0.10 to 0.20); ---------- fit to parabolic curve ($\log(k_2) = \log(k_2^\circ) + 2AZ_+Z_-\sqrt{I} - BI$) gradient at *I* 0 ($2AZ_+Z_-$) = -12.1 ± 0.5, B = -8.0 ± 0.5. Errors represent standard deviations from a least-squares fit.

different flavocytochrome b_2 concentrations, the resultant data being used to determine the second-order rate constant by linear regression analysis.

Figure 4.5 shows second-order rate constants for cytochrome *c* reduction plotted as logarithms against the square-root of ionic strength. The straight line fit for $\log(k_2)$ versus $\sqrt{I}$ according to the Debye-Hückel limiting law, has a gradient $2AZ_+Z_-$ = -5.9 ± 0.1, indicating a positive/negative interaction at the cytochrome *c* binding site. However it is clear from *Figure 4.5* that the fit is far from satisfactory, deviating strongly at high ionic strength. This is not surprising in view of the well documented non-ideal behaviour exhibited during protein:protein interactions (Koppenol, 1980; Koppenol *et al.*, 1978). Further, the ionic strength region studied (0.1 to 0.5) is well outside the range considered reasonable for an ideal solution (Robinson & Stokes,

1959) and even $NaCl_{(aq)}$ deviates from ideality. By introducing a term linearly dependent on ionic strength (with coefficient B) to the fitting function, a parabolic curve is generated. This fits better to the data, and at $I = 0$ has a gradient of $2AZ_+Z_- = -12.1 \pm 0.5$, which again indicates a significant positive/negative interaction. The theoretical basis of this equation is also limited, as the coefficient B has no simple physical meaning (Perlmutter-Hayman, 1973). Although a term linearly dependent on ionic strength will help to compensate for deviations due to short range solvent effects and to the increasing significance of the ionic radius at high concentration. However, in this case the introduction of coefficient B serves only to demonstrate the magnitude of uncertainty in the value of Z_+Z_- derived from *Figure 4.5*.

It is also worth noting that the Debye-Hückel plots derived for *H. anomala* flavocytochrome b_2 (Capeillère-Blandin & Albani, 1987) and for microsomal cytochrome b_5 (Eltis *et al.*, 1991) have slopes of similar shape and gradient.

Low ionic strength

At lower ionic strength the stopped-flow method used to obtain second-order rate constants becomes unusable. The cytochrome *c* reduction traces no longer fit to single exponential functions, suggesting that the reaction is now dependent on multiple rate-determining steps. *Figure 4.6* shows four stopped-flow traces at different ionic strengths, each fitted to a single exponential function. At lower ionic strength the amplitude of the observed reaction decreases, and the apparent rate of reaction becomes slower - although the fit quality is poor. The decrease in amplitude indicates that a larger proportion of the reaction is occurring within the stopped-flow dead-time, and is therefore happening too fast to be observed fully. This effect is to be expected if the trend of increasing second-order rate constant with decreasing ionic strength was continued as in *Figure 4.5*. The appearance of a slow phase indicates that not all the cytochrome *c* is reduced by this rapid step, but a proportion is delayed possibly by an inhibitory binding process. Such a deviation from pseudo first-order behaviour seriously limits the range of ionic strengths which can be used for the Debye-Hückel plot.

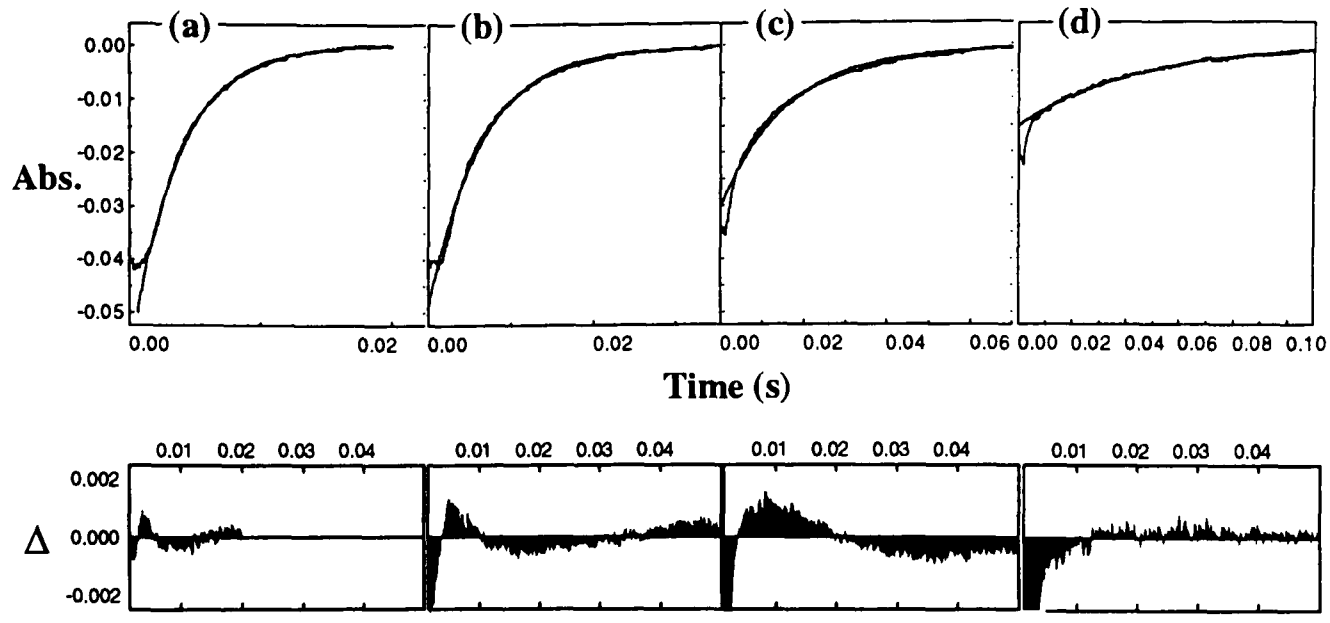

Figure 4.6 Stopped-flow traces showing cytochrome *c* reduction at low ionic strength. Pre-steady-state reduction of 1 μM cytochrome *c* by 8 μM reduced flavocytochrome b_2 was monitored at 25°C, in 10 mM Tris/HCl buffer, pH 7.5 containing 1 mM L-lactate at 4 different ionic strengths (adjusted by addition of NaCl). Each trace is fitted by non-linear least-squares regression analysis to a monophasic exponential function (shown) with rate constant *k* and amplitude A. (a) *I* 0.075, $k = 280\ s^{-1}$, A = 0.060; (b) *I* 0.050, $k = 171\ s^{-1}$, A = 0.051; (c) *I* 0.025, $k = 72\ s^{-1}$, A = 0.031; (d) *I* 0.010, $k = 24\ s^{-1}$, A = 0.015. The difference plots shown were calculated by subtracting the fit functions from the acquired data.

At low ionic strength it is likely that weak electrostatic attractions will become significant allowing cytochrome *c* molecules to bind to alternative sites. Reduction of these cytochrome *c* molecules would therefore be delayed. The amount of delay would depend on the dissociation rate constant which may in turn be influenced by ionic strength. The residual fast phase prevents the traces from fitting to mono-exponential functions (see difference plots). However, it decreases in amplitude until, at *I* 0.01 (*Figure 4.6(d)*), it has all but disappeared and the trace is essentially monophasic, as is illustrated by the difference plots. Using the Debye-Hückel limiting law to calculate a rate constant at this ionic strength (based on *Figure 4.5*) we can estimate that for a 8 μM enzyme solution $k_{obs} = 7500\ s^{-1}$. This would clearly not be observed in a stopped-flow experiment with a dead-time of 1 ms.

4.2(c) Inhibition of Cytochrome *c* Reduction

Pre-steady-state cytochrome *c* reduction by wild-type flavocytochrome b_2 was inhibited by the addition of either zinc-substituted cytochrome *c* (prepared as in *Section 2.10;* p67) or ferrocytochrome *c* to the pre-reduced enzyme, as described in *Section 2.9* (p62). Zn-cytochrome *c* has been widely used in place of ferrocytochrome *c* to study binding interactions and electron transfer (e.g. Thomas *et al.*, 1983a & b; McLendon *et al.*, 1987; Alleyne *et al.*, 1992). Recently, Anni *et al.* (1995) used NMR to assess the affect of metal substitution on the protein framework. The fact that they found no significant structural change provides justification for its extensive use. For each experiment the flavocytochrome b_2 and ferricytochrome *c* concentrations were kept constant at approximately 8 μM and 2 μM respectively, while inhibitor

---

The model used to quantify inhibition of pre-steady-state cytochrome c reduction

Pre-steady-state cytochrome *c* reduction occurs with second order rate constant k_0. Inhibition causes this to decrease to a lower value, k_r, at saturation. Assuming that there is a single primary electron transfer site per enzyme subunit which can be occupied by inhibitor, then $k_0 - k_r$ represents the second order rate constant for electron transfer at this site while k_r refers to all others cumulatively. If enzyme (**E**) and inhibitor (**I**) are in equilibrium with the complex (**E.I**), the observed rate depends on the dissociation constant:

$$\begin{array}{rll} & \mathbf{E + I} & \Rightarrow \text{ cyt}c \text{ reduction with rate } k_0[\mathbf{E}] \\ \text{dissociation constant: } & \mathbf{K_i} \uparrow\downarrow & \\ & \mathbf{E.I} & \Rightarrow \text{ cyt}c \text{ reduction with rate } k_r[\mathbf{E.I}] \end{array}$$

If the total concentrations of inhibitor and enzyme are $\mathbf{I_t}$ and $\mathbf{E_t}$ respectively then,

$$\mathbf{K_i} = \frac{[\mathbf{E}](\mathbf{I_t} - \mathbf{E_t} + [\mathbf{E}])}{\mathbf{E_t} - [\mathbf{E}]}$$

It is inappropriate to apply the approximation $\mathbf{I} = \mathbf{I_t}$ at low inhibitor concentrations, so this equation must be solved for [**E**] as a quadratic such that;

$$[\mathbf{E}] = \frac{\mathbf{E_t} - \mathbf{I_t} - \mathbf{K_i} + \sqrt{((\mathbf{E_t} - \mathbf{I_t} - \mathbf{K_i})^2 + 4\mathbf{K_i}\mathbf{Et})}}{2}$$

Since the observed rate of reaction is the sum of the two contributing factors, $k_0[\mathbf{E}] + k_r[\mathbf{E.I}]$ inhibition data can be fitted to the equation:

Equation 4.1
$$k_{obs} = k_r\mathbf{E_t} + \tfrac{1}{2}(k_0 - k_r)(\mathbf{E_t} - \mathbf{I_t} - \mathbf{K_i} + \sqrt{((\mathbf{E_t} - \mathbf{I_t} - \mathbf{K_i})^2 + 4\mathbf{K_i}\mathbf{Et})})$$

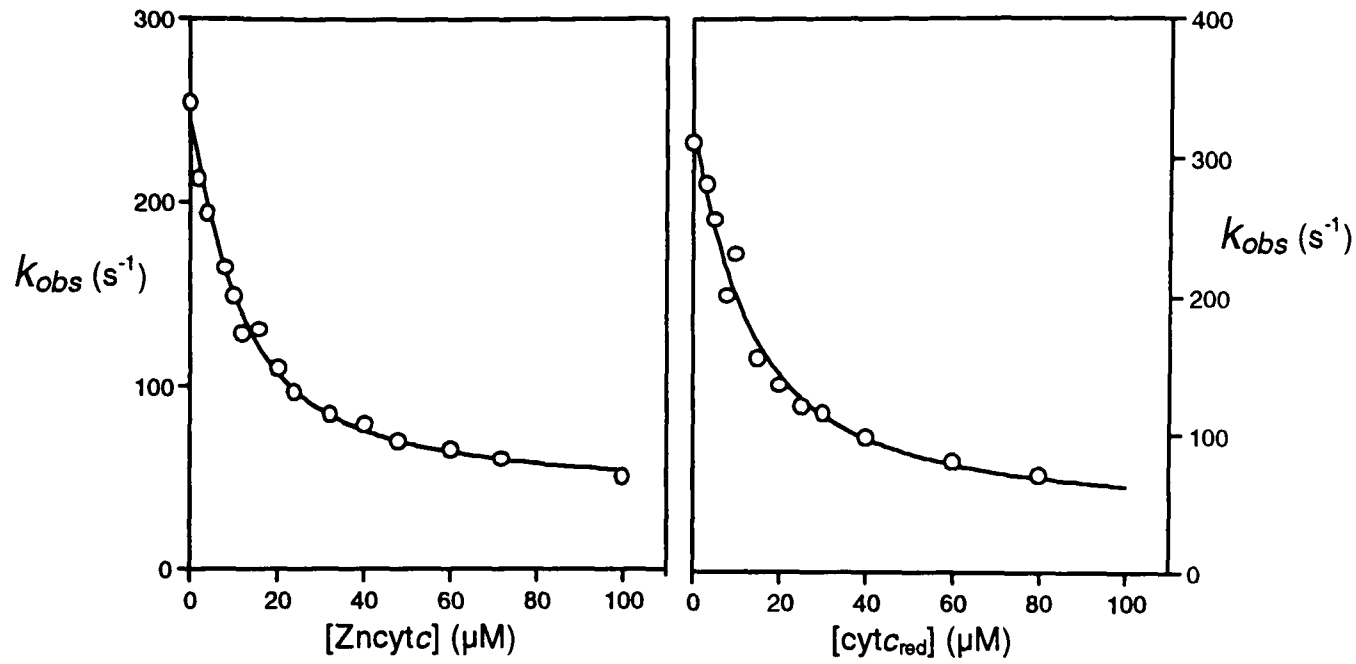

Figure 4.7 Plots showing inhibition of pre-steady-state cytochrome *c* reduction. The rate constants observed (k_{obs}) for pre-steady-state reduction of ferricytochrome *c* (2 μM) by wild-type flavocytochrome b_2 are shown plotted against inhibitor concentration. (a) Inhibitor is zinc-substituted cytochrome *c* and concentration of flavocytochrome b_2 is 8.0 μM. (b) Inhibitor is ferrocytochrome *c* and concentration of flavocytochrome b_2 is 8.3 μM. Both data sets are fitted to *Equation 4.1* by non-linear least-squares regression analysis:

Inhibitor (I)	**E_t (μM)**	**K_i (μM)**	**k_r ($\mu M^{-1}s^{-1}$)**	**k_0 ($\mu M^{-1}s^{-1}$)**
Zn-cytochrome c	8.0	7.3 ± 0.9	4.9 ± 0.5	31 ± 1
Ferrocytochrome c	8.3	8.8 ± 2.3	5.8 ± 0.9	38 ± 2

concentration was varied. The ferrocytochrome *c* generated will itself contribute to inhibition, but this is considered to be insignificant, particularly when compared to the larger amounts added prior to reaction. The inhibition curves plotted in *Figure 4.7* are clearly very similar, this indicates that the use of ferrocytochrome *c* rather than Zn-cytochrome *c* does not overtly complicate the kinetics by forcing a reverse reaction.

For a monophasic reaction reaching equilibrium, the observed rate constant is the sum of the rate constants for the forward and reverse steps, and is therefore dependent on the position of equilibrium. The redox potential difference between b_2-haem (White *et al.*, 1993) (electron donor) and cytochrome *c* (Loach, 1976) (electron acceptor) is around 270 mV, and therefore the equilibrium lies strongly in favour of cytochrome *c* reduction. In addition, L-lactate in the reaction mixture continually reduces the b_2-haem (via FMN) further displacing the equilibrium towards cytochrome *c* reduction (the redox potential difference between L-lactate/pyruvate

and cytochrome *c* reduced/oxidised is around 440 mV (Loach, 1976)). Both systems appear to exhibit partial inhibition such that at high inhibitor concentration a significant rate constant is still observed (around 20% of the maximum value). This indicates that when the primary binding site is occupied by inhibitor, cytochrome *c* reduction can still occur, albeit more slowly.

K_i values for both curves are presented in *Figure 4.7,* both Zn-cytochrome *c* and ferrocytochrome *c* appear to cause partial inhibition with a dissociation constant of around 8 μM at the primary binding site. The model used to calculate these values assumes a single cytochrome *c* binding site per subunit of flavocytochrome b_2, and introduces a residual second-order rate constant k_r to account for the minimum rate constant observed. Although the curves saturate at 50-60 s^{-1} it seems likely that this value will be dependent on the concentration of flavocytochrome b_2, and is therefore treated as a second-order process (i.e. k_r $\mu M^{-1}s^{-1}$). However it is an approximation to assume that the concentration dependence is entirely linear. Firstly, it is unreasonable to expect the alternative reaction sites utilised by this residual process to be non-binding, eventually they would be expected to become occupied by inhibitor molecules just like the primary binding site. Therefore *Equation 4.1* is only valid over an inhibitor concentration range encompassing the primary binding site, but excluding all other electron transfer sites. Secondly, it is impossible to predict electron-transfer rate constants for the alternative sites, although *Section 4.2(a)* shows that this is not a limiting factor for the primary site. It may be the case that some, or all, of the alternative sites have lower electron-transfer rate constants which, if approached, would certainly lead to deviation from linearity. The low ionic strength study in *Section 4.2(b)* provides direct evidence for poor-activity binding sites.

Overall, perhaps the most significant assumption made by *Equation 4.1* is that the stoichiometry of cytochrome *c* binding to flavocytochrome b_2 is one primary site per enzyme subunit, especially in view of the conflicting reports discussed by Tegoni (1993). The fact that the function fits the data so well can be viewed as evidence in favour of the single binding site model, although as outlined above, there are too many unknown quantities to attach any certainty to this.

Vanderkooi *et al.* (1980) conducted steady-state inhibition of cytochrome *c* reduction using porphyrin cytochrome *c* and a K_i value of 13 μM was calculated. However, according to the kinetic model discussed in *Chapter 3* (p73), competitive inhibition should only be observed at low concentrations, where *Steps 3* and *5* are rate-determining. This theory was confirmed by comparing the rates for steady-state ferricytochrome *c* reduction at saturating concentrations (100 μM cytochrome *c*) with and without an equimolar concentration of zinc-substituted cytochrome *c*. Rate constants measured in the presence of Zn-cytochrome *c* were at least 90% of those measured with no inhibitor present. Therefore steady-state inhibition can also be considered partial.

4.2(d) The Effect of Zinc-substituted Cytochrome *c* Binding on Flavocytochrome b_2 Reduction.

The possibility that inhibition by ferro-/Zn-cytochrome *c* in the steady-state may not be entirely competitive in nature was examined by monitoring flavocytochrome b_2 reduction by L-lactate in the presence of Zn-cytochrome *c*. Particular interest lies in the intramolecular electron-transfer step which presumably depends on the relative orientation and position of the two domains. Both FMN and b_2-haem reduction traces were generated on mixing 10 mM L-lactate with 10 μM flavocytochrome b_2, pre-mixed with 0, 10, 20 μM Zn-cytochrome *c* (concentrations after mixing), these are shown in *Figure 4.8*. The fact that they overlay so precisely indicates that the presence of bound Zn-cytochrome *c* has little affect on FMN reduction or FMN to b_2-haem electron transfer unless the oxidised enzyme has a substantially lower Zn-cytochrome *c* binding affinity than the reduced form.

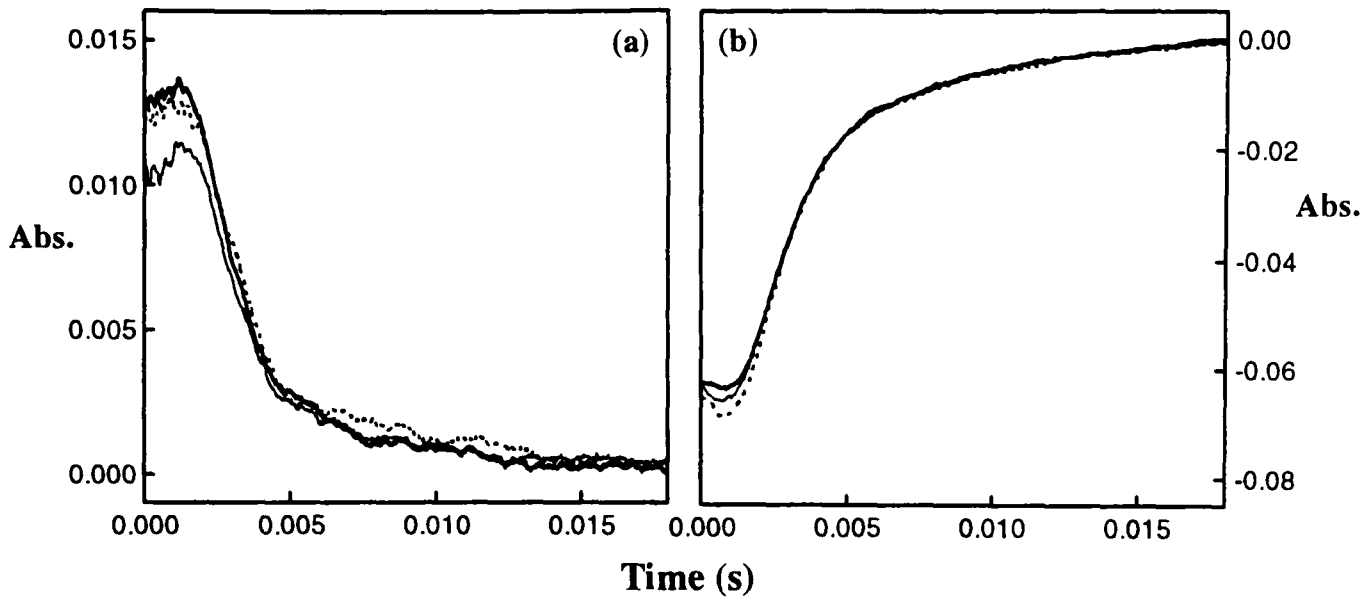

Figure 4.8 Stopped-flow traces showing flavocytochrome b_2 reduction in the presence of zinc-substituted cytochrome *c*. The traces were generated by reducing 10 μM flavocytochrome b_2 with 10 mM L-lactate in the presence of 0 (——), 10 (——), 20 (.....) μM Zn-cytochrome *c*. (a) Flavin reduction recorded at 438.3 nm (b) b_2-haem reduction recorded at 557 nm.

4.3 Discussion

The complex formed between *S. cerevisiae* flavocytochrome b_2 and cytochrome *c* appears to be stabilised by a significant electrostatic component, as demonstrated by the ionic strength study (*Section 4.2b;* p106). This behaviour correlates well with the cytochrome *c* interactions of both *H. anomala* flavocytochrome b_2 (Capeillère-Blandin & Albani, 1987) and microsomal cytochrome b_5 (Eltis *et al.,* 1991). The sequence comparison between *S. cerevisiae* b_2-haem domain, *H. anomala* b_2-haem domain and cytochrome b_5 included in *Figure 1.3* (p6), illustrates the high degree of amino-acid conservation. This qualifies as a credible starting point for identifying the active cytochrome *c* binding region, especially when coupled with the successful Salemme model for cytochrome b_5 (see *Section 1.11;* p45). There are, however, limitations in attempting to draw comparisons between cytochrome b_5 and flavocytochrome b_2. Firstly, cytochrome *c* is unlikely to be a natural substrate of microsomal cytochrome b_5, which would seriously curtail the possibility of binding-site evolution in this case. Secondly, the evidence for a strong

interaction between cytochrome *c* and the flavin domain of flavocytochrome b_2 cannot be ignored in the realistic construction of a model. Following the failure of the model proposed by Tegoni *et al.* (1993) to withstand kinetic scrutiny (Daff *et al.,* 1996b), strategic site-directed mutagenesis is currently being employed in the search for the primary cytochrome *c* binding site. The pre-steady-state inhibition studies performed with zinc-substituted cytochrome *c* are consistent with the presence of a single, dominant electron transfer binding site per flavocytochrome b_2 subunit. The observation that other, low affinity sites also contribute to electron transfer, indicates that the reaction is somewhat non-specific. The notion that flavocytochrome b_2 is a crude product of gene fusion implies that stringent molecular recognition is not a physiological necessity in this case.

The conclusion reached in *Section 4.2(a),* p104, that the intra-complex electron transfer rate constant is >1000 s^{-1} is at odds with the value of 200 s^{-1} reported by McLendon *et al.* (1987). In comparison Willie *et al.* (1992) estimate the rate constant for cytochrome b_5 to cytochrome *c* electron transfer to be 4×10^5 s^{-1}. At low ionic strength, stopped-flow traces were shown to be biphasic. This could be caused by inhibitory binding at non-productive sites, or may derive from a slow conformational change preceding electron transfer at a productive binding site. A similar effect was observed for the reaction between cytochrome b_5 and cytochrome *c* (Willie *et al.,* 1992). Factors such as these hinder theoretical analyses (e.g. the application of Marcus theory; *Section 1.9;* p28) by introducing ambiguity into both structural and kinetic data.

Since the second-order rate constant measured for cytochrome *c* reduction (35 $\mu M^{-1}s^{-1}$) appears to be equivalent to an association rate according to *model (ii); Figure 4.3* (p104), the dissociation constant derived from the inhibition studies (K_d = 8 μM) can be used to estimate the rate constant for cytochrome *c* dissociation (280 s^{-1}; although this assumes that ferro, ferri and zinc-substituted cytochrome *c* all bind with the same affinity). The relatively low dissociation rate constant may be expected to affect rapid catalytic turnover of flavocytochrome b_2 (see *Chapter 3;* p73), but the lack of zinc-cytochrome *c* inhibition observed at high ferricytochrome *c* concentrations discounts this. The availability of alternative electron transfer sites

must therefore improve the performance of this enzyme under these circumstances, whereas tight binding is clearly an advantage at low cytochrome *c* concentrations. The physiological significance of this efficient cytochrome *c* reductase ability is a more diffuse question.

CHAPTER 5

SUBSTRATE SPECIFICITY

5.1. Introduction

As established in *Section 1.2* (p3), flavocytochrome b_2 acts physiologically as a L-lactate dehydrogenase within the mitochondrial inter-membrane space of *Saccharomyces cerevisiae*. However, as discussed in *Section 1.7* (p24), it is also able to utilise several other 2-hydroxy-acids as substrates. *Figure 5.1* focuses in on the structural relationship between the product molecule, pyruvate, and the surrounding amino-acid residues, according to the X-ray crystal structure of the enzyme (Xia &

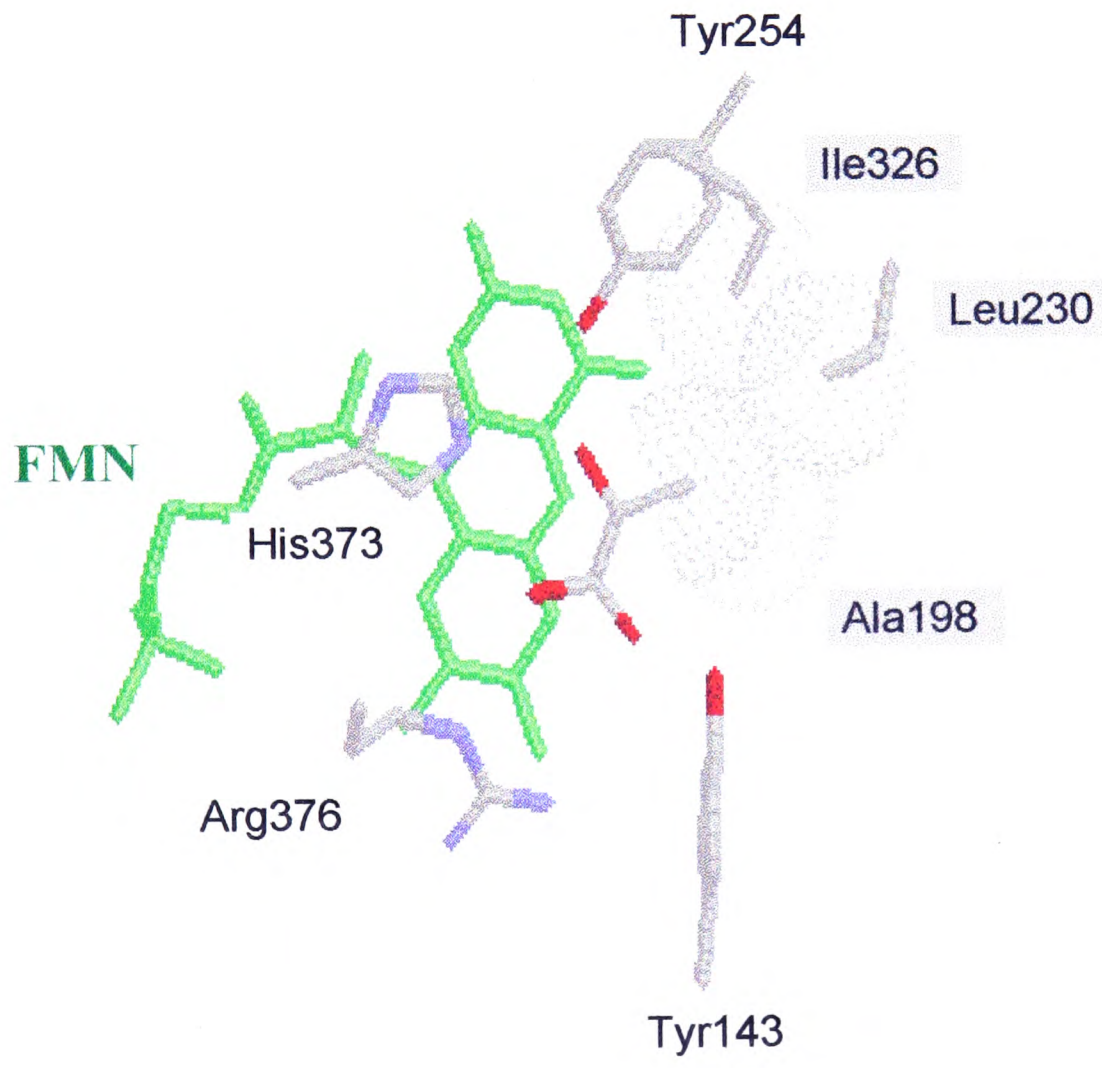

Figure 5.1 The structure of the flavocytochrome b_2 active site derived from X-ray crystallography (Xia & Mathews, 1991) illustrates how pyruvate interacts with key amino-acid residues. The side-chains of Ala198, Leu230 and Ile326 are thought to influence substrate specificity by forming hydrophobic contacts with the substrate methyl group. The dots indicate Van der Waal's contact ranges for these groups.

Mathews, 1990). The catalytic importance of several of these active site residues has already been covered in *Sections 1.5* and *1.6* (p12-23), with the conclusion that dehydrogenation is probably accomplished by hydride transfer from substrate C_2 to FMN N_5. Arg376 forms a salt-bridge with the carboxylate end of the substrate which is believed to anchor it in place, while His373 and Tyr254 are respectively thought to deprotonate and then stabilise the hydroxyl group of the substrate. Therefore, the relative orientations of these residues control the group specific nature of the enzyme (for 2-hydroxy-acids) and its stereospecificity. In accordance, the flavin binding domain of flavocytochrome b_2 is closely related to several other 2-hydroxy-acid dehydrogenases which retain the same key residues. Among these enzymes are glycolate oxidase from spinach (Volokita & Somerville, 1988), lactate oxidase from *Mycobacterium smegmatis* (Giegel *et al.*, 1990), lactate dehydrogenase from *Escherichia coli* (Dong *et al.*, 1993), mandelate dehydrogenase from *Pseudomonas putida* (Tsou *et al.*, 1990) and long-chain hydroxy-acid dehydrogenase from rat kidney (Lê & Lederer, 1991; see *Figure 1.3*, p6). The sequence homology is bolstered by the startling similarity between the active site structures of flavocytochrome b_2 and spinach glycolate oxidase from X-ray crystallography (*Figure 1.7*, p13).

In this chapter, the ability of flavocytochrome b_2 to differentiate between 2-hydroxy-acids will be considered. Therefore, the sequence comparison (*Figure 1.3*) and X-ray crystal structure (*Figure 5.1*) constitute an ideal starting point. Close inspection of the crystal structure reveals that the methyl group of pyruvate lies in a pocket of hydrophobic amino-acid side-chains (Ala198, Leu230, Leu286 and Ile326), several of which are within Van der Waal's contact range. Referring back to the sequence comparison, it is immediately apparent that, neither these nor the surrounding residues are well conserved (except with flavocytochrome b_2 from *H. anomala,* which is also a L-lactate dehydrogenase). In order to examine the role of each of these residues, site-directed mutagenesis was used to disrupt their interactions with the substrate. The strategy employed was to mutate the hydrophobic side-chains to smaller variants, thereby decreasing steric bulk in the appropriate region of the active site, in order to shift the substrate specificity of the enzyme away from L-lactate and towards larger 2-hydroxy-acids with hydrophobic substituents. The wild-type and

Table 5.1 The 2-hydroxy-acid substrates with different chain-length used to characterise the substrate specificities of wild-type and mutant flavocytochromes b_2.

Substrate	Chain-length	Structure
glycolate	2	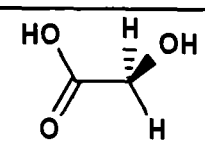
L-lactate	3	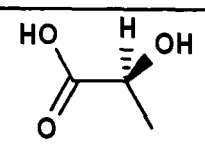
S-2-hydroxybutyrate	4	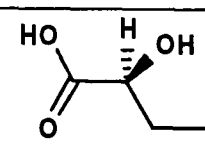
S-2-hydroxyvalerate	5	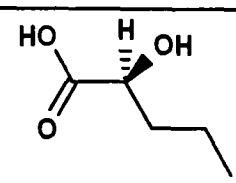
S-2-hydroxycaproate	6	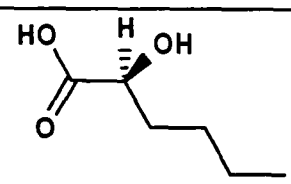
S-2-hydroxyoctanoate	8	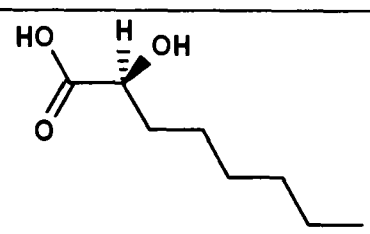

mutant enzymes were all characterised using a series of simple straight-chained 2-hydroxy-acids (see *Table 5.1*). Initially RS-substrate mixtures were used, but to avoid the unpredictability of R-substrate inhibition, as previously reported for D-lactate (Hinkson & Mahler, 1963), all parameters were re-evaluated with the optically pure S isomers. Only the latter set of parameters are presented in the following *Results* sections (the two data-sets being essentially equivalent), but the RS parameters have been reported elsewhere (see *Appendix 4*; Chapman *et al.*, 1993, *Flavins and Flavoproteins* p607-615).

All the mutants discussed in this chapter were generated by Dr F.D.C. Manson as described in *Section 2.1* (p50). However, not all the mutations gave rise to functional enzyme, or were expressed efficiently. In particular, Leu286→Ala disrupted the ability of the protein to bind FMN, the role of Leu286 therefore remains

unstudied. Ala198→Gly, Leu230→Ala and Ile326→Ala were all successful, as was a double mutation incorporating the first two. However, the double mutant of L230A and I326A failed to express a significant quantity of enzyme after transformation. Such problems probably originate during the intricacies of protein folding and remain inextricable.

Comparison with LDH from *B. stearothermophilus*

A similar study by Wilks *et al.* (1988, 1990, 1991, 1992) involved the NADH-dependent L-lactate dehydrogenase from *Bacillus stearothermophilus*. This enzyme converts pyruvate to L-lactate via hydride transfer from NADH and therefore acts in the opposite direction to flavocytochrome b_2 (due to the low redox potential of

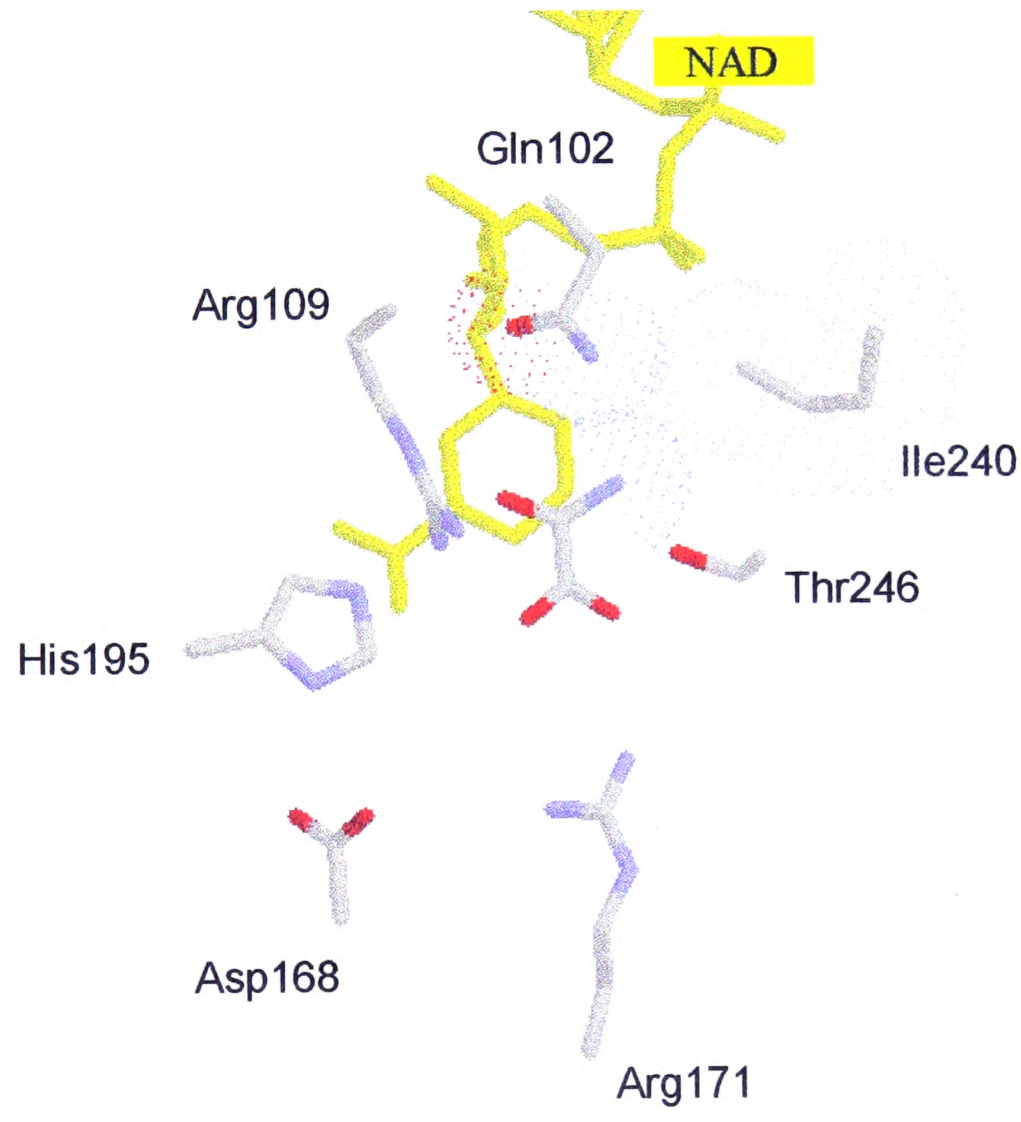

Figure 5.2 The active site of the NADH dependent L-lactate dehydrogenase from *Bacillus stearothermophilus*, as depicted in the X-ray crystal structure (2.5 Å resolution) of Wigley *et al.* (1992). The bound cofactor NAD is shown in yellow with the substrate analogue oxamate positioned centrally in a parallel plane immediately above the nicotinamide ring (compare with *Figure 5.1*)

NAD/NADH; see *Figure 1.6* p10). *Figure 5.2* shows the active site structure of L-lactate dehydrogenase cocrystallised with NAD, the competitive inhibitor, oxamate and the activator molecule fructose-1,6-biphosphate (Wigley *et al.*, 1992). There is an obvious similarity between *Figures 5.2* and *5.1* with regard to the positions of the catalytically important residues relative to the position of substrate/inhibitor. In both cases hydride transfer is thought to take place to the cofactor (FMN or NAD) lying in a parallel plane to the substrate and is initiated by hydroxyl proton abstraction by a histidine base (His373 or His195). Further, both enzymes employ an arginine residue to anchor the substrate in position (Arg376 or Arg171). However, although the basic catalytic machinery appears to be roughly equivalent, the two enzymes have no global similarity with respect to structure or sequence.

L-lactate dehydrogenase from *B. stearothermophilus* forms enzyme-substrate interactions along two lengths of polypeptide, 98-112 and 220-242, which are important in defining the enzyme's substrate specificity. The former of these is a flexible 'loop' region which is believed to undergo significant conformational change during catalysis, while the latter is a portion of an α-helix. Representative amino-acids in both regions are shown in *Figure 5.2*. Wilks *et al.* (1988, 1990, 1991, 1992) have constructed numerous mutant enzymes to investigate the role of these residues, with certain combinations exhibiting impressive specificity or diversification (summarised by Clarke *et al.*, 1989a & b; Wilks & Holbrook, 1991). Substitution of Gln102 for Arg altered the charge balance within the active site, resulting in a 10^7-fold swing in the specificity for oxaloacetate over pyruvate (oxaloacetate has a carboxylate substituent in place of pyruvate's methyl group; Wilks *et al.*, 1988). The multiple mutation of GlnLysPro102-105→MetValSer coupled with AlaAla235-236→GlyGly created a broad specificity enzyme with an increased ability to dehydrogenate 2-hydroxy-acids with larger substituents, but with less affinity for the physiological substrate (Wilks *et al.*, 1990). This latter mutation was also coupled with an insertion into the 98-112 loop region generating an enzyme 1700-fold more efficient with phenyl-pyruvate than pyruvate (Wilks *et al.*, 1992). Several of these mutants have significant commercial value, the broad-specificity enzyme opens up an easy route to

the chiral synthesis of 2-hydroxy-acids (Casy *et al.*, 1992), while the specific phenyl-lactate dehydrogenase has applications in medical diagnostics.

As mentioned in *Section 1.7* (p25), the redox capability of flavocytochrome b_2 has enabled it to form an integral part of an electronic sensor which, with the aid of protein engineering, could be 'tuned' to detect various types and quantities of 2-hydroxy-acid. Flavocytochromes are in this respect ideal biosensors, while the depth of understanding with regard to flavocytochrome b_2 make this enzyme a particularly good model system.

5.2 Results & Discussion

5.2(a) Wild-type

Native flavocytochrome b_2 has been used in several other studies of substrate specificity, but these have been under various conditions and are difficult to compare quantitatively. *Table 1.1* (p24) lists the relative activities determined with some substrates, however, some of these values were not determined from Michaelis plots, or in the presence of saturating concentrations of substrates and as a result are somewhat arbitrary.

Figure 5.3 shows a typical Michaelis plot for flavocytochrome b_2, determined from steady-state assays as described in *Section 2.7* (p59), along with parameters for the range of substrates in *Table 5.1*. The value of k_{cat} for each substrate quantifies the maximum rate of turnover in the presence of saturating amounts of substrate and electron acceptor (1 mM ferricyanide). The value of K_m, according to the Michaelis-Menten equation, is equivalent to the substrate dissociation constant (see p60), therefore, low values are usually indicative of tight binding and high values of weak binding. Values for k_{cat}/K_m are commonly used as a measure of the efficiency of the enzyme with a given substrate and relate directly to the free energy of the transition state. Throughout this chapter these parameters have been used to define 'substrate specificity profiles', which form the basis of wild-type/mutant comparisons (*Figures 5.4*, *5.7* and *5.9*).

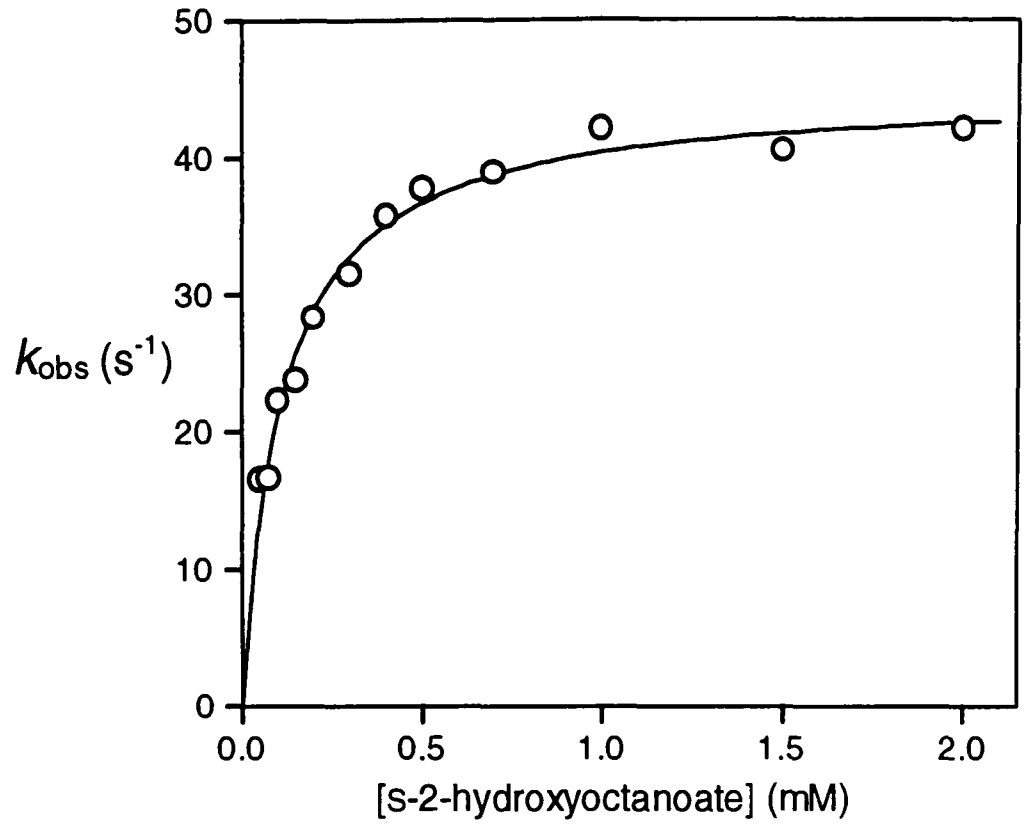

Figure 5.3 A Michaelis-Menten plot for wild-type flavocytochrome b_2 with s-2-hydroxyoctanoate. Individual points were calculated from spectrophotometric steady-state assays using the initial rate method. The data was fitted by least-squares regression analysis to the Michaelis-Menten equation, the parameters are tabulated below, along with those for a selection of straight-chained 2-hydroxy-acid substrates (see *Table 5.1*). Assays were performed in Tris/HCl buffer at 25°C (see *Section 2.7*, p59) and 1 mM ferricyanide was used as the electron acceptor. Errors in K_m are standard deviations from least-squares fitting and errors in k_{cat} are standard deviations from multiple assays at saturating substrate concentration.

Substrate	Chain-length	k_{cat} (s^{-1})	K_m (mM)	k_{cat}/K_m
glycolate	2	7 ± 1†	0.34 ± 0.05†	20 ± 3†
L-lactate	3	400 ± 10‡	0.49 ± 0.05‡	810 ± 90‡
s-2-hydroxybutyrate	4	82 ± 7	0.59 ± 0.04	140 ± 15
s-2-hydroxyvalerate	5	13 ± 1	0.22 ± 0.02	59 ± 7
s-2-hydroxycaproate	6	19 ± 1	0.11 ± 0.01	173 ± 18
s-2-hydroxyoctanoate	8	45 ± 5	0.11 ± 0.01	410 ± 60

† Taken from Miles (1992) ‡ Taken from Miles *et al.* (1992)

The most obvious trend in the data tabulated for the wild-type enzyme (*Figure 5.3*) is that K_m values are lower with long-chain 2-hydroxy-acids than with short. This phenomenon recurs in all the mutant enzymes studied (see *Figures 5.4, 5.7, 5.8 & 5.9*) and can be rationalised in terms of the increase in size of the hydrophobic 'tail' on

the substrate molecules. Large aliphatic substituents are generally repelled by solvent molecules and would bind more effectively within the protein interior, this is consistent with the notion that the methyl group of L-lactate interacts with hydrophobic side-chains as illustrated in *Figure 5.1* (p118). Despite this trend, a K_m of 0.49 mM is obtained for wild-type flavocytochrome b_2 with L-lactate, which is slightly lower than that obtained with the longer S-2-hydroxybutyrate. Furthermore the k_{cat} of 400 s^{-1}, is significantly higher than with all other substrates. Clearly the architecture of the active site has evolved to accommodate L-lactate specifically such that interactions between the methyl group and active site residues stabilise the substrate in the optimum position for dehydrogenation (see *Figure 1.11;* p21).

5.2(b) The L230A Mutation

In the X-ray crystal structure of flavocytochrome b_2 (Xia & Mathews, 1990), Leu230 lies largely in the plane of the substrate molecule and effectively makes contact with the methyl group. Its mutation to alanine removes -$CH(CH_3)_2$ from the side-chain and is designed to eliminate this contact (see *Figure 5.1;* p118):

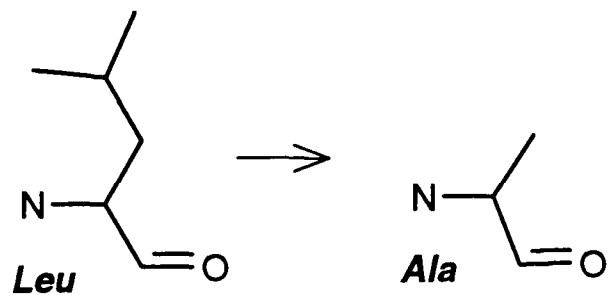

Figure 5.4 compares the substrate specificity profiles of the wild-type and L230A mutant enzymes. For L230A, catalytic efficiency (k_{cat}/K_m) increases progressively with substrate chain-length, whereas the wild-type profile includes a large peak in the L-lactate position (chain-length 3). Significantly, this peak has been all but completely eradicated in the L230A profile. It is clear from this that Leu230 is critically involved in the substrate chain-length selection process, influencing both k_{cat} and K_m for the dehydrogenation reaction such as to optimise the enzyme's efficiency with L-lactate. Substitution of this residue by Ala removes the favourable interaction between the hydrocarbon chain of Leu230 and the methyl group of the substrate, with

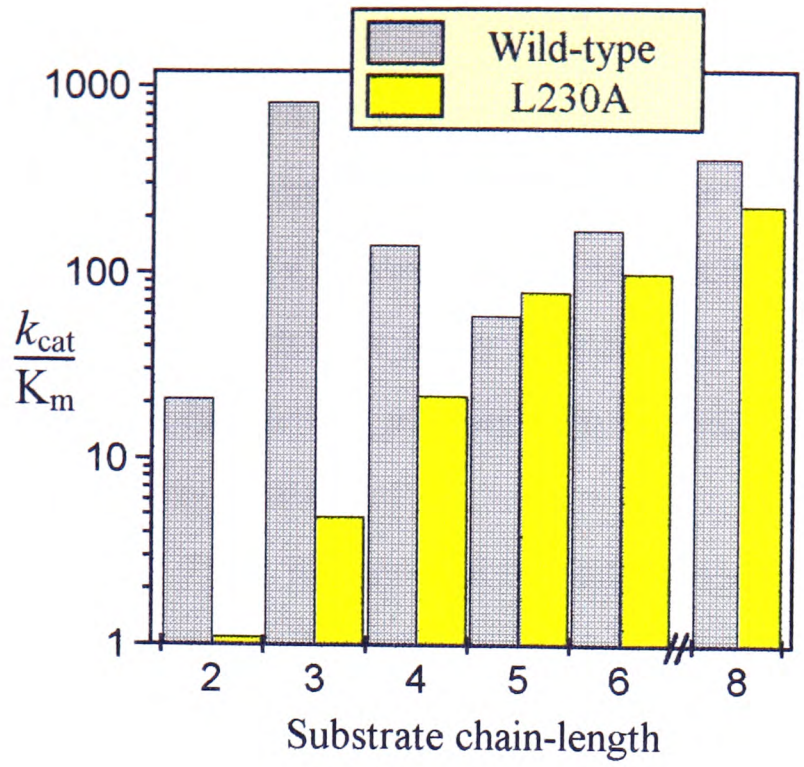

Figure 5.4 Substrate specificity profiles of wild-type and L230A mutant enzymes. Values for k_{cat}/K_m (tabulated below and in *Figure 5.3*) are represented in $mM^{-1}s^{-1}$ on a log. scale. Substrate chain-lengths (2-8) correspond to the s-2-hydroxy-acids in *Table 4.1*. The parameters were determined as described in *Figure 5.3* and see *Section 2.7*, p59.

L230A steady-state parameters

Substrate	Chain-length	k_{cat} (s^{-1})	K_m (mM)	k_{cat}/K_m
glycolate	2	3 ± 1	3 ± 1	1 ± 0.5
L-lactate	3	30 ± 3	6.1 ± 0.2	4.9 ± 0.5
s-2-hydroxybutyrate	4	18 ± 2	0.83 ± 0.05	22 ± 3
s-2-hydroxyvalerate	5	19 ± 2	0.24 ± 0.02	79 ± 10
s-2-hydroxycaproate	6	16 ± 2	0.16 ± 0.01	100 ± 14
s-2-hydroxyoctanoate	8	52 ± 5	0.23 ± 0.01	226 ± 24

the consequence of either forcing water molecules to occupy this hydrophobic pocket or inducing a significant structural change. The longer 2-hydroxy-acids, however, have hydrocarbon chains that would be able to fill this void and make contact with the new side-chain (Ala) at position 230. The observation that S-2-hydroxyvalerate (chain-length 5) has an improved catalytic efficiency with the mutant enzyme suggests that this substrate is of the appropriate length to occupy the pocket, while avoiding the negative effect of steric crowding.

The K_m values obtained for the L230A enzyme with long-chain 2-hydroxy-acids are similar to the corresponding wild-type values (see *Figure 5.3;* p124),

whereas those for short-chain substrates (glycolate and L-lactate) are 10 fold higher. This represents a large reduction in the binding affinity for smaller substrates. Further, the k_{cat} values obtained for L230A with small substrates (glycolate, L-lactate, and S-2-hydroxybutyrate) are much lower than for wild-type, in fact the k_{cat} for L-lactate decreases more than 10 fold as a consequence of the mutation. Since the k_{cat} for L-lactate with the L230A mutant is now lower than for S-2-hydroxyoctanoate, and its K_m considerably higher, L-lactate can no longer be considered the primary substrate for this mutant and has been 'deselected'.

In summary, the L230A mutant enzyme is best described as a long-chain 2-hydroxy-acid dehydrogenase, rather than a L-lactate dehydrogenase. Such is the degree of L-lactate deselection by the mutant, that it is now 40 times more efficient with S-2-hydroxyoctanoate than with L-lactate. In comparison, wild-type flavocytochrome b_2 is 2 times as efficient with L-lactate as S-2-hydroxyoctanoate. This equates to an 80-fold swing in specificity.

Stopped-flow analysis of L230A

The successful manipulation of substrate specificity requires that amino-acid mutations are as functionally selective as possible. In other words it is important to maintain the other facets of the enzyme's catalytic make-up. As such, the encouraging success of the L230A mutation prompted a more complete investigation of its kinetic properties.

Chapter 3 presents a kinetic model which accurately describes the catalytic cycle of the wild-type enzyme under steady-state conditions. The effects of the L230A mutation should therefore be interpreted on this basis. However, for convenience, the steady-state assays used to generate the substrate-specificity profiles in this chapter were conducted with ferricyanide as the electron acceptor rather than cytochrome *c*. Ferricyanide has commonly been used for this purpose, despite its physiological irrelevance, because of its high k_{cat} (400 s^{-1}) and low K_m (0.1 mM) values (obtained for wild-type in the presence of 10 mM L-lactate; Miles *et al.*, 1992). The higher k_{cat} with respect to cytochrome *c* (207 s^{-1}) can be explained by the ability of this smaller molecule to accept electrons from FMN as well as b_2-haem, which allows the rate-determining *Step 4* to be by-passed during rapid turnover (see *Figure 3.1* p73).

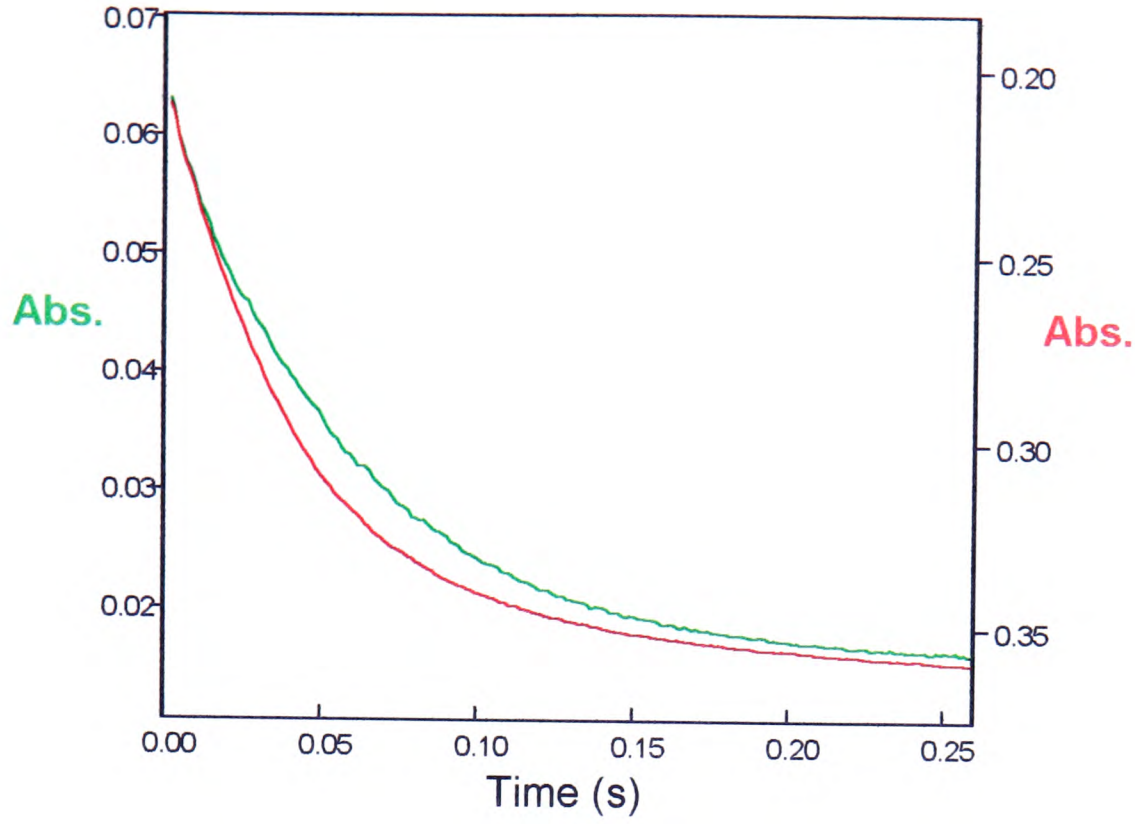

Figure 5.5 Stopped-flow traces for FMN (green) and b_2-haem (red) reduction of L230A mutant flavocytochrome b_2 collected at 438.3 nm and 557 nm respectively. Both traces (averages of 5) were generated on mixing 10 μM flavocytochrome b_2 with 50 mM L-lactate in Tris/HCl buffer (see *Section 2.7;* p59 & *2.9;* p62) at 25°C.

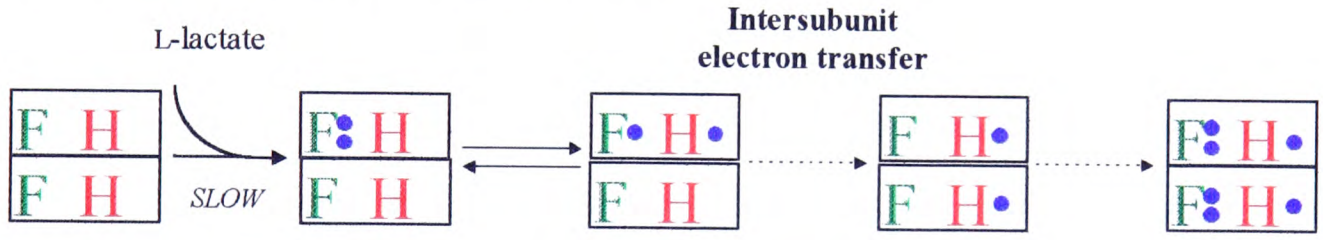

The above model considers a pair of adjacent flavocytochrome b_2 subunits undergoing reduction by L-lactate (see *Figure 1.14* legend, p28). When the rate of FMN reduction is slow, inter-subunit electron transfer becomes significant. Under extreme circumstances, the reduction of b_2-haem appears to outpace reduction of FMN.

However, the k_{cat} values derived for the mutant enzyme are much lower than these rates and turnover would be expected to be limited by the dehydrogenation step (*Step 1, Figure 3.1;* p73), if the previous deductions are justified. Consistent with this theory, the steady-state k_{cat} for L230A with L-lactate and cytochrome *c* was determined to be 27 (±3) s^{-1}, which, within error, is the same as with ferricyanide.

As discussed in *Section 3.2(a),* p76, *Step 1* can be monitored directly by following the reduction of FMN by substrate using stopped-flow spectrophotometry. *Figure 5.5* displays a sample trace from such an experiment, in which the

concentration of L-lactate (50 mM) is well in excess of the appropriate K_m value (6 mM; see *Figure 5.4*). As indicated in *Figure 3.2* (p76), b_2-haem reduction is expected to follow FMN reduction, but the haem reduction trace shown in *Figure 5.5* suggests that for this enzyme, the opposite may be the case. The only sensible explanation for this phenomenon is that flavin reduction (*Step 1*) has been slowed so much that electron transfer between subunits and probably between tetramers, becomes feasible during normal catalytic turnover. A simplified model for this electron redistribution, considering only two enzyme subunits, is included in *Figure 5.5*. Through inter-subunit electron-transfer it is possible to get complete haem reduction before FMN reduction is experimentally observable. The model presented in *Figure 3.2* (p76) for rapid enzyme reduction, includes a similar step within the '*slow phase*'.

The interpretation of this data is hampered by the complex nature of the kinetics involved, too many separate rate constants contribute to the overall effect. Fitting the traces to double exponential functions assumes that FMN reduction and electron redistribution can be considered as separate phases (as in *Section 3.2a,* p76), but the two are clearly of the same order of magnitude. This methodology has nevertheless been applied and the results are plotted in *Figure 5.6*. From the k_{max} values it appears as if b_2-haem reduction occurs 50% faster than FMN reduction at 30 s^{-1}, while from the steady-state rate constant (30 s^{-1} per mole of ferricyanide reduced; see *Figure 5.4*) one would expect *Step 1* to occur at only 15 s^{-1}. However, it is possible that the fast phase for FMN reduction may be speeded up by electron rearrangement, since FMN hydroquinone can proportionate into two semiquinones (note that ε_o for these two species is very similar at 438.3 nm; see *Figure 2.4*; p65). Therefore, although the data in *Figure 5.6* should be viewed with some scepticism, it is broadly consistent with the steady-state data obtained and indicates that *Step 1* is entirely rate-determining. It is reassuring to note that a similar effect is observed with the wild-type enzyme when the rate of flavin reduction is slowed. Pompon *et al.* (1980) observed this when using α-deuterated-L-lactate at low concentrations and low temperature (5°C).

The remainder of the catalytic cycle can be studied by monitoring the rate of flavin oxidation using stopped-flow spectrophotometry as described in *Section 3.2(c)* (p82).

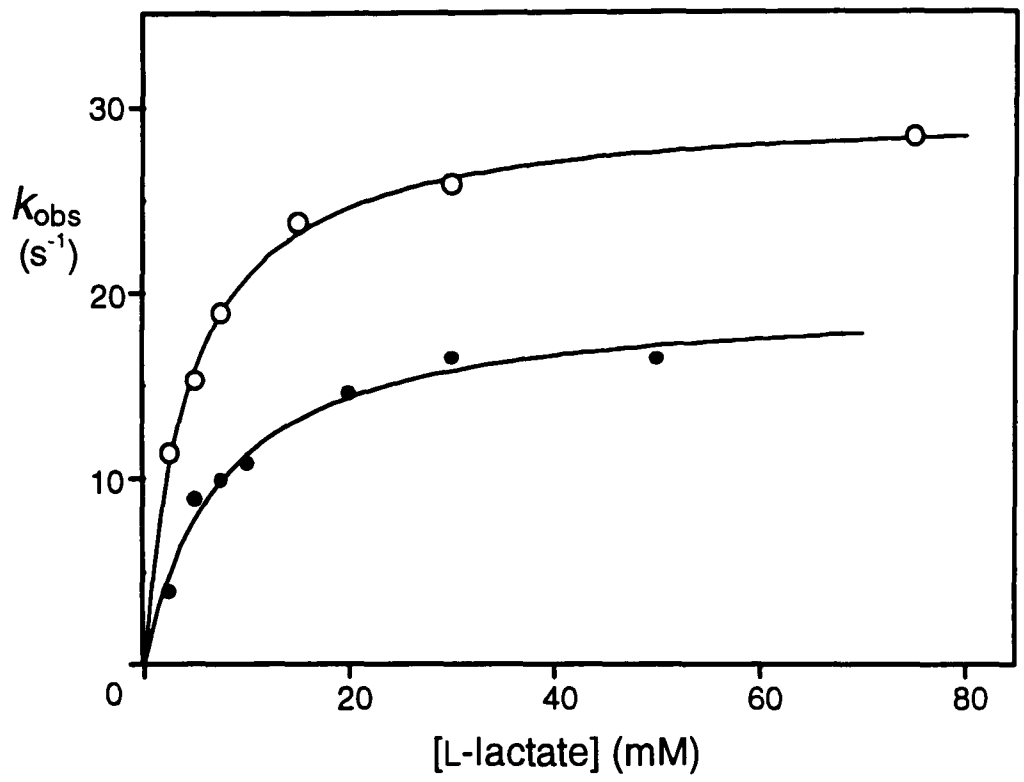

Figure 5.6 Rate constants (k_{obs}) determined for pre-steady-state FMN (•) and b_2-haem (o) reduction of L230A flavocytochrome b_2, plotted against L-lactate concentration (see *Section 2.9*, p62). The data plotted are rate constants determined from the fast phase of double exponential fits. The curves plotted are simple Michaelis-Menten fits with parameters tabulated below. Errors are standard deviations.

	k_{max} (s^{-1})	K_m (mM)
b_2-haem reduction	30 ± 0.5	4.4 ± 0.3
FMN reduction	20 ± 1.0	7.5 ± 1.2

The preliminary results obtained with L230A were very similar to those discussed for the wild-type enzyme, with the rate constants for flavin oxidation being within the range of 80 to 140 s^{-1}, but this was not studied in any detail. Overall, there is no reason to believe that the Leu230→Ala mutation had any adverse effect on any of the electron transfer processes which constitute the catalytic cycle, other than *Step 1*.

Kinetic isotope effects

The interpretation of data presented as substrate specificity profiles is also dependent on the mechanism by which FMN reduction occurs (i.e. *Step 1*) and the rate-determining factors within this step. Miles *et al.* (1992) determined a kinetic isotope effect of 8.1 (±1.4) on FMN reduction for the wild-type enzyme, when the α–

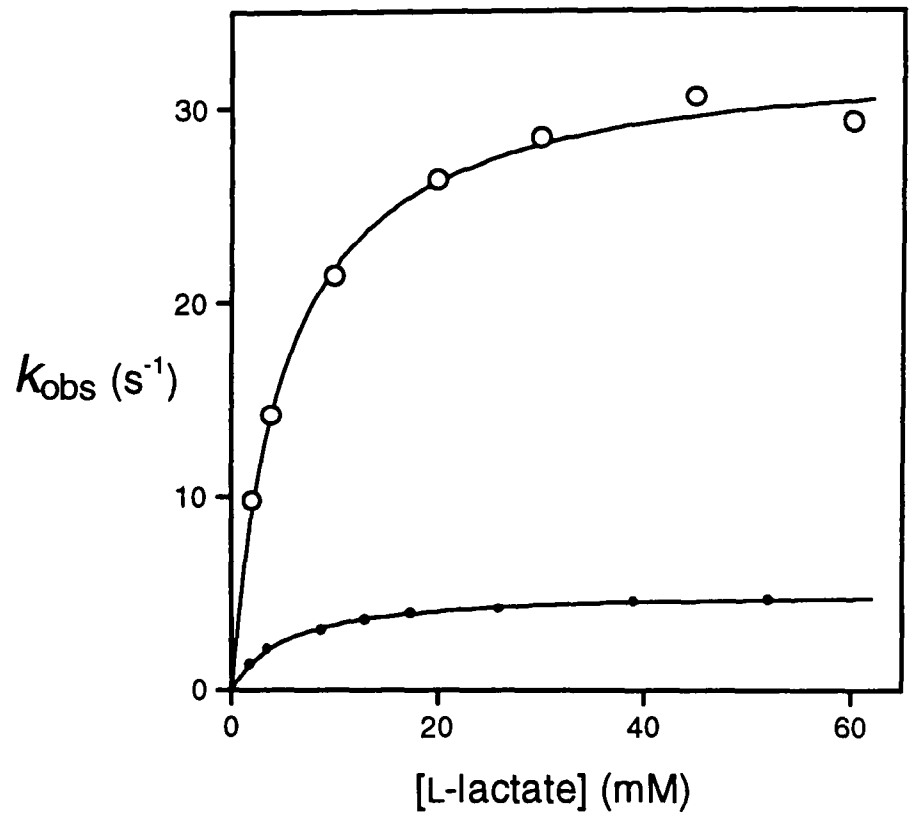

Figure 5.7 Michaelis-Menten plots determined for L230A with 2-^{1}H-L-lactate (o) and 2-^{2}H-L-lactate (•). The parameters derived from least-squares fitting are tabulated below along with the corresponding values for wild type (†taken from Miles *et al.*, 1992) and A198G. Conditions as in *Figure 5.3* (p124). Kinetic isotope effects (K.I.E.) were calculated by dividing the appropriate k_{cat} values.

Substrate	Wild-type†		A198G		L230A	
	k_{cat} (s^{-1})	K_m (mM)	k_{cat} (s^{-1})	K_m (mM)	k_{cat} (s^{-1})	K_m (mM)
L-[2-^{1}H]-Lactate	400 ± 10	0.49 ± 0.05	185 ± 5	4.1 ± 0.4	30 ± 3	6.1 ± 0.2
L-[2-^{2}H]-Lactate	86 ± 1	0.76 ± 0.06	51 ± 10	6.3 ± 1.0	5.1 ± 0.5	5.2 ± 0.3
K.I.E.	4.7 ± 0.4		3.6 ± 1.0		5.9 ± 1.3	

hydrogen of L-lactate was specifically replaced by deuterium. This translated as an isotope effect of 4.7 on the steady-state reduction of ferricyanide. As discussed in *Section 1.6* (p15), a large kinetic isotope effect indicates that α-hydrogen abstraction is the rate determining step during FMN reduction (whether the hydrogen atom is abstracted as a proton or a hydride). Therefore, in order to evaluate the mechanistic effect of the mutation, steady-state kinetic isotope effects were determined for the L230A mutant as shown in *Figure 5.7*. The 2-^{2}H-L-lactate was prepared enzymatically (see *Section 2.7,* p59) and assays were conducted as described earlier.

In view of the lower k_{cat} observed for L230A with L-lactate, it is not surprising to find that the steady-state isotope effect is slightly greater than with the wild-type enzyme, since, as already established, FMN reduction for L230A is entirely rate-

determining. Therefore, it appears that during L-lactate dehydrogenation, the same transition state is encountered for both the wild-type and L230A enzymes. This allows the kinetic data to be compared and interpreted in respect of the same fundamental model.

A kinetic isotope effect was also determined for the A198G mutant enzyme and found to be slightly lower than the value for wild type (see *Figure 5.7*). Nevertheless, a similar assumption is probably justified and accordingly, the substrate specificity profile for this mutant is discussed in the next section.

5.2(c) The A198G Mutation

The mutation of Ala198 to glycine removes a single methyl group from the active site of the enzyme:

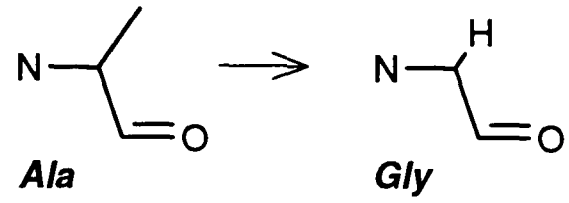

Ala ***Gly***

Although this is a very subtle change, the X-ray crystal structure places Ala198 within contact range of the substrate methyl group (see *Figure 5.1;* p118). Also, the peptide link of Ala198 appears to hydrogen-bond to the flavin N5. This latter observation may explain why the stability of this enzyme was lower than either wild-type or the other mutants characterised. Presumably the activity loss observed during analysis stemmed from FMN dissociation, as is common with certain flavoenzymes.

The substrate specificity profile for the A198G mutant is plotted in *Figure 5.8* alongside that for the wild-type enzyme. The obvious effect of this mutation was to decrease the efficiency of the enzyme with all substrates by a similar magnitude (approximately 20 fold). There is no significant change in the shape of the profile, and the enzyme is still most efficient with L-lactate. A closer insight can be gained by comparing the Michaelis parameters for the mutant with those for wild type (see *Figure 5.3;* p124). The A198G mutation causes large increases in K_m for all the

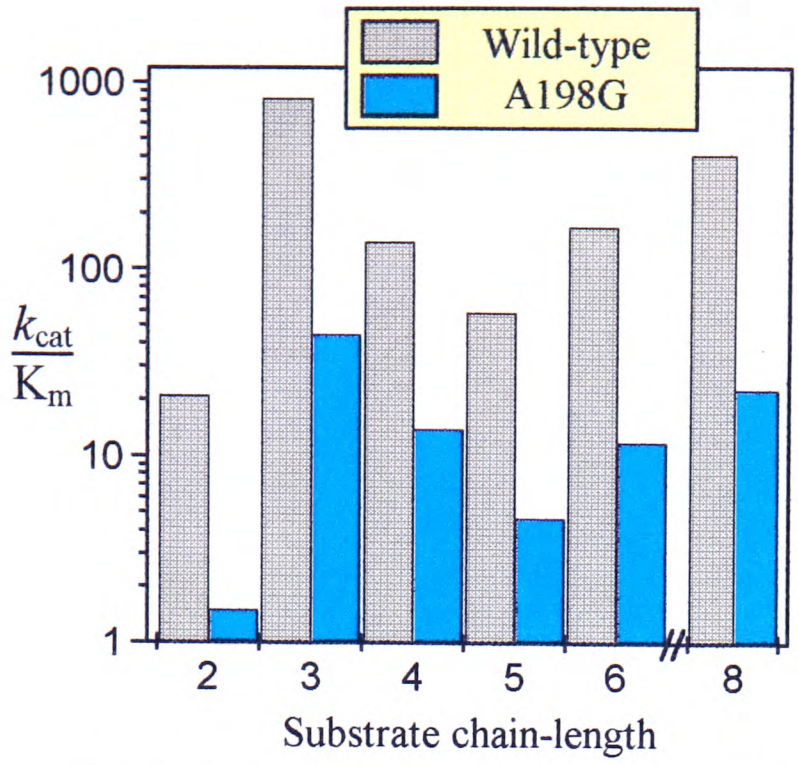

Figure 5.8 Substrate specificity profiles of wild-type and A198G mutant enzymes. Values for k_{cat}/K_m (tabulated below and in *Figure 5.3;* p124) are represented in $mM^{-1}s^{-1}$ on a log. scale. Substrate chain-lengths (2-8) correspond to the s-2-hydroxy-acids in *Table 4.1*. The parameters were determined as described in *Figure 5.3* and *Section 2.7* (p59).

A198G steady-state parameters

Substrate	Chain-length	k_{cat} (s^{-1})	K_m (mM)	k_{cat}/K_m
glycolate	2	3 ± 1	2 ± 1	1.5 ± 0.9
L-lactate	3	185 ± 5	4.1 ± 0.4	45 ± 5
s-2-hydroxybutyrate	4	34 ± 1	2.4 ± 0.3	14 ± 2
s-2-hydroxyvalerate	5	4.0 ± 0.2	0.85 ± 0.08	4.7 ± 0.5
s-2-hydroxycaproate	6	5.3 ± 0.5	0.46 ± 0.05	11.5 ± 1.5
s-2-hydroxyoctanoate	8	14 ± 1	0.60 ± 0.03	23 ± 2

substrates, indicating that substrate binding has been weakened, and the Michaelis complex destabilised. Decreases in k_{cat} throughout the substrate range suggest that the transition state is also destabilised, the effect being unspecific in both cases. A possible explanation for this is that Ala198 interacts with the β-CH_2 (possessed by all substrates bar glycolate), in an unspecific way, its removal causing universal disruption. This would be the case, if Ala198 could interact without causing a steric obstruction to the long-chain substrates. Therefore, although Ala198 clearly influences catalysis, it is not responsible for the selection of L-lactate over the other substrates studied.

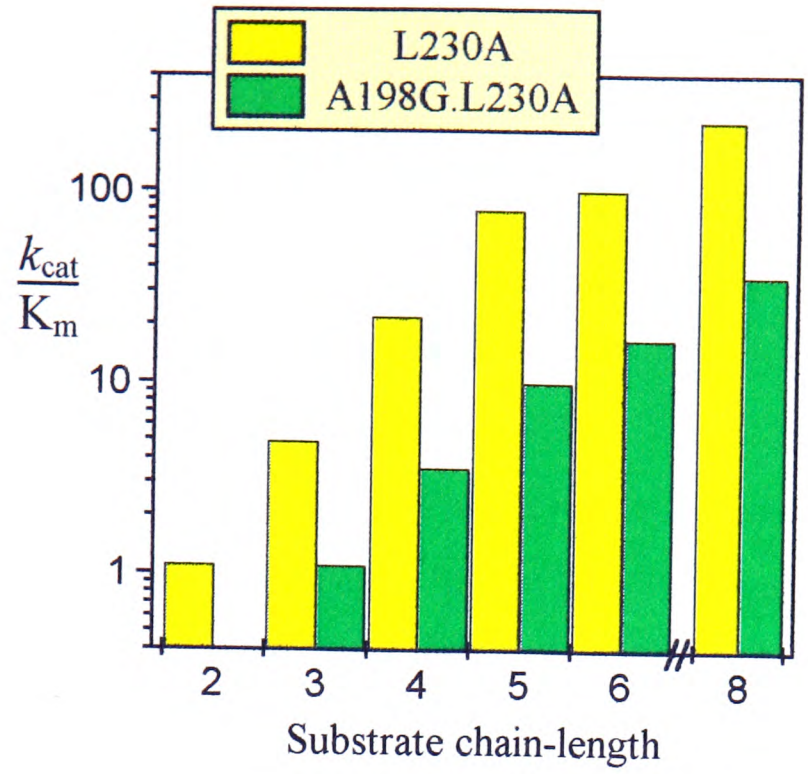

Figure 5.9 Substrate specificity profiles of L230A and L230A:A198G mutant enzymes. Values for k_{cat}/K_m (tabulated below and in *Figure 5.4;* p126) are represented in $mM^{-1}s^{-1}$ on a log. scale. Substrate chain-lengths (2-8) correspond to the s-2-hydroxy-acids in *Table 4.1*. The parameters were determined as described in *Figure 5.3* (p124) and *Section 2.7* (p59).

A198G:L230A steady-state parameters

Substrate	Chain-length	k_{cat} (s^{-1})	K_m (mM)	k_{cat}/K_m
glycolate	2	-	-	-
L-lactate	3	41 ± 2	38 ± 4	1.1 ± 0.1
s-2-hydroxybutyrate	4	13 ± 2	3.6 ± 0.5	3.6 ± 0.2
s-2-hydroxyvalerate	5	21 ± 3	2.1 ± 0.2	10 ± 2
s-2-hydroxycaproate	6	25 ± 1	1.5 ± 0.1	17 ± 1
s-2-hydroxyoctanoate	8	68 ± 3	1.9 ± 0.1	36 ± 3

The A198G:L230A mutant

The A198G mutation was also combined with the L230A mutation in the production of the double mutant, A198G:L230A. *Figure 5.9* shows the substrate specificity profile of this mutant compared to the L230A single mutant. As in the single mutant (see *Figure 5.8*) the A198G mutation caused a general decrease in enzymatic efficiency throughout the substrate range (by a factor of approximately 6-fold). However, the general shape of the A198G:L230A substrate specificity profile is remarkably similar to that of the L230A single mutant, showing a step-wise increase in efficiency as substrate chain-length is increased. It appears, therefore, that the

individual effects of the two mutations are combined within the double mutant. This observation is not as predictable as one may at first think, since one change might be expected to have a direct effect on the other. The two amino-acids are after all in very close proximity in the enzyme's active site (see *Figure 5.1;* p118).

The k_{cat} values obtained for the double mutant (*Figure 5.9*) are very similar to the values observed with the L230A single mutant (*Figure 5.4;* p126) for all the substrates. However, the K_m values, which show a universal increase, are more reminiscent of values recorded for the A198G enzyme (*Figure 5.8*), indicating a similar disruption of substrate binding. The loss of all significant activity, in the case of glycolate is presumably an extension of this phenomenon. The fact that several of the k_{cat} values obtained with longer substrates were greater than those recorded for the A198G single mutant suggests that the L230A mutation in some way compensates for the disruption caused by the Ala198→Gly mutation.

In summary, the Ala198→Gly mutation appears to destabilise the Michaelis complex and the transition state by similar amounts and is unspecific in terms of substrate affected.

5.2(d) The I326A Mutation

From studying the X-ray crystal structure, Ile326 appears to be slightly further away from the substrate than either Ala198 and Leu230, but is certainly within contact range of a larger 2-hydroxy-acid substituent. Additionally, the side-chain of Ile326 appears to make direct contact with Leu230 and may help to position this residue relative to the substrate. Therefore mutation of Ile326 to Alanine:

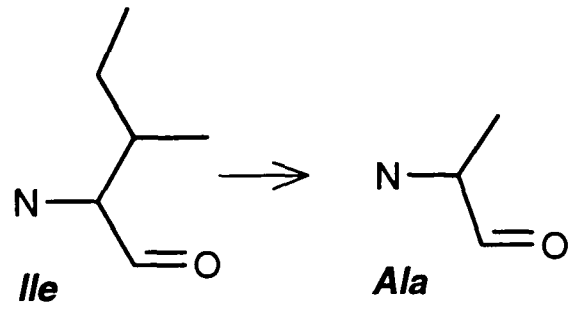

removes a significant amount of steric bulk from the active site and is designed to affect the protein-substrate interactions both directly (in the case of large

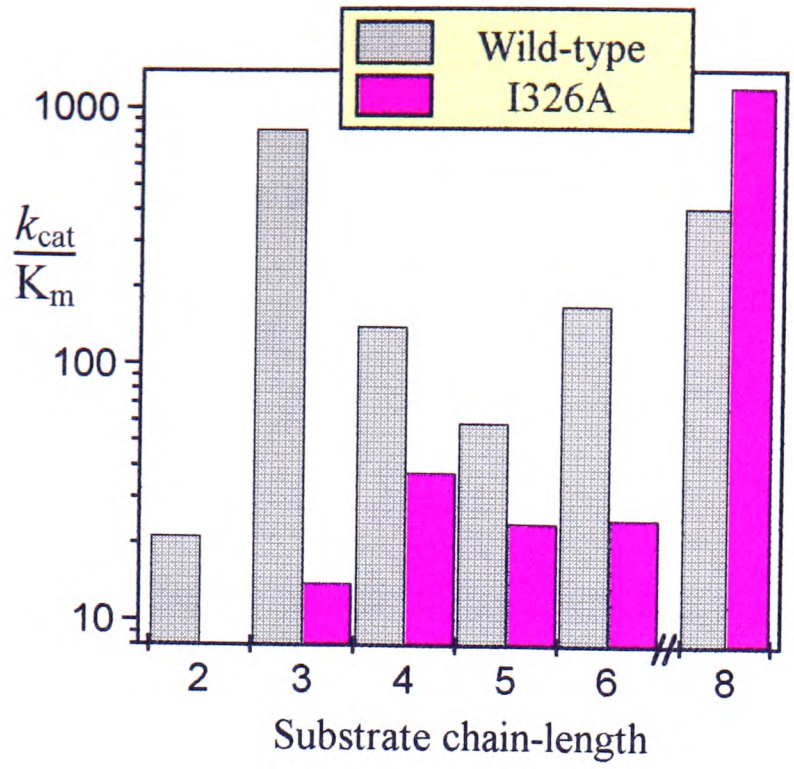

Figure 5.10 Substrate specificity profiles of wild-type and I326A mutant enzymes. Values for k_{cat}/K_m (tabulated below and in *Figure 5.3;* p124) are represented in $mM^{-1}s^{-1}$ on a log. scale. Substrate chain-lengths (2-8) correspond to the s-2-hydroxy-acids in *Table 4.1*. The parameters were determined as described in *Figure 5.3* and *Section 2.7* (p59). †The K_m value for this mutant was determined using cytochrome *c* as electron acceptor.

I326A steady-state parameters

Substrate	Chain-length	k_{cat} (s^{-1})	K_m (mM)	k_{cat}/K_m
glycolate	2	1.3 ± 0.1	2.1 ± 0.4	0.5 ± 0.1
L-lactate	3	11.0 ± 0.4	0.76 ± 0.07	14.5 ± 1.4
S-2-hydroxybutyrate	4	19 ± 2	0.52 ± 0.03	38 ± 1
S-2-hydroxyvalerate	5	11.4 ± 0.6	0.48 ± 0.04	24 ± 2
S-2-hydroxycaproate	6	2.0 ± 0.1	0.08 ± 0.01	25 ± 3
S-2-hydroxyoctanoate	8	11.8 ± 0.6	0.01†	1200†

substrates) and indirectly in the case of L-lactate. The substrate specificity profile for the I326A mutant is shown in *Figure 5.10* compared to the wild-type profile. As observed for the L230A mutant, the shape of the profile is drastically different to that for wild-type, but in this case it is not uniform. As chain-length increases, the enzyme efficiency appears to reach a peak at chain-length 4, due to increases in k_{cat}. However, a second peak is created at chain-length 8 due to rapidly decreasing K_m values. In fact the K_m for S-2-hydroxyoctanoate with I326A is some six-fold less than with the wild-type enzyme, whereas the other substrates give rise to K_m values which are

remarkably similar in both mutant and wild-type enzymes. Therefore we can conclude that the extra space generated in the active site by the Ile326→Ala mutation stabilises the Michaelis complex for S-2-hydroxyoctanoate in preference to the other substrates, although some of the transition state stability for shorter substrates seems to have been retained.

5.3 Conclusions

This study has confirmed the role of certain aliphatic amino-acid side-chains in defining the substrate specificity of *S. cerevisiae* flavocytochrome b_2. Leu230 and Ile326 were observed to have the largest influence, since their mutation to Alanine caused gross changes in the shape of the respective substrate specificity profiles (see *Figures 5.4;* p126 *& 5.10;* p136). Ala198 was identified as being important for stabilising the Michaelis complex of the enzyme, but did not appear to influence substrate specificity.

In addition to the latent value of this information, the study has also demonstrated how substrate activity parameters can be manipulated strategically for a chosen application. In this respect much has been gained from each one of the mutants. Even the Ala198→Gly mutation, which failed to influence substrate specificity, demonstrated how K_m values can be increased for a range of substrates. Such a tool would be useful in the creation of biosensors with large concentration ranges. In terms of substrate specificity the L230A and I326A mutations respectively caused 80-fold and 160-fold swings in the selection of S-2-hydroxyoctanoate over L-lactate by the enzyme.

APPENDIX 1

REFERENCES

Allen, J.P., Feher, G., Yeates, T.O., Komiya, H. & Rees, D.C. (1987) *Proc. Natl. Acad. Sci. USA 84*, 5725-5729.

Alleyne, T.A., Wilson, M.T., Antonini, G., Malatesta, F., Vallone, B., Sarti, P. & Brunori, M. (1992) *Biochem. J. 287*, 951-956.

Anni, H., Vanderkooi, J.M. & Mayne, L. (1995) *Biochemistry 34*, 5744-5753.

Appleby, C.A. & Morton, R.K. (1954) *Nature (London) 173*, 749-752.

Averill, B.A., Schonbrunn, A., Abeles, R.H., Weinstock, L.T., Cheng, C.C., Fisher, J., Spencer, R. & Walsh, C. (1975) *J. Biol. Chem. 250*, 1603-1605.

Baldwin, J.E. & Krebs, H. (1981) *Nature 291*, 381-382.

Balme ,A., Brunt, C.E., Pallister, R.L., Chapman, S.K., & Reid, G.A. (1995) *Biochem. J. 309*, 601-605.

Bach, S.J., Dixon, M. & Keilin, D. (1942a) *Nature (Letters to the Editor) 149*, 21.

Bach, S.J., Dixon, M. & Zerfas, L.G. (1942b) *Nature (Letters to the Editor) 149*, 48-49.

Banner, D.W., Bloomer, A.C., Petsko, G.A., Phillips, D.C., Pogson, C.I., Wilson, I.A., Corran, P.H., Furth, A.J., Milman, J.D., Offord, R.E., Priddle, J.D. & Waley, S.G. (1975) *Nature 255*, 609-614.

Bernheim, F. (1928) *Biochem. J. 22*, 1178-1192.

Bjerrum, M.J., Casimiro, D.R., Chang, I-J., Di Bilio, A.J., Gray, H.B., Hill, M.G., Langen, R., Mines, G.A., Skov, L.K., Winkler, J.R. & Wuttke, D.S. (1995) *J. Bioenerg. Biomemb. 27*, 295-302.

Black, M.T., White, S.A., Reid, G.A. & Chapman, S.K. (1989) *Biochem. J. 258*, 255-259.

Blankenhorn, G. (1977) in *Pyridine-Nucleotide-Dependent Dehydrogenases* (Sund, H. ed., Verlag de Gruyter, Berlin.) 185-198.

Bright, H.J. & Porter, D.J.T. (1975) in *The Enzymes 12*, 421.

Brunt, C.E., Cox, M.C., Thurgood, A.G.P., Moore, G.R., Reid, G.A. & Chapman, S.K. (1992) *Biochem. J. 283*, 87-90.

Casy, G., Lee, T.V., Lovell, H., Nichols, B.J., Sessions, R.B. & Holbrook, J.J. (1992) *Chem. Com. 13*, 924-926.

Chang, C.H., Tiede, D., Tang, J., Smith, U., Norris, J. & Schiffer, M. (1986) *FEBS. Lett. 205*, 82-86.

Capeillère-Blandin, C. (1975) *Eur. J. Biochem. 56*, 91-101.

Capeillère-Blandin, C. (1982) *Eur. J. Biochem. 128*, 533-542.

Capeillère-Blandin, C. (1991) *Biochem. J. 274*, 207.

Capeillère-Blandin, C. & Albani, J. (1987) *Biochem. J. 245*, 159-165.

Capeillère-Blandin, C., Bray, R.C., Iwatsubo, M., & Labeyrie, F. (1975a) *Eur. J. Biochem. 54*, 549-566.

Capeillère-Blandin, C., Bray, R.C., Iwatsubo, M., & Labeyrie, F. (1975b) *Eur. J. Biochem. 56*, 91-101.

Capeillère-Blandin,C., Iwatsubo,M., Testylier,G. and Labeyrie,F. (1980) in *Flavins and Flavoproteins* (Yagi,K. and Yamamoto,T., eds.), pp. 617-630, Japan Scientific Societies Press, Tokyo.

Chapman, S.K. & Mount, A.R. (1995) *Nat. Prod. Rep. 12*, 93-100.

Chapman, S.K, Reid, G.A., Bell, C., Short, D. & Daff, S. (1995) *Biochem. Soc. Trans. 24*, 73-77.

Chapman, S.K, Reid, G.A., Daff, S., Sharp, R.E., White, P.W., Manson, F.D.C. & Lederer, F. (1994) *Biochem. Soc. Trans. 22*, 713-718.

Chapman, S.K., White, S.A. and Reid, G.A.(1991) *Adv. Inorg. Chem. 36*, 257-301.

Choong, Y.S. & Massey, V. (1980) *J. Biol. Chem. 255*, 8672-8677.

Clarke, A.R., Atkinson, T. & Holbrook, J.J. (1989a) *Trends Biochem. Sci. 14*, 101-105.

Clarke, A.R., Atkinson, T. & Holbrook, J.J. (1989b) *Trends Biochem. Sci. 14*, 145-148.

Coulson, A.F.W., Erman, J.E. & Yonetani, T. (1971) *J. Biol. Chem. 246*, 917-924.

Curry, W.B., Grabe, M.D., Kurnikov, I.V., Skourtis, S.S., Beratan, D.N., Regan, J.J., Aquino, A.J.A., Beroza, P. & Onuchic, J.N. (1995) *J. Bioenerg. Biomemb. 27*, 285-293.

Daff, S., Ingledew, W.J., Reid, G.A. & Chapman, S.K. (1996a) *Biochemistry (in press).*

Daff, S., Manson, F.D.C., Reid, G.A. & Chapman, S.K. (1994) *Biochem. J. 301*, 829-834.

Daff, S., Sharp, R.E., Short, D.M., Bell, C., White, P., Manson, F.D.C., Reid, G.A., & Chapman, S.K. (1996b) *Biochemistry, (in press).*

Daum, G., Böhni, P.C., & Schatz, G. (1982) *J. Biol. Chem. 275*, 13028-13033.

Dawson, R.M.C., Elliott, D.C., Elliott, W.H. and Jones, K.M. (1987) *Data for Biochemical Research 3rd edn.* pp126-127, Oxford University Press.

Dong, J.M., Taylor, J.S., Latour, D.J., Iuchi, S., and Lin, E.C.C. (1993) *J. Bacteriol. 175*, 6671-6678.

Durham, B., Fairris, J.L., McLean, M., Millett, F., Scott, J.R., Sligar, S.G. & Willie, A. (1995) *J. Bioenerg. & Biomemb. 27*, 331-340.

Eltis, L.D., Herbert, R.G., Barker, P.D., Mauk, A.G. & Northrup, S.H. (1991) *Biochemistry 30*, 3663-3674.

Eley, C.G.S. & Moore, G.R. (1983) *Biochem. J. 215*, 11-21.

Fersht, A. (1985) *Enzyme Structure & Mechanism* (2nd. Ed., Freeman).

Fitzgerald, M.M., Churchill, M.J., McRee, D.E. & Goodin, D.B. (1994) *Biochemistry 33*, 3807-3818.

Forestier, J-P. & Baudras, A. (1971) in *Flavins & Flavoproteins* (Kamin, H. ed.) University Park Press, Baltimore, 599-605.

Gasser, S.M., Ohashi, A., Daum, G., Böhni, P.C., Gibson, J., Reid, G.A., Yonetani, T. & Schatz, G. *(1982) Proc. Natl. Acad. Sci. USA 79*, 267.

Ghisla, S. (1982) in *Flavins & Flavoproteins* (Massey, V. & Williams, C.H. eds., Elsevier), 133-142.

Ghisla, S. & Massey, V. (1980) *J. Biol. Chem.*, 5688-5696.

Ghisla, S. & Massey, V. (1991) in *Chemistry and Biochemistry of Flavoenzymes vol II* (F. Müller, ed. CRC Press, Boca Raton, Florida) 243-289.

Ghisla, S., Ogata, H., Massey, V., Schonbrunn, A., Abeles, R.H. & Walsh, C.T. (1976) *Biochemistry 15*, 1798.

Giegel, D.A., Williams, C.H.Jr. and Massey, V. (1990), *J. Biol. Chem. 256*, 6626-6632.

Gruschus, J.M. & Kuki, A. (1993) *J. Phys. Chem. 97*, 5581-5593.

Guillemette, J.G., Barker, P.D., Eltis, L.D., Lo, T.P., Smith, M., Brayer, G.D. & Mauk, A.G. (1994) *Biochemie 76*, 592-604.

Hasegawa, H. (1962) *J. Biochem. 52*, 12-15.

Hayash, H. (1995) *J. Biochem. 118*, 463-473.

Hazzard, J.T., Cusanovich, M.A., Tainer, J.A., Getzoff, E.D. & Tollin, G. (1986) *Biochemistry 25*, 3318-3328.

Hazzard, J.T., McDonough, C.A. & Tollin, G. (1994) *Biochemistry 33*, 13445-13454.

Hemmerich, P., Massey, V. & Fenner, H. (1977) *Febs. Letters 84*, 5-21.

Hinkson, J.W. and Mahler, H.R.(1963) *Biochemistry 2*, 216-220.

Ingraham, L.L. & Meyer, D.L. (1985) *Biochemistry of Dioxygen*, Plenum Press (NewYork).

Iwatsubo, M., Mével-Ninio, M. & Labeyrie, F. (1977) *Biochemistry 16*, 3558-3566.

Jacq, C. & Lederer, F. (1972) *Eur. J. Biochem. 25*, 41-48.

Jacq, C. & Lederer, F. (1974) *Eur. J. Biochem. 41*, 311-320.

Janot, J-M., Capeillère-Blandin, C., & Labeyrie, F. (1990) *Biochem. Biophys. Acta 1016*, 165-176.

Koppenol, W.H. (1980) *Biophys. J. 29*, 493-508.

Koppenol, W.H., Vroonland, C.A.J. & Braams, R. (1978) *Biochim. Biophys. Acta. 503*, 499-508.

Kunkel, T.A. (1985) *Proc. Natl. Acad. Sci. U.S.A. 82*, 488-492.

Labeyrie, F., Baudras, A. & Lederer, F. (1978) in *Methods in Enzymology* (S. Fleischer & L. Packer eds., Academic Press, New York) *53*, 238-256.

Labeyrie, F., Beloeil, J.C. & Thomas, M.A. (1988) *Biochem. Biophys. Acta 953*, 134-141.

Lammli, U.K. (1970) *Nature 227*, 680-685.

Lè, K.H.D. and Lederer, F. (1991) *J. Biol. Chem. 266*, 20877-20881.

Lederer, F. (1978) *Eur. J. Biochem. 88*, 425-431.

Lederer, F.(1991) in *Chemistry and Biochemistry of Flavoenzymes* vol II Ch.7, (F. Müller ed., CRC Press, Boca Raton, Florida).

Lederer, F., Ghrir, R., Guiard, B., Cortial, S. & Ito, A. (1983) *Eur. J. Biochem. 132*, 95-102.

Lederer, F. and Simon, A-M.(1971) *Eur. J. Biochem. 20*, 469-474.

Liu, R-Q., Hahm, S., Miller, M.A., Han, G.W., Geren, L., Hibdon, S., Kraut, J., Durham, B. & Millett, F. (1994) *Biochemistry 33*, 8678-8685.

Lloyd, E., Chapman, K., Chapman, S.K., Jia, Z-S., Lim, M-C., Tomkinson, N.P., Salmon, G.A. & Sykes, A.G. (1994) *J. Chem. Soc. Dalton Trans.* 675-681.

Loach, P.A. (1976) in *Handbook of Biochemistry & Molecular Biology (Physical & Chemical Data Vol. 1)* 3rd. Edn. (Fasman G.D. ed.), CRC Press Inc., Cleveland, 122-130.

Macheroux, P., Kiewig, V., Massey, V., Söderlind, E., Stenberg, K. & Lindquist, Y. (1993) *Eur. J. Biochem. 213*, 1047-1054.

Marcus, R.A. & Sutin, N. (1985) *Biochem. Biophys. Acta 811*, 265-322.

Margoliash, E. & Walasek, O.F. (1967) *Methods Enzymol. 10*, 339.

Massey, V., Müller, F., Feldberg, R., Schuman, M., Sullivan, P.A., Howell, L.G., Mayhew, S.G., Mathews, R.G. & Foust, G.P. (1969) *J. Biol. Chem. 244*, 3999.

Mauk, A.G. (1991) *Struct. Bonding 75*, 131.

Mauk, A.G., Mauk, M.R., Moore, G.R. & Northrup, S.H. (1995) *J. Bioenerg. & Biomemb. 27*, 331-330.

Mauk, M.R., Barker, P.D. & Mauk, A.G. (1991) *Biochemistry 30*, 9873-9881.

Mauk, A.G., Mauk, M.R., Weber, P.C. & Mathew, J.B. (1986) *Biochemistry 25*, 7085-7091.

Mauk, M.R., Reid, L.S. & Mauk, A.G. (1982) *Biochemistry 21*, 1843-1846.

Mayhew, S.G. & Ludwig, M.L. (1975) *Enzymes* (3rd Ed.) *12*, 57-118.

McLendon, G. & Hake, R. (1992) *Chem. Rev. 92*, 481-490.

McLendon, G., Pardue, K. & Bak, P. (1987) *J. Am. Chem. Soc. 109*, 7540-7541.

Michel, H., Deisenhofer, J. & Eppo, O. (1986) *EMBO. J. 5*, 2445-2451.

Miles, C.S., *PhD Thesis*, University of Edinburgh, (1992).

Miles, C.S., Rouviere, N., Lederer, F., Mathews, F.S., Reid, G.A., Black, M.T., & Chapman, S.K. (1992) *Biochem. J. 285*, 187-192.

Miller, M.A., Lui, R-Q., Hahm, S., Geren, L., Hibdon, S., Kraut, J., Durham, B. & Millett, F. (1994) *Biochemistry 33*, 8686-8693.

Millett, F., Miller, M.A., Geren, L. & Durham, B. (1995) *J. Bioenerg. Biomemb. 27*, 341-351.

Moodie, A., Mitchell, R. and Ingledew, W.J. (1990) *Analytical Biochemistry 189*, 103-106.

Moore, G.R. & Pettigrew, G.W. (1987) *Cytochromes c: Evolutionary, Structural & Physiological Aspects* (Springer-Verlag).

Moser, C.C., Page, C.C., Farid, R. & Dutton, P.L. (1995) *J. Bioenerg. & Biomemb. 27*, 263-274.

Müh, U., Williams, C.H. & Massey, V. (1994a) *J. Biol. Chem. 269*, 7982-7988.

Müh, U., Williams, C.H. & Massey, V. (1994b) *J. Biol. Chem. 269*, 7994-8000.

Müh, U., Williams, C.H. & Massey, V. (1994c) *J. Biol. Chem. 269*, 7989-7993.

Newton, M.D. (1988) *J. Phys. Chem. 92*, 3049-3056.

Ng, S., Smith, M.B., Smith, H.T. & Millett, F. (1977) *Biochemistry 16*, 4975-4978.

Northrup, S.H., Boles, J.O & Reynolds, J.C.L. (1988) *Science 241*, 67-71.

Northrup, S.H., Thomasson, K.A., Miller, C.M., Barker, P.D., Eltis, L.D., Guillemette, J.G., Inglis, S.C. & Mauk, A.G. (1993) *Biochemistry 32*, 6613-6623.

Ogura,Y. and Nakamura,T. (1966) *J.Biochem. (Tokyo) 60*, 77-86.

Pajot, P. & Groudinsky, O. (1970) *Eur. J. Biochem. 12*, 158-164.

Pelletier, H. & Kraut, J. (1992) *Science 254*, 1748-1755.

Perlmutter-Hayman, B. (1973) in *Progress in Reaction Kinetics* (Jennings, K.R. & Cundall, R.B. ed.), Pergamon Press Oxford, 6, 239-267.

Pompon, D. (1980) *Eur. J. Biochem. 106*, 151-159.

Pompon, D., Iwatsubo, M. & Lederer, F. (1980) *Eur. J. Biochem. 104*, 479-488.

Pompon, D. & Lederer, F. (1979) *Eur. J. Biochem. 96*, 571-579.

Porter, D.J.T., Voet, J.G. & Bright, H.J. (1973) *J. Biol. Chem. 248*, 4400.

Pettigrew, G.W. & Moore, G.R. (1987) *Cytochromes c: Biological Aspects* (Springer-Verlag).

Poulos, T.L. & Kraut, J. (1980) *J. Biol. Chem. 255*, 10322-10330.

Purcell, W.L. & Erman, J.E. (1976) *J. Am. Chem. Soc. 98*, 7033-7037.

Reid, G.A.,White, S.A., Black, M.T., Lederer, F., Mathews, F.S. and Chapman, S.K. (1988) *Eur. J. Biochem. 178*, 329-333.

Robinson, R.A. & Stokes, R.H. (1959) *Electrolyte Solutions*, 2nd Edn., Butterworth & Co. Ltd., London. 230-231.

Rodgers, K.K., Pochapsky, T.C. & Sligar, S.G. (1988) *Science 240*, 1657-1659.

Rodgers, K.K. & Sligar, S.G. (1991) *J. Mol. Biol. 221*, 1453-1460.

Salemme, F.R. (1976) *J. Mol. Biol. 102*, 563-568.

Sambrook, J., Fritsch, E.F. & Maniatis, T. (1989) *Molecular Cloning: A Laboratory Manual,* 2nd edn., Cold Spring Harbor Laboratoy Press, Cold Spring Harbor, NY.

Shapiro, S.S. & Dennis, D. (1965) *Biochem. 4*, 2283.

Sharp, R.E., White, P.W., Chapman, S.K. & Reid, G.A. (1994) *Biochemistry 33*, 5115-5120.

Sharp, R.E., Chapman, S.K. & Reid, G.A. (1996a) *Biochemistry 35, 891-899.*

Sharp, R.E., Chapman, S.K. & Reid, G.A. (1996b) *Biochem. J.(in press).*

Siddarth, P. & Marcus, R.A. (1993) *J. Phys. Chem. 97*, 13078-13082.

Smith, M.B., Stonehuerner, J., Ahmed, A.Q.J., Staudenmeyer, N. & Millett, F. (1980) *Biochim. Biophys. Acta 592*, 303-313.

Stankovich, M. & Fox, B. (1983) *Biochemistry 22*, 4466-4472.

Tegoni, M., Janot, J.M. & Labeyrie, F. (1986) *Eur. J. Biochem. 155*, 491-503.

Tegoni, M., Janot, J-M, & Labeyrie, F. (1990) *Eur. J. Biochem. 190*, 329-342.

Tegoni, M. & Mathews, F.S. (1988) *J. Biol. Chem. 263*, 19278.

Tegoni, M., Mozzarelli, A., Rossi, G.L. & Labeyrie, F.(1983) *J. Biol. Chem. 258*, 5424-5427.

Tegoni, M., White, S.A., Roussel, A., Mathews, F.S. & Cambillau, C. (1993) *Proteins 16*, 408-422.

Thomas, M.A., Favoudon, V. & Pochon, F. (1983a) *Eur. J. Biochem. 135*, 569-576.

Thomas, M.A., Gervais, M., Favaudon, V. & Valat, P. (1983b) *Eur. J. Biochem. 135*, 577-581.

Tsou, A.Y., Ransom, S.C. and Gerlt, J.A. (1990) *Biochemistry 29*, 9856-9862.

Urban, P., Alliel, P.M., & Lederer, F. (1983) *Eur. J. Biochem. 134*, 275-281.

Urban, P. & Lederer, F. (1984) *Eur. J. Biochem. 144*, 345-351.

Urban, P. & Lederer, F. (1985) *J. Biol. Chem. 260*, 11115-11122.

Vanderkooi, J.M., Adar, F. & Erecinska, M. (1976) *Eur. J. Biochem. 64*, 381-387.

Vanderkooi, J.M. & Erecinska, M. (1975) *Eur. J. Biochem. 60*, 199-207.

Vanderkooi, J.M., Glatz, P., Casadei, J. & Woodrow, G.V. (1980) *Eur. J. Biochem. 110*, 189-196.

Volokita, M. and Somerville, C.R. (1987) *J. Biol. Chem. 262*, 15825-15828.

Walker, M.C., & Tollin, G. (1991) *Biochemistry 30*, 5546-5555.

Wendolski, J.J., Matthew, J.B., Weber, P.C. & Salemme, F.R. (1987) *Science 238*, 794-797.

White, P., Manson, F.D.C., Brunt, C.E., Chapman, S.K. & Reid, G.A. (1993) *Biochem. J, 291*, 89-94.

Whitford, D., Concar, D.W., Veitch, N.C. & Williams, R.J.P. (1990) *Eur. J. Biochem. 192*, 715-721.

Wigley, D.B., Gamblin, S.J., Turkenburg, J.P., Dodson, E.J., Piontek, K., Muirhead, H. & Holbrook, J.J., (1992) *J. Mol. Biol. 223*, 317.

Williams R.F. & Bruice T.C. (1976) *J. Am. Chem. Soc. 98*, 7752-7768.

Williams, R.J.P. (1989) *Chem. Scripta 29*, 63.

Willie, A., McLean, M., Liu, R.Q., Hilgen-Willis, S., Saunders, A.J., Pielak, G.J., Sligar, S.G., Durham, B. & Millett, F. (1993) *Biochemistry 32*, 7519-7525.

Willie, A., Stayton, P.S., Sligar, S.G., Durham, B. & Millett, F. (1992) *Biochemistry 31*, 7237.

Wilks, H.M., Halsall, D.J., Atkinson, T., Chia, W.N., Clarke, A.R. & Holbrook, J.J. (1990) *Biochemistry 29*, 8587-8591.

Wilks, H.M., Hart, K.W., Feeney, R., Dunn, C.R., Muirhead, H., Chia, W.N., Barstow, D.A., Atkinson, T., Clarke, A.R. & Holbrook, J.J. (1988) *Science 242*, 1541-1544.

Wilks, H.M. & Holbrook, J.J. (1991) *Curr. Opin. Biochem. 2*, 561.

Wilks, H.M., Moreton, K.M., Halsall, D.J., Hart, K.W., Sessions, R.D., Clarke, A.R. & Holbrook, J.J. (1992) *Biochemistry 31*, 7802-7806.

Winkler, J.R. & Gray, H.B. (1992) *Chem. Rev. 92*, 369-379.

Witt, H., Zickermann, V. & Ludwig, B. (1995) *Biochem. Biophys. Acta 1230*, 74-76.

Xia, Z-X. & Mathews, F.S., (1990) *J. Mol. Biol. 212*, 837-863.

APPENDIX 2

ABBREVIATIONS

Amino acids

	Code	Symbol
Alanine	Ala	A
Arginine	Arg	R
Asparagine	Asn	N
Aspartic acid	Asp	D
Cysteine	Cys	C
Glutamic acid	Glu	E
Glutamine	Gln	Q
Glycine	Gly	G
Histidine	His	H
Isoleucine	Ile	I
Leucine	Leu	L
Lysine	Lys	K
Methionine	Met	M
Phenylalanine	Phe	F
Proline	Pro	P
Serine	Ser	S
Threonine	Thr	T
Tryptophan	Trp	W
Tyrosine	Tyr	Y
Valine	Val	V

Mutations

Amino acid mutations are represented as: code|number→code where the number gives the position on the polypeptide chain. The mutant enzymes produced are referred to as in the following example:

Ala198→Gly would generate the mutant A198G

Kinetic Parameters

K_m	Michaelis constant
k_{cat}	Rate constant at saturation
K_i	Inhibition constant
K_d	Dissociation constant
k_{et}	Electron transfer rate constant
k_2	Second-order rate constant
t	Time

Standard units

m	metre	°C	degree Celsius
g	gram	M	molar
s	second	V	volt
l	litre	Å	Angstrom

Textual abbreviations

Abs.	Absorbance
ADH	Alcohol dehydrogenase
ATP	Adenosine-5'-triphosphate
CAPS	3(Cyclohexylamino)-1-propanesulphonic acid
Da	Daltons
DNA	Deoxyribonucleic acid
E. coli	*Escherichia coli*
EDTA	Ethylenediaminetetraacetic acid
EPR	Electron paramagnetic resonance (spectroscopy)
FMN	Flavin mononucleotide
ΔG	Free energy change
H. anomala	*Hansenula anomala*
HPLC	High performance liquid chromatography
I	Ionic strength
LDH	Lactate dehydrogenase
MOPS	3-(Morpholino)-propanesulphonic acid
M_r	Molecular weight
M. smegmatis	*Mycobacterium smegmatis*
NMR	Nuclear magnetic resonance (spectroscopy)
NAD	β-Nicotinamide adenine dinucleotide
PAGE	Polyacrylamide gel electrophoresis
PMSF	Phenylmethylsulphonyl fluoride
P. putida	*Pseudomonas putida*
PTFE	Polytetrafluoroethene
Rb. sphaeroides	*Rhodobacter spheroides*
Rp. viridis	*R viridis*
S. cerevisiae	*Sacharomyces cerevisiae*
SDS	Sodium dodecyl sulphate
TEMED	N,N,N',N'-Tetramethylethylene diamine
Tris	Tris(hydroxymethyl)aminomethane
UV	Ultraviolet
Vis	Visible

APPENDIX 3

COURSES & CONFERENCES

Courses Attended

Undergraduate Lectures

Structure & function of proteins (4th year biochemistry).

Microbiology & biotechnology (4th year chemistry).

Postgraduate Lectures

NMR, EPR, X-ray crystallography, Database searching.

Department of Chemistry Colloquia

External Courses

Chemistry of metals in biological systems:

EEC-ESF advanced course (Wavre, May 14-24; *poster presented*).

Conferences Attended

Scottish Protein Structure Group Meetings at:

Stirling

Edinburgh

Aberdeen *(as speaker).*

Hannah Research Institute

Fifth International Conference of Bioinorganic Chemistry:

San Diego, California *(abstract & poster presented).*

Biochemical Society Meetings at:

Cardiff *(abstract & poster presented).*

Dublin *(poster presented).*

Harden Conference on Biological Electron-Transfer:

Wye College, Kent *(poster presented).*

FLAPS Network Meeting:

Wageningen, Netherlands *(as speaker, poster presented).*

APPENDIX 4

PUBLICATIONS

Probing the Structure and Function of Flavocytochrome b_2 Using Protein Engineering Methods

Chapman, S.K, White, P.W., Daff, S., Reid, G.A., Sharp, R.E. & Manson, F.D.C. (1993) in *Flavins & Flavoproteins* (Walter de Gruyter & Co., Berlin) 607-615.

Flavin to haem electron transfer in flavocytochrome b_2

Chapman, S.K, Reid, G.A., Daff, S., Sharp, R.E., White, P.W., Manson, F.D.C. & Lederer, F. (1994) *Biochem. Soc. Trans.* 22, 713-718.

Strategic manipulation of the substrate specificity of *Saccharomyces cerevisiae* flavocytochrome b_2

Daff, S., Manson, F.D.C., Reid, G.A. & Chapman, S.K. (1994) *Biochem. J. 301*, 829-834.

Flavocytochrome b_2: an ideal model system for studying protein-mediated electron transfer

Chapman, S.K, Reid, G.A., Bell, C., Short, D. & Daff, S. (1995) *Biochem. Soc. Trans. 24*, 73-77.

New Insights into the Catalytic Cycle of Flavocytochrome b_2

Daff, S., Ingledew, W.J., Reid, G.A. & Chapman, S.K. (1996) *Biochemistry (in press).*

Interaction of Cytochrome *c* with Flavocytochrome b_2

Daff, S., Sharp, R.E., Short, D.M., Bell, C., White, P., Manson, F.D.C., Reid, G.A., & Chapman, S.K. (1996) *Biochemistry, (in press).*

Probing the Structure and Function of Flavocytochrome b_2 Using Protein Engineering Methods.

Stephen K. Chapman, Patricia White, Simon Daff

Department of Chemistry, University of Edinburgh, West Mains Road, Edinburgh EH9 3JJ, Scotland, U.K.

Graeme A. Reid, R. Eryl Sharp, Forbes D.C. Manson

Institute of Cell and Molecular Biology, University of Edinburgh, Edinburgh EH9 3JR, Scotland U.K.

Introduction

Protein engineering techniques are now commonplace. The ability to design and construct altered forms of enzymes is now well established as an important method for the study of enzyme structure and function (1). The successful application of protein engineering is dependent on three requirements: i) the availability of the DNA that encodes the protein; ii) a high-resolution three-dimensional structure of the protein; and iii) a system allowing expression and isolation of engineered forms of the protein. All of these conditions have been met for the enzyme flavocytochrome b_2 from *Saccharomyces cerevisiae*.

Flavocytochrome b_2 (L-lactate:cytochrome *c* oxidoreductase, EC 1.1.2.3) is a soluble component of the intermembrane space of yeast mitochondria (2) where it catalyses the oxidation of L-lactate to pyruvate and transfers electrons to cytochrome *c* (3). The crystal structure of flavocytochrome b_2 from *S. cerevisiae* has been solved to 0.24 nm resolution (4). The enzyme is a tetramer of identical subunits of M_r 57,500 (5). Each subunit consists of two distinct domains; an N-terminal haem-containing cytochrome domain, and a C-terminal FMN-containing flavodehydrogenase domain. The DNA encoding *S. cerevisiae* flavocytochrome b_2 has been cloned and sequenced (6). The successful expression of flavocytochrome b_2 at a high-level in *E.coli* (7), followed by the independent expression of the haem- and FMN- containing domains (8,9), opened up the way for extensive protein engineering studies on the enzyme. These have involved: active site residues important in lactate oxidation (10,11); structural features such as the C-terminal tail (12) and

Flavins and Flavoproteins 1993

interdomain hinge (13); and ligand residues of the haem iron (14). These studies have proved invaluable in furthering our understanding of the mechanism of lactate oxidation and cytochrome *c* reduction catalysed by flavocytochrome b_2. We are now using this knowledge to help us in redesigning certain parts of flavocytochrome b_2 to "tailor" the enzyme in specific ways. In this paper we report progress in shifting the selectivity of the enzyme towards substrates of differing chain length, and the effects of altering the hinge region which links the two domains of flavocytochrome b_2.

Results and Discussion

Redesigning substrate specificity

Although flavocytochrome b_2 is a L-lactate dehydrogenase it is by no means exclusive in terms of substrate, but does have somewhat poorer activity with longer chain 2-hydroxyacids. It appears that selectivity for the methyl group of lactate is controlled by interactions with bulky non-polar residues, particularly Leu230, Ala198 and Leu286 as illustrated in Figure 1.

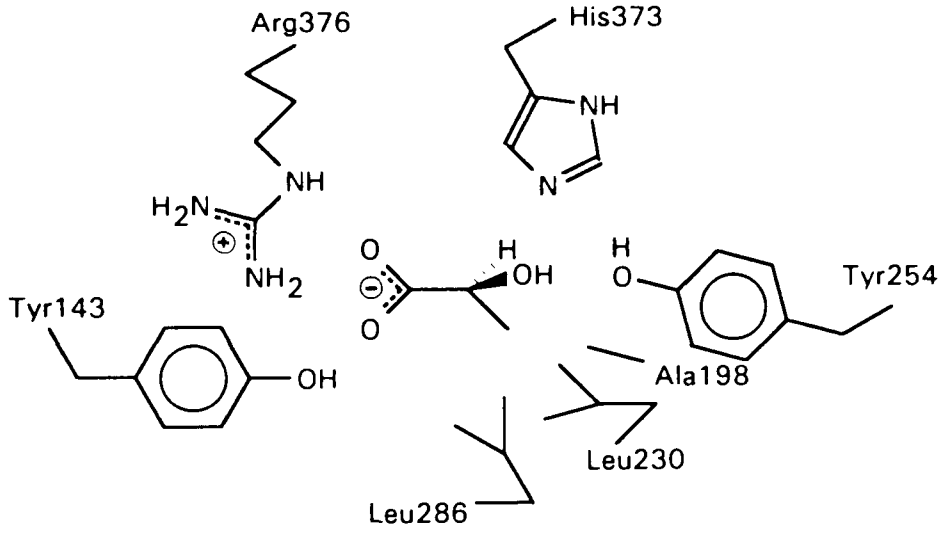

Figure 1. Schematic representation of the active site of flavocytochrome b_2 (in this view the FMN group, which is not shown, lies directly behind residues 376 and 373)

Using Figure 1 as a guide, the obvious way to change the specificity of flavocytochrome b_2 towards longer chain length substrates would be to decrease the size of the sidechains of residues 198, 230 and 286. Using this strategy we have used site-directed mutagenesis to

generate the following mutations: Ala198->Gly (A198G); Leu230->Ala (L230A); and Leu286->Ala (L286A). We have also made the double mutant A198G,L230A.

In order to investigate the effect of these mutations on the substrate specificity of the enzyme we have determined k_{cat} and K_m values for the series of D,L-2-hydroxyacids of increasing chain length shown in Figure 2.

glycolate (2)

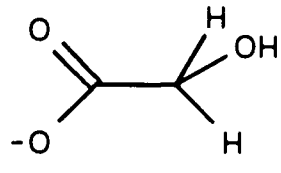

lactate (3)

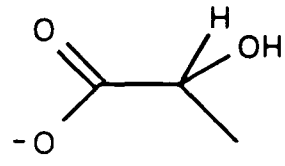

2-hydroxybutyrate (4)

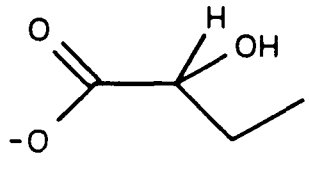

2-hydroxyvalerate (5)

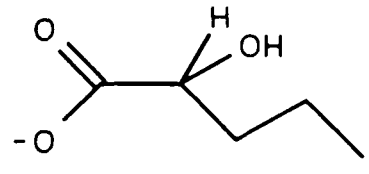

2-hydroxycaproate (6)

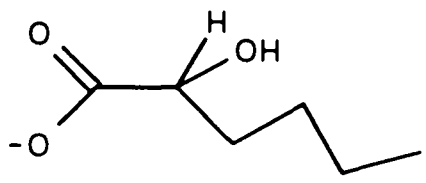

2-hydroxyoctanoate (8)

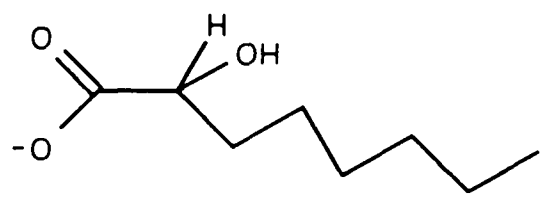

Figure 2. The series of 2-hydroxyacids used in the substrate specificity studies. Chain length is indicated in brackets.

The efficiency (as judged by k_{cat}/K_m values) of wild-type and mutant flavocytochromes b_2 at oxidising the above D,L-2-hydroxyacids is summarised in Table 1 on the next page. For the wild-type enzyme there is, not surprisingly, a definite maximum value of k_{cat}/K_m with D,L-lactate as substrate. With other substrates the general trend for the wild-type enzyme is for the efficiency to increase with increasing substrate chain length. The A198G mutant

enzyme shows a similar trend but with k_{cat}/K_m values being an order of magnitude lower than those seen for the wild-type enzyme. The difference in k_{cat}/K_m values is mainly due to larger K_m values in the A198G enzyme implying that this mutation has primarily disturbed the formation of the Michaelis complex.

Table 1. Kinetic parameters for the oxidation of D,L-2-hydroxyacids by wild-type and mutant flavocytochromes b_2. All experiments were carried out under steady-state conditions at 25°C in Tris/HCl buffer, pH 7.5 (I = 0.10 M). Ferricyanide was used as electron acceptor at a concentration of 1 mM.

Substrate	Chain length	Wild-type k_{cat}/K_m ($M^{-1}s^{-1}$)	A198G k_{cat}/K_m ($M^{-1}s^{-1}$)	L230A k_{cat}/K_m ($M^{-1}s^{-1}$)	A198G,L230A k_{cat}/K_m ($M^{-1}s^{-1}$)
glycolate	2	2.1×10^4	1.0×10^3	9.3×10^2	-
D,L-lactate	3	8.1×10^5	3.8×10^4	6.1×10^3	$\sim 2 \times 10^2$
D,L-2-hydroxy-butyrate	4	1.1×10^5	9.0×10^3	2.3×10^4	1.3×10^3
D,L-2-hydroxy-valerate	5	5.5×10^4	-	7.7×10^4	7.2×10^3
D,L-2-hydroxy-caproate	6	1.3×10^5	1.3×10^4	1.2×10^5	8.0×10^3
D,L-2-hydroxy-octanoate	8	4.2×10^5	1.0×10^4	2.1×10^5	1.8×10^4

The L230A mutation is far more interesting and results in a true alteration in the substrate specificity of the enzyme. The largest k_{cat}/K_m value for the L230A-enzyme is seen with D,L-2-hydroxyoctanoate as substrate (Table 1). In fact the efficiency of the L230A-enzyme with D,L-2-hydroxyoctanoate is some 30-fold higher than with D,L-lactate as substrate. This is in marked contrast to the wild-type enzyme which is 2-fold more efficient with D,L-lactate than with D,L-2-hydroxyoctanoate. This means that in the L230A-mutant enzyme we have in effect achieved a 60-fold swing in substrate selectivity from a substrate with a 3-carbon chain length towards a substrate with a 8-carbon chain length. One might, therefore, reasonably describe the L230A-enzyme as a long-chain 2-hydroxyacid dehydrogenase rather than a lactate dehydrogenase. Essentially what the L230A mutation does is to de-tune the efficiency of the enzyme with D,L-lactate whilst

retaining efficiency with the longer chain 2-hydroxyacids. This is most clearly demonstrated in Figure 3.

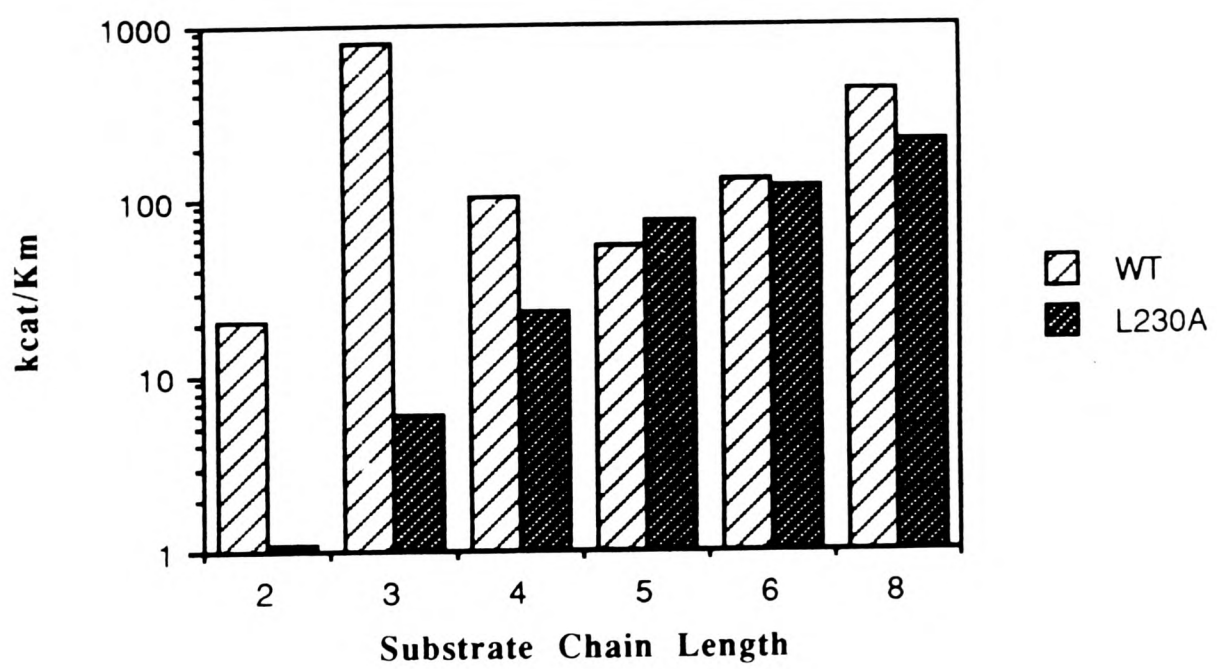

Figure 3. Enzyme efficiency vs substrate chain length for wild-type and L230A flavocytochromes b_2.

Results for the double mutant, A198G,L230A, represent a combination of the effects of the two single mutants producing a much lower activity enzyme which acts best on the longer chain 2-hydroxyacids.
We are now repeating this work using the pure L-(+)-isomers of all of the 2-hydroxyacids. It is already clear that the trend is exactly the same as reported here with the D,L-compounds.

From the work described above we have demonstrated the potential for manipulating substrate specificity in flavocytochrome b_2 using protein engineering methods. In clarifying the roles of residues A198 and L230 we have clearly shown that L230 is crucial for substrate chain length selectivity.

Altering the hinge region

The two distinct domains of flavocytochrome b_2 are linked by a typical hinge peptide. This is illustrated schematically in Figure 4. The role of this hinge in electron transfer between the domains has already been investigated by the construction of interspecies hybrids of flavocytochrome b_2 (13). However it was clear from this previous work that a more subtle approach was needed to provide more detail on the function of the hinge. We have therefore constructed a mutant enzyme, HΔ3, which has a three amino acid deletion (residues Ala98 ,Pro99, Gly100) in the hinge region.

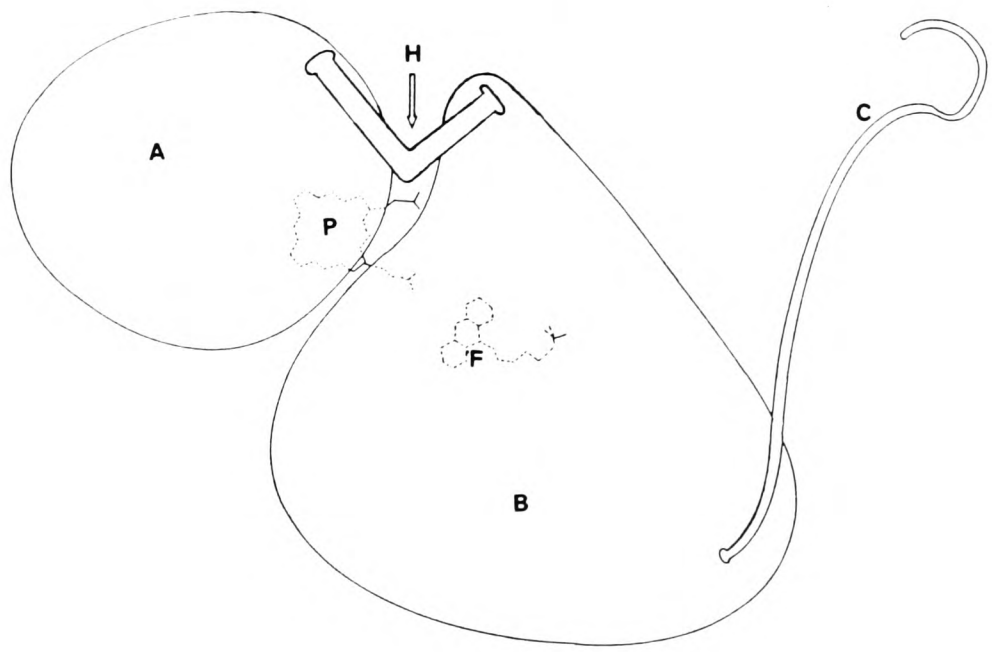

Figure 4. Schematic representation of a flavocytochrome b_2 subunit. A, haem domain; B, flavin domain; C, C-terminal tail; F, FMN; P, protohaem IX; H, interdomain hinge.

Kinetic studies were carried out on the HΔ3-enzyme (at 25°C in Tris/HCl buffer, pH 7.5, I = 0.10 M) and indicated that HΔ3-flavocytochrome b_2 remains a good L-lactate dehydrogenase. Under steady-state conditions, with ferricyanide as electron acceptor, the value of k_{cat} for L-lactate oxidation seen with the HΔ3-enzyme was 257 s^{-1} which is around two-thirds the value of 400 s^{-1} seen for the wild-type enzyme. The cytochrome *c* reductase function of the enzyme is, on the other hand, severely impaired by the HΔ3-

mutation. Under steady-state conditions the k_{cat} value for cytochrome *c* reduction falls over five-fold from 207 s^{-1} in the wild-type enzyme to 39 s^{-1} in the mutant. Since cytochrome *c* can only receive electrons from the haem group of flavocytochrome b_2 (15,16), the fall in k_{cat} could be due either to disruption of FMN → b_2-haem or b_2-haem → cytochrome *c* electron transfer. Stopped-flow experiments reveal that the k_{cat} for b_2-haem reduction has fallen from 445 s^{-1} in the wild-type enzyme to 93 s^{-1} in the HΔ3-mutant enzyme. Therefore, if we consider the steady-state and stopped-flow results together, it is clear that the HΔ3-mutation affects <u>both</u> intramolecular electron transfer from FMN to b_2-haem <u>and</u> intermolecular electron transfer from b_2-haem to cytochrome *c*. Further evidence for this was provided from the determination of the second-order rate constants for the flavocytochrome b_2 reduction of cytochrome *c* measured directly using stopped-flow spectrophotometry. Values for cytochrome *c* reduction were 4.7 x 10^7 $M^{-1}s^{-1}$ with wild-type enzyme and 4.0 x 10^6 $M^{-1}s^{-1}$ with the HΔ3-mutant enzyme. This order of magnitude difference is indicative of a significant effect on the flavocytochrome b_2 - cytochrome *c* interaction caused by the HΔ3-mutation.

To investigate the effect of the HΔ3-mutation on the binding of cytochrome *c* to flavocytochrome b_2 directly we have used NMR spectroscopy. NMR spectra were recorded at 25°C in 20 mM phosphate buffer at pH 7.0 and >98% D_2O using a 600 MHz spectrometer. Flavocytochrome b_2 concentrations were 0.1 mM tetramer (*i.e.* 0.4 mM subunit) and cytochrome *c* aliquots were titrated into the flavocytochrome b_2 sample (both proteins were kept oxidised throughout). The linewidths due to cytochrome *c* haem-methyl resonances at 34.0 and 32.5 ppm were monitored throughout the titration. If significant binding of cytochrome *c* to flavocytochrome b_2 occurs then the linewidths should broaden significantly whereas if there were no binding at all then the linewidths would be identical to free cytochrome *c*. A plot of linewidth at 34.0 ppm against 1/[cytochrome *c*] for both wild-type and HΔ3-enzyme is shown in Figure 5.

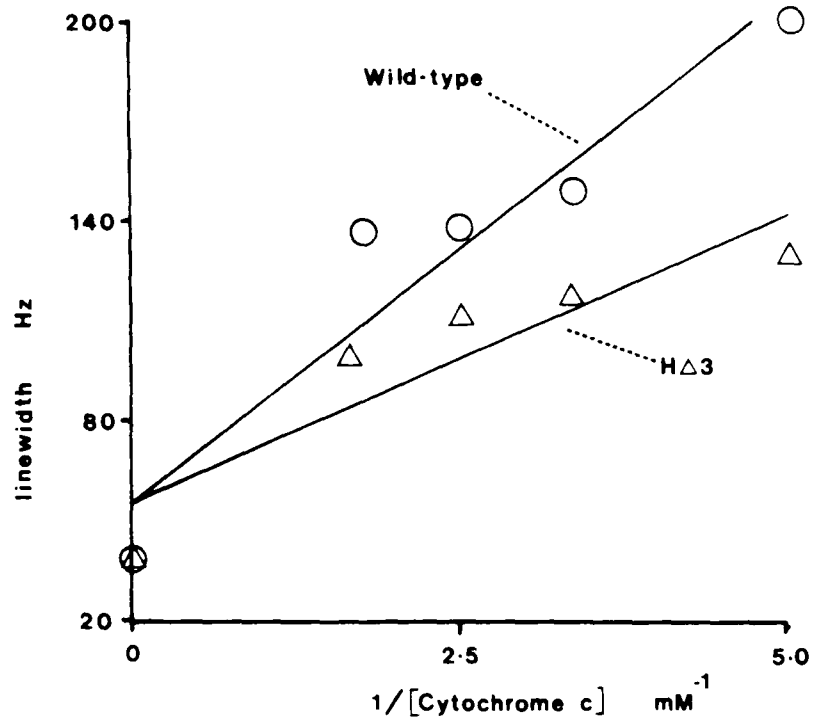

Figure 5. Plot of the linewidth at 34.0 ppm against 1/[cytochrome *c*] for the wild-type and HΔ3 flavocytochromes b_2

The degree of binding is indicated by the gradient of the lines; the steeper the gradient the stronger the binding. Thus from Figure 5 it is clear that the wild-type enzyme binds cytochrome *c* far more strongly than the HΔ3-mutant enzyme. Thus, at least qualitatively, we can confirm from the NMR studies that the HΔ3-mutation does disrupt cytochrome *c* binding to flavocytochrome b_2.

From our work on the HΔ3-mutant enzyme we conclude that: the interdomain hinge has little importance in the lactate dehydrogenase function of the enzyme; the hinge plays a central role in mediating interdomain electron transfer from FMN to b_2-haem; the hinge is also important for binding and electron transfer to cytochrome *c*.

Acknowledgements

This work was supported by the Science and Engineering Research Council through research studentships awarded to PW, SD and RES and research grants to GAR and SKC. We are grateful to John Parkinson for help with the nmr experiments and to Florence

Lederer, Scott Mathews, Mariella Tegoni and Christian Cambillau for fruitful discussions.

References

1. Chapman, S.K. and G.A. Reid. 1993. Chem. in Brit. *29*:202-204.

2. Daum, G., P.C. Böhni and G. Schatz. 1982. J. Biol. Chem. *257*:13028-13033.

3. Appleby, C.A. and R.K. Morton. 1954. Nature *173*:749-752.

4. Xia, Z.-X. and F.S. Mathews. 1990. J. Mol. Biol. *212*:837-863.

5. Jacq, C. and F. Lederer. 1974. Eur. J. Biochem. *41*:311-320.

6. Guiard, B. 1985. EMBO. J. *4*:3265-3272.

7. Black, M.T., S.A. White, G.A. Reid and S.K. Chapman. 1989. Biochem. J. *258*:255-259 .

8. Pallister, R.L., G.A. Reid, C.E. Brunt, C.S. Miles and S.K. Chapman. 1990. In Flavins and Flavoproteins (B. Curti, S. Ronchi, G. Zanetti eds.), Walter de Gruyter, Berlin, pp. 787-790.

9. Brunt C.E., M.C. Cox, A.G.P. Thurgood, G.R. Moore, G.A. Reid and S.K. Chapman. 1992. Biochem. J. *283*:87-90.

10. Dubois, J., S.K. Chapman, F.S. Mathews, G.A. Reid and F. Lederer. 1990. Biochemistry *29*:6393-6400.

11. Miles, C.S., N. Rouvière-Fourmy, F. Lederer, F.S. Mathews, G.A. Reid, M.T. Black and S.K. Chapman. 1992. Biochem.J. *285*:187-192.

12. White, S.A., M.T. Black, G.A. Reid and S.K. Chapman, 1989. Biochem. J. *263*:849-853.

13. White, P., F.D.C. Manson, C.E. Brunt, S.K. Chapman and G.A. Reid. 1993. Biochem. J. *291*:89-94.

14. Miles, C.S., F.D.C. Manson, G.A. Reid and S.K. Chapman. 1993, Biochim. Biophys. Acta. (in press).

15. Ogura, Y. and T. Nakamura. 1966. J. Biochem. *60*:77-86.

16. Capeillère-Blandin, C., M. Iwatsubo, G. Testylier and F. Labeyrie. 1980. In: Flavins and Flavoproteins (K. Yagi and T. Yamamoto, eds.) Japan Scientific Societies Press, Tokyo. pp. 617-630.

electron transfer and haem oxygen binding are very rapid. Therefore the initial optical spectrum observed will be that of the haem oxy-complex and flavin radical. Flavin radical is then oxidized by oxygen at a rate of 0.15 s^{-1}, re-generating FAD. However, in the presence of oxygen bound at the haem site, flavin reduction by NAD(P)H is inhibited, and the flavin remains oxidized in the steady state. While attractive, such a model requires more direct evidence of haem–flavin interactions and oxygen consumption by $FAD^{\bullet}$, before it is confirmed.

Hmp binds oxygen and reduces it and oxidizes NAD(P)H. This intriguing diaphorase might, therefore, be able to 'sense' NAD(P)H/NAD(P) ratios and/or cellular oxygen concentrations. Experiments to investigate both possibilities are in progress in these laboratories.

We thank the SERC (R.K.P.) and the MRC (C.E.C.) for financial support and Helen Cooper for technical assistance.

1 Appleby, C. A. (1984) Annu. Rev. Plant Physiol. **35**, 443–478
2 Zhu, H. and Riggs, A. F. (1992) Proc. Natl. Acad. Sci. U.S.A. **89**, 5015–5019
3 Kroneck, P. M. H., Jakob, W., Webster, D. A. and DeMaio, R. (1991) Biol. Met. **4**, 119–125
4 Ioannidis, N., Cooper, C. E. and Poole, R. K. (1992) Biochem. J. **288**, 649–655
5 Orii, Y., Ioannidis, N. and Poole, R. K. (1992) Biochem. Biophys. Res. Commun. **187**, 94–100
6 Vasudevan, S. G., Armarego, W. L., Shaw, D. C., Lilley, P. E., Dixon, N. E. and Poole, R. K. (1991) Mol. Gen. Genet. **226**, 49–58
7 Andrews, S. C., Shipley, D., Keen, J. N., Findlay, J. B., Harrison, P. M. and Guest, J. R. (1992) FEBS Lett. **302**, 247–252
8 Jakob, W., Webster, D. A. and Kroneck, P. M. H. (1992) Arch. Biochem. Biophys. **292**, 29–33
9 Poole, R. K., Ioannidis, N. and Orii, Y. (1994) Proc. Roy. Soc. London B **255**, 251–258
10 Massey, V., Palmer, G. and Ballou, D. (1971) in Flavins and Flavoproteins (Kamin, H., ed.), pp. 349–361, Butterworths, London
11 Boerman, S. and Webster, D. A. (1982) J. Gen. Appl. Microbiol. **28**, 35–43
12 Khosla, C. and Bailey, J. E. (1988) Nature (London) **331**, 633–635
13 Khosla, C. and Bailey, J. E. (1989) J. Mol. Biol. **210**, 79–89
14 Eschenbrenner, M., Coves, J. and Fontecave, M. (1994) Biochem. Biophys. Res. Commun. **198**, 127–131
15 Spiro, S. and Guest, J. R. (1991) Trends Biochem. Sci. **16**, 310–314
16 Cammack, R. and Cooper, C. E. (1992) Methods Enzymol. **227**, 353–384

Received 21 April 1994

Flavin to haem electron transfer in flavocytochrome b_2

Stephen K. Chapman*§, Graeme A. Reid†, Simon Daff*, R. Eryl Sharp†, Patricia White*, Forbes D. C. Manson† and Florence Lederer‡

*Department of Chemistry, University of Edinburgh, West Mains Road, Edinburgh EH9 3JJ, U.K., †Institute of Cell and Molecular Biology, University of Edinburgh, Mayfield Road, Edinburgh EH9 3JR, U.K., and ‡Centre National de la Recherche Scientifique, URA 1561, Hôpital Necker, 161 rue de Sèvres, 75743 Paris Cédex 15, France

Introduction

Flavocytochrome b_2 is a homotetrameric enzyme from yeast mitochondria which catalyses the oxidation of L-lactate to pyruvate with subsequent electron transfer to cytochrome *c* [1,2]. The enzyme from *Saccharomyces cerevisiae* has been successfully expressed at a high level in *Escherichia coli* [3] and it has been shown that the kinetic properties of flavocytochrome b_2 isolated from both yeast and *E. coli* are identical [3].

The X-ray crystal structures have been determined for the enzyme from both *S. cerevisiae* [4] and *E. coli* [5] and these are essentially isostructural and clearly show that each subunit is composed of two distinct domains: an N-terminal, haem-containing, cytochrome domain and a C-terminal, FMN-containing, flavodehydrogenase domain, the shortest distance between the flavin and haem groups being ~9.7 Å [4]. The crystal structure of

Abbreviation used: RDS, rate-determining step.

§To whom correspondence should be addressed.

flavocytochrome b_2 exhibits two crystallographically distinguishable subunits in the asymmetric unit [4]. In subunit 1, the electron-density map clearly shows the presence of both cytochrome and flavodehydrogenase domains, with Tyr-143 hydrogen bonding to a haem propionate (Figure 1). However, in subunit 2, the cytochrome domain is not visible, due to positional disorder (Gly-100 is the first visible residue), and Tyr-143 is seen to be hydrogen bonded to the carboxylate of a pyruvate molecule (the reaction product) which is located in the active site of the flavodehydrogenase domain.

Analysis of this three-dimensional information has allowed the identification of particular structural elements and amino acid residues which might be important in controlling electron transfer from one prosthetic group to another. For example, the two domains are linked by a typical hinge peptide and it is clear that this region of the protein has a significant influence on flavin to haem electron transfer [6,7]. In addition, it has been clearly demonstrated that one particular interface residue, Tyr-143 (Figure 1), plays a pivotal role in the modulation of interdomain electron transfer [8]. In the present paper we shall draw together previous work and new results to give an overall view of flavin to haem electron transfer in flavocytochrome b_2.

Figure 1

The arrangement of the flavin and haem groups seen in one of the two crystallographically distinguishable subunits [4]

Tyr-143 is seen hydrogen-bonding to one of the haem propionates. The shortest distance between the haem and flavin rings is 9.7 Å (from haem C-2A to flavin N-5). W664 is a water molecule.

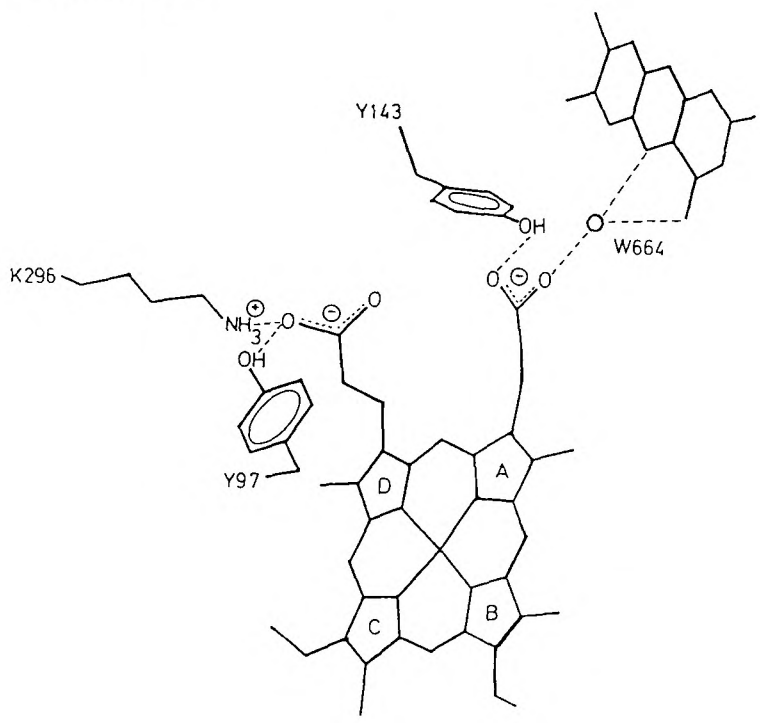

Materials and methods

DNA manipulation

Standard methods for growth of *E. coli*, DNA manipulation and transformation were performed as described by Sambrook et al. [9]. Site-directed mutagenesis was performed as described elsewhere [10].

Enzymes

Wild-type and mutant flavocytochromes b_2 were isolated from *E. coli* cells and purified as previously reported [3].

Kinetic analysis

All kinetic parameters reported here were determined at 25 ± 0.1°C in 0.01 M Tris/HCl, pH 7.5, with I adjusted to 0.10 by addition of NaCl. Steady-state results were obtained as previously described [8]. Pre-steady-state kinetic measurements were made using an Applied Photophysics SF.17MV stopped-flow spectrophotometer as previously described [8]. Analysis of data was performed using the SF.17MV software and simulations were carried out using the Applied Photophysics Global Analysis package.

Results and discussion

How fast is flavin to haem electron transfer in flavocytochrome b_2?

The electron flow through flavocytochrome b_2 proceeds from L-lactate to flavin, from flavin to b_2-haem and finally from b_2-haem to cytochrome *c*. This process includes two intramolecular electron-transfer steps [11,12]: electron transfer from fully reduced flavin to b_2-haem, and electron transfer from flavin semiquinone to b_2-haem. Under pre-steady-state conditions, in the absence of any electron acceptor such as cytochrome *c*, the full reduction of flavocytochrome b_2 proceeds as illustrated in Scheme 1. The various electron-transfer

Scheme 1

The electron-transfer processes occurring in one subunit of flavocytochrome b_2 during full reduction of the enzyme by L-lactate

Step 1, reduction of flavin; step 2, flavin to haem electron transfer. Step 3 is the entry of a third electron per subunit to generate fully reduced enzyme. F, flavin; H, haem; black dots denote electrons.

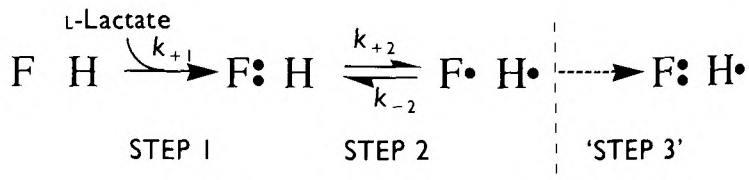

steps in this process have been studied by stopped-flow spectrophotometry [8] in which the reduction of the flavin and haem can be monitored at 438.3 nm (an isosbestic point in the visible spectrum of the haem) and 557 nm respectively [11,13]. As in previous studies, under most conditions the kinetic traces could be satisfactorily analysed as the sum of two exponentials.

Two models have been proposed to explain the reduction process [14,15]. In these models, the rapid first phase is a two-step process in which two electrons from L-lactate enter a subunit at the flavin level and are redistributed between flavin and haem in each subunit. The slower second phase is dominated by the entry of a third electron per subunit (corresponding to four electrons from two L-lactate molecules entering the full tetramer), which is made possible by inter-subunit electron transfer. This slow phase (equivalent to step 3 in Scheme 1) is kinetically irrelevant during catalytic turnover of the enzyme when it acts as a two-electron transferase [11,13].

In this paper we are focusing on flavin to haem electron transfer, which is step 2 in Scheme 1. This step is reversible, with the position of the equilibrium lying 85% in favour of reduced haem (as calculated from redox potentials [16]). The preceding step, flavin reduction by L-lactate, has a measured rate constant of $604 \pm 60\ s^{-1}$ [8], which corresponds to k_{+1} in Scheme 1. The absorbance versus time trace for haem reduction yields a rate constant of $445 \pm 50\ s^{-1}$ if fitted to a biphasic model [8]. However, the fact that these traces show an appreciable lag behind flavin reduction, coupled with the fact that there are three steps in Scheme 1, clearly indicates that fitting such data to a biphasic model is an approximation. Consequently, the value of the rate constant for haem reduction will have contributions from all three steps in Scheme 1. Step 3, however, contributes only ~15% of the total absorbance change and is much slower than steps 1 and 2. Therefore, during the initial 80% of the haem absorbance change the contribution of step 3 is comparatively small. Hence, in this region of the trace, the proportion of reduced haem can be described by the function

$$\frac{1 + (k_a e^{-k_b t} - k_b e^{-k_a t})}{k_b - k_a}$$

This function describes the accumulation of C in an A→B→C consecutive process, the second step of which may be an equilibrium. By fixing k_a to be the value of k_{+1} in Scheme 1, i.e. $604 \pm 60\ s^{-1}$, and fitting the above function to the initial 80% of the haem absorbance change, a value for k_b of $1600 \pm 300\ s^{-1}$ can be deduced. The value of k_b is, however, still slightly influenced by the rate of step 3, which perturbs the equilibrium of step 2. In order to take all the possible contributions into account, the limiting conditions must be considered. If step 3 is rapid and irreversible, the equilibrium in step 2 would be displaced and k_b would be equal to k_{+2}. If, on the other hand, step 3 is detectably slow, then k_b would be equal to $k_{+2} + k_{-2}$. The ratio of k_2 to k_{-2} can be calculated, from the equilibrium constant, to be 5.5:1 and this allows the limiting values for k_{+2} and k_{-2} to be calculated. From the limiting values one can estimate values for the rate constants k_{+2} ($1500 \pm 500\ s^{-1}$) and k_{-2} ($270 \pm 90\ s^{-1}$). Simulations indicate that this is a valid approach, especially in the absence of a more detailed understanding of step 3. These rate constants have been evaluated previously under very different experimental conditions [14,15]. Thus, at 25°C and at pH 7.5, the rate constant for electron transfer from fully reduced flavin to b_2-haem is $\sim 1500\ s^{-1}$.

The rate of electron transfer from flavin semiquinone to b_2-haem is more difficult to estimate however. This step has been more extensively studied using the enzyme from *Hansenula anomala* with experimental approaches involving T-jump relaxation [17], stopped-flow spectrophotometry [18], stopped-flow coupled with e.p.r. [19,20] and laser flash photolysis [16,21]. The major conclusion from these experiments is that the stability of the flavin semiquinone is greatly enhanced in the presence of pyruvate, which causes an increase in the oxidized/semiquinone redox couple of ~100 mV. There is at present conflicting evidence about how this affects electron transfer from flavin semiquinone to b_2-haem [16,18,19,21].

Is the hinge important for interdomain electron transfer?

As mentioned in the introduction, the cytochrome and flavodehydrogenase domains of flavocytochrome b_2 are linked by a segment of polypeptide chain which constitutes the interdomain hinge. This allows the cytochrome domain to be mobile with respect to the flavodehydrogenase domain, as demonstrated by crystallographic work [4] and supported by n.m.r. data [22]. The primary structure of the hinge region is strikingly different between flavocytochromes b_2 from two yeast species, *S. cerevisiae* and *Hansenula anomala*, even though there is 60% identity between the amino acid sequences of the two enzymes as a whole [23].

In order to probe the role of the hinge, an interspecies hybrid enzyme was constructed which consisted of the bulk of the *Saccharomyces* enzyme but had the hinge region replaced with that from the *Hansenula* enzyme [6]. This 'hinge-swap' enzyme retained the ability to be a good L-lactate dehydrogenase but was a very poor cytochrome *c* reductase. It was clear that the major effect of the hinge-swap was on flavin to haem electron transfer, which was at least 300-fold slower in the hybrid enzyme compared with wild-type [6] (Table 1). The implication was that structural integrity around the hinge was crucial in mediating electron transfer between the domains.

To probe more subtly this effect, two hinge mutations of flavocytochrome b_2 (HΔ3 and HΔ6) were constructed. The HΔ3 enzyme has a three-amino-acid deletion of residues 98–100 (APG) and the HΔ6 enzyme a six-amino-acid deletion of residues 95–100 (PPYAPG). These residues were chosen for deletion since they lie within the hinge region at the interdomain boundary. Both HΔ3 and HΔ6 enzymes remain good L-lactate dehydrogenases; flavin reduction is only 15% slower than for the wild-type enzyme (Table 1), implying that the hinge is of little importance in flavin reduction by L-lactate. The most striking effect of these deletions is, not surprisingly, on the rate of haem reduction, indicating that flavin to haem electron transfer has been impaired. The $k_{cat.}$ values for haem reduction in the HΔ3 and HΔ6 enzymes are some 5-fold and 17-fold lower respectively than in the wild-type enzyme (Table 1). These results show that as the hinge segment is sequentially truncated the rate of flavin to haem electron transfer decreases. One possible explanation for this is that the truncation restricts the flexibility of the hinge, thereby impairing productive recognition between the two domains. In any case, it is now clear that the nature of the hinge region is critical for efficient electron transfer from flavin to haem.

Does Tyr-143 control flavin to haem electron transfer?

From Figure 1, Tyr-143 appears to be uniquely placed to play a central role in mediating electron transfer both from lactate to flavin and from flavin to haem. The role of this residue has been examined by the construction and extensive characterization of a mutant flavocytochrome b_2 (Y143F-b_2) in which Tyr-143 has been replaced by phenylalanine [8,24]. The most significant effect of the mutation was found to be a change in the rate-determining step (RDS) for the enzyme. In the wild-type enzyme the main RDS is proton abstraction at C-2 of L-lactate, as shown by the primary ^{2}H-kinetic isotope effect [8,13]. However, in Y143F-b_2 the RDS is intramolecular electron transfer from flavin to haem. The rate of flavin reduction is identical (within error; Table 1) for the mutant and wild-type enzymes under the conditions employed in [8], whereas the $k_{cat.}$ for haem reduction in Y143F-b_2, as determined from stopped-flow experiments, is some 20-fold lower than that measured for wild-type enzyme (Table 1) [8]. Therefore we can conclude immediately that Tyr-143 plays a key role in facilitating electron transfer from flavin to haem.

Table 1

Values of $k_{cat.}$ for the reduction of flavin and haem by L-lactate for wild-type and mutant flavocytochromes b_2

All values were determined by the stopped-flow method at 25°C in Tris/HCl buffer, pH 7.5, $I = 0.10$. Values, obtained from non-linear least-squares fit of Michaelis–Menten curves, are expressed as number of prosthetic groups reduced per second (mean ± S.D.). Data were collected and analysed as described previously [8].

	$k_{cat.}$ (s^{-1})		
Enzyme	Flavin reduction	Haem reduction	Reference
Wild-type	604 ± 60	445 ± 50	[8]
Y143F	735 ± 80	21 ± 2	[8]
HΔ3	518 ± 17	91 ± 3	[7]
HΔ6	520 ± 12	26 ± 1	R. E. Sharp, unpublished work
Hinge-swap	240 ± 12	1.6 ± 0.4	[6]

Why does the Y143F mutation have such an effect on flavin to haem electron transfer? It is known that the effect is not due to gross structural changes since the X-ray crystal structure of Y143F-b_2 is essentially the same, overall, as that of the wild-type enzyme [25]. The most likely explanation is that the mutation removes a critical inter-domain hydrogen bond between the phenolic OH of Y143 and a haem propionate (Figure 1) and this removal significantly impairs interaction and electron transfer between the domains.

Does pH influence flavin to haem electron transfer?

The catalytic activity of flavocytochrome b_2 is pH-dependent and pre-steady-state kinetics indicate that the rate of flavin to haem electron transfer is substantially decreased at low pH. This suggests that protonation of an ionizable group close to the haem or flavin has a significant influence on this electron-transfer step. The pK_a of this ionizable group is estimated, from kinetic experiments, to be a little above 5.0. One can suggest, from Figure 1, that a suitable candidate for this group would be haem-propionate 7 (HP7) which hydrogen-bonds to Tyr-143. N.m.r. experiments on the isolated cytochrome domain indicate that HP7 has a pK_a of 4.8 [26], and a similar n.m.r. study on a monomeric form of flavocytochrome b_2 gives a value of ~5.0 (P. White, unpublished work). These results are consistent with HP7 being the ionizable group which affects flavin to haem electron transfer. It is possible to visualize the protonation of HP7 causing a disruption of the network of hydrogen-bonding between the flavin and haem (Figure 1) with the resulting effect on electron transfer between the two redox centres.

Conclusions

There are several factors which affect the rate of electron transfer in proteins, such as the driving force, the distance between redox centres and the intervening medium between these centres. In this paper we have focused on electron transfer from flavin to haem in flavocytochrome b_2. It has been shown that this intramolecular electron-transfer step is strongly influenced by a number of structural features of the enzyme, including the inter-domain hinge, Tyr-143 and haem-propionate 7. In addition, it is now evident that properties such as domain mobility are important in modulating inter-domain electron transfer.

We are indebted to Professor F. S. Mathews, Dr. M. Tegoni and Dr. C. Cambillau for helpful discussions. This work was supported by the Science and Engineering Research Council (SERC) through research grants and by the Royal Society through an equipment grant. We are grateful to SERC for postdoctoral support for P.W. and F.D.C.M. and for postgraduate support for S.D. and R.E.S. We thank the European Community FLAPS network for travel funds.

1 Chapman, S. K., White, S. A. and Reid, G. A. (1991) Adv. Inorg. Chem. **36**, 257–301
2 Lederer, F. (1991) in The Chemistry and Biochemistry of Flavoenzymes (Müller, F., ed.), vol. 2, pp. 154–242, CRC Press, Boca Raton, FL
3 Black, M. T., White, S. A., Reid, G. A. and Chapman, S. K. (1989) Biochem. J. **258**, 255–259
4 Xia, Z.-X. and Matthews, F. S. (1990) J. Mol. Biol. **212**, 837–863
5 Tegoni, M. and Cambillau, C. (1994) Protein Sci. **3**, 303–813
6 White, P., Manson, F. D. C., Brunt, C. E., Chapman, S. K. and Reid, G. A. (1993) Biochem. J. **291**, 89–94
7 Sharp, R. E., White, P., Chapman, S. K. and Reid, G. A. (1994) Biochemistry **33**, 5115–5120
8 Miles, C. S., Rouvière-Fourmy, N., Lederer, F., Mathews, F. S., Reid, G. A., Black, M. T. and Chapman, S. K. (1992) Biochem. J. **285**, 187–192
9 Sambrook, J., Fritsch, E. F. and Maniatis, T. (1989) Molecular Cloning: A Laboratory Manual, 2nd edn., Cold Spring Harbor Laboratory Press, Cold Spring Harbor, NY
10 Kunkel, T. A. (1985) Proc. Natl. Acad. Sci. U.S.A. **82**, 488–492
11 Capeillère-Blandin, C., Bray, R. C., Iwatsubo, M. and Labeyrie, F. (1975) Eur. J. Biochem. **54**, 549–566
12 Capeillère-Blandin, C. (1982) Eur. J. Biochem. **128**, 533–542
13 Pompon, D., Iwatsubo, M. and Lederer, F. (1980) Eur. J. Biochem. **104**, 479–488
14 Capeillère-Blandin, C. (1975) Eur. J. Biochem. **56**, 91–101
15 Pompon, D. (1980) Eur. J. Biochem. **106**, 151–159
16 Walker, M. C. and Tollin, G. (1991) Biochemistry **30**, 5546–5555
17 Tegoni, M., Silvestrini, M. C., Labeyrie, F. and Brunori, M. (1984) Eur. J. Biochem. **140**, 39–45
18 Janot, J.-M., Capeillère-Blandin, C. and Labeyrie, F. (1990) Biochim. Biophys. Acta **1016**, 165–176
19 Capeillère-Blandin, C., Barber, M. J. and Bray, R. C. (1986) Biochem. J. **238**, 745–756
20 Capeillère-Blandin, C. (1991) Biochem. J. **274**, 207–217
21 Walker, M. C. and Tollin, G. (1992) Biochemistry **31**, 2798–2805
22 Labeyrie, F., Beloeil, J. C. and Thomas, M. A. (1988) Biochim. Biophys. Acta **953**, 134–141

23 Black, M. T., Gunn, F. J., Chapman, S. K. and Reid, G. A. (1989) Biochem. J. **263**,973–976
24 Rouvière-Fourmy, N., Capeillère-Blandin, C. and Lederer, F. (1994) Biochemistry **33**, 798–806
25 Tegoni, M. and Cambillau, C. (1994) Biochimie, in the press
26 Brunt, C. E., Cox, M. C., Thurgood, G. P., Moore, G. R., Reid, G. A. and Chapman, S. K. (1992) Biochem. J. **283**, 87–90

Received 9 March 1994

Metal–redox centre interactions in photosynthetic reaction centres

Michael C. W. Evans*, Matthew C. Berry, Peter J. Bratt, Olga Kaminskaya and Jonathan H. A. Nugent
Department of Biology, University College London, Gower Street, London WC1E 6BT, U.K.

Introduction

Photosynthetic reaction centres are supramolecular structures which convert light energy into electrochemical energy [1]. The general design of these structures and the mechanism of energy conversion is the same in all chlorophyll-containing photosynthetic organisms. The photochemically driven electron-transfer process depends on a highly organized electron-transfer chain containing a mixture of metal centres and organic redox centres. The latter are held in a protein matrix which provides them with very precise positions and orientations. The efficiency of the photochemical system depends on the positioning of the redox components, which controls the rate of electron transfer. The precise positioning and close relationship of the organic and metal redox centres results in magnetic interactions between the centres which can be detected by magnetic resonance techniques, providing information about the distances between the centres and a sensitive measure of changes in the local environment of the centres. These interactions can provide comparative information to allow modelling of reaction centre structures and mechanisms and also provide novel information about the mechanism of electron transfer.

The essential reaction centre structure contains a primary photochemically activated electron donor and an acceptor. The basic photochemical mechanism appears to be essentially the same in all reaction centres:

$$\text{Photochemical donor} \xrightarrow{\text{Light}} \text{first acceptor} \longrightarrow \text{secondary acceptors}$$

However, there are two types of reaction centres, in which the protein structure and the nature of the redox centres of the electron acceptor complex are very different. One type (type A) is found in purple anoxygenic photosynthetic bacteria, some green bacteria and photosystem 2 of oxygenic organisms. It is well characterized, with X-ray crystal structures available for two purple bacterial reaction centres and extensive spectroscopic characterization of reaction centres available for both oxygenic and anoxygenic organisms. Type A has two major polypeptides which bind the redox components and show significant sequence similarities among the different groups of organism. In these reaction centres the first electron acceptor is a pheophytin and the secondary acceptors are two quinone molecules coupled to a ferrous iron atom. In bacteria, the electron donors to this type of centre are cytochromes, and in photosystem 2 the water-oxidizing complex is the electron donor.

The second type of reaction centre (type B), found in green sulphur bacteria, Heliobacteria and photosystem 1 of oxygenic photosynthetic organisms, is less well characterized structurally. Crystals of cyanobacterial photosystem 1 are available, but the structure has not yet been completed, although data at 6 Å has been published [2]. Again two main polypeptides bind the initial redox components; however, these are much larger than in type A, share no sequence similarity with type A polypeptides and bind a large number of light-harvesting chlorophyll molecules as well as the redox-active components. There are a number of smaller polypeptides associated with type B reaction centres, one of which binds two iron-sulphur centres of the electron acceptor complex. In these reaction centres the first electron acceptor is a chlorophyll and the secondary acceptors include both quinone and iron-sulphur centres. While the purple bacterial reaction centre is the best characterized type A centre, with much of our knowledge of photosystem 2 coming from application of the bacterial model, photosystem 1 is the best known type B centre, with the green bacteria and Heliobacterial centres rather poorly understood because

*To whom correspondence should be addressed.

Strategic manipulation of the substrate specificity of *Saccharomyces cerevisiae* flavocytochrome b_2

Simon DAFF,* Forbes D. C. MANSON,† Graeme A. REID† and Stephen K. CHAPMAN*‡

*Edinburgh Centre for Molecular Recognition, Department of Chemistry, University of Edinburgh, West Mains Road, Edinburgh EH9 3JJ, Scotland, U.K.
and †Edinburgh Centre for Molecular Recognition, Institute of Cell and Molecular Biology, University of Edinburgh, Mayfield Road, Edinburgh EH9 3JR, Scotland, U.K.

Flavocytochrome b_2 from *Saccharomyces cerevisiae* acts physiologically as an L-lactate dehydrogenase. Although L-lactate is its primary substrate, the enzyme is also able to utilize a variety of other (*S*)-2-hydroxy acids. Structural studies and sequence comparisons with several related flavoenzymes have identified the key active-site residues required for catalysis. However, the residues Ala-198 and Leu-230, found in the X-ray-crystal structure to be in contact with the substrate methyl group, are not well conserved. We propose that the interaction between these residues and a prospective substrate molecule has a significant effect on the substrate specificity of the enzyme. In an attempt to modify the specificity in favour of larger substrates, three mutant enzymes have been produced: A198G, L230A and the double mutant A198G/L230A. As a means of quantifying the overall kinetic effect of a mutation, substrate-specificity profiles were produced from steady-state experiments with (*S*)-2-hydroxy acids of increasing chain length, through which the catalytic efficiency of each mutant enzyme with each substrate could be compared with the corresponding wild-type efficiency. The Ala-198→Gly mutation had little influence on substrate specificity and caused a general decrease in enzyme efficiency. However, the Leu-230→Ala mutation caused the selectivity for 2-hydroxyoctanoate over lactate to increase by a factor of 80.

INTRODUCTION

Saccharomyces cerevisiae flavocytochrome b_2 is a soluble L-lactate dehydrogenase found in the mitochondrial intermembrane space. It is a tetrameric protein, each subunit consisting of an amino acid chain 511 residues in length. Its X-ray-crystal structure, solved to 2.4 Å (0.24 nm) resolution [1], identifies two distinct domains within each subunit. The largest of these contains the enzyme's active site, of which FMN is an integral component. The flavin-binding domain is connected via a short hinge region to a smaller haem-binding domain which functions as an electron-transfer mediator, and as such passes electrons from the catalytically essential FMN to the physiological electron acceptor, cytochrome *c*, direct transfer being prohibited [2,3]. The substrate range of the enzyme is limited to (*S*)-2-hydroxy acids, many of which are efficiently oxidized to their 2-keto derivatives in the active site (Scheme 1) [4]. The key residues involved in catalysis have been pinpointed in the crystal structure (Figure 1), and a carbanion mechanism proposed [4,5].

The aim of this work is to investigate the origins of substrate specificity amongst 2-hydroxy acids, which lies in favour of L-lactate, and to examine the possibility of its strategic manipulation using site-directed mutagenesis.

Steady-state kinetic analysis of the wild-type enzyme with a series of substrates of increasing chain length has enabled a substrate-specificity profile to be developed, which describes how enzyme efficiency varies with substrate size. Furthermore, close examination of the active-site structure (Figure 2), coupled with sequence comparisons of *S. cerevisiae* flavocytochrome b_2 with related enzymes (Figure 3), has allowed two residues to be identified as being most likely to control this selectivity, these being Ala-198 and Leu-230. In an attempt to modify the selectivity of the enzyme in favour of larger substrates, three mutant enzymes have been constructed: Ala-198→Gly (A198G), Leu-230→Ala (L230A) and the double mutant A198G/L230A. All three mutants have been characterized by steady-state kinetics, and substrate-specificity profiles developed.

MATERIALS AND METHODS

DNA manipulation, strains and growth

Site-directed mutagenesis was performed by the Kunkel method of non-phenotypical selection [6] using the oligonucleotides 347N (CTGCTAACAGGTTTGTGTAAAC) and 346N (GATATCT-ACTGCTGCTTCATGT) for the A198G and L230A mutations respectively and the single-stranded plasmid, pGR401 [7], as template. A double mutant was also constructed using both oligonucleotides listed above. The oligonucleotides were prepared by Oswel DNA Service, University of Edinburgh, Edinburgh, Scotland, U.K. Mutants were subjected to DNA sequence analysis of the entire flavocytochrome b_2-coding region to ensure the absence of unwanted secondary mutations. The A198G, L230A and A198G/L230A mutant sequences were transferred into the expression vector pDSb2 [8] by replacing the wild-type flavocytochrome b_2-coding sequence. Standard methods for growth of *Escherichia coli*, plasmid purification, DNA manipulation and transformation were used as described previously [9].

Enzymes

Wild-type and mutant flavocytochromes b_2 expressed in *E. coli* were isolated from cells, which had been stored at −20 °C, using a previously reported purification procedure [8]. Purified enzyme samples were stored under nitrogen at 4 °C as precipitates from 70 %-satd. $(NH_4)_2SO_4$ solution.

Purified mutant enzymes were demonstrated to be 'intact' rather than 'cleaved' by SDS/PAGE [10], and to be in possession of a full complement of flavin. This was shown by directly measuring the amounts of dissociated flavin and protein-bound

Abbreviations used: KIE, kinetic isotope effect; Caps, 3-cyclohexylamino-1-propanesulphonic acid.
‡ To whom correspondence should be addressed.

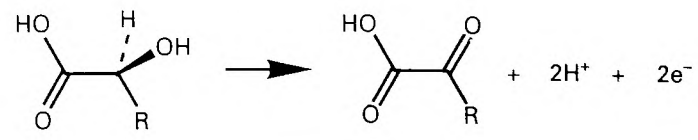

Scheme 1 (*S*)-2-Hydroxy acid dehydrogenation

R is the only variable in the catalytic dehydrogenation reaction performed by flavocytochrome b_2. For the physiological substrate L-lactate, R is $-CH_3$.

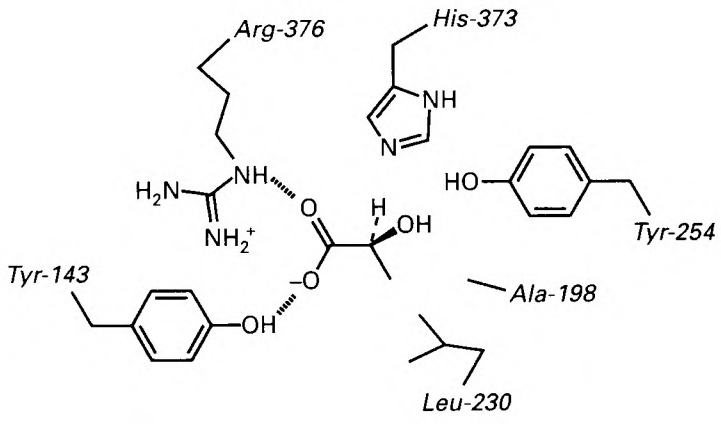

Figure 1 Schematic diagram of the flavocytochrome b_2 active site

The diagram is based on the X-ray-crystal structure of the enzyme, which identifies active-site residues. A substrate molecule (L-lactate) is shown in its appropriate binding orientation. FMN, although not shown in this diagram, lies in a parallel plane directly beneath the His-373 residue and substrate molecule.

haem separated on a Sephadex G-25 gel-filtration column (1.5 cm × 15 cm; Sigma), equilibrated and eluted with Caps (3-cyclohexylamino-1-propanesulphonic acid) buffer (Sigma), pH 11, *I* 0.10 mol/l at 4 °C in darkness, using their known visible absorption maxima [11,12]. The Caps buffer consisted of 0.01 M NaOH titrated against Caps solution to pH 11 and adjusted to *I* 0.10 mol/l using NaCl.

Kinetic analysis

All steady-state kinetic measurements were performed at 25.0 ± 0.1 °C in Tris/HCl buffer, pH 7.5, *I* 0.10 mol/l. The buffer

```
                    198                                   230
                     ↓                                     ↓
Scb2 PFYVSATALC KLGNPLEGEK DVARGCGQGV TKVPQMISTL ASCSPEEIIE
Hab2 PFYISATALA KLGHP.EGEV AIAKGAGRE. .DVVQMISTL ASCSFDEIAD
Gox  PIMIAPTAMQ KMAHP.EGEY ATARAASAA. .GTIMTLSSW ATSSVEEVAS
Hao  PICISPTAFH SIAWP.DGEK STARAAQEA. .NICYVISSY ASYSLEDIVA
Mdh  PLLIGPTGLN GALWP.KGDL ALARAATKA. .GIPFVLSTA SNMSIEDLAR
Lox  PMFFAPIGVI ALC.AQDGHG DAASAQASAR TGVPYITSTL AVSSLEDIRK
LctD PVALAPVGLC GMYAR.RGEV QAAKAADAH. .GIPFTLSTV SVCPIEEVA.
```

Figure 3 Sequence comparison of flavocytochromes b_2 and other 2-hydroxy acid dehydrogenases

The sequence of *S. cerevisiae* flavocytochrome b_2 (Scb2) is shown between residues 191 and 240, and is aligned with the corresponding sequences from *Hansenula anomala* flavocytochrome b_2 (Hab2), spinach glycollate oxidase (Gox), rat hydroxy acid oxidase (Hao), *Pseudomonas putida* mandelate dehydrogenase (Mdh), *Myobacterium smegmatis* lactate oxidase (Lox) and L-lactate dehydrogenase from *E. coli* (LctD). The positions of Ala-198 and Leu-230 are indicated.

consisted of 0.01 M HCl titrated against Tris solution to pH 7.5, and adjusted to *I* 0.10 mol/l by addition of NaCl.

Rates of reduction of 1 mM ferricyanide (potassium salt; BDH Chemicals) by enzyme/substrate combinations were measured on a Beckman DU52 spectrophotometer as previously described [13].

Substrate solutions were prepared in Tris/HCl buffer, and titrated with 0.25 M NaOH to pH 7.5 before use; they contained glycollic acid (Aldrich), L-lactate (lithium salt; Sigma) and the following enantiomerically pure long-chain 2-hydroxy acids (produced by Oxford Asymmetry Ltd.), which correspond to the same stereochemistry as L-lactate: (*S*)-2-hydroxybutyric acid {$[\alpha]_D^{25}$ 12.7° (*c* 1.1 in chloroform)}; (*S*)-2-hydroxyvaleric acid {$[\alpha]_D^{25} - 1.9°$ (*c* 1.0 in ethanol)}; (*S*)-2-hydroxyhexanoic acid ($[\alpha]_D^{25} - 1.9°$ (*c* 1.0 in ethanol)}; (*S*)-2-hydroxyoctanoic acid {$[\alpha]_D^{25}$ 1.0° (*c*. 1.0 in ethanol)}.

Kinetic isotope effects (KIEs) were measured as previously reported [13], using L-[2-^{2}H]lactate prepared as described in [14].

RESULTS

Steady-state kinetic parameters

Table 1 presents the data collected from steady-state kinetic analyses of wild-type and mutant flavocytochromes b_2, with

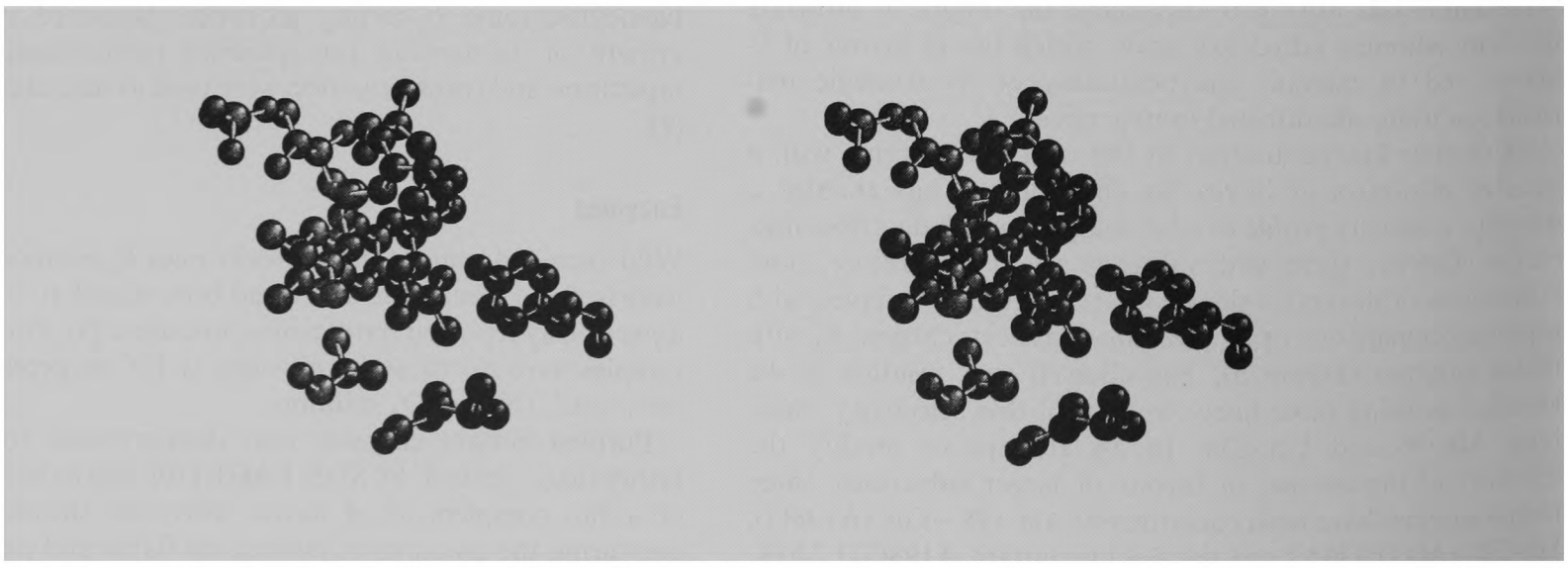

Figure 2 A parallel-vision stereoscopic view of the flavocytochrome b_2 active site

Pyruvate is shown in the centre of the diagram with residues Leu-230 and Ala-198 bottom right and bottom left respectively. Arg-376 lies to the left of pyruvate, and His-373 at the top. FMN is shown in a parallel plane directly behind the substrate.

Table 1 Steady-state parameters for wild-type and mutant flavocytochromes b_2 with substrates of different chain length

All experiments were carried out at 25.0 ± 0.1 °C in Tris/HCl buffer, pH 7.5 (/ 0.10). Values for $k_{cat.}$ represent the rates of reduction, at saturating substrate concentration, of 1 mM ferricyanide in electrons transferred /s per molecule of enzyme. As each substrate is a 2-electron donor, $k_{cat.}$ values should be halved to give rates in terms of substrate molecules consumed. K_m values are expressed in terms of mM substrate concentration. All substrates used are the simple straight-chained 2-hydroxy acids with two to eight carbon atoms. Errors quoted represent standard deviations from a non-linear least-squares fit.

Substrate	Chain length	Wild-type		A198G		L230A		A198G/L230A	
		$k_{cat.}$ (s^{-1})	K_m (mM)	$k_{cat.}$ (s^{-1})	K_m (mM)	$k_{cat.}$ (s^{-1})	K_m (mM)	$k_{cat.}$ (s^{-1})	K_m (mM)
Glycollate	2	7 ± 1*	0.34 ± 0.05*	3 ± 1	2 ± 1	3 ± 1	3 ± 1	–	–
L-Lactate	3	400 ± 10†	0.49 ± 0.05†	185 ± 5	4.1 ± 0.4	30 ± 3	6.1 ± 0.2	41 ± 2	38 ± 4
(*S*)-2-Hydroxybutyrate	4	82 ± 7	0.59 ± 0.04	34 ± 1	2.4 ± 0.3	18 ± 2	0.83 ± 0.05	13 ± 2	3.6 ± 0.5
(*S*)-2-Hydroxyvalerate	5	13 ± 1	0.22 ± 0.02	4.0 ± 0.2	0.85 ± 0.08	19 ± 2	0.24 ± 0.02	21 ± 3	2.1 ± 0.2
(*S*)-2-Hydroxyhexanoate	6	19 ± 1	0.11 ± 0.01	5.3 ± 0.5	0.46 ± 0.05	16 ± 2	0.16 ± 0.01	25 ± 1	1.5 ± 0.1
(*S*)-2-Hydroxyoctanoate	8	45 ± 5	0.11 ± 0.01	14 ± 1	0.60 ± 0.03	52 ± 5	0.23 ± 0.01	68 ± 3	1.9 ± 0.1

* Taken from [16].
† Taken from [13].

Table 2 [^{2}H]Lactate KIEs

All experiments were carried out at 25.0 ± 0.1 °C in Tris/HCl buffer, pH 7.5 (/ 0.10). Ferricyanide was used as the electron acceptor, at a concentration of 1 mM. Values of $k_{cat.}$ and K_m are expressed as in Table 1.

Substrate	Wild-type*		A198G		L230A	
	$k_{cat.}$ (s^{-1})	K_m (mM)	$k_{cat.}$ (s^{-1})	K_m (mM)	$k_{cat.}$ (s^{-1})	K_m (mM)
L-[2-^{1}H]Lactate	400 ± 10	0.49 ± 0.05	185 ± 5	4.1 ± 0.4	30 ± 3	6.1 ± 0.2
L-[2-^{2}H]Lactate	86 ± 1	0.76 ± 0.06	51 ± 10	6.3 ± 1.0	5.1 ± 0.5	5.2 ± 0.3
KIE	4.7 ± 0.4		3.6 ± 1.0		5.9 ± 1.3	

* Taken from [13].

substrates of increasing chain length. All substrates used were enantiomerically pure *S*-isomers, to avoid complications caused by *R*-isomer inhibition, as observed for D-lactate [15].

The first point to note is that for a given enzyme, K_m values are lower with long-chain 2-hydroxy acids than with short. As it has been demonstrated that the reaction closely follows Michaelis–Menten kinetics (although substrate inhibition is observed at high concentration) [17], in which K_m is equated to $1/K_d$, K_m values can be used as an indication of the enzyme's relative substrate-binding affinity. Hence the apparent relationship between long chains and stronger binding can be rationalized in terms of the increase in size of the hydrophobic 'tail' on the substrate molecules. Such large non-polar substituents, repelled by solvent molecules, would clearly bind more effectively within the protein interior. Despite this trend, a K_m of 0.49 mM is obtained for wild-type flavocytochrome b_2 with L-lactate, which is slightly lower than that obtained with the longer (*S*)-2-hydroxybutyrate. Furthermore the $k_{cat.}$ of 400 s^{-1} is significantly higher than with all other substrates. On this evidence L-lactate is the optimum substrate for the enzyme.

For the A198G mutant enzyme the highest $k_{cat.}$ is also observed with L-lactate, although it is less than half the value observed with wild-type. Similarly $k_{cat.}$ values obtained with the other substrates are two or three times lower than the corresponding wild-type values. In addition to this universal decrease in $k_{cat.}$, there is an increase in K_m across the substrate range; however, the increase for L-lactate is slightly out of proportion, resulting in this being the weakest binding of all the substrates. Since the changes in $k_{cat.}$ and K_m which arise from the A198G mutation are of a universal nature, the overall effect on substrate specificity is modest.

The K_m values obtained for the L230A enzyme with long-chain 2-hydroxy acids are similar to the corresponding wild-type values, whereas those for short-chain substrates (glycollate and L-lactate) are 10-fold higher. Therefore, compared with wild-type, this represents a large decrease in the binding affinity of the L230A enzyme for the smaller substrates. In addition to this, the $k_{cat.}$ values obtained for L230A with small substrates [glycollate, L-lactate and (*S*)-2-hydroxybutyrate] are much lower than for the wild-type enzyme, $k_{cat.}$ for L-lactate showing a decrease of more than 10-fold as a consequence of the L230A mutation. As $k_{cat.}$ for L-lactate with the L230A mutant is now lower than for (*S*)-2-hydroxyoctanoate, and its K_m considerably higher, L-lactate can no longer be considered the primary substrate for this mutant. Other more subtle kinetic changes caused by the L230A mutation include an increase in $k_{cat.}$ for (*S*)-2-hydroxyvalerate, and increases in K_m values for both (*S*)-2-hydroxyhexanoate and (*S*)-2-hydroxyoctanoate. The double mutation A198G/L230A causes the collective swings in kinetic performance demonstrated by the single mutants. As such, $k_{cat.}$ values obtained for this enzyme are very similar to the values observed with the L230A mutant, throughout the substrate range. However, the K_m values, which show a universal increase, are more reminiscent of values recorded for the A198G enzyme, showing further disruption of substrate binding. The loss of all significant activity in the case of glycollate is presumably an extension of this phenomenon.

KIEs

Abstraction of the α-H from L-lactate is known to be the major rate-limiting step in the dehydrogenation pathway of flavocytochrome b_2. This is demonstrated by the large KIE of 4.7 [13] observed during steady-state reduction of ferricyanide with L-[2-^{2}H]lactate as substrate. Table 2 presents similar parameters obtained for the A198G and L230A mutant enzymes. As the KIEs remain large for the mutants, it is most likely that the rate-determining step and transition state are identical in both mutant and wild-type enzymes.

DISCUSSION

Flavocytochrome b_2 from *S. cerevisiae* is physiologically an L-lactate dehydrogenase, but it is also able to utilize other 2-hydroxy acids as substrates. The high-resolution crystal structure of the enzyme reveals a product molecule, pyruvate, bound in the active site by Arg-376 and Tyr-143 at the carboxylate end and His-373 and Tyr-254 at the carbonyl. These residues are believed to be responsible for the group-specific nature of the enzyme. However, it is clear that they cannot be responsible for the ability of the enzyme to distinguish between L-lactate and other 2-hydroxy acids, i.e. its substrate specificity. The selectivity of wild-type flavocytochrome b_2 for L-lactate over 2-hydroxy acids of different chain length is illustrated by the substrate-specificity profiles in Figures 4(a) and 4(b), which show a conspicuously large peak in enzyme efficiency for chain length 3. The reason for this discrimination must arise from the extra stability gained by the Michaelis complex and transition state of the enzyme from interactions between the L-lactate/pyruvate methyl group and strategically positioned amino acid side chains. The underlying trend in the substrate-specificity profile is a general increase in enzyme efficiency with increasing chain length, which can be attributed to the greater binding affinity of longer, more hydrophobic substrates for the active site, as mentioned above. Despite this trend, L-lactate is a more efficient substrate than (*S*)-2-hydroxyoctanoate by a factor of 2.

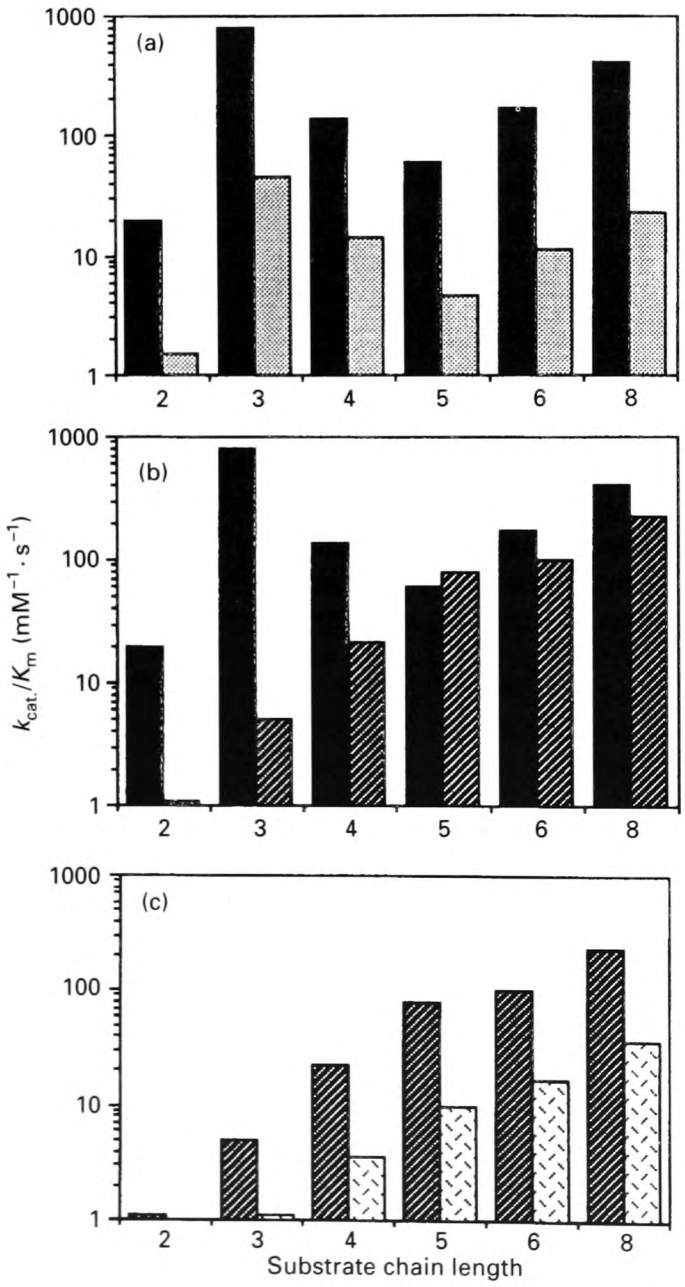

Figure 4 Substrate-specificity profiles of wild-type and mutant enzymes

(**a**) Comparison of wild-type (■) with A198G (▨); (**b**) comparison of wild-type (■) with L230A (▨); (**c**) comparison of L230A (▨) with A198G/L230A (▨). Values for $k_{cat.}/K_m$ are taken from Table 3 and are presented in mM$^{-1}\cdot$s^{-1} on a log scale. Substrate chain lengths (2–8) correspond to the (*S*)-2-hydroxy acids in Table 1.

The flavin-binding domain of flavocytochrome b_2 is closely related to several other 2-hydroxy acid dehydrogenases with different substrate specificities. These include the glycollate oxidase from spinach [18], lactate oxidase from *Mycobacterium smegmatis* [19], lactate dehydrogenase from *E. coli* [20], mandelate dehydrogenase from *Pseudomonas putida* [21] and long-chain hydroxy acid dehydrogenase from rat kidney [22]. The catalytically important residues are well conserved throughout this family but we have sought to determine the structural basis for substrate selectivity. The crystal structure of *S. cerevisiae* flavocytochrome b_2 indicates that the side chains of Ala-198 and Leu-230 interact closely with the methyl group of pyruvate, the product of lactate oxidation, which is found at the active site of the enzyme. The amino acid sequences of flavocytochrome b_2 and its relatives are compared for this region of the polypeptide chain in Figure 3. Ala-198 is replaced by glycine in some members of the family, whereas the position of Leu-230 is occupied by the larger tryptophan side chain in glycollate oxidase and by the smaller alanine in mandelate dehydrogenase. It thus appears plausible that these residues play some role in substrate selection. In an attempt to demonstrate the importance of these residues in controlling the substrate specificity in this series of enzymes, three mutant flavocytochromes b_2 were constructed: A198G, L230A and the double mutant A198G/L230A. As such, in each mutant enzyme, bulk had been removed from the appropriate region of the active site, and we expected that this would swing the substrate specificity of the enzyme away from L-lactate and towards bulkier 2-hydroxy acids. A similar study by Wilks et al. [23] involved the NAD$^+$-dependent L-lactate dehydrogenase from *Bacillus stearothermophilus*. The enzyme was modified to become a broad-specificity 2-hydroxy acid dehydrogenase by the removal of a large amount of steric bulk from the active site. Although the mechanism and direction of the enzyme-catalysed reaction are different in this case, the general principle is the same.

As a means of quantifying the effect of each mutation on substrate specificity, steady-state analyses were carried out on the wild-type and mutant enzymes for a range of 2-hydroxy acids of increasing chain length. The results have been used to build up substrate-specificity profiles for each enzyme, as represented in Figure 4, and in Table 3.

By comparing the relative rates of reaction of L-[2-^{1}H]- and L-[2-^{2}H]-lactate with the A198G and L230A enzymes, KIEs were calculated. The large primary effects observed served to confirm that α-H abstraction is the rate-determining step in both cases. As the same result has been reported for the wild-type enzyme,

Table 3 Second-order rate constants for wild-type and mutant flavocytochromes b_2 with substrates of different chain length

All values are calculated from the data presented in Table 1.

Substrate	Chain length	Wild-type $k_{cat.}/K_m$ ($mM^{-1} \cdot s^{-1}$)	A198G $k_{cat.}/K_m$ ($mM^{-1} \cdot s^{-1}$)	L230A $k_{cat.}/K_m$ ($mM^{-1} \cdot s^{-1}$)	A198G/L230A $k_{cat.}/K_m$ ($mM^{-1} \cdot s^{-1}$)
Glycollate	2	20 ± 3*	1.5 ± 0.9	1 ± 0.5	–
L-Lactate	3	810 ± 90†	45 ± 5	4.9 ± 0.5	1.1 ± 0.1
(*S*)-2-Hydroxybutyrate	4	140 ± 15	14 ± 2	22 ± 3	3.6 ± 0.2
(*S*)-2-Hydroxyvalerate	5	59 ± 7	4.7 ± 0.5	79 ± 10	10 ± 2
(*S*)-2-Hydroxyhexanoate	6	173 ± 18	11.5 ± 1.5	100 ± 14	17 ± 1
(*S*)-2-Hydroxyoctanoate	8	410 ± 60	23 ± 2	226 ± 24	36 ± 3

* Taken from [16].
† Taken from [13].

it is safe to assume that the mechanism followed and transition state passed through are consistent in all three enzymes. This allows the kinetic data to be compared and interpreted with respect to the same fundamental model.

For example, the A198G mutation causes increases in K_m for all the substrates, indicating that substrate binding has been weakened, and the Michaelis complex destabilized. Decreases in $k_{cat.}$ throughout the substrate range suggest that the transition state is also destabilized, the effect being unspecific in both cases. A possible explanation for this is that Ala-198 interacts with the β-CH_2 (possessed by all substrates except glycollate), in an unspecific way, its removal causing universal disruption. This would be the case if Ala-198 could interact without causing a steric obstruction to the long-chain substrates. Figure 4(a) shows the substrate-specificity profile of A198G in comparison with the wild-type profile, enzyme efficiency ($k_{cat.}/K_m$) being plotted against substrate chain length. It is clear that wild-type flavocytochrome b_2 is a far more efficient 2-hydroxy acid dehydrogenase than A198G, by an order of magnitude, but that the substrate specificity is largely unaffected by the mutation. Although Ala-198 clearly influences catalysis, it is not responsible for the selection of L-lactate over the other substances studied.

L230A on the other hand has a substrate-specificity profile which differs dramatically from the wild-type profile, as illustrated in Figure 4(b). The catalytic efficiency ($k_{cat.}/K_m$) of the mutant enzyme increases progressively with substrate chain length, whereas the wild-type profile includes a large peak in the L-lactate position (chain length 3). Significantly, this peak has been all but completely eradicated in the L230A profile. It is clear therefore that Leu-230 is critically involved in the substrate chain-length selection process, influencing both $k_{cat.}$ and K_m for the dehydrogenation reaction such as to optimize the enzyme's efficiency with L-lactate. Replacement of this residue by alanine removes the favourable interaction between the hydrocarbon chain of Leu-230 and the methyl group of L-lactate, with the possible consequence of forcing water molecules to occupy this hydrophobic pocket. However, the longer 2-hydroxy acids have hydrocarbon chains that would be able to contact the mutated Ala-230 residue, causing an interaction similar to the alkyl–alkyl interaction believed to occur with Leu-230. The observation that (*S*)-2-hydroxyvalerate (chain length 5) has an improved catalytic efficiency with the mutant suggests that this substrate is of the appropriate length to occupy the pocket, thus avoiding the possibility of steric crowding.

The result of the L230A mutation is therefore an enzyme that is best described as a long-chain 2-hydroxy acid dehydrogenase,

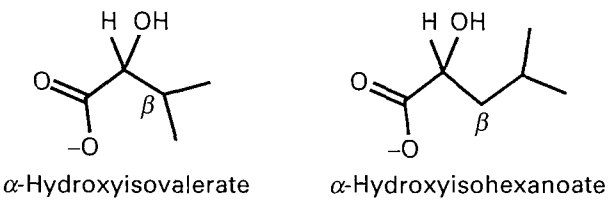

α-Hydroxyisovalerate α-Hydroxyisohexanoate

Figure 5 Branching at the β position of the substrate chain impedes the catalytic dehydrogenation reaction

rather than an L-lactate dehydrogenase. Such is the degree of L-lactate deselection by the mutant that it is now 40 times more efficient with (*S*)-2-hydroxyoctanoate than with L-lactate. In comparison, wild-type flavocytochrome b_2 is twice as efficient with L-lactate as with (*S*)-2-hydroxyoctanoate. Therefore the L230A mutation has caused an 80-fold swing in selectivity.

Progression to the double mutation A198G/L230A causes even larger increases in the K_m values, signifying a large disruption to the substrate-binding properties of the enzyme. However, the $k_{cat.}$ values are similar to those recorded with the L230A mutant enzyme, rather than those obtained with the A198G mutant, which are somewhat lower. This suggests that the L230A mutation in some way compensates for the A198G mutation with respect to $k_{cat.}$. The substrate-specificity profile of the A198G/L230A mutant (Figure 4c) therefore resembles the L230A profile in shape, but poor substrate-binding properties cause the enzyme to be far less efficient in every case.

An additional observation was that none of the mutants studied showed any activity with (*S*)-2-hydroxyisovalerate (Figure 5), whereas the activity with *S*-2-hydroxyisohexanoate was similar to that observed with (*S*)-2-hydroxyhexanoate. It appears therefore that, whereas branching at C-4 causes no ill effect, branching at C-3 invokes steric interference, presumably from a different active-site residue, which exerts its own influence on substrate specificity. One possibility is Tyr-254, the aromatic ring of which is seen to be within contact distance of the pyruvate methyl group in the crystal structure. Mutation of this residue will be the subject of further investigation.

In conclusion, the substrate-specificity studies that we have carried out on wild-type flavocytochrome b_2 and the A198G, L230A and A198G/L230A mutant enzymes have shown that Leu-230 is a key residue responsible for selecting L-lactate as the primary substrate for the enzyme in preference to other 2-hydroxy acids. Further, in generating the L230A mutant we have

demonstrated the possibilities for successfully redesigning the enzyme to select other 2-hydroxy acids in preference to the natural substrate. This mutant enzyme is more efficient at utilizing long-chain 2-hydroxy acids, such as (*S*)-2-hydroxyoctanoate, by a factor of 40.

This work was supported by the Science and Engineering Research Council (SERC) via project grants and postgraduate support to S.D.

REFERENCES

1 Xia, Z.-X. and Mathews, F. S. (1990) J. Mol. Biol. **212**, 837–863
2 Ogura, Y. and Nakamura, T. (1966) J. Biochem. (Tokyo) **60**, 77–86
3 Capeillère-Blandin, C., Iwatsubo, M., Testylier, G. and Labeyrie, F. (1980) in Flavins and Flavoproteins (Yagi, K. and Yamamoto, T., ed.), pp. 617–630, Japan Scientific Societies Press, Tokyo
4 Chapman, S. K., White, S. A. and Reid, G. A. (1991) Adv. Inorg. Chem. **36**, 257–301
5 Lederer, F. (1991) in Chemistry and Biochemistry of Flavoenzymes (Müller, F., ed.), vol. 2, chapter 7, CRC Press, Boca Raton, FL
6 Kunkel, T. A. (1985) Proc. Natl. Acad. Sci. U.S.A. **82**, 488–492
7 Reid, G. A., White, S. A., Black, M. T., Lederer, F., Mathews, F. S. and Chapman, S. K. (1988) Eur. J. Biochem. **178**, 329–333
8 Black, M. T., White, S. A., Reid, G. A. and Chapman, S. K. (1989) Biochem. J. **258**, 255–259
9 Sambrook, J., Fritsch, E. F. and Maniatis, T. (1989) Molecular Cloning: A Laboratory Manual, 2nd edn., Cold Spring Harbor Laboratory Press, Cold Spring Harbor, NY
10 Lederer, F. and Simon, A.-M. (1971) Eur. J. Biochem. **20**, 469–474
11 Pajot, P. and Groudinsky, O. (1970) Eur. J. Biochem. **12**, 158–164
12 Dawson, R. M. C., Elliott, D. C., Elliott, W. H. and Jones, K. M. (1987) Data for Biochemical Research, 3rd edn., pp. 126–127, Oxford University Press, Oxford
13 Miles, C. S., Rouviére-Fourmy, N., Lederer, F., Mathews, F. S., Reid, G. A. and Chapman, S. K. (1992) Biochem. J. **285**, 187–192
14 Pompon, D., Iwatsubo, M. and Lederer, F. (1980) Eur. J. Biochem. **104**, 479–488
15 Hinkson, J. W. and Mahler, H. R. (1963) Biochemistry **2**, 216–220
16 Miles, C. S. (1991) PhD Thesis, University of Edinburgh
17 Hasegawa, H. (1962) J. Biochem. (Tokyo) **52**, 12–15
18 Volokita, M. and Somerville, C. R. (1987) J. Biol. Chem. **262**, 15825–15828
19 Giegel, D. A., Williams, C. H. Jr. and Massey, V. (1990) J. Biol. Chem. **265**, 6626–6632
20 Dong, J. M., Taylor, J. S., Latour, D. J., Iuchi, S. and Lin, E. C. C. (1993) J. Bacteriol. **175**, 6671–6678
21 Tsou, A. Y., Ransom, S. C. and Gerlt, J. A. (1990) Biochemistry **29**, 9856–9862
22 Le, K. H. D. and Lederer, F. (1991) J. Biol. Chem. **266**, 20877–20881
23 Wilks, H. M., Halsall, D. J., Atkinson, T., Chia, W. N., Clarke, A. R. and Holbrook, J. J. (1990) Biochemistry **29**, 8587–8591

Received 20 December 1993/1 March 1994; accepted 15 March 1994

Flavocytochrome b_2: an ideal model system for studying protein-mediated electron transfer

S. K. Chapman‡, G. A. Reid†, C. Bell*, D. Short* and S. Daff*

*Department of Chemistry, University of Edinburgh, West Mains Road, Edinburgh EH9 3JJ, Scotland, UK, and †Institute of Cell and Molecular Biology, University of Edinburgh, Mayfield Road, Edinburgh EH9 3JR, Scotland, UK

Introduction

Most of the recent intense scientific effort towards providing an understanding of electron transfer in proteins has focused on intraprotein electron transfer and on the pathway between the donor (D) and acceptor (A) redox centres. These centres are usually fixed within the protein matrix as in the case of the photosynthetic reaction centre [1], or involve attaching an artificial redox centre onto the surface of a protein at a fixed distance from the natural centre, e.g. in 'ruthenated' proteins [2]. Such studies usually reduce to an analysis of whether the electron travels from D to A directly through space (i.e. treating the intervening protein medium as homogeneous like an 'organic glass'), or whether it travels through a distinct σ-tunnelling pathway involving specific covalent bonds, hydrogen bonds, etc. (i.e., treating the protein medium as heterogeneous). As well as the distance between D and A, the rate of electron transfer is also influenced by the driving force of the reaction, ΔG°, and the reorganization energy, λ [1].

In addition to intraprotein electron transfer, in which the redox centres are fixed within one protein, there is also intense interest in bimolecular reactions between proteins which result in interprotein electron transfer. Here, one must consider the dynamics of the interactions between the two proteins involved. Do the two proteins form one defined complex with a specific electron transfer path between redox centres? Are there a number of possible sites on the proteins where binding followed by electron transfer can occur? An interesting example is the complex between cytochrome *c* and cytochrome *c* peroxidase for which there is now a crystal structure [3]. Based on this structure a σ-tunnelling pathway linking the two haem groups has been proposed [3]. However an NMR study of the dynamics of the cytochrome *c*–cytochrome *c* peroxidase interaction indicates that the complex in solution is highly mobile and probably does not have a discrete architecture with one specific electron transfer pathway [4].

‡To whom correspondence should be addressed.

It is apparent then that to probe fully protein-mediated redox processes a model system is needed that can allow both the study of intraprotein electron transfer, between redox centres within the same protein, and interprotein electron transfer between centres in separate protein partners. Flavocytochrome b_2 is arguably the ideal model system for such studies for the following reasons: (i) it is soluble and easily obtained; (ii) the enzyme has been expressed at a high level in *Escherichia coli* [5] and a number of mutant enzymes have been generated [6–8]; (iii) crystal structures of the native and recombinant enzymes are available [9,10]; (iv) the crystal structure of the natural redox partner cytochrome *c* is also available [11]; (v) the structure of a hypothetical complex between flavocytochrome b_2 and cytochrome *c* has been proposed [12]; (vi) the redox potentials of all the prosthetic groups have been determined and there is a wealth of data on the mechanism of action of the enzyme [13,14].

Background to the flavocytochrome b_2 system

Flavocytochrome b_2 (L-lactate:cytochrome *c* oxidoreductase) from *Saccharomyces cerevisiae* is a homotetramer with subunit M_r of 57 500. It is a soluble component of the mitochondrial intermembrane space, where it catalyses the transfer of electrons from L-lactate to cytochrome *c* [13]. We have cloned the DNA encoding the enzyme and expressed it at a high level in *E. coli*. (Note that the kinetic properties of flavocytochrome b_2 from yeast and the recombinant enzyme from *E. coli* are identical [5]). This has given us the ability to produce large amounts of fully active wild-type and mutant enzyme, which has facilitated our studies on the mechanism of action of the enzyme [6–8]. The X-ray crystal structures have been determined for the native enzyme from *S. cerevisiae* [9], and for the recombinant enzyme from *E. coli* [10]. These are isostructural and clearly show that each subunit is composed of two distinct domains as illustrated in Figure 1. One of these contains haem (the cytochrome domain) and the other flavin mononucleotide

(the flavin domain) [9]. The edge-to-edge distance between the flavin and haem groups is about 9.7 Å. The two domains are connected by a single segment of polypeptide chain, which constitutes an interdomain 'hinge'. This raises the question of whether or not mobility permitted by the hinge influences the interdomain electron transfer rate.

Although there is no X-ray structure available for the flavocytochrome b_2-cytochrome c complex there is now a hypothetical model for how these two proteins interact [12]. This model predicts that the b_2 and c haem groups are coplanar with an edge-to-edge distance of around 14 Å and with a possible σ-tunnelling electron-transfer pathway linking the two haems, involving residues 50–52 of flavocytochrome b_2 (Figure 2). The model also predicts a number of key electrostatic interactions between the two proteins, the most promiment of which is a salt bridge between Glu-91 of flavocytochrome b_2 and Arg-13 of cytochrome c [12].

We address in this paper two specific aspects of electron transfer in flavocytochrome b_2: (i) how can we probe the effect of domain mobility on interdomain electron transfer and (ii) is the published hypothetical complex between flavocytochrome b_2 and cytochrome c correct?

How can we probe the effect of interdomain mobility on electron transfer in flavocytochrome b_2?

In many cases, redox centres in proteins are rigidly locked in the protein matrix, an obvious example being the photosynthetic reaction centre [1]. In such cases it is relatively easy to measure the distance between donor and acceptor redox centres, since this distance will have a definite fixed value. However, what happens if the redox centres within a protein are not at a fixed distance, i.e. there is intraprotein fluxionality? A classic example would be where two domains in a protein (one containing D and the other A) are mobile with respect to each other. Is the rate of electron transfer in such a case regulated by the frequency of motion between the two domains?

Flavocytochrome b_2 is an ideal system to address this question since the cytochrome and flavin domains of the enzyme are connected by an interdomain 'hinge' (arrowed in Figure 1) that allows mobility of the domains with respect to each other. The occurrence of Interdomain mobility in flavocytochrome b_2 is supported by crystallographic [9] and NMR evidence [15] as follows. (1) Crystallographic evidence. The crystal structure of flavocytochrome b_2 shows two crystallographically distinguishable subunits in the asymmetric unit [9]. In subunit 1 the electron density map shows the presence of both

Figure 1

A single subunit of wild-type flavocytochrome b_2. The α-helices are shown as ribbons, β-sheets as arrows and the remaining α-carbon backbone as wire

The prosthetic groups are shown as ball and stick representations. The interdomain hinge is arrowed.

Figure 2

The proposed ρ-tunnelling pathway for electron transfer from the flavocytochrome b_2 haem to the cytochrome c haem, based on the hypothetical complex proposed by Tegoni et al. [12]

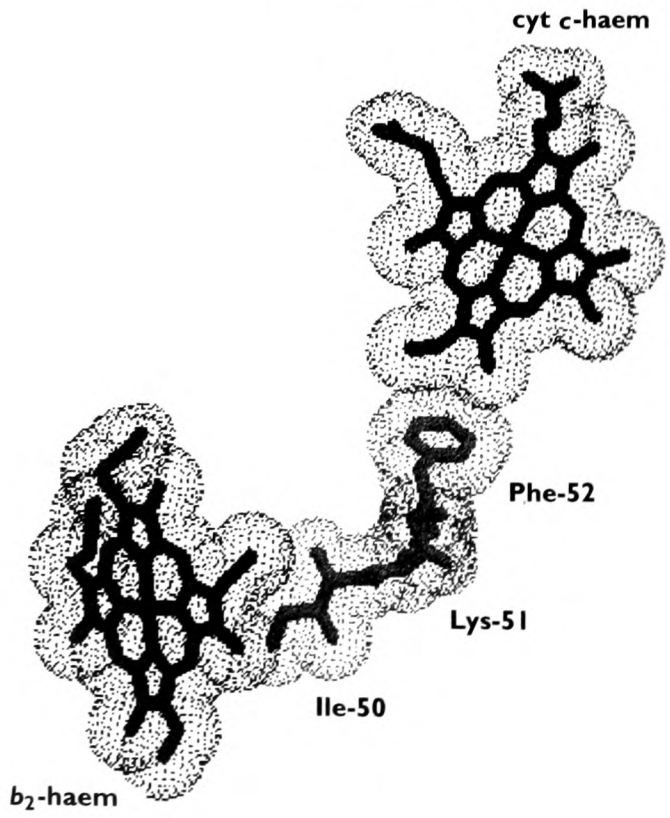

cytochrome and flavin domains. However in subunit 2, no electron density for the cytochrome domain is resolved owing to positional disorder (Gly-100 is the first visible residue), indicating that the haem domain can move with respect to the flavin domain. (2) NMR evidence. The linewidths of haem proton resonances in the intact enzyme are far sharper than would be expected if the cytochrome domain had no free motion relative to the flavin domain [15]. This implies that the hinge region allows the cytochrome domain a considerable degree of mobility. From a number of studies on site-directed mutant forms of flavocytochrome b_2 with alterations in the hinge [7,8] and interface residues [6], it has now become clear that the rate of electron transfer from the fully reduced flavin to the haem is governed by the mobility of the two domains and the frequency of productive encounters between them.

To analyse further the effect of interdomain mobility on the rate of intramolecular electron transfer in flavocytochrome b_2 a methodology is needed that can be used to prevent interdomain mobility reversibly. For this reason we decided to introduce a disulphide bridge between the two domains to act as a 'reversible lock' on mobility. The power of this methodology has already been beautifully demonstrated in the case of some non-redox proteins. For example in the case of the sulphate-binding protein (SBP) from *E. coli* [16], two cysteines have been introduced into the protein to form a disulphide bond across the ligand binding site cleft that lies between two domains. This disulphide bond dramatically reduces domain flexibility in the protein [16]. Similarly, to regulate catalytic activity, a disulphide bond has been introduced across the active site cleft of T4 lysozyme. This disulphide link lowers mobility and completely removes catalytic activity [17]. Reductive cleavage of the disulphide link restores the enzyme to full activity, thus demonstrating the possibility of using an artificial disulphide bridge as a reversible lock.

In the case of flavocytochrome b_2, a suitable location needed to be identified to introduce cysteine residues that might form a disulphide bridge linking the domains and restricting mobility. Analysis of the three-dimensional structure of the enzyme using molecular graphics allowed us to identify possible locations at the interface of the two domains where suitable disulphide linkages might be introduced. One such analysis indicated that a cysteine introduced at residue 67 (normally an alanine) in the cytochrome domain could form a disulphide bridge with an existing cysteine in the flavin domain at position 233. Using site-directed mutagenesis we have generated the Ala-67→Cys (A67C-b_2) mutant enzyme. Our preliminary studies on A67C-b_2 indicate that a disulphide bridge does indeed form in oxidizing conditions and that this bridge can be broken using reductants such as dithiothreitol. For example, Ellman assays on A67C-b_2 isolated from *E. coli* under oxidizing conditions revealed one fewer free cysteine than for wild-type enzyme, whereas Ellman assays on A67C-b_2 in the presence of reductants gave one more free cysteine. These results are exactly as would be expected if we had a reversible disulphide link as indicated schematically in Figure 3. We shall refer to the mutant enzyme with the disulphide bridge in place as the 'locked' form and in the absence of the bridge as the 'open' form.

Our preliminary kinetic studies on A67C-b_2 have produced some interesting results. Firstly, it is clear that in the presence of dithiothreitol, i.e. in the open form, the mutant enzyme has

Figure 3

Schematic representation of a flavocytochrome b_2 subunit showing the haem- and flavin-containing domains

The cysteine at position 67 was introduced by site-directed mutagenesis, whereas C233 is a naturally occurring cysteine residue. When there is no disulphide bridge, i.e. the open form, the haem domain is mobile with respect to the flavin domain. In the presence of a disulphide bridge, the locked form, domain mobility is restricted.

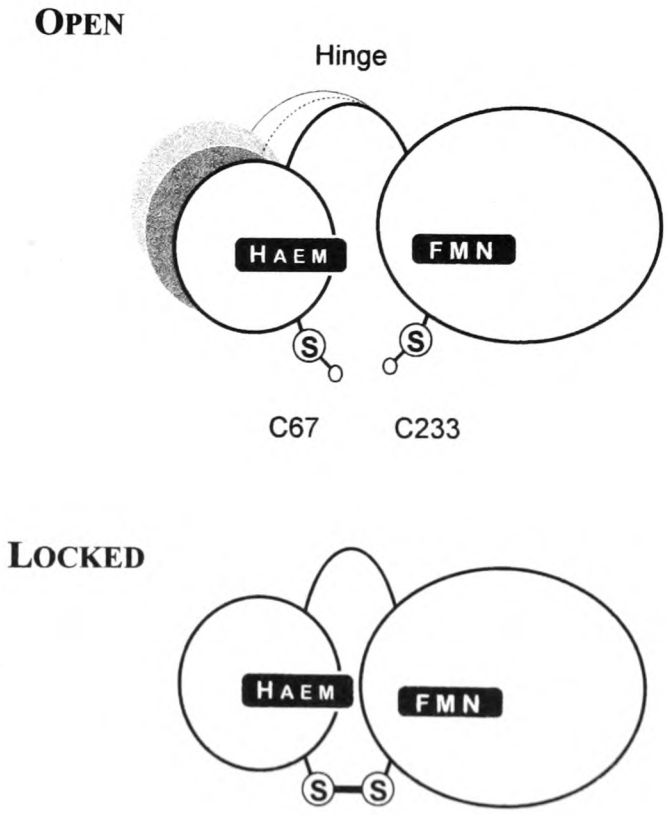

kinetic properties very similar to wild-type flavocytochrome b_2. For example, the rate constants for flavin and haem reduction measured under presteady-state conditions using stopped-flow spectrophotometry are the same within experimental error for both A67C-b_2 and wild-type enzyme. However, in the absence of dithiothreitol, in the locked form, the kinetic properties of A67C-b_2 are remarkably different from those of wild-type b_2. For A67C-b_2 in the locked form, the rate constant for haem reduction is some 10-fold lower than the value seen for the open form or for the wild-type enzyme. In contrast, the rate constant for flavin reduction in the locked form is only slightly affected. This is direct evidence that disulphide bridge formation has a major effect on flavin-to-haem electron transfer but not on the reduction of flavin by L-lactate. These preliminary data demonstrate the feasibility of placing a reversible lock on interdomain mobility in flavocytochrome b_2 and open up exciting possibilities for further analyses of intraprotein electron transfer in this system.

Is the published hypothetical complex between flavocytochrome b_2 and cytochrome c correct?

As mentioned above, a hypothetical model for the complex formed between a flavocytochrome b_2 tetramer and four cytochromes c has been proposed [12]. This model predicts a number of polar contacts between the two proteins, a notable example being that between Arg-13 of cytochrome c and Glu-91 of flavocytochrome b_2. In this case, the distance between the Arg and the Glu is suggested to be around 2.6 Å [12]. In order to test the importance of this electrostatic interaction for complex formation, we have used site-directed mutagenesis to replace Glu-91 with Lys to generate E91K-b_2. Such a change introduces a coulombic barrier, which should have a large effect on the kinetics of complex formation.

The model also indicates a possible σ-tunnelling pathway linking the b_2 and c haems that might act as the electron transfer route (Figure 2). From Figure 2 it is clear that the aromatic side chain of Phe-52 provides the link to the cytochrome c haem. To test the validity of this proposed pathway, we mutated Phe-52 to an Ala, generating F52A-b_2. This change will effectively interrupt the tunnelling pathway and would be expected to have a marked effect on the electron transfer rate from flavocytochrome b_2 to cytochrome c.

The two mutant enzymes, E91K-b_2 and F52A-b_2, have been characterized kinetically. The second-order rate constant for cytochrome c reduction by wild-type flavocytochrome b_2 has been found to be $35 \pm 1/\mu$M/s (at 25°C, pH 7.5, $I = 0.10$ M + 10 mM lactate) and the values for the two mutant enzymes are identical to this within experimental error. This rather surprising result indicates that the catalytically competent site on flavocytochrome b_2 at which cytochrome c binds is unlikely to be the one proposed from the published hypothetical complex. The results are also inconsistent with the proposed electron transfer pathway shown in Figure 2. It would appear then that the published hypothetical complex between the two proteins [12] does not represent a catalytically competent entity. We are now re-examining the structure of flavocytochrome b_2 to try and find alternative locations at which cytochrome c might bind in a catalytically competent way.

We are indebted to Professor F. S. Matthews, Dr F. Lederer, Dr M. Tegoni and Dr C. Cambillau for helpful discussions. This work was supported by the BBSRC through research grants. We are grateful to the EPSRC and BBSRC for postgraduate support for S.D. and D.S. and to the EU through the Human Capital and Mobility Programme (FLAPS Network contract no. ERBCHRXCT930166).

1 Moser, C. C., Keske, J. M., Warncke, K., Farid, R. S. and Dutton, P. L. (1992) Nature (London) **355**, 796–802
2 Lloyd, E., Chapman, K. E., Chapman, S. K., Jia, Z.-S., Lim, M.-C., Tomkinson, N. P., Salmon, G. A. and Sykes, A. G. (1994) J. Chem. Soc. Dalton. Trans. 675–681
3 Pelletier, H. and Kraut, J. (1992) Science **258**, 1748–1755
4 Jeng, M.-F., Englander, S. W., Pardue, K., Rogalskyj, J. S. and McLendon, G. (1994) Nature. Struct. Biol. **1**, 234–238
5 Black, M. T., White, S. A., Reid, G. A. and Chapman, S. K. (1989) Biochem. J. **258**, 255–259
6 Miles, C. S., Rouvière-Fourmy, N., Lederer, F., Mathews, F. S., Reid, G. A., Black, M. T. and Chapman, S. K. (1992) Biochem. J. **258**, 187–192
7 White, P., Manson, F. D. C., Brunt, C. E., Chapman, S. K. and Reid, G. A. (1993) Biochem. J. **291**, 89–94
8 Sharp, R. E., White, P., Chapman, S. K. and Reid, G. A. (1994) Biochemistry **33**, 5115–5120
9 Xia, Z.-X. and Mathews, F. S. (1990) J. Mol. Biol. **212**, 837–863
10 Tegoni, M. and Cambillau, C. (1994) Protein Sci.

3, 303–313
11 Louie, G. V., Brayer, G. D. (1990) J. Mol. Biol. **214**, 527–555
12 Tegoni, M., White, S. A., Roussel, A., Mathews, F. S. and Cambillau, C. (1993) Proteins **16**, 408–422
13 Chapman, S. K., White, S. A. and Reid, G. A. (1991). Adv. Inorg. Chem. **36**, 257–301
14 Lederer, F. (1991) in The Chemistry and Biochemistry of Flavoenzymes (Müller F., ed.) Vol. 2, pp. 154–242, CRC Press, Boca Raton
15 Labeyrie, F., Beloeil, J. C. and Thomas, M. A. (1988) Biochim. Biophys. Acta **953**, 131–141
16 Jacobson, B. L., He, J. J., Verersch, P. S., Lemon, D. D. and Quiocho, F. A. (1991) J. Biol. Chem. **266**, 5220–5225
17 Matsumura, M. and Mathews, B. W. (1989) Science **243**, 792–794

Received 17 August 1995

The chemical mechanism of flavoprotein-catalysed α-hydroxy acid dehydrogenation: a mutational analysis

F. Lederer, A. Belmouden and M. Gondry
URA 1461, CNRS and Université Paris V, Hôpital Necker, 75743 Paris Cedex 15, France

The family of FMN-dependent L-2-hydroxy acid oxidizing enzymes

The oxidation of 2-hydroxy acids to keto acids is catalysed by both nicotinamide-linked and FMN-dependent enzymes. The two classes form distinct evolutionary families, which are believed to operate via different chemical mechanisms. Nicotinamide-dependent reactions are classically considered to proceed by transfer of a hydride ion, whereas the flavoenzymes are assumed to first abstract the substrate α-hydrogen as a proton, a step followed by flavin reduction (carbanion mechanism) [1].

The family of FMN-dependent α-hydroxy acid-oxidizing enzymes encompasses at present a dozen proteins with known sequences, including one open reading frame (ORF) in data banks [2–7]. The alignment, based on the comparison between the crystal structures of flavocytochrome b_2 from *Saccharomyces cerevisiae* (Flb_2) and spinach glycolate oxidase (GO) [2,8,9], indicates 31 totally invariant residues and 85 strongly conserved residues, out of about 350 positions aligned. The two structures [10–13] show a $\beta_8\alpha_8$ barrel fold for the flavodehydrogenase (FDH) domains with an rms difference of 0.93 Å for 311 superimposed Cα-atoms [8]. The most variable area between the two structures corresponds to β-barrel loop 4, which follows a different course in space over part of its length and for which, in both cases, a few residues cannot be located, owing to their mobility. In the overall sequence alignment, it is also the most variable region, including from about 45 to 75 residues with practically no similarity. This segment was assigned the role of membrane-binding anchor for mandelate dehydrogenase from *Pseudomonas putida* [3]. There is also indirect evidence concerning Flb_2 and long-chain α-hydroxy acid oxidase (HAO) ([9,14–16], A. Belmouden and F. Lederer, unpublished work) that loop 4 may modulate catalysis by interacting with the active site, even though the edges of the invisible segment lie some 15–20 Å away from it in the two known structures [10–12].

The Flb_2 structure afforded a picture of pyruvate, the reaction product, bound at the active site, where FMN is most likely under the semiquinone form. This led us to propose a binding mode for the substrate, lactate, and to assign to active site residues a role compatible with a carbanion mechanism [15,17,18], the validity of which rests on work carried out mainly with lactate mono-oxygenase from *Mycobacterium smegmatis* (LMO) [19] and Flb_2 [20]. Figure 1 shows the hypothetical substrate binding mode, which implies participation of R-376, Y-143 and Y-254. H-373 is the postulated catalytic general base, which removes the substrate α–H as a proton. Carbanion formation is assisted by the electrostatic interaction between the imidazolium ion and D-282. In the next step, electron transfer to FMN is facilitated by the K-349 positive charge which stabilizes the reduced flavin anionic form, irrespective of the exact mechanism of electron transfer [1,18]. All the side chains mentioned above are strictly conserved in all members of the family except for a substitution in HAO of F for Y-254 (Figure 1). Their good superposition in the crystal structures indicates a similar role for these side chains in GO and hence probably in all other family members. The observed shift between Flb_2 and GO in the flavin position relative to the

Figure 1

Proposed catalytic roles for active site side chains in flavocytochrome b_2

The substrate binding mode is deduced from that of pyruvate observed in the first Flb_2 crystal structure [10]. (A) Michaelis complex and abstraction of the substrate α proton by H-373. (B) Flavin reduction by the carbanion.

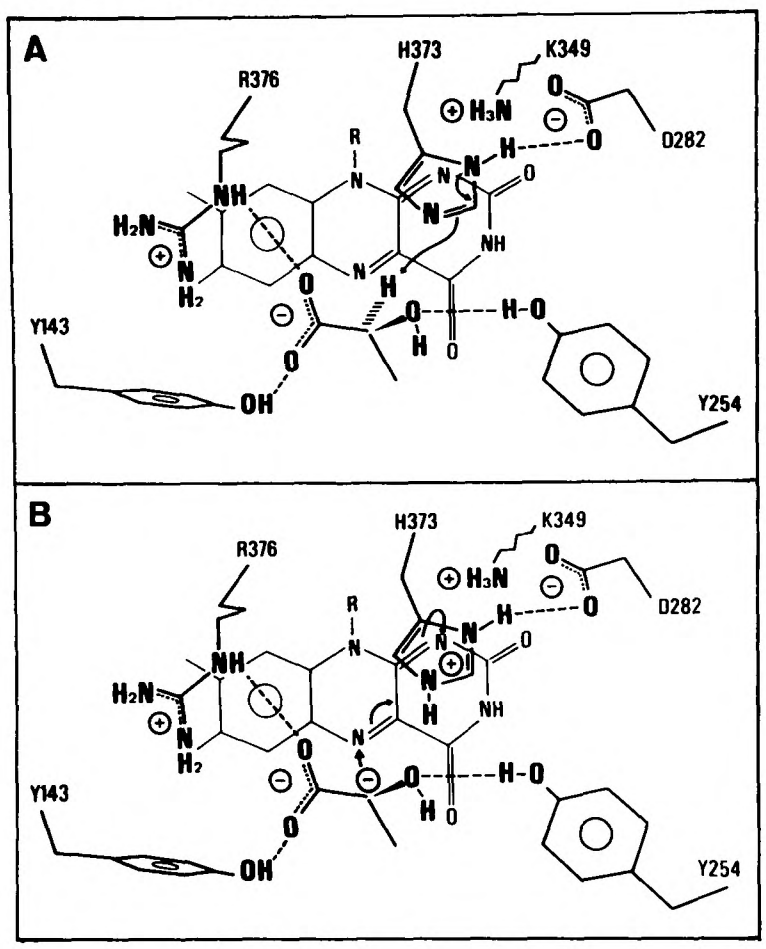

barrel backbone is possibly related to oxygen reactivity, and will not be discussed further here [8]. In the last few years, the study of site-directed mutant forms of Flb_2, GO, LMO and HAO, combined with modelling attempts, provided the means of probing the various aspects of catalysis mentioned above.

The active site histidine is the catalytic base

The critical role of H-373 (Figure 1) was demonstrated by mutating this residue and its LMO homologue H-290 to Q [21,22]. These two mutant enzymes had very low, if any, activity (Table 1). In Flb_2, the exact value of the intrinsic activity was obscured by the fact that the mutant enzyme preparations were contaminated by a trace of wild-type (WT) enzyme, presumed to arise from translational errors during biosynthesis. These results are compatible with a role of general base for H373 and its homologues. However it must be stressed that in a hydride transfer mechanism in which this residue would abstract the hydroxyl proton, a similar activity loss would be expected [30].

On the role of Y-254 and its homologues

The initial hypotheses predicted that Y-254 should form a hydrogen bond with the substrate in the Michaelis complex and that it could facilitate flavin reduction by acting as a second general base with respect to the substrate hydroxyl group at the carbanion stage [15,17–19]. Nevertheless, studies of the Y-254F and Y-254L variants of Flb_2 showed that it was α-proton abstraction that was slowed down [16,23,31]. The variations of k_{cat}/K_m values induced by the Y to F mutation indicated that the H-bond between substrate and tyrosine hydroxyl groups stabilizes the transition state (Table 1). It was suggested that this effect arises from the oritentation effect of the H-bond, leading to a correct positioning of the Cα-H-bond with respect to H-373 [23]. The Y to L mutation destabilizes the transition state even more (Table 1). For Y-152F LMO and Y-129F GO, the similarity in the energy level differences suggests that the effect of the mutation can be rationalized in the same way.

Contrary to expectations, mutations at position 254 and its homologues led either to no alteration of apparent affinities or even to a 10-fold increase in the case of LMO (Table 1). Should one then conclude that Y-254 does not contribute to Michaelis complex stabilization? The idea that lactate could have no other interactions in the enzyme–substrate (ES) complex than those with Y-143 and R-376 (Figure 1) is difficult to entertain in view of the fact that propionate behaves as a competitive inhibitor of lactate with $K_i = 28$ mM [32]. Modelling studies suggested that lactate could adopt a different conformation in the active site, but this would entail a switch to a hydride transfer mechanism, which was experimentally excluded for Y-254 Flb_2 [23]. Furthermore, an enzyme structural alteration possibly leading to a different lactate-binding mode was ruled out by crystal structure results for the Y-129F GO and Y-254F Flb_2 mutants [26,33]; these showed no protein structural change other than the loss of the tyrosine hydroxyl. A tentative explanation can be offered to rationalize these results. The apparent binding energy deduced from K_d values is the result of the replacing enzyme–solvent and substrate–solvent interactions by enzyme–substrate interactions. We may explain the lack of effect of the

New Insights into the Catalytic Cycle of Flavocytochrome b_2[†]

Simon Daff,[‡] W. John Ingledew,[§] Graeme A. Reid,[∥] and Stephen K. Chapman*[,‡]

Department of Chemistry and Institute of Cell and Molecular Biology, University of Edinburgh, King's Buildings, West Mains Road, Edinburgh, Scotland, U.K., and School of Biological & Medical Sciences, University of St. Andrews, St. Andrews, Fife, Scotland, U.K.

Received September 20, 1995; Revised Manuscript Received January 16, 1996[⊗]

ABSTRACT: Flavocytochrome b_2 from *Saccharomyces cerevisiae* couples L-lactate dehydrogenation to cytochrome *c* reduction in the mitochondrial intermembrane space. The catalytic cycle for this process can be described in terms of five consecutive electron-transfer events. L-Lactate dehydrogenation results in the two-electron reduction of FMN. The two electrons are individually passed to b_2-heme (intramolecular electron transfer) and then onto cytochrome *c* (intermolecular electron transfer). At 25 °C, *I* 0.10, in the presence of saturating concentrations of ferricytochrome *c* and L-lactate, the catalytic cycle progresses with rate constant 104 (± 5) s^{-1} [per L-lactate oxidized; Miles, C. S., Rouviere-Fourmy, N., Lederer, F., Mathews, F. S., Reid, G. A., & Chapman, S. K. (1992) *Biochem. J. 285*, 187−192]. Stopped-flow spectrophotometry has been used to show that the major rate-limiting step in the catalytic cycle is electron transfer from flavin semiquinone to b_2-heme. This conclusion is based on the observation that pre-steady-state flavin oxidation by ferricytochrome *c* takes place at 120 s^{-1}. Although flavin oxidation involves several other electron transfer steps, these are considered too fast to contribute significantly to the rate constant. It was also shown that the reaction product, pyruvate, is able to inhibit pre-steady-state flavin oxidation (K_i = 40 ± 17 mM) consistent with reports that it acts as a noncompetitive inhibitor in the steady state at high concentrations [K_i = 30 mM; Lederer, F. (1978) *Eur. J. Biochem. 88*, 425−431]. This novel way of measuring the electron transfer rate constant is directly applicable to the catalytic cycle and has enabled us to derive a self-consistent model for it, based also on data collected for enzyme reduction [Miles, C. S., Rouviere-Fourmy, N., Lederer, F., Mathews, F. S., Reid, G. A., & Chapman, S. K. (1992) *Biochem. J. 285*, 187−192] and its interaction with cytochrome *c* [Daff, S., Sharp, R. E., White, P., Short, D. M., Manson, F. D. C., Reid, G. A., & Chapman, S. K. (1996) *Biochemistry 35*, 0000−0000]. Rapid-freezing quenched-flow EPR has been used to confirm the model by demonstrating that during steady-state turnover of the enzyme approximately 75% of the flavin is in the semiquinone oxidation state.

Flavocytochrome b_2 from *Saccharomyces cerevisiae* is a soluble L-lactate cytochrome *c* oxidoreductase found in the mitochondrial intermembrane space (Daum et al., 1982). It is a homotetramer, with each 511 amino acid subunit consisting of two distinct domains. The first 100 residues fold to form a heme binding domain which is connected via a short hinge region to a flavin mononucleotide (FMN) binding domain. Finally, a 20 amino acid C-terminal tail winds around the 4-fold axis of the tetramer forming several interactions with each of the other subunits. The X-ray crystal structure, solved to 2.4 Å resolution (Xia & Mathews, 1990), identifies the site for L-lactate dehydrogenation which is constructed around the FMN prosthetic group. The two electrons generated by L-lactate dehydrogenation are used to reduce FMN to its hydroquinone form. They are then individually passed to two ferricytochrome *c* molecules via the b_2-heme. Direct flavin to cytochrome *c* electron transfer is negligible (Forestier & Baudras, 1971; Iwatsubo et al., 1977; Balme et al., 1995). The rate constant for enzyme turnover under the saturating conditions of 10 mM L-lactate and excess cytochrome *c* is 104 (± 5) s^{-1} per mol of lactate per mol of enzyme (which is equivalent to 207 (± 10) s^{-1} per mol of cytochrome *c* reduced), whereas the rate constant for the flavin reduction/lactate oxidation process is 604 (± 60) s^{-1} (Miles et al., 1992). The latter value is subject to a ^2H kinetic isotope effect of 8.1 (± 1.4), whereas in the cycle as a whole this has been eroded to 3.0 (± 0.6). Clearly there is a slower step in the cycle which limits the enzyme's turnover rate. The catalytic cycle can be represented by a series of five consecutive electron-transfer steps which form the basis of the model described in Figure 1. Following FMN reduction/L-lactate oxidation (step 1) there are two FMN to b_2-heme intramolecular electron transfers (steps 2 and 4), and two b_2-heme to cytochrome *c* electron transfers (steps 3 and 5). The cytochrome *c* reduction steps are considered in detail by Daff *et al.* (1996) with the conclusion that the effect of these steps on the overall rate of the cycle is minimal. Intramolecular electron transfer from FMN hydroquinone to b_2-heme (step 2) has been studied extensively by using stopped-flow spectrophotometry to monitor b_2-heme reduction (Capeillère-Blandin, 1975; Capeillère-Blandin et al., 1975; Pompon et al., 1980; Pompon, 1980;

* To whom correspondence should be addressed. Fax: (44)131 650 4743. Email: S.K.Chapman@ed.ac.uk.

† This work was funded by the Biotechnology and Biological Science Research Council (U.K.), by The European Commission (FLAPS Network) and via a studentship from the Engineering and Physical Sciences Research Council (U. K.) to S.D.

‡ Department of Chemistry, University of Edinburgh.

§ University of St. Andrews.

∥ Institute of Cell and Molecular Biology, University of Edinburgh.

⊗ Abstract published in *Advance ACS Abstracts*, Xxxxxxxxx YY, ZZZZ.

S0006 2960(95)02255 0 CCC: $12.00

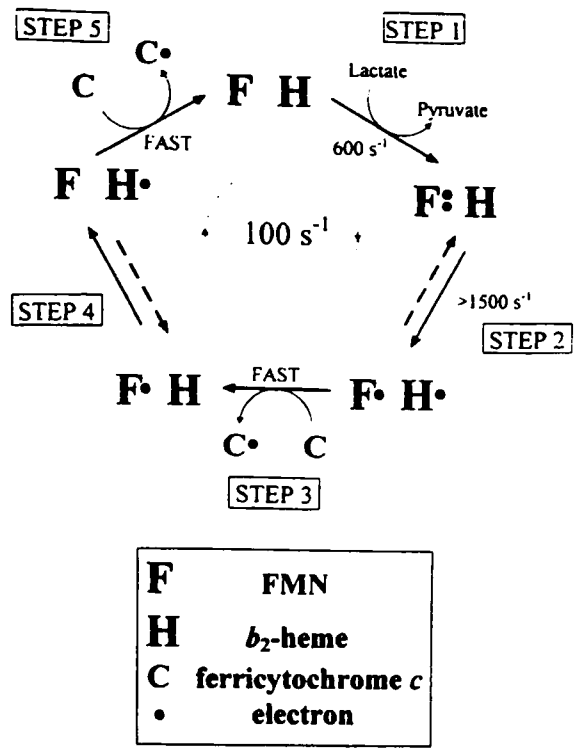

FIGURE 1: Model proposed to explain the catalytic cycle of flavocytochrome b_2 based on individual electron-transfer processes. The action of a single subunit of the enzyme is described as it turns over at its maximum rate of ~100 s^{-1} in the presence of saturating amounts of L-lactate and ferricytochrome *c* at 25 °C in 10 mM Tris-HCl buffer, pH 7.5, *I* 0.10. Two equivalents of cytochrome *c* are reduced in each turnover so in these terms the k_{cat} is 207 (± 10) s^{-1} (Miles et al., 1992). (Step 1) Reduction of FMN to its hydroquinone form, and oxidation of L-lactate to pyruvate. (Step 2) Interdomain electron transfer from fully reduced FMN to b_2-heme, generating reduced heme and FMN semiquinone. (Steps 3 and 5) Binding and reduction of ferricytochrome *c* by b_2-heme. (Step 4) Interdomain electron transfer from FMN semiquinone to b_2-heme.

Chapman et al., 1994), laser flash photolysis to monitor b_2-heme re-reduction (Hazzard et al., 1994), and site-directed mutagenesis to investigate the importance of the protein framework (Miles et al., 1992; Sharp et al., 1994; White et al., 1993). All of these experiments confirm that step 2 is several times faster than catalytic turnover, and, under our particular conditions, the rate constant is likely to be in excess of 1500 s^{-1} (Chapman et al., 1994). The second intramolecular electron transfer (step 4), which occurs from FMN semiquinone to b_2-heme, is less well understood but has been studied recently using laser flash photolysis (Walker & Tollin, 1991). However, electron transfer was only observed in the presence of pyruvate and in the reverse direction. Pyruvate is known to cause complex inhibition during the steady-state turnover of flavocytochrome b_2 (Lederer, 1978) and is able to stabilize the semiquinone redox state of FMN in both the *S. cerevisiae* (Walker & Tollin, 1991) and related *Hansenula anomala* enzymes (Tegoni et al., 1986, 1990).

In the present paper we describe how the use of stopped-flow spectrophotometry to study FMN oxidation in the presence of excess ferricytochrome *c* has enabled step 4 of the catalytic cycle to be monitored in the pre-steady-state, both in the absence and presence of pyruvate. The evidence obtained suggests that FMN semiquinone to b_2-heme electron transfer is the major rate-limiting step in the catalytic cycle, and that pyruvate inhibits this process. This has allowed a self-consistent kinetic model to be derived for the catalytic cycle (Figure 1) based on the electron transfers occurring when the enzyme is turning over in the presence of saturating concentrations of its physiological substrates. Confirmatory evidence for the model has been obtained from rapid-freezing quenched-flow EPR spectrometry which has enabled free-radical quantities to be calculated for reaction mixtures frozen while in steady-state turnover.

MATERIALS AND METHODS

Enzyme Preparations. Flavocytochrome b_2 expressed in *Escherichia coli* was isolated from cells stored temporarily at −20 °C using a previously reported purification procedure (Black et al., 1989). Purified enzyme samples were stored in the short term under nitrogen at 4 °C as precipitates from 70% saturated $(NH_4)_2SO_4$ solution. Alternatively, long term storage was secured by snap-freezing drops of enzyme in liquid nitrogen and maintaining these at below −180 °C. Before freezing, the enzyme was desalted using a Sephadex G25 gel filtration column (1.5 cm × 15 cm) (Sigma) equilibrated and eluted with 10 mM Tris-HCl buffer, pH 7.5, *I* 0.10. The buffer consisted of 10 mM HCl titrated against Tris solution to pH 7.5 and adjusted to *I* 0.10 by addition of NaCl. All enzyme solutions used for kinetic analysis were found to have >90% activity based on the maximum steady-state rate of 400 s^{-1} (Miles et al., 1992) measured in the presence of 1 mM ferricyanide (potassium salt, BDH) and 10 mM L-lactate (Sigma). Enzyme concentrations were calculated using previously published extinction coefficients (Pajot & Groudinsky, 1970).

Stopped-Flow Kinetics. All stopped-flow experiments were carried out in 10 mM Tris, HCl buffer, *I* 0.10 at 25.0 (± 0.1) °C, using an Applied Photophysics SF.17 MV stopped-flow spectrofluorimeter, as described previously (Miles et al., 1992), analysis of kinetic data was performed using the SF.17 MV software and Origin (Microcal), both of which use nonlinear least-squares regression analysis. FMN and b_2-heme reduction were monitored as described previously (Miles et al., 1992) by following absorbance changes at 438.3 and 557 nm, respectively; in addition, pyruvate was introduced into the syringe containing L-lactate to ascertain its effect on these processes. The re-reduction of b_2-heme by flavin, following rapid oxidation by horse-heart cytochrome *c* (Sigma), was monitored at 408.4 nm, an isosbestic point in the cytochrome *c* spectrum. For this experiment 40 μM flavocytochrome b_2 reduced by 10 mM L-lactate was used in conjunction with 4 μM cytochrome *c*. Absorbance is then converted to percent b_2-heme oxidized, based on the quantity of cytochrome *c* used (4 μM), and the standard absorbance change for deflavoflavocytochrome b_2 calculated from an oxidized/reduced difference spectrum to be 44 000(± 5000) M^{-1} s^{-1}.

FMN oxidation by an excess of cytochrome *c*, as illustrated in Figure 4, was monitored at the b_2-heme isosbestic wavelength of 438.3 nm, where standard absorption coefficients for the various redox states have been previously determined to be approximately 1200, 3000, and 10 000 M^{-1} cm^{-1} for reduced, semiquinone, and oxidized, respectively (Capeillère-Blandin, 1991). Flavocytochrome b_2 was initially reduced by 1 mM glycolate (Sigma), a poor substrate with maximum turnover rate of 3.5 mol of substrate s^{-1}, in order to prevent rapid re-reduction of the enzyme. Since 438.3 nm is not an isosbestic for cytochrome *c*, its absorbance contribution at this wavelength had to be subtracted. This was achieved by generating a cytochrome *c* reduction trace at the b_2-heme/FMN isosbestic of 544.8 nm (Figure 3) (Janot et al., 1990). A pure FMN trace could be produced according to Absorbance(438.3 nm) + 107%[Absorbance(544.8 nm)]. The traces were collected using a split time-base, and the period of slow turnover, dependent on glycolate oxidation,

was used to determine the addition percentage used above. During a true steady-state period the absorbance of the FMN will be constant, and therefore the modified trace should be flat. In addition, once all the cytochrome *c* has reacted, the enzyme is reduced by the excess of glycolate and should therefore return to its original absorbance. Bearing these facts in mind, the value was derived by inspection. The error in this method, although difficult to quantify, can be expected to be less than 5%. Once modified, the fast phase of each trace, representing the time course for flavin oxidation and occurring largely within the first 100 ms, was fitted to a single-exponential function. The effect of the addition error on these rate constants is estimated to be less than 10%.

Inhibition of FMN oxidation by pyruvate (Sigma) was studied by introducing a range of different concentrations (0−50 mM) via the cytochrome *c* syringe. The kinetic analysis was then carried out as described above.

Quenched-Flow EPR Kinetics. The rapid quenched-flow EPR experiment was performed in 10 mM MOPS (morpholinopropanesulfonic acid, Sigma)/KOH buffer, pH 7.5, adjusted to *I* 0.10 by addition of NaCl. For each experimental data point, 1 mL of reaction mixture containing 470 μM oxidized cytochrome *c*, 20 μM flavocytochrome b_2, and 10 mM L-lactate was generated by a rapid mixer and forced through a variable length of HPLC steel tubing before being sprayed into a bath of isopentane (Probalo), maintained at −140 °C by a liquid nitrogen cooled cryostat (Moodie et al., 1990). In order to vary the time-base for the experiment, different lengths of steel tube were used, to allow different degrees of aging. The frozen reaction mixture was then packed into an EPR tube and stored in liquid nitrogen. All EPR measurements were performed on a Bruker instrument. Integrals were calculated for the FMN semiquinone signal at −184 °C relative to a 1 mM Cu^{II} standard, and for the ferricytochrome *c* signal at −270 °C relative to a 1 mM ferricytochrome *c* standard. These were corrected for packing with respect to a standard ferricytochrome *c* sample produced in an identical way but in the absence of flavocytochrome b_2. The ferricytochrome *c* integrals were used to calibrate the time base for the data in Figure 6 by fixing them to a spectrophotometrically collected cytochrome *c* trace which had been adjusted to account for the higher concentration of flavocytochrome b_2 and faster reaction rate observed in the quenched-flow experiment.

RESULTS AND DISCUSSION

The catalytic cycle for flavocytochrome b_2 is illustrated in Figure 1 in terms of its component electron transfer processes. This provides a convenient frame of reference for experiment since each electron transfer corresponds to a change in the visible absorption spectrum. It is important to note, however, that the rate determining factor in each electron transfer step may be dependent on a chemical or conformational change directly preceding the electron transfer, such that the observed color changes serve only as convenient observation points.

Step 1. FMN reduction by L-lactate has been studied previously using stopped-flow spectrophotometry (Miles et al., 1992). The rate constant for this process is reported as 604 (± 60) s^{-1} with a ^2H kinetic isotope effect of 8.1 (± 1.4) on α-H abstraction. This step is 6-fold faster than the overall turnover rate, and for this reason it should contribute little toward rate limitation.

Step 2. b_2-Heme reduction has been studied in tandem with FMN reduction and appears to lag behind by only a small amount. This suggests that the rate constant for electron transfer from FMN to b_2-heme is faster than for FMN reduction. A conservative estimate of the rate constant for the electron-transfer process has been given as 1500 (± 500) s^{-1} (Chapman et al., 1994) by considering the magnitude of the lag phase. However, accuracy is limited by the stopped-flow procedure which cannot generate reliable data for reactions which occur at this velocity and faster. Laser flash photolysis has also been used to study this electron-transfer process, providing a value for the rate constant of 1900 s^{-1} (Hazzard et al., 1994) at 24 °C in pH 7, 100 mM phosphate buffer, which is in agreement with the stopped-flow observations.

If pre-steady-state rate constants are to be applied directly to a steady-state situation, it is important to match the conditions as closely as possible. In the b_2-heme reduction experiment described above, intramolecular electron transfer is only observed after FMN reduction and, in this respect, mimics step 1 and step 2 of the catalytic cycle. However, one factor missing from this experiment is the presence of cytochrome *c* which may bind strongly to the enzyme and affect either step. For this reason b_2-heme reduction was carried out in the presence of zinc-substituted cytochrome *c*, a redox inactive form of the electron acceptor known to bind to flavocytochrome b_2. The results are presented by Daff et al. (1996) and show that the stopped-flow traces overlay almost exactly, demonstrating that the binding of cytochrome *c* to flavocytochrome b_2 is unlikely to affect either step 1 or step 2.

In order to study FMN to b_2-heme electron transfer in the presence of redox-active cytochrome *c*, the rapid b_2-heme to cytochrome *c* electron-transfer process was exploited. This intermolecular step is dependent on the concentration of enzyme, and at high concentration (>25 μM) is known to occur within the dead-time of a stopped-flow experiment (Daff et al., 1996). By inducing the FMN to b_2-heme electron transfer in fully reduced enzyme using a substoichiometric amount of cytochrome *c* to first partially oxidize the b_2-heme, a "b_2-heme re-reduction" trace is generated. The absorbance change observed gives the percent of oxidized b_2-heme relative to the amount of ferricytochrome *c* used. The proportion of oxidized b_2-heme reaches a maximum of 20−30%, meaning that electron transfer from the fully reduced FMN to b_2-heme is happening too fast to be observed by this method; i.e., the rate constant must be in excess of 1000 s^{-1}. Some oxidized heme is observed because electron transfer from the fully reduced FMN to oxidized b_2-heme will initially result in an equilibrium being established between the two prosthetic groups, based on their electrode potentials (Capeillère-Blandin, 1975; Chapman et al., 1994). This equilibrium is eventually disrupted by disproportionation of flavin semiquinones followed by reduction by L-lactate. This is an overall slower process than the initial electron transfer but leads to fully reduced enzyme which accommodates three electrons (i.e., back to the starting absorbance). This experiment was repeated using different substrates at different concentrations to reduce the enzyme, but in each case the maximum absorbance observed was never significantly different from that described above. In these experiments it is very unlikely that substrate (e.g., L-lactate) is bound in the active site when the enzyme is fully reduced (Urban et al., 1983), especially at low substrate

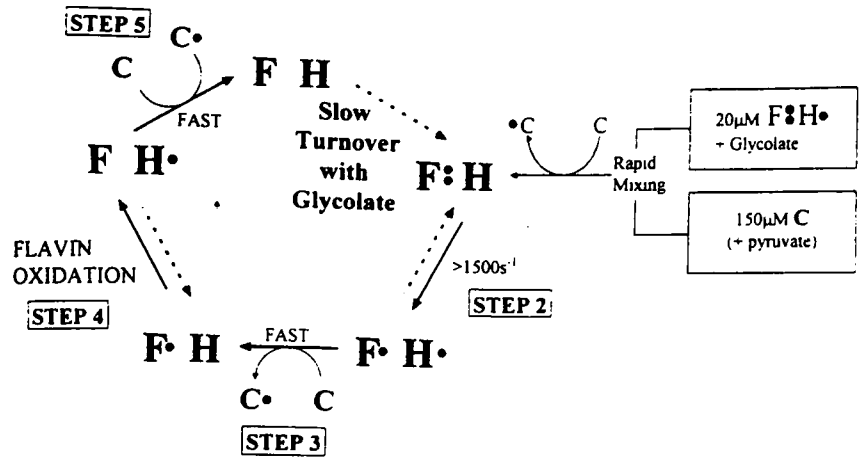

FIGURE 2: Electron-transfer processes occurring during the flavin oxidation stopped-flow experiment (see Materials and Methods). An excess of ferricytochrome *c* is used to oxidize flavocytochrome b_2 by entering the catalytic cycle (see Figure 1) immediately before step 2. The use of glycolate as substrate enables the enzyme to be fully reduced initially but dramatically slows down the overall turnover rate at step 1 (see Figure 1). This allows step 4, FMN oxidation, to be monitored as a pre-steady-state process. Examples of the stopped-flow traces derived from this experiment are illustrated in Figures 3 and 4. The introduction of pyruvate into the ferricytochrome *c* solution before mixing allows inhibiton to be studied in the pre-steady-state.

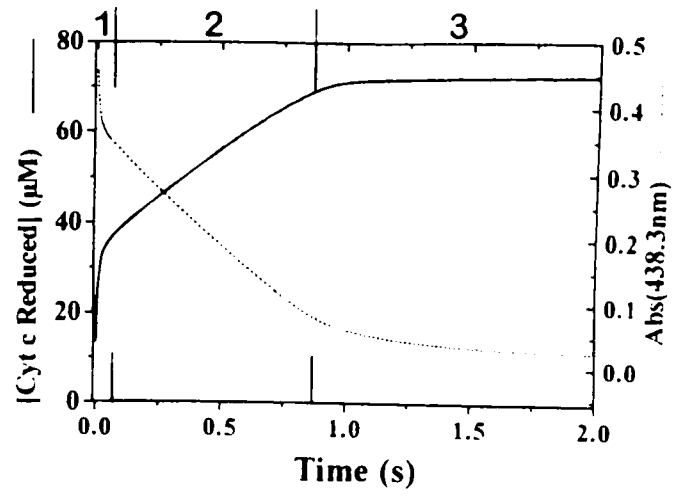

FIGURE 3: Examples of stopped-flow traces generated from a flavin oxidation experiment (see Figure 2) containing 10 μM flavocytochrome b_2, 75 μM cytochrome *c*, and 15 mM pyruvate at 25 °C in 10 mM Tris-HCl buffer, pH 7.5, *I* 0.10. The cytochrome *c* trace (left axis) was recorded at the b_2-heme isosbestic of 544.8 nm where an absorbance increase is observed as ferricytochrome *c* is reduced. The *y*-axis for this trace has been converted to concentration of ferrocytochrome *c* by using $\Delta\epsilon = 7000$ (see Materials and Methods). This allows the steps described in Figure 2 to be followed in terms of molar equivalents; i.e., since flavocytochrome b_2 is present at a concentration of 10 μM (after mixing), each 10 μM ferrocytochrome *c* produced represents one molar equivalent. The cytochrome *c* trace is split into three distinct phases: 1, a rapid pre-steady-state phase in which 3 molar equivalents of ferrocytochrome *c* are generated; 2, a slow steady-state phase in which turnover is limited by glycolate oxidation; 3, turnover ends when all the cytochrome *c* has been reduced. The trace recorded at the b_2-heme isosbestic 438.3 nm (right axis) is almost a mirror image of the cytochrome *c* trace, due to a large negative contribution from cytochrome *c* to the absorbance change at this wavelength. However, there is a significant contribution from the flavin manifested in phase 1, due to flavin oxidation, and phase 3, as flavin reduction occurs. Weighted addition of the two traces to eliminate the common cytochrome *c* contribution leads to the flavin time course illustrated in Figure 4.

concentrations. Further, since the product (e.g., pyruvate) is present only in a slight excess over the enzyme, this is also unlikely to be bound. Therefore, rapid FMN to b_2-heme electron transfer must be possible when the active site of the enzyme is empty. This observation is therefore complementary to the b_2-heme reduction experiment, which demonstrates that rapid electron transfer occurs directly after FMN reduction by L-lactate. In this case it is possible that pyruvate is still bound in the active site during the electron-transfer event. Therefore, we can conclude either that the presence of pyruvate has little effect on this electron-transfer step in terms of the catalytic cycle or that pyruvate dissociation is too fast to cause a detectable change in the rate.

In summary, there is no evidence to show that there is any significant impediment to the electron transfer from fully reduced FMN to b_2-heme that would contribute to limiting the overall turnover rate to 100 s^{-1}.

Steps 3 and 5. Both these steps represent electron transfers from the b_2-heme to cytochrome *c* but also involve binding and dissociation processes. These are discussed in detail in Daff et al. (1996) which concludes that the effects on the catalytic cycle are negligible.

Step 4. Flavin oxidation traces were collected as described in Materials and Methods (see Figures 2–4). By using the poor substrate, glycolate, to pre-reduce a solution of enzyme (20 μM before mixing) and mixing with an excess of ferricytochrome *c* (150 μM before mixing), step 4 of the cycle could be studied with the assurance that step 1, flavin reduction, would be slowed down enough to effectively rate-limit enzyme turnover. As already discussed, steps 2 and 3 occur too fast to be detected by stopped-flow spectrophotometry, and therefore the change observed with regard to FMN absorbance at 438.3 nm is limited to the conversion of the semiquinone to oxidized FMN. The cytochrome *c* trace monitored at 544.8 nm gives an overall indication of the processes occurring. The fast phase (first 100 ms) corresponds to a large absorbance change, corresponding to approximately three electron equivalents. These three electrons are removed on the first rapid circuit of the catalytic cycle, before flavin re-reduction by glycolate slows turnover dramatically. Once this point has been reached, a steady state period occurs of approximately 1 s, in which glycolate is oxidized at the expense of cytochrome *c*. Finally, after around 7.5 electron equivalents, all of the cytochrome c has been reduced and turnover stops. The ferricytochrome *c* concentration was chosen to be as high as possible to ensure that the first two electron equivalents could be reduced while the flavocytochrome b_2 was still saturated. The K_m for cytochrome *c* reduction has been measured to be 10 (± 1) μM (Miles et al., 1992), and so even after the first two electron equivalents have been reduced (≡20 μM), 55 μM remains, i.e., 5-fold in excess of the K_m.

The corresponding flavin trace shows a rapid absorbance increase initially caused by FMN oxidation, a flat period during steady-state, and finally a slow reduction phase once all the cytochrome *c* has been reduced. The amplitude of the FMN contribution to the absorbance change at 438.3 nm was typically around 0.07. This is compatible with the expected change for the semiquinone to oxidized FMN redox change based on previously determined absorption coefficients (Capeillère-Blandin, 1991). The rate constant for the flavin oxidation process was determined to be 120 s^{-1} by fitting the stopped-flow trace to a single-exponential function. Therefore, although several other steps occur before flavin oxidation they were deemed to be too fast to affect the shape of the trace, and Figure 4 was treated as a single-step reaction. The quality of fit typically achieved by this method suggests that this is a valid assumption. However, one should not ignore the implications of this when considering the error involved in the rate constant. Taking this into account, along with errors generating from the

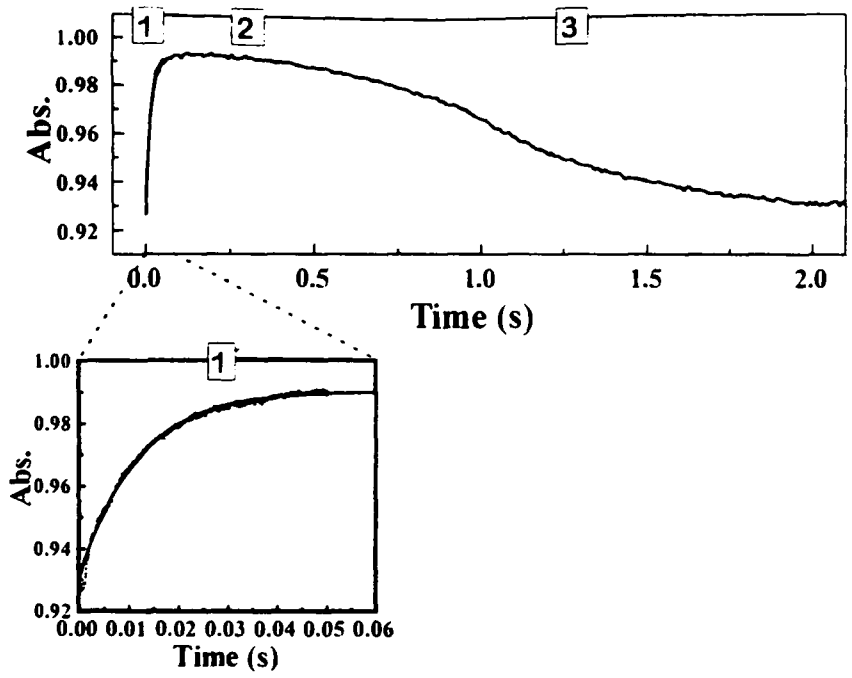

FIGURE 4: Example of a flavin absorbance time course generated by the addition of the stopped-flow traces shown in Figure 3 according to Abs(438.3 nm) + 1.07Abs(544.8 nm). The three phases described for Figure 3 are apparent here as follows: 1, flavin oxidation causes an absorbance increase at 438.3 nm; 2, steady-state period during which time the flavin absorbance is approximately constant; 3, flavin reduction which occurs in the presence of excess glycolate once exhaustion of ferricytochrome *c* has ended the steady-state reaction and returns the absorbance back to its starting point. Phase 1 is shown expanded to illustrate the flavin oxidation process. Although the entire trace contains 1000 data points, the use of split time bases has enabled this small region of the time course to contain 500 data points, allowing it to be accurately fitted to a single-exponential function (as shown).

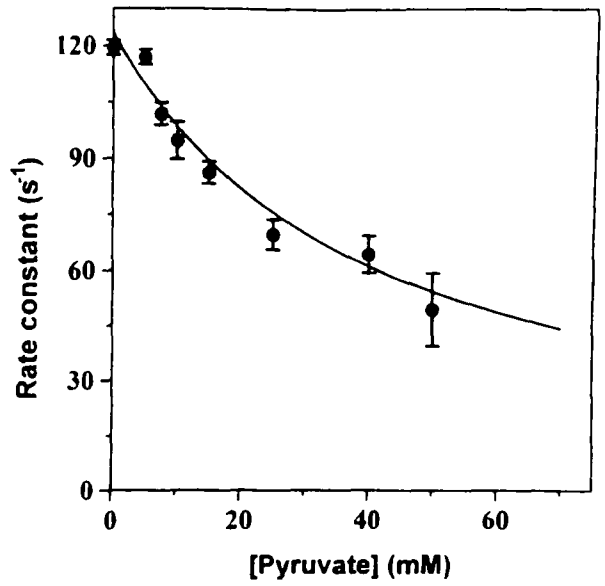

FIGURE 5: Inhibition plot of flavin oxidation rate vs pyruvate concentration. All experiments were conducted as described in the Materials and Methods, 10 μM flavocytochrome b_2 and 75 μM cytochrome *c* (after mixing), in 10 mM Tris-HCl buffer, pH 7.5, I 0.10, at 25 °C. Data were fitted to a Michaelis–Menten partial inhibition function using nonlinear least-squares regression analysis. k_0 is the rate constant in the absence of inhibitor, and k_x is the minimum rate constant at saturation. This was constrained to >0 during fitting. The error bars represent the range of values collected at each concentration from at least five experiments. K_i = 40 (± 17) mM, k_0 = 123 (± 2) s^{-1}, k_x = 0 (± 26) s^{-1}.

subtraction of cytochrome *c* absorbance (see Materials and Methods), the actual rate constant for FMN semiquinone to b_2-heme electron transfer is estimated to be 120 s^{-1} with an error of 10–20%.

Electron transfer from flavin semiquinone to b_2-heme has also been studied by laser flash photolysis (Walker & Tollin, 1991), but no electron transfer was observed by this method in the absence of product (pyruvate). Therefore the steps preceding flavin oxidation within the catalytic cycle appear to be critical in determining the rate constant observed.

Pyruvate Inhibition. The flavin oxidation process, seen to occur with rate constant 120 s^{-1} is inhibited by addition of the product pyruvate to the reaction mixture with a K_i of 40 (±17) mM (Figure 5). These experiments were performed by introducing pyruvate into the ferricytochrome *c* solution before mixing (see Figure 2). The reason for this was to avoid FMN oxidation by excess pyruvate, although this process is sufficiently slow so as not to compete with the usual catalytic cycle (Urban et al., 1983). Pyruvate is known to be a noncompetitive inhibitor of flavocytochrome b_2 in the steady-state, and the K_i of 30 mM (Lederer, 1978) is consistent with the above result. Conversely, increases in ionic strength or addition of oxalate (a competitive inhibitor) cause the flavin oxidation process to occur more rapidly. However, the single-exponential functions obtained under the initial conditions become more complex, as presumably different steps begin to contribute to rate limitation. This problem is also observed as the rate is slowed down by addition of pyruvate. Contributing factors to the complexity include the effect of increasing ionic strength with increasing pyruvate concentration and also deviation from ideality with respect to pyruvate binding, i.e., the association/dissociation rates may be too slow to create a genuine equilibrium for binding during the pre-steady-state reaction. For this reason pyruvate concentrations are limited to less than 50 mM, over which range the data are reliable. However, using such a narrow range limits the accuracy of the K_i derived. For example, it is impossible to say whether the inhibition tends to zero at infinite pyruvate concentrations. Although the accuracy is poor, it is clear that inhibition does occur during this rate-determining electron-transfer step. There are several possibilities for the mechanism of inhibition based on pyruvate binding to the semiquinone form of the enzyme: (1) pyruvate acts as a physical barrier to electron transfer from FMN to b_2-heme by changing the properties of the intervening medium. (2) Pyruvate stabilizes the semiquinone state thereby altering its redox potential and making electron transfer thermodynamically less favorable [this possibility is discussed in detail by Tegoni et al. (1990) for the related enzyme from *H. anomala* and supported by Walker and Tollin (1991) for the *S. cerevisiae* enzyme]. (3) Pyruvate competes with one of the heme propionates for a key hydrogen bond causing the heme group to be "disconnected" from the active site. This could result in an increase in the flavin–heme separation which would disfavor the electron transfer. Tyr 143 is a suitable candidate for this role in that it is observed to be within hydrogen-bonding distance of both pyruvate and one of the propionates in the enzyme's crystal structure (Xia & Mathews, 1990). Further, it has been demonstrated that mutation of this residue to phenylalanine greatly disrupts both intramolecular electron transfer and substrate binding (Miles et al., 1992).

Regardless of the mechanism, the fact that pyruvate is able to cause this inhibition suggests that, immediately prior to electron transfer, dissociation of pyruvate has already occurred, and that the active site is vacant. Furthermore, the observation that step 4 (in the absence of pyruvate) occurs at the same rate as in the catalytic cycle suggests that pyruvate dissociation contributes little to the overall rate of turnover.

Quenched-Flow EPR. In order to test the model derived for the catalytic cycle, quenched-flow EPR was used to quantify the amount of flavin semiquinone present when the

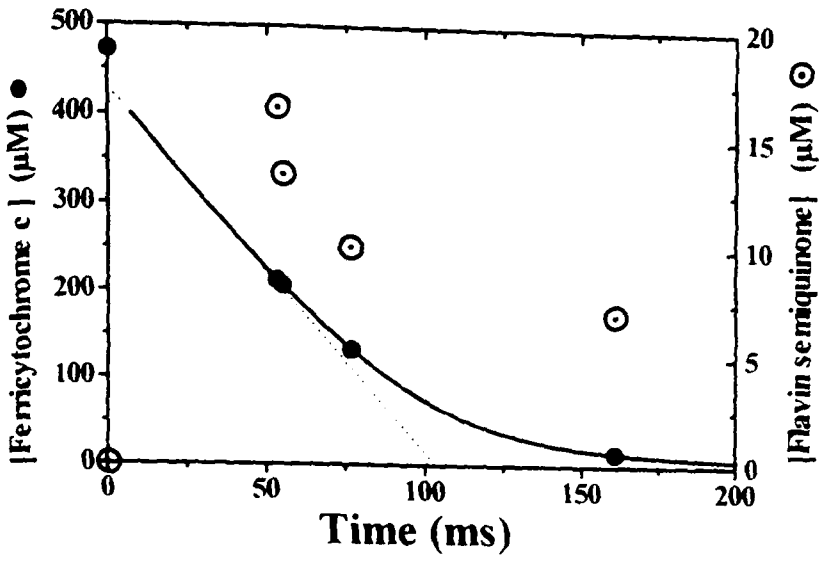

FIGURE 6: Plot of free radical concentrations for both ferricytochrome c and flavin semiquinone derived from EPR spectroscopic quantifications of frozen samples of a reaction mixture containing 470 μM cytochrome *c*, 10 mM L-lactate, and 20 μM flavocytochrome b_2 mixed at 25 °C in 10 mM MOPS buffer, *I* 0.10, pH 7.5, and freeze-quenched in isopentane liquid at −140 °C. The ferricytochrome *c* quantities have been used to calibrate the time-base for this plot by fixing them to a simulation of the reaction (—), derived by scaling up an assay collected by a visible spectrophotometer with a catalytic amount of flavocytochrome b_2. Each of the EPR quantifications have been corrected for the dilution caused by loose packing of the frozen, powdered sample in the EPR tube relative to a standard ferricytochrome *c* sample. Inconsistencies in packing are likely to constitute most of the significant error in the data.

enzyme is turning over at its maximum rate in the presence of saturating amounts of L-lactate (10 mM) and cytochrome *c* (470 μM). Figure 6 plots the concentrations, calculated using EPR spectrometry, of flavin semiquinone and ferricytochrome *c* in each frozen sample relative to the reaction time base. The ferricytochrome *c* quantitations provide an internal indication of the extent of the reaction and therefore allow the semiquinone concentration values to be fixed to their correct positions along the time axis. This calibration was performed using a spectrophotometrically collected trace identical to the above reaction, but using only a catalytic amount of flavocytochrome b_2, which was then scaled up to provide an approximate simulation of the quenched-flow experiment. Although the free radical concentrations are imprecise, due mainly to the problem of achieving uniform sample packing within the EPR tube, the data show that after 50 ms, during the rapid turnover period, around 75% of the total enzyme present is in the semiquinone form. This result is entirely compatible with the kinetic model derived.

CONCLUSIONS

Many of the steps within the catalytic cycle of flavocytochrome b_2 have been studied before, but the intramolecular electron transfer between FMN semiquinone and b_2-heme has proved difficult to observe. In this paper we demonstrate a method for achieving this which is of particular relevance to the catalytic cycle, by observing the rate of FMN oxidation by ferricytochrome *c* using stopped-flow spectrophotometry. The rate constant obtained for the electron transfer is 120 s^{-1}, which appears to rate-limit the overall catalytic cycle to 100 s^{-1}. Confirmation of this comes from quenched-flow EPR experiments which show that, during steady-state turnover, around 75% of the enzyme is in the FMN semiquinone form. We also show that FMN oxidation is inhibited by pyruvate binding. The inhibition constant obtained (K_i = 40 (±17) mM) is consistent with the steady-state value for noncompetitive inhibition.

The reason why FMN semiquinone to b_2-heme electron transfer is so slow in comparison to that from FMN hydroquinone to b_2-heme (> 1500 s^{-1}) is unclear. Based on electrode potentials for the redox couples involved in the two one-electron transfers, one would expect semiquinone to heme electron transfer to be faster than that for hydroquinone to heme (Walker & Tollin, 1991). The scope for conformational influences on electron-transfer rate constants is extensive in this case owing to the significant mobility of the two prosthetic groups with respect to each other. Such factors mean that the electron-transfer rate constants are likely to be altogether less predictable than for systems in which electron-transfer distance and prosthetic group orientation are fixed. Evidence for the mobility of the b_2-heme domain is derived from crystallographic (Xia & Mathews, 1990) and NMR data (Labeyrie et al., 1988), while the significance of the interdomain hinge region has been studied by mutagenesis (Sharp et al., 1994; White et al., 1993).

REFERENCES

Balme, A., Brunt, C. E., Pallister, R. L., Chapman, S. K., & Reid, G. A. (1995) *Biochem. J. 309*, 601−605.

Black, M. T., White, S. A., Reid, G. A., & Chapman, S. K. (1989) *Biochem. J. 258*, 255−259.

Capeillère-Blandin, C. (1975) *Eur. J. Biochem. 56*, 91−101.

Capeillère-Blandin, C. (1991) *Biochem. J. 274*, 207.

Capeillère-Blandin, C., Bray, R. C., Iwatsubo, M., & Labeyrie, F. (1975) *Eur. J. Biochem. 54*, 549−566.

Chapman, S. K., Reid, G. A., Daff, S., Sharp, R. E., White, P., Manson, F. D. C., & Lederer, F. (1994) *Biochem. Soc. Trans 22*, 713−718.

Daff, S., Sharp, R. E., White, P., Short, D. M., Manson, F. D. C., Reid, G. A., & Chapman, S. K. (1996) *Biochemistry 35*, 0000−0000.

Daum, G., Böhni, P. C., & Schatz, G., (1982) *J. Biol. Chem. 252*, 13028−13033.

Forestier, J-P., & Baudras, A. (1971) in *Flavins & Flavoproteins* (Kamin, H., Ed.) pp 599−605, University Park Press, Baltimore, MD.

Hazzard, J. T., McDonough, C. A., & Tollin, G. (1994) *Biochemistry 33*, 13445−13454.

Iwatsubo, M., Mével-Ninio, M., & Labeyrie, F. (1977) *Biochemistry 16*, 3558−3566.

Janot, J.-M., Capeillère-Blandin, C., & Labeyrie, F. (1990) *Biochim. Biophys. Acta 1016*, 165−176.

Labeyrie, F., Beloeil, J. C., & Thomas, M. A. (1988) *Biochim. Biophys. Acta 953*, 134−141.

Lederer, F. (1978) *Eur. J. Biochem. 88*, 425−431.

Miles, C. S., Rouviere-Fourmy, N., Lederer, F., Mathews, F. S., Reid, G. A., & Chapman, S. K. (1992) *Biochem. J. 285*, 187−192.

Moodie, A., Mitchell, R., & Ingledew, W. J. (1990) *Anal. Biochem. 189*, 103−106.

Pajot, P., & Groudinsky, O. (1970) *Eur. J. Biochem. 12*, 158−164.

Pompon, D. (1980) *Eur. J. Biochem. 106*, 151−159.

Pompon, D., Iwatsubo, M., & Lederer, F. (1980) *Eur. J. Biochem. 104*, 479−488.

Sharp, R. E., White, P., Chapman, S. K., & Reid, G. A. (1994) *Biochemistry 33*, 5115−5120.

Tegoni, M., Janot, J.-M., & Labeyrie, F. (1986) *Eur. J. Biochem. 155*, 491−503.

Tegoni, M., Janot, J.-M, & Labeyrie, F. (1990) *Eur. J. Biochem. 190*, 329−342.

Urban, P., Alliel, P. M., & Lederer, F. (1983) *Eur. J. Biochem. 134*, 275−281.

Walker, M. C., & Tollin, G. (1991) *Biochemistry 30*, 5546−5555.

White, P., Manson, F. D. C., Brunt, C. E., Chapman, S. K., & Reid, G. A. (1993) *Biochem. J. 291*, 89−94.

Xia, Z.-X., & Mathews, F. S. (1990) *J. Mol. Biol. 212*, 837−863.

BI9522559

Interaction of Cytochrome *c* with Flavocytochrome b_2[†]

Simon Daff,[‡] R. Eryl Sharp,[§] Duncan M. Short,[‡] Cameron Bell,[‡] Patricia White,[‡] Forbes D. C. Manson,[∥] Graeme A. Reid,[∥] and Stephen K. Chapman*,[‡]

Department of Chemistry and Institute of Cell and Molecular Biology, Edinburgh Centre for Molecular Recognition, University of Edinburgh, West Mains Road, Edinburgh EH9 3JJ, Scotland, U.K., and Johnson Research Foundation, B501 Richards Building, Department of Biochemistry and Biophysics, University of Pennsylvania, 37th and Hamilton Walk, Philadelphia, Pennsylvania 19104

Received September 20, 1995; Revised Manuscript Received March 11, 1996[⊗]

ABSTRACT: Flavocytochrome b_2 from *Saccharomyces cerevisiae* couples L-lactate dehydrogenation to cytochrome *c* reduction. At 25 °C, 0.10 M ionic strength, and saturating L-lactate concentration, the turnover rate is 207 s^{-1} [per cytochrome *c* reduced; Miles, C. S., Rouviere, N., Lederer, F., Mathews, F. S., Reid, G. A., Black, M. T., & Chapman, S. K. (1992) *Biochem. J. 285*, 187−192]. The second-order rate constant for cytochrome *c* reduction in the pre-steady-state has been determined by stopped-flow spectrophotometry to be 34.8 (± 0.9) μM^{-1} s^{-1} in the presence of 10 mM L-lactate. This rate constant has been found to be dependent entirely on the rate of complex formation, the electron-transfer rate in the pre-formed complex being in excess of 1000 s^{-1}. Inhibition of the pre-steady-state reduction of cytochrome *c* by either zinc-substituted cytochrome *c* or ferrocytochrome *c* has led to the estimation of a K_d for the catalytically competent complex of 8 μM, and from this the dissociation rate constant of 280 s^{-1}, a value much less than the actual electron-transfer rate. The inhibition observed is only partial which indicates that electron transfer from the 1:1 complex to another cytochrome *c* can occur and that alternative electron transfer sites exist. The cytochrome *c* binding site proposed by Tegoni et al. [Tegoni, M., White, S. A., Roussel, A., Mathews, F. S., & Cambillau, C. (1993) *Proteins 16*, 408−422] has been tested using site-directed mutagenesis. Mutations designed to affect the complex stability and putative electron-transfer pathway had little effect, suggesting that the primary cytochrome *c* binding site on flavocytochrome b_2 lies elsewhere. The combination of tight binding and multiple electron-transfer sites gives flavocytochrome b_2 a low K_m and a high k_{cat}, maximizing its catalytic efficiency. In the steady-state, the turnover rate is therefore largely limited by other steps in the catalytic cycle, a conclusion which is discussed in the preceding paper in this issue [Daff, S., Ingledew, W. J., Reid, G. A., & Chapman, S. K. (1996) *Biochemistry 35*, 0000−0000].

Over recent years there has been a huge amount of research directed at understanding the rate and specificity of interprotein electron transfer (Marcus & Sutin, 1985; McLendon & Hake, 1992; Chapman & Mount, 1995; Moser et al., 1995). To date much of the work done to address this question has been based on the reactions of the promiscuous protein cytochrome *c*, with both its physiological (e.g., cytochrome *c* peroxidase) and nonphysiological (e.g., cytochrome b_5) redox partners. In this paper, we discuss the less well characterized interaction of cytochrome *c* with another of its physiological partners, flavocytochrome b_2.

Flavocytochrome b_2 (L-lactate:cytochrome *c* oxidoreductase, EC 1.1.2.3) from baker's yeast (*Saccharomyces cerevisiae*) is a homotetramer of subunit molecular weight 57 500 (Jacq & Lederer, 1974). It is a soluble component of the mitochondrial intermembrane space (Daum et al., 1982) where it catalyzes the oxidation of L-lactate to pyruvate with subsequent electron transfer to cytochrome *c* (Appleby & Morton, 1954). The crystal structure of flavocytochrome b_2 determined to 2.4 Å resolution (Xia & Mathews, 1990) shows that each subunit consists of two distinct domains: an N-terminal domain containing protoheme IX ("b_2-heme domain") and a C-terminal domain containing flavin mononucleotide ("flavin domain"). It has been shown that direct electron transfer from FMN to cytochrome *c* is insignificant (Forestier & Baudras, 1971; Iwatsubo et al., 1977; Balme et al., 1995), and that the role of the b_2-heme domain is to mediate this process. Therefore, the route of electron transfer in this system is L-lactate → FMN → b_2-heme → cytochrome *c*. The intraprotein FMN → heme electron transfer reactions of *S. cerevisiae* flavocytochrome b_2 have been extensively investigated (Capeillère-Blandin et al., 1975; Pompon et al., 1980; Miles et al., 1992; Walker & Tollin, 1991; Hazzard et al., 1994; White et al., 1993; Sharp et al., 1994; Chapman et al., 1994; Daff et al., 1996). However, the rather more intractable problem of investigating the interprotein electron transfer to cytochrome *c* has been performed with flavocytochrome b_2 from the yeast *Hansenula anomala* (Capeillère-Blandin, 1982), for which the crystal structure is not yet known.

Recently, in view of the unsuccessful attempts to obtain cocrystals of *S. cerevisiae* flavocytochrome b_2 and cyto-

[†] This work was funded by research grants from the Biotechnology and Biological Science Research Council (U.K.), which also provided studentships for R.E.S., and D.M.S., and by The European Commission (FLAPS Network) and the Engineering and Physical Sciences Research Council (U.K.), which provided a studentship for S.D.

* To whom correspondence should be addressed. Fax: (44)131 650 4743. E-mail: S.K.Chapman@ed.ac.uk.

[‡] Department of Chemistry, University of Edinburgh.

[§] University of Pennsylvania.

[∥] Institute of Cell and Molecular Biology, University of Edinburgh.

[⊗] Abstract published in *Advance ACS Abstracts*, Xxxxxxxxx YY, ZZZZ.

S0006-2960(95)02256-2 CCC: $12.00

chrome *c*, Tegoni et al. (1993) have proposed a hypothetical complex for the interaction between crystalline flavocytochrome b_2 and cytochrome *c*. The model binding site consists of an electrostatic interaction in which the positively charged side chains of cytochrome *c* (Arg13, Arg38, Lys54, and Lys79.) are positioned in the immediate vicinity of acidic flavocytochrome b_2 residues, and several hydrogen bonds are developed. Residue Glu91 of flavocytochrome b_2 is implicated in a number of these interactions and plays a key role in defining the model. As well as presenting a model binding site, Tegoni et al. (1993) suggest a possible pathway for electron transfer. This pathway proceeds from the b_2-heme through residues 50−51 and emerges on the enzyme surface at the side chain of Phe52.

In this paper we (i) report new solution studies on the flavocytochrome b_2-cytochrome *c* interaction and (ii) test the hypothetical complex using site-directed mutagenesis.

MATERIALS AND METHODS

DNA Manipulation, Strains, and Growth. Site-directed mutagenesis was performed by the Kunkel method of nonphenotypical selection (Kunkel, 1985) using the oligonucleotides G1194 (GTTATCAAGGCTAATGCCGG) and G1193b (ATGCCTCCTAAACTTGTCTG) to construct F52A and E91K, respectively (Oswel DNA Service, University of Edinburgh, Edinburgh, Scotland, U.K.). Standard methods for growth of *Escherichia coli*, plasmid purification, DNA manipulation, and transformation were performed as described in Sambrook et al. (1989). *E. coli* strains AR120 and TG1 were used for expression of mutant and wild-type flavocytochromes b_2, respectively.

Enzymes. Flavocytochrome b_2. Wild-type and mutant flavocytochromes b_2 expressed in *E. coli* were isolated from cells which had been stored at −20 °C. The purification procedure was essentially as described previously (Brunt et al., 1992; Black et al., 1989). Purified enzyme preparations were either stored in the reduced state under a nitrogen atmosphere at 4 °C as precipitates from 70% saturated $(NH_4)_2SO_4$ solution or as concentrated aliquots (approximately 100 μM) in the oxidized state, snap-frozen, and stored in liquid nitrogen. Under the former conditions, the enzymes retained full activity for several weeks and indefinitely when frozen in liquid nitrogen. Enzyme concentrations were calculated using previously published extinction coefficients (Pajot & Groudinsky, 1970).

Zinc-Substituted Cytochrome c. Porphyrin cytochrome *c* was prepared essentially as described by Vanderkooi and Erecinska (1975). Approximately 100 mg of freeze-dried horse-heart cytochrome *c* (Sigma) was placed in an open PTFE test tube and cooled in liquid nitrogen. HF gas was then condensed onto the cytochrome *c* while stirring with a PTFE rod. The HF was generated by bubbling nitrogen gas through a HF-saturated pyridine solution (Sigma) contained in a sealed PTFE vessel, the only exit from which lead directly to the cytochrome *c* via a length of PTFE tubing. This apparatus was contained within a well ventilated fume hood. Once the cytochrome *c* was covered entirely by solid HF, the flow was stopped and reaction tube removed from liquid nitrogen. While stirring, the HF was evaporated in a steady stream of nitrogen gas. Purification was conducted as described by Vanderkooi and Erecinska (1975). The porphyrin cytochrome *c* was converted entirely to zinc-substituted cytochrome *c* as described by Vanderkooi et al. (1976). The Zn-cytochrome *c* was dialyzed into 10 mM Tris, HCl buffer, pH 7.5, *I* 0.10, and concentrated using Centricon tubes (Amicon) to approximately 250 μM. Aliquots were stored at −20 °C. Concentrations were calculated from previously reported extinction coefficients (Vanderkooi et al., 1976).

Kinetic Analysis. All kinetic experiments were carried out at 25 ± 0.1 °C in 10 mM Tris-HCl at pH 7.5, *I* 0.10. The buffer consisted of 10 mM HCl titrated against Tris solution to pH 7.5 and adjusted to *I* 0.10 by addition of NaCl. For experiments involving ionic strength effects, *I* was adjusted by addition of the appropriate amount of NaCl. Steady-state kinetic measurements involving the enzymatic oxidation of L-lactate were performed using a Shimadzu UV2101PC or a Beckman DU62 spectrophotometer. Horse-heart cytochrome *c* (type VI, Sigma) was used as the electron acceptor. Collection and analysis of the steady-state data was as previously described (Miles et al., 1992). The K_m and k_{cat} parameters were determined using nonlinear regression analysis.

Pre-steady-state kinetics were performed on an Applied Photophysics SF.17 MV stopped-flow spectrofluorimeter as previously described (Miles et al., 1992; Sharp et al., 1994). Cytochrome *c* reduction by prereduced flavocytochrome b_2 was monitored at 416.5 nm, a flavocytochrome b_2-heme isosbestic point. To ensure that the reduction occurred under pseudo-first-order conditions, flavocytochrome b_2 was always present in excess. Reduction was carried out over a range of flavocytochrome b_2 concentrations, typically 2−10 μM. The cytochrome *c* concentration was 1 μM after mixing. The traces were fitted to monophasic exponentials by nonlinear regression analysis. At least five runs were performed at each flavocytochrome b_2 concentration. Throughout each set of experiments involving ionic strength variation, L-lactate was added to the flavocytochrome b_2 solution to a concentration of 2 mM (before mixing), to fully reduce the enzyme. Over the time scale of the experiment (5 min) no autooxidation of the enzyme occurred and it remained fully reduced. For all other experiments the L-lactate concentration was 10 mM after mixing. For cytochrome *c* reduction by b_2-core, 0.1 μM wild-type flavocytochrome b_2 (a catalytic amount) was added to achieve full b_2-core reduction prior to mixing. Precautions were taken to prevent aerobic oxidation of b_2-core by handling all solutions under an N_2 atmosphere. Second-order-rate constants were determined by plotting k_{obs} for cytochrome *c* reduction against flavocytochrome b_2 concentration and fitting the data to a linear regression analysis.

Inhibition of pre-steady-state cytochrome *c* reduction by reduced or zinc-substituted cytochrome *c* was performed essentially as described above, except that the pre-reduced flavocytochrome b_2 was mixed with a known concentration of reduced or zinc-substituted cytochrome *c*. Flavocytochrome b_2 was kept at approximately 8 μM and inhibitor concentration was varied from 2 to 100 μM (after mixing). Cytochrome *c* reduction (2 μM after mixing) was monitored at 544.8 nm, a b_2-heme isosbestic point. The inhibition constant for cytochrome *c* reduction was determined by plotting the rate of cytochrome *c* reduction against the concentration of inhibiting cytochrome *c* and the data fitted to the equation shown in Chart I.

Chart 1[a]

$$k_{obs} = k_R E_T + \tfrac{1}{2}(k_2 - k_R)\left(E_T - I_T - K_i \mp \sqrt{(E_T - I_T - K_i)^2 + 4E_T K_i} \right)$$

k_2	Second-order rate constant at $I_T = 0$.
k_R	Residual second-order rate constant (at $I_T = \infty$).
E_T	Total enzyme concentration.
I_T	Total inhibitor concentration.
K_i	Dissociation constant for inhibitor at primary binding site.

[a] Cytochrome *c* reacts at a single primary binding site per flavocytochrome b_2 subunit with second-order rate constants k_2–k_R. It also reacts at alternative positions whether the primary site is occupied or not. The cumulative effect of these electron-transfer encounters is accounted for by introducing a residual second-order rate constant k_R. The potential binding properties of these alternative electron-transfer sites is ignored for simplicity. Inhibitor binds to the primary binding site with dissociation constant K_i and prevents further reaction at this position. Since $I_T \ll E_T$, it is considered inappropriate to use a classical Michaelis–Menten function for the fitting process.

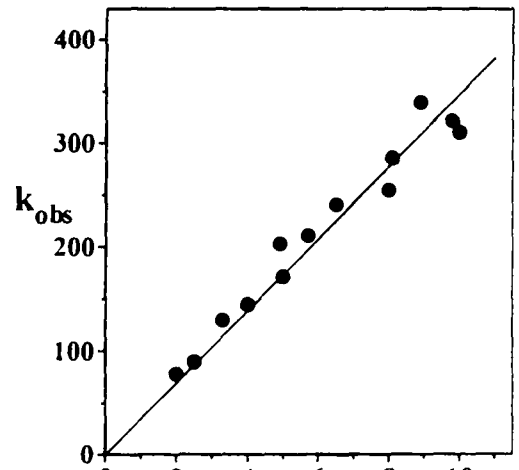

FIGURE 1: Determination of the second-order rate constant for cytochrome *c* reduction by pre-reduced wild-type flavocytochrome b_2 performed at 25 °C in 10 mM Tris–HCl buffer, pH 7.5, I 0.10, containing 10 mM L-lactate. k_{obs} is the pseudo-first-order rate constant for cytochrome *c* reduction derived from stopped-flow spectrophotometry at 416.5 nm (see Materials and Methods). The data are fitted by linear regression analysis. The gradient $k_2 = 34.8 \pm 0.9\ \mu M^{-1}\ s^{-1}$.

Reduction of wild-type flavocytochrome b_2-heme by L-lactate in the presence of zinc-substituted cytochrome *c* was monitored by stopped-flow spectrophotometry at 557 nm as described previously (Miles et al., 1992). The final concentrations were 5 μM flavocytochrome b_2, 10 mM L-lactate, and 0, 10, and 20 μM Zn-cytochrome *c*. Each trace shown in Figure 5 is an average of at least five different runs.

All data fitting was conducted by least-squares regression analysis using either Applied Photophysics software or Origin (Microcal).

RESULTS

Pre-Steady-State Reduction of Cytochrome c. Reduction of a substoichiometric amount of cytochrome *c* by reduced flavocytochrome b_2 was monitored by stopped-flow spectrophotometry as described in Materials and Methods. Figure 1 shows a plot of the observed rate constant against wild-type flavocytochrome b_2 concentration, which shows a linear dependency up to 10 μM, with the rate constant approaching 400 s^{-1}. Each of the generated traces fitted well to a single-exponential function (see Figure 3a), indicating that the reduction process is controlled by a single rate-determining

Scheme 1: Pre-Steady-State Reduction of Cytochrome *c* by Excess Flavocytochrome b_2 under Standard Conditions Follows a Single-Exponential Function[a]

(i) $F{:}H^{\bullet} + \text{cyt}c \overset{\text{Fast}}{\rightleftharpoons} [F{:}H^{\bullet}\text{cyt}c] \xrightarrow{\text{Slow}} [F{:}H\ \text{cyt}c^{\bullet}]$

(ii) $F{:}H^{\bullet} + \text{cyt}c \overset{\text{Slow}}{\rightleftharpoons} [F{:}H^{\bullet}\text{cyt}c] \xrightarrow{\text{Fast}} [F{:}H\ \text{cyt}c^{\bullet}]$

binding **electron transfer**

[a] This is only possible if one of the two schemes illustrated above is satisfied by the reaction mechanism. Therefore either (i) cytochrome *c* binding is fast and reversible and electron transfer slow by comparison, or (ii) cytochrome *c* association/dissociation is slow and electron transfer is fast. F, flavin mononucleotide; H, b_2-heme; cytc, cytochrome *c*; ●, represents an electron thereby indicating redox state.

Table 1: Second-Order Rate Constants for the Reduction of Cytochrome *c* by Pre-Reduced Wild-Type and Mutant Flavocytochromes b_2[a]

	second-order rate constant ($\mu M^{-1}\ s^{-1}$)
wild-type	34.8 ± 0.9
E91K	37.7 ± 1.2
F52A	34.3 ± 1.4
b_2-core	16.2 ± 0.3

[a] All experiments were performed at 25 °C in 10 mM Tris-HCl buffer, pH 7.5, I 0.10 containing 10 mM L-lactate. The second-order rate constants were determined as described in Materials and Methods and as illustrated in Figure 1. Errors represent standard deviations from least-squares fit.

step. The two possibilities for this mechanism are shown in Scheme 1. Either (i) complex formation is rapid and reversible, while electron transfer within the pre-formed complex is slow, or (ii) cytochrome *c* binding is slow while electron transfer is faster than both binding and dissociation. Model (i) would generally produce a hyperbolic curve saturating at the electron-transfer rate with $K_m = K_d$ for the bound complex. The linear region observed in Figure 1 would therefore have to occur at concentrations much less than the K_d for the bound complex. Model (ii) would generate a linear plot until the rate of binding approached the rate of electron transfer at which point single-exponential functions would no longer fit to the experimental traces. The second-order rate constant for cytochrome *c* reduction by wild-type flavocytochrome b_2 derived from Figure 1 is presented in Table 1 along with comparable values for the mutant enzymes E91K, F52A, and b_2-core (the separately expressed heme domain; Brunt et al., 1992). Neither point mutation has any effect on the rate of cytochrome *c* reduction, whereas the b_2-core mutant has a second-order rate constant less than half that of the wild-type value. Therefore residues E91 and F52 are unlikely to be important components of the cytochrome *c* binding site.

Variation of the Second-Order Rate Constant for Cytochrome c Reduction with Ionic Strength. The second-order rate constants for cytochrome *c* reduction by wild-type flavocytochrome b_2 at different ionic strengths are plotted in Figure 2. The straight line fit for log k_2 versus $\sqrt{I}$ according to the Debye–Hückel equation has a gradient $2AZ_+Z_- = -5.9 \pm 0.1$, indicating a positive/negative interaction at the cytochrome *c* binding site. However, it is clear from Figure 2 that the fit is far from satisfactory, deviating strongly at high ionic strength. This is not surprising in view of the well documented nonideal behavior

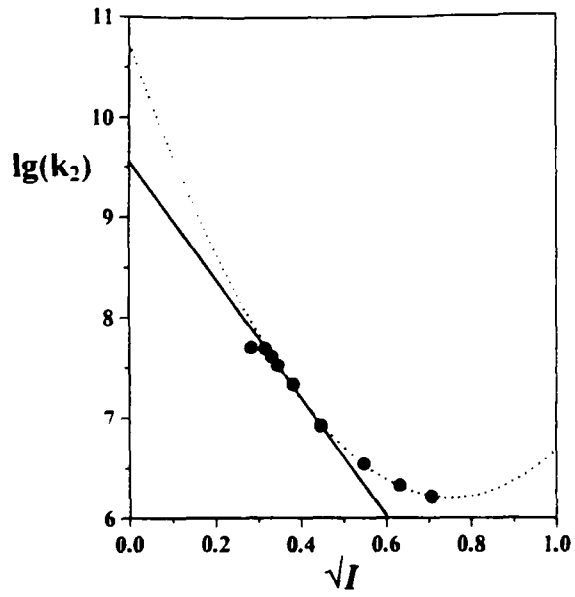

FIGURE 2: Log of the second-order rate constant (k_2) for cytochrome *c* reduction by wild-type flavocytochrome b_2 plotted against the square root of buffer ionic strength (10 mM Tris−HCl, pH 7.5 + NaCl + 1 mM L-lactate). (—) Fit to the Debye−Hückel equation ($\log k_2 = \log k_2^\circ + 2AZ_+Z_-\sqrt{I}$) gradient ($2AZ_+Z_-$) = −5.9 ± 0.1 (NB/Fit restricted to five data points I 0.10−0.20); (---) Fit to parabolic curve ($\log k_2 = \log k_2^\circ + 2AZ_+Z_-\sqrt{I} - BI$) gradient at I 0 ($2AZ_+Z_-$) = −12.1 ± 0.5. Errors represent standard deviations from a least-squares fit.

exhibited during protein−protein interactions (Koppenol, 1980; Koppenol et al., 1978). Further, the ionic strength region studied (0.1−0.5) is well outside the range considered reasonable for an ideal solution (Robinson & Stokes, 1959). By introducing a term linearly dependent on ionic strength (with coefficient B) to the fitting function, a parabolic curve is generated. This fits better to the data and at $I = 0$ has a gradient of $2AZ_+Z_- = -12.1 \pm 0.5$, which again indicates a significant positive/negative interaction. The theoretical basis of this equation is also limited, as the coefficient B has no simple physical meaning (Perlmutter-Hayman, 1973). Its use in this case demonstrates the magnitude of uncertainty in the value of Z_+Z_- derived from Figure 2. Alternative more elaborate approaches use additional information to calculate the magnitude of charge−charge stabilization in a complex [e.g., Watkins et al. (1994)]. However, for the flavocytochrome b_2−cytochrome *c* complex the binding site location is unknown and such methods therefore inaccessible.

At lower ionic strength the stopped-flow method used to obtain second-order rate constants becomes unusable. The cytochrome *c* reduction traces no longer fit to single-exponential functions, suggesting that the reaction is now dependent on multiple rate-determining steps. Figure 3a−d shows four stopped-flow traces at different ionic strengths, each fitted to a single-exponential function. At lower ionic strength the amplitude of the observed reaction decreases and the apparent rate of reaction becomes slower, although the fit quality is poor. The decrease in amplitude indicates that a larger proportion of the reaction is occurring within the stopped-flow dead-time and is therefore happening too fast to be observed fully. This effect is to be expected if the trend of increasing second-order rate constant with decreasing ionic strength was continued as in Figure 2. The appearance of a slow phase indicates that not all the cytochrome *c* is reduced by this rapid step, but a proportion is delayed possibly by an inhibitory binding process. Such a deviation from pseudo-first-order behavior seriously limits the range of ionic strengths which can be used for the Debye−Hückel plot.

Inhibition of Cytochrome c Reduction. Pre-steady-state cytochrome *c* reduction by wild-type flavocytochrome b_2 was inhibited by the addition of either zinc-substituted cytochrome *c* or ferrocytochrome *c* to the prereduced enzyme. The inhibition curves generated are plotted in Figure 4. The general similarity of the two data sets indicates that the use of the redox-inactive Zn−cytochrome *c* is unnecessary for this type of experiment. The electrode potential of cytochrome *c* (Loach, 1976) is some 270 mV more positive than that of the b_2-heme (White et al., 1993), and it is therefore unlikely that a significant reverse reaction would occur. Both systems appear to exhibit partial inhibition such that at high inhibitor concentration a significant rate constant is still observed (around 20% of the maximum value). This indicates that although the primary binding site is occupied rapidly by the inhibitor, cytochrome *c* reduction still occurs, albeit more slowly. K_i values for both curves in Figure 4 are presented in Table 2 along with the residual second-order rate constants (k_R). The model used to calculate these values assumes a single cytochrome *c* binding site per subunit of flavocytochrome b_2 and introduces a residual second-order rate constant k_R to account for the minimum rate constant observed. Both Zn−cytochrome *c* and ferrocytochrome *c* appear to cause partial inhibition with a dissociation constant of around 8 μM at the primary binding site. The additional data in Table 2 refers to the mutant E91K which shows no significantly different behavior with regard to inhibition by ferrocytochrome *c*, further supporting the view that this is not an important residue for binding cytochrome *c*.

Effect of Zinc-Substituted Cytochrome c Binding on b_2-Heme Reduction. Figure 5 shows three b_2-heme reduction traces for wild-type flavocytochrome b_2 generated by mixing with excess L-lactate in the presence of 0, 10, and 20 μM zinc-substituted cytochrome *c*. The Zn−cytochrome *c* is at high enough concentrations to ensure that a significant proportion of the binding sites are occupied (shown by the inhibition studies). The three traces overlay almost exactly, which indicates that there is no significant affect on either FMN to b_2-heme electron transfer or on the preceeding step, FMN reduction.

DISCUSSION

There have been several attempts to characterize the complexation between flavocytochrome b_2 and cytochrome *c*; however, the lack of correlation between these studies has made interpretation difficult. For example, stoichiometries reported vary between one cytochrome *c* per flavocytochrome b_2 tetramer to one per subunit (Tegoni et al., 1993). Previous studies on the flavocytochrome b_2 from *H. anomala* (60% sequence identity with the *S. cerevisiae* enzyme; Black et al., 1989) have lead to the conclusion that the cytochrome *c* binding site involves both flavin and b_2-heme domains (Thomas et al., 1983a,b; Capeillère -Blandin & Albani, 1987). A similar conclusion can be drawn for the *S. cerevisiae* enzyme since the isolated heme domain (b_2-core) has a second-order rate constant for cytochrome *c* reduction which is less than half the value for the intact enzyme (Table 1). In addition, Capeillère-Blandin (1982) reported that the catalytically competent *H. anomala* flavocytochrome b_2−cytochrome *c* complex is stabilized by electrostatic attraction. Similar conclusions hold for the *S. cerevisiae* enzyme (see Figure 2 and Results). In line with the above results, Tegoni et al. (1993) proposed a model for the complex between

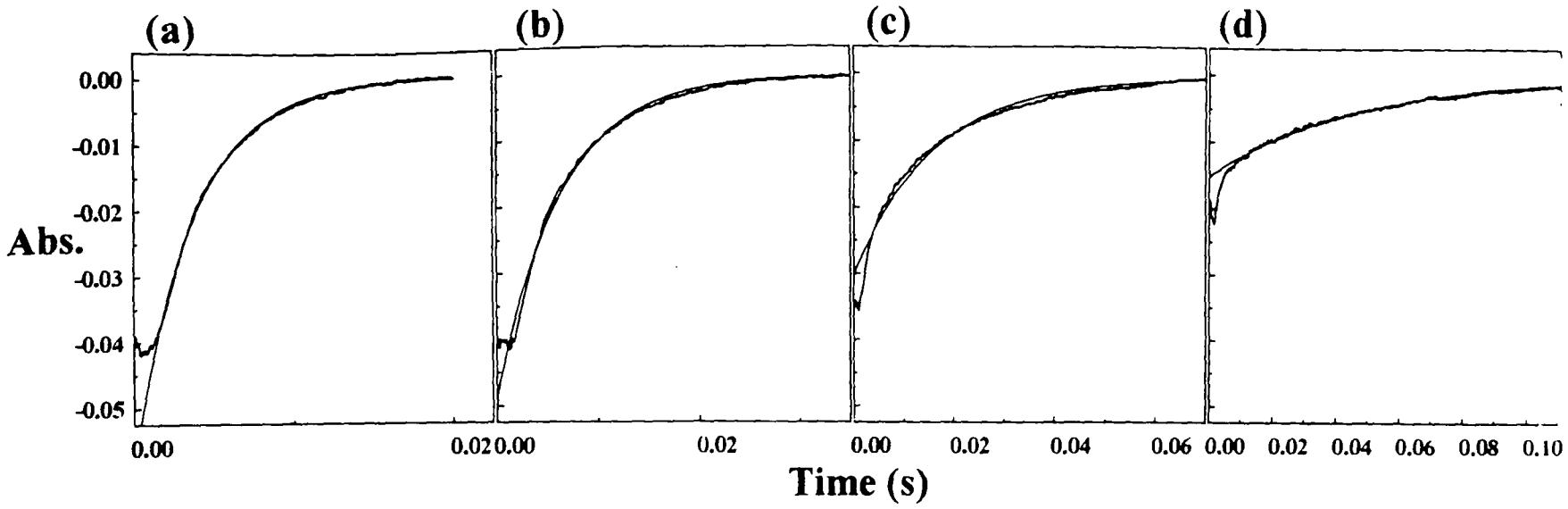

FIGURE 3: Stopped-flow traces showing pre-steady-state reduction of 1 μM cytochrome *c* by 8 μM reduced flavocytochrome b_2 at 25 °C, in 10 mM Tris-HCl buffer, pH 7.5, containing 1 mM L-lactate at four different ionic strengths (adjusted by addition of NaCl). Each trace is fitted by nonlinear least-squares regression analysis to a monophasic exponential function (shown) with rate constant *k* and amplitude *A*. (a) *I* 0.075, $k = 280\ s^{-1}$, $A = 0.060$; (b) *I* 0.050, $k = 171\ s^{-1}$, $A = 0.051$; (c) *I* 0.025, $k = 72\ s^{-1}$, $A = 0.031$; (d) *I* 0.010, $k = 24\ s^{-1}$, $A = 0.015$.

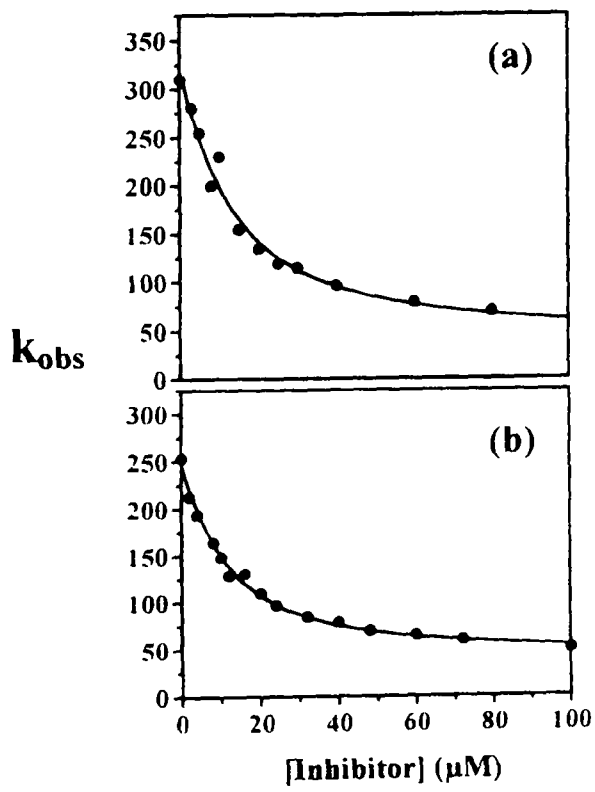

FIGURE 4: Rate constants observed (k_{obs}) for pre-steady-state reduction of ferricytochrome *c* (2 μM) by wild-type flavocytochrome b_2 are shown plotted against inhibitor concentration. (a) Inhibitor is ferrocytochrome *c* and concentration of flavocytochrome b_2 is 8.3 μM. (b) Inhibitor is zinc-substituted cytochrome *c* and concentration of flavocytochrome b_2 is 8.0 μM. Both data sets are fitted to the equation in Chart 1 by nonlinear least-squares regression analysis; (a) $K_i = 8.8 \pm 2.3\ \mu$M (b) $K_i = 7.3 \pm 0.9\ \mu$M.

flavocytochrome b_2 and cytochrome *c* dominated by electrostatic interactions and involving both heme and flavin domains. They also imposed a stoichiometry of one cytochrome *c* per subunit. We have constructed mutants of flavocytochrome b_2 to test this model. E91K reverses the charge of a flavocytochrome b_2 residue postulated to be involved in an electrostatic interaction critical to cytochrome *c* binding, and F52A removes a phenyl ring suggested to be a crucial part of the electron transfer pathway between the two hemes. If the hypothetical model were correct, both mutations would be expected to have a profound affect on the cytochrome *c* reductase ability of the enzyme. The results in Table 1 show that this is not the case.

Since the Tegoni model is unlikely to be correct, we have analyzed the flavocytochrome b_2–cytochrome *c* interaction in more detail. For wild-type flavocytochrome b_2, the rate

Table 2: Inhibition Constants (K_i) and Residual Second-Order Rate Constants (k_R) Calculated for Inhibition by either Zinc-Substituted Cytochrome *c* or Ferrocytochrome *c* of the Pre-Steady-State Reduction of Ferricytochrome *c* by Both Wild-Type and Mutant (E91K) Flavocytochromes b_2[a]

enzyme	inhibitor	K_i (μM)	k_R (μM^{-1} s^{-1})
wild-type	zinc-cytochrome *c*	7.3 ± 0.9	4.9 ± 0.6
wild-type	ferrocytochrome *c*	8.8 ± 2.3	4.5 ± 2.0
E91K	ferrocytochrome *c*	6.0 ± 2.0	7.5 ± 0.8

[a] Performed at 25 °C in 10 mM Tris-HCl buffer, pH 7.5 (*I* 0.10), containing 10 mM L-lactate. Rate constants generated by fitting stopped-flow data to monophasic exponential functions were plotted against inhibitor concentration, and fitted to the equation in Chart 1 by nonlinear regression analysis (as in Figure 4). Errors represent standard deviations from the least-squares fit.

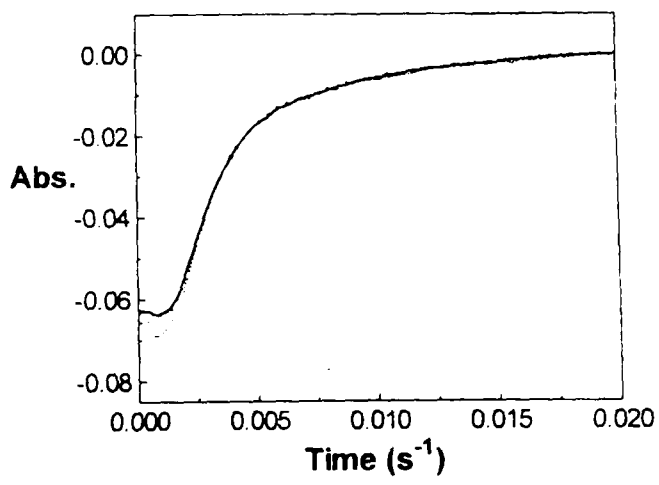

FIGURE 5: b_2-heme reduction traces for wild-type flavocytochrome b_2 (5 μM) on mixing with L-lactate (10 mM) in the presence of zinc-substituted cytochrome *c*: (—) 0 μM; (---) 10 μM; (···) 20 μM. The traces were collected at 557 nm using stopped-flow spectrophotometry at 25 °C in 10 mM Tris–HCl buffer, pH 7.5, *I* 0.10.

constant for electron transfer from b_2-heme to cytochrome *c* within the pre-formed complex has been estimated by photochemical excitation to be 200 (± 80) s^{-1} at 25 °C (McLendon et al., 1987). For the *H. anomala* enzyme, the rate constant has been determined from stopped-flow/ionic strength experiments to be 380 s^{-1} at 5 °C (Capeillère-Blandin, 1982). In our experiments on the *S. cerevisiae* enzyme (at 25 °C), cytochrome *c* reduction occurs at rates beyond the reliable range of the stopped-flow technique and must be in excess of 1000 s^{-1}. While the second value is not inconsistent with this (in view of the lower temperature

used and different enzyme form), it seems unlikely that the electron-transfer rate constant could be as low as 200 s^{-1} as determined by photochemical excitation. At low ionic strength biphasic kinetic behavior is observed (Figure 3), the slow phase of which is probably caused by the inhibitory binding of cytochrome *c* to low activity sites on flavocytochrome b_2, as weaker electrostatic forces become more significant. At *I* 0.01 the amplitude is greatly diminished as the fast phase can no longer be resolved. Using the Debye–Hückel equation to calculate a rate constant at this ionic strength (based on Figure 2), we can estimate that for a 8 μM enzyme solution $k_{obs} = 7500\ s^{-1}$. This would clearly not be observed in a stopped-flow experiment with a dead-time of 1 ms.

In order to resolve the confusion regarding cytochrome *c* binding to flavocytochrome b_2, kinetics can be used to discriminate for interactions at the catalytically active binding site. Vanderkooi et al. (1980) used iron free cytochrome *c* to inhibit the steady-state turnover of flavocytochrome b_2 and obtained a $K_i = 13\ \mu M$. The catalytic cycle for flavocytochrome b_2 is discussed in Daff et al. (1996), and it is clear from the model presented that competitive inhibition would only occur at low cytochrome *c* concentrations. To demonstrate this, we conducted several steady-state assays in which redox-inactive zinc-substituted cytochrome *c* was used as an inhibitor. Zn–cytochrome *c* has been widely used in place of ferrocytochrome *c* to study binding interactions and electron transfer [e.g., Thomas et al. (1983a,b), McLendon et al. (1987) and Alleyne et al. (1992)] and has been shown to be structurally identical to the native protein (Anni et al., 1995). At high concentrations of ferricytochrome *c* (> 100 μM) assays containing an equimolar amount of Zn–cytochrome *c* retained at least 90% of the rate observed in the absence of Zn–cytochrome *c*. Inhibition by Zn–cytochrome *c* was also followed in the pre-steady-state to ensure that the inhibition constants were as close as possible to dissociation constants. Figure 4 panels a and b plot observed rate constants against ferrocytochrome *c* and Zn–cytochrome *c* concentrations, respectively, for the pre-steady-state reduction of ferricytochrome *c*. In both cases the K_i was found to be around 8 μM based on the use of the equation in Chart 1. The fact that this equation fits the data suggests that the stoichiometry is one cytochrome *c* per flavocytochrome b_2 subunit, for the main catalytically active binding site [in agreement with Vanderkooi et al. (1980)]. However, the need to introduce a residual second-order rate constant indicates that this is not the sole site for b_2-heme to cytochrome *c* electron transfer, and that cytochrome *c* reduction occurs even when the main binding site is occupied. The equation in Chart 1 does not, however, take account of the number or nature of these alternative reaction sites and so is flawed in this respect. Nevertheless, if these reaction sites are numerous and binding to them is weak, the equation can be applied over a limited range. Pre-steady-state cytochrome *c* reduction is a single step reaction, which is dependent entirely on cytochrome *c* binding. Therefore, the K_i determined is likely to be equivalent to the actual dissociation constant for ferrocytochrome *c*. Since the protein–protein interaction is expected to be similar in the ferricytochrome *c*–flavocytochrome b_2 complex, as a first approximation the K_d for the catalytically active complex would be expected to be the same. In view of this, it seems unlikely that model (i), Scheme 1 could represent the pre-steady-state reaction. As explained in Results, this model requires that $K_d \gg 10\ \mu M$. Model (ii), Scheme 1 can therefore be used to explain some of the effects already described. The rate constant for electron transfer has already been shown to be > 1000 s^{-1}, which is consistent with this model. The rate constant for cytochrome *c* association would be equal to the second-order rate constant for cytochrome *c* reduction (i.e., 34.8 $\mu M^{-1}\ s^{-1}$). Finally, the dissociation rate must be less than the electron-transfer rate. By using the association rate constant and the inhibition constant, the dissociation rate constant can be estimated to be 280 s^{-1}. Although this value is significant when compared to the rate of enzyme turnover (207 s^{-1}) (Miles et al., 1992), the inhibition constant on which it is based is derived from partial inhibition. So although cytochrome *c* dissociation may be slow, the presence of alternative electron transfer sites means that at high concentration the turnover rate remains unaffected, whereas at low cytochrome *c* concentrations the binding affinity for cytochrome *c* remains high.

The possibility that inhibition by ferro-/Zn–cytochrome *c* in the steady-state may not be entirely competitive in nature was examined by monitoring flavocytochrome b_2 reduction by L-lactate in the presence of Zn–cytochrome *c*. Since b_2-heme reduction requires that both FMN reduction and FMN to b_2-heme intramolecular electron transfer take place, this was considered an appropriate experiment. Particular interest lies in the intramolecular electron transfer step which presumably depends on the relative orientation and position of the two domains. The traces displayed in Figure 5 overlay almost exactly suggesting either that the presence of bound Zn–cytochrome *c* has little affect on the enzyme's other catalytic processes or that the oxidized enzyme has a substantially lower Zn–cytochrome *c* binding affinity than the reduced form. Our current research is directed toward defining the precise location for cytochrome *c* reduction on flavocytochrome b_2.

ACKNOWLEDGMENT

We thank Prof. F. S. Mathews and Drs. F. Lederer, M. Tegoni, and C. Cambillau for helpful discussions.

REFERENCES

Alleyne, T. A., Wilson, M. T., Antonini, G., Malatesta, F., Vallone, B., Sarti, P., & Brunori, M. (1992) *Biochem. J. 287*, 951–956.

Anni, H., Vanderkooi, J. M., & Mayne, L. (1995) *Biochemistry 34*, 5744–5753.

Appleby, C. A., & Morton, R. K. (1954) *Nature 173*, 749–752.

Balme, A., Brunt, C. E., Pallister, R. L., Chapman, S. K., & Reid, G. A. (1995) *Biochem. J. 309*, 601–605.

Black, M. T., White, S. A., Reid, G. A., & Chapman, S. K. (1989) *Biochem. J. 258*, 255–259.

Brunt, C. E., Cox, M. C., Thurgood, A. G. P., Moore, G. R., Reid, G. A., & Chapman, S. K. (1992) *Biochem. J. 283*, 87–90.

Capeillère-Blandin, C. (1982) *Eur. J. Biochem. 128*, 533–542.

Capeillère-Blandin, C., & Albani, J. (1987) *Biochem. J. 245*, 159–165.

Capeillère-Blandin, C., Bray, R. C., Iwatsubo, M., & Labeyrie, F. (1975) *Eur. J. Biochem. 56*, 91–101.

Chapman, S. K., & Mount, A. R. (1995) *Nat. Prod. Rep. 12*, 93–100.

Chapman, S. K, Reid, G. A., Daff, S., Sharp, R. E., White, P. W., Manson, F. D. C., & Lederer, F. (1994) *Biochem. Soc. Trans. 22*, 713–718.

Daff, S., Ingledew, W. J., Reid, G. A., & Chapman, S. K. (1996) *Biochemistry* 35, 0000–0000.

Daum, G., Böhni, P. C., & Schatz, G. (1982) *J. Biol. Chem. 275*, 13028−13033.
Forestier, J-P., & Baudras, A. (1971) in *Flavins & Flavoproteins* (Kamin, H., Ed.) pp 599−605, University Park Press, Baltimore, MD.
Hazzard, J. T., McDonough, C. A., & Tollin, G. (1994) *Biochemistry 33*, 13445−13454.
Iwatsubo, M., Mével-Ninio, M., & Labeyrie, F. (1977) *Biochemistry 16*, 3558−3566.
Jacq, C., & Lederer, F. (1974) *Eur. J. Biochem. 41*, 311−320.
Koppenol, W. H. (1980) *Biophys. J. 29*, 493−508.
Koppenol, W. H., Vroonland, C. A. J., & Braams, R. (1978) *Biochim. Biophys. Acta 503*, 499−508.
Kunkel, T. A. (1985) *Proc. Natl. Acad. Sci. U.S.A. 82*, 488−492.
Loach, P. A. (1976) in *Handbook of Biochemistry & Molecular Biology (Physical & Chemical Data Vol. 1)* (Fasman, G. D., ed.), 3rd ed., pp 122−130, CRC Press Inc., Cleveland, OH.
Marcus, R. A., & Sutin, N. (1985) *Biochim. Biophys. Acta 811*, 265−322.
McLendon, G., & Hake, R. (1992) *Chem. Rev. 92*, 481−490.
McLendon, G., Pardue, K., & Bak, P. (1987) *J. Am. Chem. Soc. 109*, 7540−7541.
Miles, C. S., Rouviere, N., Lederer, F., Mathews, F. S., Reid, G. A., Black, M. T., & Chapman, S. K. (1992) *Biochem. J. 285*, 187−192.
Moser, C. C., Page, C. C., Farid, R., & Dutton, P. L. (1995) *J. Bioenerg. Biomembr.* (in press).
Pajot, P., & Groudinsky, O. (1970) *Eur. J. Biochem. 12*, 158−164.
Perlmutter-Hayman, B. (1973) in *Progress in Reaction Kinetics* (Jennings, K. R., & Cundall, R. B., Ed.) Vol. 6, pp 239−267, Pergamon Press Oxford.

Pompon, D., Iwatsubo, M., & Lederer, F. (1980) *Eur. J. Biochem. 104*, 479−488.
Robinson, R. A., & Stokes, R. H. (1959) *Electrolyte Solutions*, 2nd ed., pp 230−231, Butterworth & Co. Ltd., London.
Sambrook, J., Fritsch, E. F., & Maniatis, T. (1989) *Molecular Cloning: A Laboratory Manual*, 2nd ed., Cold Spring Harbor Laboratoy Press, Cold Spring Harbor, NY.
Sharp, R. E., White, P. W., Chapman, S. K., & Reid, G. A. (1994) *Biochemistry 33*, 5115−5120.
Tegoni, M., White, S. A., Roussel, A., Mathews, F. S., & Cambillau, C. (1993) *Proteins 16*, 408−422, and references therein.
Thomas, M. A., Favoudon, V., & Pochon, F. (1983a) *Eur. J. Biochem. 135*, 569−576.
Thomas, M. A., Gervais, M., Favaudon, V., & Valat, P. (1983b) *Eur. J. Biochem. 135*, 577−581.
Vanderkooi, J. M., & Erecinska, M. (1975) *Eur. J. Biochem. 60*, 199−207.
Vanderkooi, J. M., Adar, F., & Erecinska, M. (1976) *Eur. J. Biochem. 64*, 381−387.
Vanderkooi, J. M., Glatz, P., Casadei, J., & Woodrow, G. V. (1980) *Eur. J. Biochem. 110*, 189−196.
Walker, M. C., & Tollin, G. (1991) *Biochemistry 30*, 5546−5555.
Watkins, J. A., Cusanovich, M. A., Meyer, T. E., & Tollin, G. (1994) *Protein Sci. 3*, 2104−2114.
White, P., Manson, F. D. C., Brunt, C. E., Chapman, S. K., & Reid, G. A. (1993) *Biochem. J. 291*, 89−94
Witt, H., Zickermann, V., & Ludwig, B. (1995) *Biochim. Biophys. Acta 1230*, 74−76.
Xia, Z.-X., & Mathews, F. S. (1990) *J. Mol. Biol. 212*, 837−863.

BI9522561